



Impact of ocean acidification and ocean warming on the oxidation of dissolved Fe(II) in coastal and open Southern Ocean water

By

Helene Aflenzer,

B.Sc., M.Sc.

Submitted in fulfilment of the requirements for the Degree of
Doctor of Philosophy (Natural and Physical Sciences)

University of Tasmania, July 2022

DECLARATION OF ORIGINALITY

This thesis contains no material which has been accepted for a degree or diploma by the University or any other institution, except by way of background information and duly acknowledged in the thesis, and to the best of my knowledge and belief no material previously published or written by another person except where due acknowledgement is made in the text of the thesis, nor does the thesis contain any material that infringes copyright.

Date: 20.12.2021

Signed:

AUTHORITY OF ACCESS

This thesis is not to be made available for loan or copying for two years following the date this statement was signed. Following that time, the thesis may be made available for loan and limited copying and communication in accordance with the *Copyright Act 1968*.

Date: 20.12.2021

Signed:

Acknowledgements

None of this would have been possible without the vision and support of my supervisors Andrew Bowie, Kathrin Wuttig, Philip Boyd, and Pier van der Merwe. Thank you for sharing your knowledge and skills with me, for letting me work with sensitive equipment and for hiring me as a PhD candidate to begin with.

I would like to especially thank Andy for initiating numerous meetings to develop my project, for comments on my written work and mostly for not giving up on me.

Kathrin, I am so glad we met, and I am entirely grateful for your continuous support and patience with me in the lab and during my write-up process. If it was not for you, I think I would have thrown the towel. I would also like to thank you for being an outstanding supervisor and an inspiring mother in science.

Pier, I know we had our differences, and several things went wrong. I still appreciate your help in the lab, your insights into science and your technical know-how. I don't think I would have gotten my current position if not for your inspiration with programming, soldering and the Arduino work.

Also, a major thanks to Thomas Holmes, who was in the same boat as me regarding FIA work. I am so never-ending grateful for your input in my write-up stage and for helping me move my PhD along. I have not met anyone as friendly, open and relaxed as you are, but also professional at the same time.

Further appreciation goes to Linn Hoffmann, Robert Strzepek and Kristen Karsh for giving me insights into biology linked processes. I especially thank Linn Hoffmann for her help with my biotic chapter and shaping this data.

Thank you to Thomas Holmes, Christina Schallenberg, Delphine Lannuzel, Julie Jansen, Matthieu Bressac and Manon Tonnard - I cannot guarantee that the FIA-instruments would not have found their way through the window at some point if it was not for you. I genuinely say thank you to all of you and that I consider myself lucky to have had the chance to work with all of you.

I would like to further express my gratitude to Christina McGraw and Damon Britton for sharing your OA knowledge. I want to thank Pam Quayle, Toby Bolton, and Rob King for facility and equipment-based issues. Thank you to Cathryn Wynn-Edwards for being a close friend and helping me out in the laboratory while already pregnant. Thank you to Lavenia Ratnarajah for guidance on how to structure my written work. Thank you to Cristina Genovese for giving me an insight into voltammetry and sharing her lab ideas with me. Thank you to Nils Jansen for his analytical work and discussions. I would also like to thank Morgane Perron for her help preparing the voyage and Pauline Latour for analysing data from my 4th chapter and the great time on the *RV Investigator*.

A special thank you to Julia Blanchard, Delphine Lannuzel, Joanne Whittaker, and Jaqueline Halpin - my research coordinators - for guiding me through a forest of paperwork along with a very emotional research experience as a PhD candidate.

Thank you to Michael Ellwood, Andrew Bowie, and the Marine National Facilities for making it possible for me to join a research cruise in 2018 – it was a dream of mine, and it was a blast!

I feel lucky to have been funded by the Antarctic Gateway Partnership and the Antarctic and Climate Ecosystems – CRC. Thank you to Donna Saward, Wenneke ten Hout, Jenna Patterson and Richard Coleman for their organising and administrative contribution.

Finally, thank you to my family and friends from home and all the friends I made along the way. A special thank you to my beloved husband Martin for giving me the chance to follow my dream to develop my career by supporting our move to a different country while evolving in your field – I am so proud of you! Thank you also for being such a caring, supporting father and family man who never fails to make me smile.

Table of contents

Acknowledgements	iv
Table of contents	vi
List of Figures	ix
List of Tables	xiii
List of Tables in Appendix	xiv
Thesis Abstract	xvii
Chapter 1: Introduction	1
1.1 The Southern Ocean	1
1.2 The oceanic carbon pumps	2
1.3 The limiting micronutrient iron	4
1.3.1 Sinks and sources of iron.....	4
1.3.2 Iron concentrations and half-lives	6
1.3.3 Iron fractionation and sizes	7
1.3.4 Dissolved Fe(II) and dFe(III)	7
1.4 Iron biochemistry & parameters influencing the dFe(II) and dFe(III) redox couple	8
1.4.1 Kinetics of dFe(II) with oxygen & hydrogen peroxide	8
1.4.2 Ocean acidification, pH changes & its effects on iron	10
1.4.3 Ocean acidification & its effects on biology	11
1.4.4 Temperature, ocean warming & its effects on iron	12
1.4.5 Temperature & ocean warming & its effects on biology	13
1.4.6 Impact of light for iron	14
1.5 Importance of iron for phytoplankton	15
1.5.1 Bioavailability and uptake	16
1.6 Present knowledge gaps and aims	17
1.7 References	19
Chapter 2: Dissolved iron(II) oxidation in coastal and open ocean waters under future scenarios	33
2.1 Introduction	35
2.2 Material and Methods.....	38
2.2.1 Cleaning and sample handling	38
2.2.2 Seawater collection.....	39
2.2.3 Analysis of dFe(II)	39

2.2.4 Analysis of sub-parameters	44
2.2.5 Calculations & modelling.....	46
2.2.6 Experimental overview.....	47
2.2.7 Methodological caveats	48
2.3 Results	49
2.3.1 Temperature Experiments	49
2.3.2 CO ₂ Experiment	53
2.3.3 Comparison of actual observations vs. calculated values	56
2.4 Discussion	57
2.4.1 Role of temperature for the dFe(II) oxidation in open and coastal water in combination with trace metals, ligands and nutrients	57
2.4.2 Trace metals	58
2.4.3 Ligands	59
2.4.4 Nutrients	60
2.4.5 Role of UV and visible light for the dFe(II) oxidation in open and coastal water ..	60
2.4.6 Filtered vs. non-filtered open ocean water	61
2.4.7 Role of pH in combination with temperature on the oxidation rate of dFe(II) in coastal and open ocean water	62
2.4.8 Modelling and suggestions for future models	62
2.4.9 Results for the oxidation of dFe(II) at realistic values of pH and temperature	66
2.5 Conclusion.....	68
2.6 Suggested Improvements	68
2.7 References	70

Chapter 3: Effect of dissolved iron (II) and temperature on the growth of the Southern Ocean species *Fragilariopsis cylindrus* and *Phaeocystis antarctica* 77

3.1 Introduction	79
3.2 Methods.....	82
3.2.1 Experimental overview.....	82
3.2.2 Cleaning.....	83
3.2.3 Seawater	84
3.2.4 Study organisms	84
3.2.5 Temperature, pH and salinity	84
3.2.6 Macronutrients.....	85
3.2.7 Trace elements.....	85
3.2.8 Voltammetry.....	85
3.2.9 Growth rates	86
3.2.10 Statistical analysis	87
3.3 Results	87
3.3.1 Seawater	87
3.3.2 Growth rates	88
3.3.3 Iron-binding organic ligands	90
3.4 Discussion	91
3.4.1 Growth rates	91
3.4.2 Iron binding organic ligands.....	94
3.5 Conclusions	95
3.6 References	97

Chapter 4: Processes governing distribution and cycling of Fe(II) and H₂O₂ in the South Tasman Sea and northern subantarctic zone	102
4.1 Introduction	104
4.2 Methods	106
4.2.1 Oceanographic setting	106
4.2.2 Study area	107
4.2.3 Sample collection and preparation	108
4.2.4 Analysis	109
4.3 Results	112
4.3.1 Hydrography	112
4.3.2 Macronutrients	116
4.3.3 Chlorophyll- <i>a</i>	118
4.3.4 Dissolved Fe(II) distribution	118
4.3.5 Dissolved iron distributions	120
4.3.6 Dissolved H ₂ O ₂ distribution	122
4.3.7 Rainwater and sediment pore water	124
4.4 Discussion	125
4.4.1 Dissolved Fe(II), H ₂ O ₂ and dFe concentrations in the Southern Ocean	125
4.4.2 Impact of physico-chemical parameters for the H ₂ O ₂ and dFe(II) concentration	128
4.4.3 Dissolved Fe(II) from rain and sediment pore water sources	133
4.4.4 Ocean acidification and temperature impacts on dFe(II)	135
4.5 Conclusions	138
4.6 References	140
Chapter 5: General Discussion and Conclusion	148
5.1 Summary and aims of this work	148
5.2 Future recommendations	154
5.3 Conclusion	157
5.4 References	157
Appendix A	160
Appendix B	167
Appendix C	168
Appendix D	182

List of Figures

- Figure 1.1** Map of the annual mean surface NO_3^- based on the World Ocean Atlas 2001 (Conkright et al., 2002, Sarmiento, 2013). The three major HNLC areas are annotated: The Southern Ocean (a), Northeast Subarctic Pacific (b) and the Equatorial Pacific (c)..... 1
- Figure 1.2** The Oceans' Carbon Pumps: solubility/physical pump (left) and the biological pumps (right) exports carbon into deeper water. The Solubility pump is a physical process driven by absorption leading to heat and gas exchanges. The biological pump consists of the organic carbon pump and the soft tissue carbon pump (BCP). (Figure is drawn and modified after Oscar Schofield, Rutgers University) 3
- Figure 1.3** External supply of Fe comes from hydrothermal vents, sediments, river runoff, aerosol deposition and sea ice melting. Internal processes include biological uptake and sinking particles, while the whole cycle is enhanced by reducing reactions from dFe(III) to dFe(II) . The surface is supplied with Fe via upwelling and deep mixing processes..... 5
- Figure 1.4** Left (a): Transect from the SAZ (Subantarctic Zone) Sense voyage 2006/2007, overlaid over satellite chlorophyll-*a* imagery. Right (b): vertical profile of Fe from 0 to 1000 m from station P2 at the Polar Front (PF). Circles denote dissolved Fe ($< 0.2 \mu\text{m}$), green squares particulate Fe ($> 1.0 \mu\text{m}$) (Bowie et al., 2009). 6
- Figure 1.5** Schematic of trace metal fractionation after Raiswell and Canfield (2012). 7
- Figure 1.6** Modelled oxidation of dFe(II) in saline water ($S = 36.24$) at pH 8.17 at O_2 concentrations of $210 \mu\text{M}$ and varying H_2O_2 concentrations from 50 to 728 nM (González-Dávila et al., 2006). 9
- Figure 1.7** (a) The modelled dependance of the $t_{1/2}$ of dFe(II) to pH (Millero et al., 2009) and (b) the modelled pH dependent speciation of dFe(II) in seawater resulting in fractionation changes (Millero et al., 1995). 11
- Figure 1.8** The oxidation rate constant k for dFe(II) in seawater at salinity of 35 as a function of pH (Millero et al., 1987). 13
- Figure 1.9** Photochemical cycle of Fe modified after (Turner and Hunter, 2001)..... 15
- Figure 1.10** Chemical structure of photo pigment Chl-*a* with a porphyrin ring and a central magnesium atom; Scheer (1991)..... 16
- Figure 1.11** Iron uptake by siderophore exchange, after Braun et al. (1998) and Wilhelm (1995): Low intracellular Fe induces the synthesis of transporters such as siderophores and Fe-siderophore uptake at the outer cell membrane. Once the siderophore is outside the cell, it chelates and solubilizes Fe and iron hydroxide (Fe(OH)_3). The siderophore is transported (FeT) into the cell, where Fe is released, and an Fe protein (FeE) is synthesized. The free siderophore is then transported back outside the cell. Fe(OH)_3 is complexed by a siderophore, which enables transport into the cell where Fe is synthesized and the siderophore leaves the cell again. 17
- Figure 2.1** Schematic of processes in the cycling of surface dissolved Fe. Abbreviations: FeL_s , Fe complexed by strong ligand; FeL_w , Fe complexed by weak ligand; dFe(II) ,

sum of all dFe(II) species; Fe', sum of all inorganic dFe(III) species; hv (photon flux); O₂, CO₂ and H₂O₂. Schematic modified for the SO after Croot and Heller (2012). ...35

Figure 2.2 Flow injection analysis for dFe(II) sampling from a temperature cooled tank system, placed inside an iso class-5 laminar flow hood (LMFH): Luminol or ultrapure water(UPW), switched by a 3-port valve, and a sample are pulled from the bottles placed in the cooled tanks located inside a LMFH. Once the reagent and the sample are mixed in the y-piece, they are drawn into a mirrored coil and detected through a photon multiplying tube (PMT). The pH-electrode and buffers were kept at the same temperature as the experimental bottles.41

Figure 2.3 Schematic for one of the two custom-made acrylic tanks (inlet and outlet not shown).41

Figure 2.4 Filtered CO₂ from a cylinder and filtered O₂ from a pump get mixed together. This mix is used to bubble seawater to a pH of 6, 7, 7.5 and 7.9 through a lid with one inlet and one outlet port.44

Figure 2.5 Oxidation curves of dFe(II) over time (minutes) at natural pH at temperatures of 15°C (red), 10°C (yellow) and 5°C (blue) in 0.2 μm filtered coastal water (a-c), filtered open ocean water (d-f), and unfiltered open ocean water (g-h). sw = seawater. Thick datapoints denote replicate averages (n=3), transparent datapoints in the respective colours display the standard deviation for the three replicates. For each water type, dark (a, d, g), light (b, e, h) and UV (c, f, i) treatments were applied.51

Figure 2.6 Filtered (0.2) dFe(II) oxidation under varying pH in coastal water at 10°C and 15°C (a & b) and in open ocean water at 5°C, 10°C and 15°C (c, d, & e). Panels f, g and h display enlarged data from the oxidation in open ocean water. Thick datapoints represent averaged values (n = 3), transparent datapoints represent the standard deviation (n = 3).55

Figure 2.7 Scatterplots with Pearson correlation comparison of measured values from open (A, B) and coastal (C, D) seawater for temperature and t^{1/2} (A, C) and pH and t^{1/2} (B, D). In open ocean water dark (black), light (blue), UV (green), filtered, unfiltered (cyan) and CO₂ (red) treatments are considered. In coastal water no values for unfiltered water were assessed. The black line displays the linear fit for all values in each plot including the R². The correlation coefficient r and its p-value and respective sample numbers n are also shown. P – values are significant at 0.01 level (2-tailed) and are marked with **.64

Figure 2.8 Scatterplots with Pearson correlation comparison of modelled values from open (A, B) and coastal (C, D) seawater for temperature and t^{1/2} (A, C) and pH and t^{1/2} (B, D). In open ocean water dark (black), light (blue), UV (green), filtered, unfiltered (cyan) and CO₂ (red) treatments are considered whereas in coastal water no values for unfiltered water were assessed. The black line displays the linear fitting for all values in each plot including the respective R². The correlation coefficient r and its

p-value and respective sample numbers n are also given below the legend. P – values are significant at 0.05 level (2-tailed) and are marked with * or ** for $p = 0.01$65

- Figure 2.9** Coastal water (a) and open ocean (c) oxidation rates based on **Table 2.8**. Oxidation rates calculated using the functions shown in a and c for: b (open ocean) and d (coastal).67
- Figure 2.10** Summary of the oxidation of dFe(II) with an increase of 1°C and a decrease in pH by 0.2 units (right) based on measured values **Supplementary Table 1**. 68
- Figure 3.1** Experimental hypothesis for coastal and open ocean water from the SO, showing respective Fe concentrations and resulting primary production..... 81
- Figure 3.2** Experimental overview: Growth rate experiment at 3°C (left), 5°C (middle) and 7°C (right) for *Phaeocystis cylindrus* (blue) and *Fragilariopsis cylindrus* (green); with and without an addition (+) of 5 nM dFe(II) in coastal (shaded in yellow) and open ocean water (shaded in red). 83
- Figure 3.3** Specific growth rate (μ , d⁻¹) of *Phaeocystis antarctica* (a, b) and *Fragilariopsis cylindrus* (c, d) grown in coastal (a, c) and open ocean (b, d) water, with the addition (dark colour) and without the addition (light colour) of 5 nM dFe(II). Error bars are standard deviation, n = 3, p-values derived through one-way ANOVAs (**Supplementary Table 11**) comparing for with and without dFe(II) additions are given above the respective bars. 89
- Figure 3.4** Visual summary of Fe : Ligand ratio and their states in coastal and open ocean water. 95
- Figure 4.1** Inset: The locations of the East Australian Current (EAC, orange) and the Sub-Tropical Front (STF, blue) with respect to the Australian continent. Main: the 12 sampling stations and 2 transects (E-W and N-S) sampled during IN2018-V04 on the R/V *Investigator* during September and October 2018. PS = Process station; TS = Transit station. The colour bar indicates depth. 107
- Figure 4.2** Temperature (a), salinity (b) and oxygen (c) along transects N-S and E-W from 0 to 5000 m. The colour bar indicates concentrations, black dots indicate sampling depths for each station, including neutral density contours (γ^n ; kg m⁻², white lines). Antarctic Intermediate Water (AAIW, b) and Subantarctic Mode water (SAMW, c) was defined in the surface and followed by upper (U) and lower (L) Circumpolar Deep Water (CDW) below. Below section (c) the northern Subantarctic Front (SAF) is displayed followed by the northern Subantarctic Zone (SAZ-N) and the Subtropical Front (STF). This figure also outlines the Subtropical Zone (STZ) and the Tasman Front (TF), followed by the East Australian Current (EAC). The red

rectangle displayed in a) indicates the position of a cyclonic eddy observed during this voyage.....	114
Figure 4.3 Depth profiles of temperature ($^{\circ}\text{C}$; green), salinity (orange) and O_2 (μM ; purple) for stations TS 9 to TS 2 (N-S transect) and stations PS 2 to PS 1 (E-W transect). .	115
Figure 4.4 Macronutrient concentrations in the water column along the transects E-W and N-S: a) NO_3^- , (b) PO_4^{3-} and c) SiO_4^{2-} including neutral density contours (γ^n ; kg m^{-2} , white lines).	116
Figure 4.5 Depth profiles of macronutrients NO_3^- (μM , green), PO_4^{3-} (μM , orange) and SiO_4^{2-} (μM , purple) for all stations. Stations TS 9 to TS 2 are summarised as the N-S transect and stations PS 2 to PS 1 as the E-W transect.	117
Figure 4.6 Chl- <i>a</i> concentrations (μg) along both transects in the upper 200 m of the water column. White lines denote neutral density contours (γ^n ; kg m^{-2}).	118
Figure 4.7 Dissolved Fe(II) concentrations (nM) along the transect into depths in the upper 500 m (a) and below 4000 m (b) with neutral density contours (γ^n ; kg m^{-2} , white lines). The colour bar indicates concentrations of dFe(II), black dots display stations labelled at the top. The full data set can be found in Supplementary Table 13 . The red rectangle displayed in a) indicates the position of a cyclonic eddy observed during this voyage.....	119
Figure 4.8 DFe (nM) following N-S and E-W transects of (a) concentration from surface to 500 m depth, and (b) concentration from surface to below 4000 m with neutral density contours (γ^n ; kg m^{-2} , white lines). DFe values presented were used from Barrett et al., (2021).	120
Figure 4.9 Concentrations of dFe(II) (nM, green) and dFe (nM, orange) and the ratio of dFe(II) to dFe (blue) for all 12 stations. Stations TS 9 to TS 2 (N-S transect) is followed by stations PS 2 to PS 1 (E-W transect). The dFe data was used from Barrett et al., (2021).	121
Figure 4.10 Dissolved H_2O_2 concentrations (nM) along the transect in the upper 500 m (a) and below 4000 m (b) with neutral density contours (γ^n ; kg m^{-2} , white lines). Colour bar indicates concentrations of H_2O_2 (nM), black dots display stations, labelled at the top. The full data set can be found in the appendix.....	122
Figure 4.11 Deep profiles from surface to below 4000 m. Samples taken for dFe(II) (green), H_2O_2 (orange) and O_2 (blue) in the N-S transect (TS 9 to TS 2) following the E-W	

transect (PS 2 to PS 1). The full data set is displayed in the appendix (Supplementary Table 13).	123
Figure 4.12 Apparent oxygen utilisation in the upper 500 m (a) and 5000 m (b). White lines in a) denote Chl- <i>a</i> contours. White lines in b) denote neutral density contours (γ^n ; kg m ⁻²).	126
Figure 4.13 DFe (nM) with H ₂ O ₂ contours (white lines) for the upper 1500 m.	127
Figure 4.14 Chl- <i>a</i> concentrations averaged over the time of the voyage. (NOAA, VIIRS; Wang et al., 2017).	132
Figure 4.15 Current movement and speed from the surface (0-5m) from 12 th of September (left) to 22 nd of September (right) 2018.	133
Figure 4.16 Rainwater data (mm) during the time of the voyage. The plot was generated using the averaged data (port and starboard) for the iso surface mode from ODV (Schlitzer, 2015).	134
Figure 4.17 Schematic summary of the key findings of the for the V04_2018 voyage.....	138
Figure 5.1 Summary of key findings for the dFe(II) oxidation from chapter 2 comparing coastal and open ocean seawater.	149
Figure 5.2 Dissolved Fe(II) oxidations comparing coastal and open ocean water (a), impacts of a temperature increase by 5°C (b) and comparing pH decreases by 0.2 units (c). (a) and (b) are based on the measured findings of Table 2.2 from Chapter 2 and (c) is based on modelled values presented in Table 2.4	150
Figure 5.3 Summary of findings for chapter 3.	153

List of Tables

Table 2.1 Overview of experimental treatments from temperature and CO ₂ experiments in coastal and open ocean water.	48
Table 2.2 Temperature based dFe(II) oxidations in coastal and open ocean water for 0.2 μ m filtered (f.) and unfiltered (unf.) treatments. A dark (control, grey), light (yellow) and a UV treatment (purple) was considered at 5°C (blue), 10°C (orange) and 15°C (red). In the left columns are the general parameters temperature (T), pH, salinity (S), dissolved oxygen (DO) and ionic strength (<i>I</i>), followed by the 1 st and 2 nd <i>t</i> _{1/2} , with <i>t</i> _{1/2} , <i>k</i> ' and Log <i>K</i> _{app} reported from each experiment. The calculated values for <i>t</i> _{1/2} and <i>k</i> ' are also shown.	52
Table 2.3 Oxidation of dFe(II) at altering pH via CO ₂ manipulation and varying temperatures of 5°C (blue), 10°C (orange) and 15°C (red). Measured parameters include temperature (T°C), pH, salinity (S) and ionic strength (<i>I</i>). Calculated values of <i>k</i> ' and <i>t</i> _{1/2} are also included.	54
Table 2.4 Modelled approach of CO ₂ experiment: Input parameters were obtained from observations T, (°C), pH, salinity and ionic strength (<i>I</i>) from Table 2.2) from which	

k' and $t_{1/2}$ were calculated using equation 4. ‘-‘ denotes that no value was derived through the calculation.	56
Table 2.5 Trace metal concentrations for open and coastal seawater obtained through ICP-MS analysis (n = 1).	58
Table 2.6 Chromophoric dissolved organic matter (CDOM) concentrations for open and coastal water (n = 1).	60
Table 2.7 Nutrient concentrations in coastal and open ocean water (n = 1).	60
Table 2.8 Summary of read out data obtained by using data from Table 2.3.	66
Table 3.1 Salinity (n = 3), pH (n = 3), dissolved trace metal and nutrient composition of surface (0 -15 m) coastal and open ocean water.	88
Table 3.2 Dissolved (d) Fe is the concentration of Fe, L (nM) is the ligand concentration in the respective seawater samples, $\text{Log}K'_{\text{Fe} \cdot \text{L}}$ is the ligand-binding strength or complexation capacity, L' the freely available ligand, L/dFe displays the ratio of ligand to dFe concentrations, Fe' (pM) the freely available Fe, %FeL is the percentage concentration of dFe organically complexed, and $\text{log}\alpha'_{\text{Fe} \cdot \text{L}}$ is a parameter describing the reactivity for new binding capacities.	91
Table 4.1 Left: Concentrations of dFe(II) 16 hours after collection from 25 cm followed by concentrations below the surface from approximately -1 cm to - 10 cm. Each concentration was analysed 3 times (n = 3). Right: Figure of the measured concentrations of dFe(II) nM.	125
Table 4.2 Summary of N-S and E-W data for the main parameters H_2O_2 , dFe, dFe(II) and the biological parameters PAR and Chl- <i>a</i> for from 0 to 250 m depth.	131
Table 4.3 Comparison of TS 7 and PS 1 for modelled dFe(II) changes, based on pH, temperature, and salinity.	138

List of Tables in Appendix

Supplementary Table 1 Tukey's HSD post hoc test comparing the light treatments in coastal water for the 1 st t $\frac{1}{2}$	161
Supplementary Table 2 Tukey's HSD post hoc test comparing the light treatments in open ocean water for the 1 st t $\frac{1}{2}$	161
Supplementary Table 3 ANOVA for the 1 st t $\frac{1}{2}$ in open ocean water comparing filtered vs. unfiltered conditions.....	162
Supplementary Table 4 Tukey's HSD post hoc test comparing filtered light treatments in open ocean water for the 1 st t $\frac{1}{2}$	162
Supplementary Table 5 Tukey's HSD post hoc test comparing unfiltered light treatments in open ocean water for the 1 st t $\frac{1}{2}$	163
Supplementary Table 6 Tukey's HSD post hoc test comparing filtered light treatments in coastal ocean water for the 2 nd t $\frac{1}{2}$	163
Supplementary Table 7 Tukey's HSD post hoc test comparing filtered coastal water for all light treatments in the 1 st and 2 nd t $\frac{1}{2}$	164
Supplementary Table 8 Tukey's HSD post hoc test comparing open ocean pH in the 1 st t $\frac{1}{2}$ during the CO ₂ experiment.....	164
Supplementary Table 9 Tukey's HSD post hoc test comparing coastal ocean pH in the 1 st t $\frac{1}{2}$ during the CO ₂ experiment.....	165
Supplementary Table 10 Calculated t $\frac{1}{2}$ for coastal and open ocean water at pH 8.1 and 7.9 for temperature range from 0°C to 20°C.....	166
Supplementary Table 11 Summary of the p-values from the statistical analysis. Significant values are shown in bold.	168
Supplementary Table 12 Depth (cm), salinity, pH, temperature, and dilution factors for the analysis of sediment samples.	169
Supplementary Table 13 Location, depth, CTD and nutrient data (NO ₃ ⁻ , PO ₄ ³⁻ , SiO ₄ ²⁻ , NH ⁴⁺) with Chl- <i>a</i> together with the data of dFe(II), dFe and H ₂ O ₂ from V04_2018.170	
Supplementary Table 14 Pearson correlations matrix for all data.....	177
Supplementary Table 15 Correlations of proximity to landmass and/or seamounts for the first 250 m of dFe(II), H ₂ O ₂ and dFe.	178
Supplementary Table 16 People & tasks thankfully performed by them for each chapter	182

Thesis Abstract

The Southern Ocean is the largest region where major nutrients such as nitrate, silicate and phosphate are present in excess, yet the crucial micronutrient element iron (Fe) is scarce. It is well established that the Southern Ocean is key in exporting carbon to greater depths through biomass production by phytoplankton, but Fe is metabolically required for photosynthesis. Changes in uptake of carbon and heat to the ocean will impact ocean acidification and ocean warming. These anthropogenically linked processes are projected to lead to a drop in ocean pH by 0.2 units and an increase in the ocean's temperature by 2°C by the end of the century and are already known to have tremendous ecological impacts on the ocean's flora and fauna. However, little is known about how changes in ocean temperature and pH could alter the nutrient composition in future oceans.

Regarding nutrients, this work focuses on the dissolved (d) element Fe. It is essential for photosynthesis, but also a limiting element in the Southern Ocean due to limiting sources leading to low availability. Iron exists in two redox states in seawater. While the species dFe(III) is stable in seawater and occurs in relatively higher concentrations, its redox partner dFe(II) is tied to several physico-chemical processes impacting its oxidation time and overall presence. The importance of dFe(II) also lies with its accessibility for phytoplankton in its reduced oxidative state. The overall aim of this study was to investigate changes in concentration, speciation, and availability of the 'more' bioavailable, rapidly oxidizing Fe species dFe(II) under a changing Southern Ocean scenario.

Chapter 2 addressed the redox behaviour of dFe(II) and dFe(III), where several questions were explored for further experimental planning. The main question was how the coastal and open ocean systems differ in their dFe(II) concentrations and how ocean acidification and ocean warming impact Fe redox chemistry in both systems. I therefore performed controlled acidification and temperature alteration experiments in coastal and open ocean water taken from the Tasmanian coast and the Southern Ocean. This large dataset enabled us to project for future ocean dFe(II) concentrations and oxidation rates. I observed that a reduction in ocean pH by 0.2 units doubles the dFe(II) oxidation time in the open ocean and tripled in coastal water through model-based experiments. In contrast to these high impacts from pH, an increase in temperature by 1°C accelerated the oxidation by ~ 1.1 times (13% in coastal water and 8% in open ocean water). Therefore, realistic changes in temperature are likely to have small impacts on the oxidation of dFe(II) in both water systems compared to the proposed changes in pH.

For phytoplankton, these results pose contradicting outcomes, and studies display mixed results once parameters such as ocean warming, and acidification are combined. An increase in temperature might lead to less or no growth once a certain temperature threshold is crossed. Similarly, a decrease in pH is also thought to impact phytoplankton physiology. It also depends on the severity of acidification and the phytoplankton species itself. Ocean warming could reduce phytoplankton growth, despite increased Fe availability due to higher solubility in warmer water. Regarding ocean acidification, on the other hand, dFe(II) could become available for an extended time, therefore enabling further uptake of dFe(II) by phytoplankton for that time. When comparing mixed effects of ocean acidification and warming, a reduction in pH might have a greater impact on the dFe(II) oxidation than just temperature. Temperature changes, however, might be a greater concern in the near future before ocean acidification becomes relevant.

Due to this projection of temperature being a more imminent concern, I targeted the limiting element Fe in its less investigated form dFe(II). I observed how temperature alone impacts growth of two Southern Ocean phytoplankton species. I therefore ran an dFe(II)-enrichment incubation experiment in Chapter 3 with differing temperatures (3°C, 5°C, and 7°C) in coastal and open ocean water from the Southern Ocean using the well-studied haptophyte *Phaeocystis antarctica* and the diatom *Fragilariopsis cylindrus*. These enrichment experiments with altered temperatures overall confirmed that phytoplankton growth was elevated once 5 nM dFe(II) were added. In other words, freely available dFe(II) was present, almost regardless of the temperature increase from 3°C to 7°C. This could implicate that an increase in temperature has beneficial effects on growth in the case of higher concentrations of freely available dFe(II). However, these values of future dFe(II) concentrations and oxidation rates under acidified and warmer scenarios are only laboratory-based projections, to better understand the dFe(II) presence and demand by phytoplankton species in a future Southern Ocean.

In Chapter 4, a one-month field study onboard the *RV Investigator* was conducted east of the Australian continent along the East Australian Current (EAC) into nutrient-rich but Fe poor water in the Southern Ocean. I observed the overall distribution of dFe(II) and hydrogen peroxide in this understudied region. The findings suggest that dFe(II) concentrations are very low in the observed area of the open Southern Ocean (< 0.1 nM) compared to coastal waters (> 0.5 nM), likely driven by differences in terrestrial Fe inputs. Hydrogen peroxide was generally higher in the southern stations within the upper 200 m (~60 nM) while the dFe(II) : dFe ratios are 10 % higher than reported for previous Southern Ocean studies. High biological activity in

the upper water extending to the frontal mixing zone where the two major currents meet (EAC and STF), may further have led to the observed low dFe concentrations and high H₂O₂ concentrations. Occasional higher dFe(II) peaks found in this area in surface water may be the result of several external sources such as rain or vertical transport from seamounts but also due to biological or physico-chemical impacts such as photochemical reduction or uptake by phytoplankton.

Overall, the work in this study advances our understanding of the coupled effects of the climate change parameters ocean acidification and ocean warming on the dFe(II) oxidation, with implications for its availability to phytoplankton and overall sources in the region east and south-east of Tasmania in coastal and open ocean water. The experimental approaches taken suggest a higher impact of ocean acidification compared to ocean warming and a potential benefit for phytoplankton species preferring dFe(II).

Chapter 1: Introduction

1.1 The Southern Ocean

The Southern Ocean (SO) is the largest High Nutrient-Low Chlorophyll (HNLC) area (**Figure 1.1; a**) in the world (Boyd et al., 2004, Okin et al., 2011). Other major HNLC areas are the Northeast Subarctic Pacific (**b**) and the Equatorial Pacific (**c**). The SO is defined by high concentrations of macronutrients such as nitrate (NO_3^-) and phosphate (PO_4^{3-}) all year round. At the same time, the vital nutrient for microbial growth - iron (Fe) - is limited in that area (Martin and Fitzwater, 1988, Martin et al., 1990, Gran, 1931). The importance of the SO lies in its size and ability to store carbon (C), which makes it the most critical area for uptake of anthropogenic carbon dioxide (CO_2) (Sarmiento et al., 1998, Gloor et al., 2003). While the SO only makes up about 20% of the Earth's oceans, it can take up to 40% of atmospheric CO_2 (Takahashi et al., 2002, IPCC, 2014, Gruber et al., 2019).

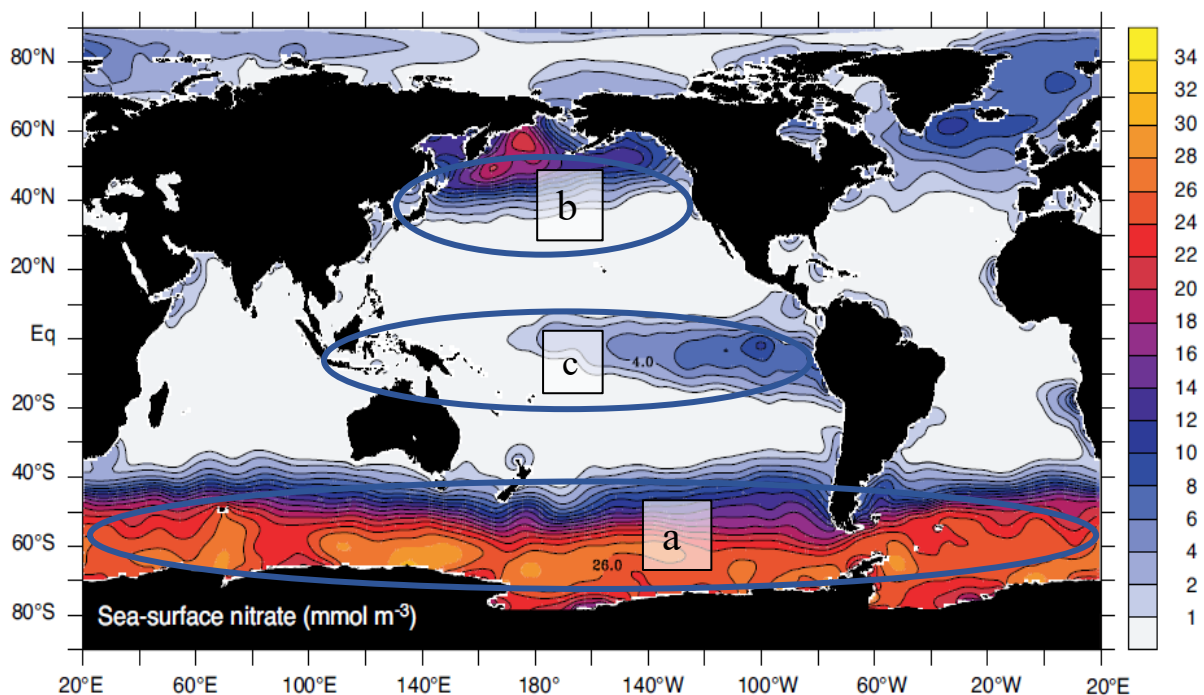


Figure 1.1 Map of the annual mean surface NO_3^- based on the World Ocean Atlas 2001 (Conkright et al., 2002, Sarmiento, 2013). The three major HNLC areas are annotated: The Southern Ocean (a), Northeast Subarctic Pacific (b) and the Equatorial Pacific (c).

1.2 The oceanic carbon pumps

Nutrients are essential for life on earth. In biology, they mostly serve metabolic and enzymatic processes to build and maintain the functions within a cell (see section 1.5). One can distinguish them into macro-nutrients, for example, NO_3^- , C and silicate (SiO_4^{2-}) and micro-nutrient such as Fe or zinc (Zn) (Lohan and Tagliabue, 2018). While the availability of many nutrients is subject to redistribution by currents and upwelling systems, others are a matter of seasonality, distance to their sources, light, temperature, and pH. Nutrients in the ocean not only influence ecological processes (Birkeland, 2015, Moore et al., 2013) but also impact one another (Moore et al., 2001, Gonzalez et al., 2010) and furthermore the oceanic carbon pumps (Falkowski et al., 2000).

The ocean carbon pumps play an important biochemical role on earth, depleting the surface oceans of CO_2 . The pump consists of the physical pump (also solubility pump) and biological pumps consisting of the carbonate pump, the soft tissue carbon pump (BCP, also called organic or biological pumps) and the microbial carbon pump (MCP) (Legendre et al., 2015). The physical pump transports CO_2 from the atmosphere into the ocean's surface, called the solubility pump (**Figure 1.2**). As a result, gas and heat are constantly exchanging (Volk and Hoffert, 2013, Jiao et al., 2010). This pump is highly influenced by sea surface temperature, and therefore, uptake of CO_2 is higher at high latitudes because cold water can hold more gas, whereas, at low latitudes, where the water is warmer, less CO_2 is taken up. This is also intensified by strong winds and waves (Raven and Falkowski, 1999). As a result, when those cold waters in high latitudes come back up to the surface in upwelling systems, they hold a greater amount of CO_2 compared to the atmosphere. Hence, they release CO_2 to reach equilibrium (Watson and Liss, 1998, Zeebe and Wolf-Gladrow, 2001). The BCP (**Figure 1.2**, middle) is started by phytoplanktonic photosynthesis, where C is assimilated, and a small percentage is transported to depth through sinking of dead cells, faecal pellets etc. (Passow and Carlson, 2012, Raven and Falkowski, 1999). Most organisms on earth store and fix C simply by growth; hence they also contribute to the storage of C (Duarte and Cebrian, 1996). The carbonate pump is also part (**Figure 1.2**, right) of the biological pumps and acts by releasing CO_2 from calcification and creating a flux of calcium carbonate (CaCO_3) within the aphotic zone. While the above pumps maintain a vertical gradient of carbon between the surface and deep waters, the recently described MCP (not displayed) maintains a gradient between short and long lived dissolved

organic carbon (> 100 years) (Legendre et al., 2015).

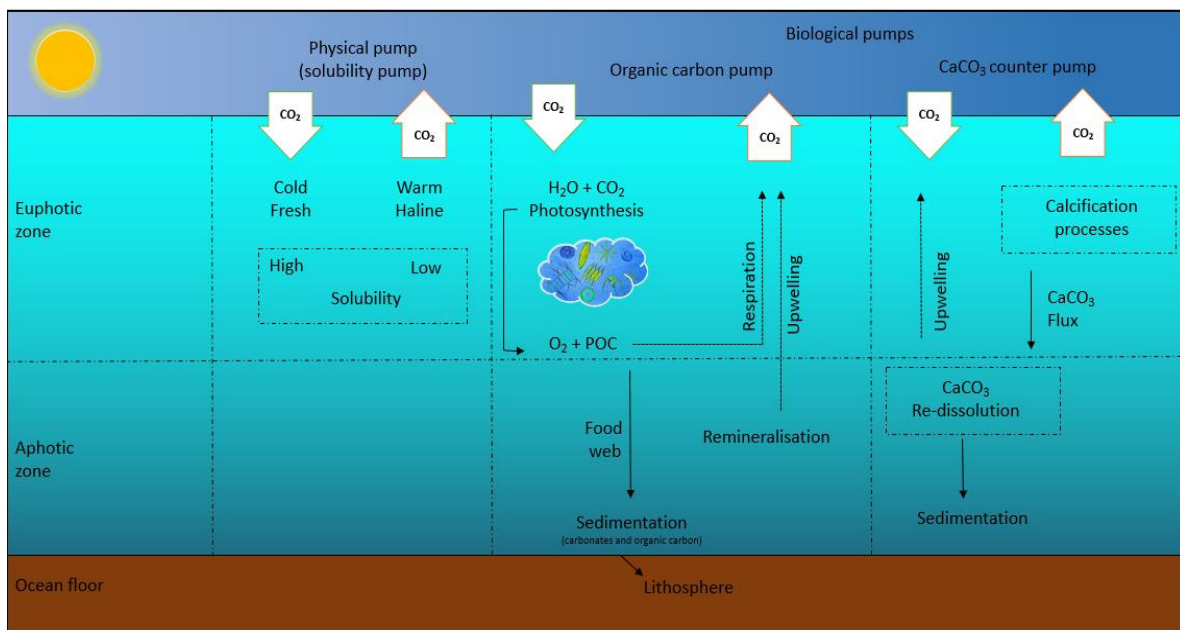


Figure 1.2 The Oceans' Carbon Pumps: solubility/physical pump (left) and the biological pumps (right) exports carbon into deeper water. The Solubility pump is a physical process driven by absorption leading to heat and gas exchanges. The biological pump consists of the organic carbon pump and the soft tissue carbon pump (BCP). (Figure is drawn and modified after Oscar Schofield, Rutgers University).

Phytoplankton growth, accounts for approximately 40% of the global C-fixation (Falkowski, 1997), which is what makes them important. Furthermore, calcifies as corals, molluscs, and some phytoplankton are dependent on sufficient carbonate ions to form their exoskeletons and shells. During this process, they also fix additional C. Calcifying organisms are affected by a decrease in pH, which leads to the dissolution of their outer structures and shells (Ries et al., 2009). There will be a flux of CO₂ from the ocean to the atmosphere if the partial (p) pressure of CO₂ from seawater is larger than the pCO₂ in the air; a process called the carbonate counter pump (**Figure 1.2**, right) (Rost and Riebesell, 2004, IPCC, 2007).

Ever since the industrial revolution, the oceans have been facing several climate change-related issues. Previously mentioned CO₂ accumulation in the oceans and the atmosphere have led to an increase in temperature due to what is known as the greenhouse effect. This temperature increase (see section 1.4.5) has already led to an increase in temperature in the SO by 0.2 °C,

reaching down to 700 m depth (Bindoff and Rintoul, 2011). Due to its size and role in global overturning circulation, the SO is regarded as a global thermal regulator and can buffer for relatively sudden changes in temperature (Takahashi et al., 2002). While this buffering capacity for temperature changes is in jeopardy, accumulations of CO₂ are also leading to a decrease in pH (see section 1.4.2) with adverse outcomes for biology (e.g. Shi et al., 2010, Hoffmann et al., 2012, Taucher et al., 2015, Britton et al., 2016, Millero et al., 2009). Both parameters, temperature increase and a decrease in pH, impact biology and the chemical composition and speciation of nutrients such as Fe in seawater with feedbacks on the ecological dynamic of marine ecosystems (e.g. Laws et al., 2000, Riebesell et al., 2007).

1.3 The limiting micronutrient iron

Nutrients are essential for plants (Uchida, 2000, Imran and Gurmani, 2011) and life on earth. Macronutrients such as NO₃⁻ (Wheeler, 1983, Maldonado and Price, 2000), PO₄³⁻ (Arrigo et al., 1999, Kuffner and Paul, 2001, Harvey, 1940) or SiO₄²⁻ (Tréguer and Jacques, 1992) mainly serve in metabolic and enzymatic processes. Micro-nutrients such as Fe however play an essential role during nitrogen fixation (Price et al., 1991), photosynthesis, and respiration (see section 1.5; Raven et al., 1999). As described in the next sections (1.3.1 to 1.3.4), Fe in the ocean has many sources and comes in several forms and species. Concerning current climate change stressors, I will further elaborate on how Fe is impacted and how this may negatively affect ecosystem processes (Van de Waal and Litchman, 2020, Millero et al., 2009).

1.3.1 Sinks and sources of iron

The groundwork for a modern understanding of the ocean Fe cycle was laid when John Martin (1990) postulated that low concentrations of Fe limit phytoplankton growth in the SO. Many small and large-scale studies followed, exploring the fertilising effect of Fe for phytoplankton (e.g. Langmann et al., 2010, Duggen et al., 2007, Bowie et al., 2001, Peeken et al., 2006, Boyd et al., 2000, Blain et al., 2008). Although Fe is the fourth most abundant element on the earth's crust, its concentration in SO surface waters is low (< 0.3 nM; Boyd and Ellwood, 2010). This mainly results from the low solubility of Fe in the modern, oxygenated ocean and a lack of sources within observed regions of the SO. Major Fe sources (see **Figure 1.3**) are linked to the proximity of continental margins such as sediment resuspension (Bowman and McCuaig, 2003,

Hawkings et al., 2016, Johnson et al., 1999) and river runoff (Chase et al., 2007, Hodson et al., 2017). Hydrothermal vents may also add to the Fe pool but are linked to plate boundaries rather than to continental margins (Ardyna et al., 2019). Aeolian sources contribute to the Fe budget through aerosols (Strzelec et al., 2020, Perron et al., 2020), dust (Bowie et al., 2009, Gabric et al., 2016), particles from bushfires (Ito et al., 2020) or ash from volcanic eruptions (Achterberg et al., 2013). Closer to the Antarctic continent, melting sea ice also delivers a substantial amount of Fe into the ocean in spring (Sedwick and DiTullio, 1997, Lannuzel et al., 2007, Schallenberg et al., 2016). Internal processes within the water column such as vertical and lateral transport, remineralisation (Maldonado et al., 2016, Tagliabue et al., 2017, Boyd et al., 2017), and biological scavenging (Boyd et al., 2015) alter the Fe distributions and concentration. Moreover, biological uptake and chemical removal make up the Fe sink (Tagliabue et al., 2017), removing it from the cyclic process. Seasonally linked upwelling and deep mixing processes (Hutchins et al., 1999a, Thuróczy et al., 2012, Arrigo et al., 2015, Schallenberg et al., 2018), as well as photochemical reduction (Miller et al., 1995, Barbeau et al., 2001), can increase available Fe at the ocean surface (**Figure 1.3**). Further details on the photochemical Fe cycle can be found in **Figure 1.9**.

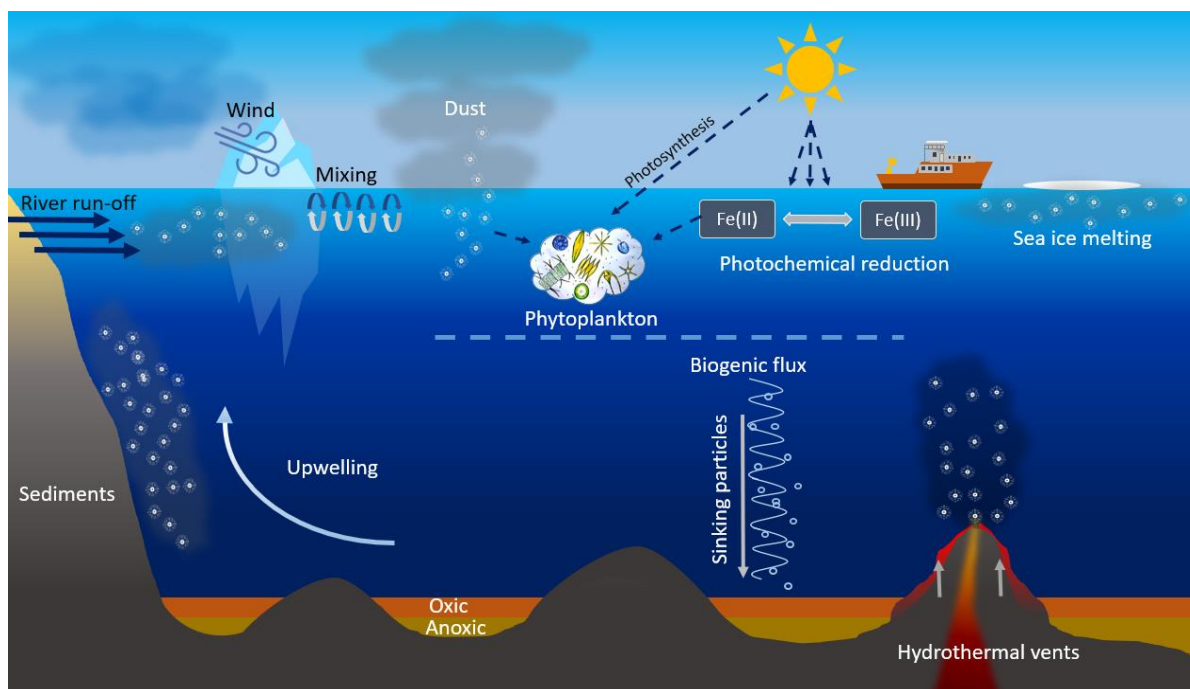


Figure 1.3 External supply of Fe comes from hydrothermal vents, sediments, river runoff, aerosol deposition and sea ice melting. Internal processes include biological uptake and sinking particles, while the whole cycle is enhanced by reducing reactions from dFe(III) to dFe(II). The surface is supplied with Fe via upwelling and deep mixing processes.

1.3.2 Iron concentrations and half-lives

Surface (0 to ~250 m depth) concentrations of Fe in the SO are exceptionally low, with values below 0.3 nM in the open ocean (Boyd and Ellwood, 2010) and increasing concentrations towards sediments and coasts (1.1 – 1.5 nM), including subantarctic islands such as Heard Island or McDonald Island in the Indian sector of the SO (Holmes et al., 2019). Iron resides within the upper water column from approximately 18 to 300 days (Jickells and Spokes, 2001, Jickells et al., 2016) with increasing half-lives in deep water from 70-200 years (Ussher et al., 2004). The short half-life in surface water is linked to rapid uptake and removal through biological processes by phytoplankton (Johnson et al., 1997, Hutchins et al., 1993) or other physico-chemical processes. In deeper SO waters from 200 to 1000 m depth (**Figure 1.4**, a and b), the Fe concentrations can increase up to 0.4 nM (Bowie et al., 2009, Lannuzel et al., 2011), due to lower consumption of primary producers and bacterial remineralisation of sinking particles. Closer to the sediments, it can be much higher with > 25 nM (König et al., 1999).

However, the concentration and speciation largely determine Fe availability and therefore drive phytoplankton growth, which will be explored in each of the following chapters.

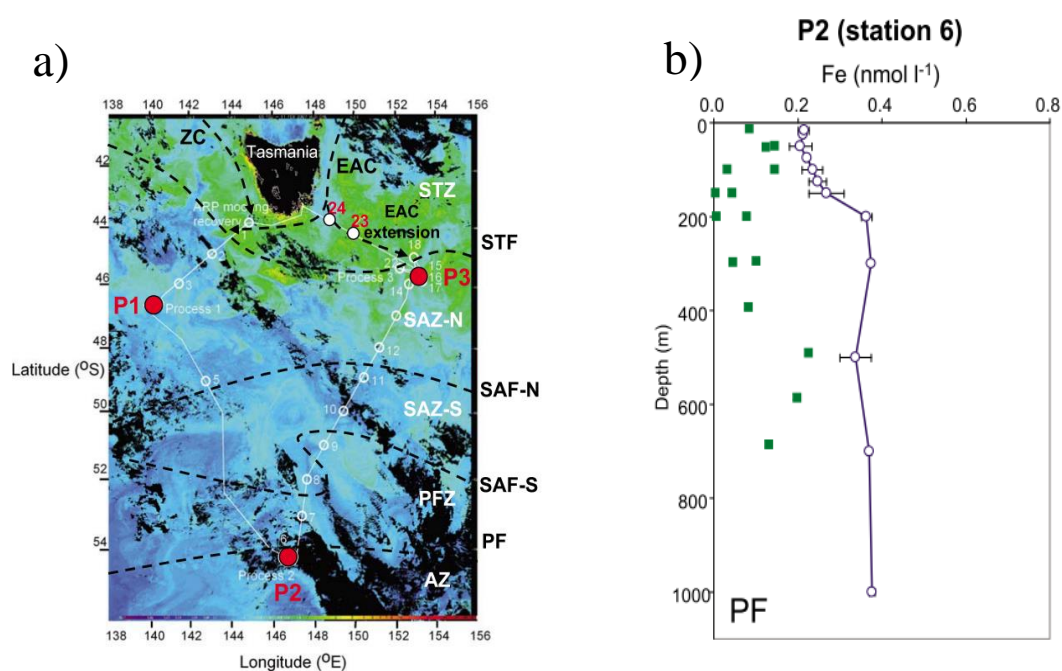


Figure 1.4 Left (a): Transect from the SAZ (Subantarctic Zone) Sense voyage 2006/2007, overlaid over satellite chlorophyll-*a* imagery. Right (b): vertical profile of Fe from 0 to 1000 m from station P2 at the Polar Front (PF). Circles denote dissolved Fe ($< 0.2 \mu\text{m}$), green squares particulate Fe ($> 1.0 \mu\text{m}$) (Bowie et al., 2009).

1.3.3 Iron fractionation and sizes

Different forms of Fe are characterised by particle size fractionation derived from biological or physico-chemical complexation (Gledhill and Buck, 2012). These sizes (**Figure 1.5**) determine the availability of Fe for phytoplankton uptake at the cell surface (Sunda and Huntsman, 1995, Shaked and Lis, 2012). Commonly identified forms of Fe are the particulate form, representing particles larger than $0.4 \mu\text{m}$, and the dissolved (d) form ($< 0.4 \mu\text{m}$).

In coastal areas, Fe occurs in high concentrations ($> 1 \text{ nM}$) compared to the open ocean ($0.05\text{--}1 \text{ nM}$) (Boyd et al., 2000). Dissolved Fe and trace metals can be further divided into soluble Fe ($< 0.02 \mu\text{m}$) and colloidal Fe ($0.02 \mu\text{m} - 0.2 \mu\text{m}$) (Fitzsimmons and Boyle, 2014). Particulates consist of biogenic, lithogenic and detrital particles at sizes of $> 0.2 \mu\text{m}$ (Price and Morel, 1998).

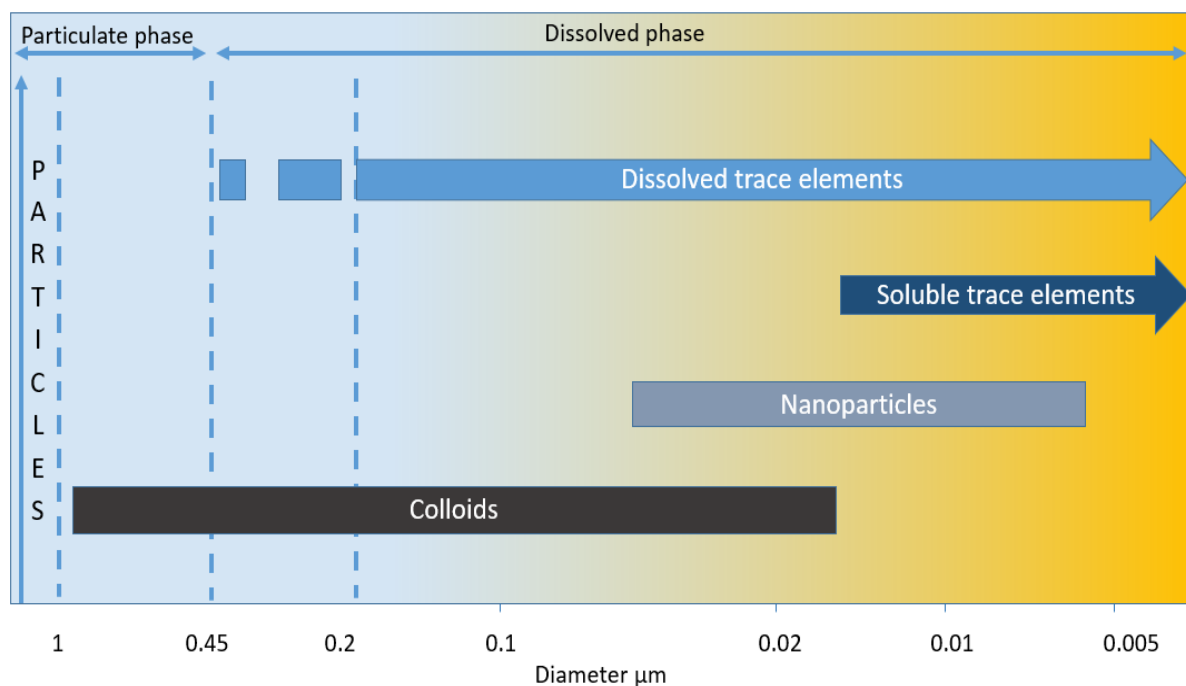


Figure 1.5 Schematic of trace metal fractionation after Raiswell and Canfield (2012).

1.3.4 Dissolved Fe(II) and dFe(III)

During the past decades of oceanic Fe-research, two Fe redox states have been identified as important: dFe(III) and dFe(II) (**Figure 1.3** & **Figure 1.9**). Dissolved Fe(III) is more commonly measured in experimental fieldwork (e.g., Bowie et al., 2001, Boyd et al., 2000, Maldonado et al., 2001, Strzepek et al., 2019) due to its greater stability at the current oceanic pH of ~8.1, which makes it easier to analyse.

A less commonly studied species is dFe(II), a highly reactive and reduced species with short half-lives of minutes to hours in the modern oxygenated ocean (Millero et al., 1987). During the Archean and Proterozoic eon however, the oceans were anoxic and therefore the dFe(II) concentrations were thermodynamically stable (Planavsky et al., 2011). Today, its concentrations are often a magnitude lower (picomolar) than its redox partner dFe(III) (Bowie et al., 2002). Dissolved Fe(II) is considered an important Fe species because, during its oxidation, it is in an unbound state and therefore potentially easily accessible to phytoplankton (Shaked and Lis, 2012). However, its half-life in the ocean and its availability to phytoplankton is subject to several physico-chemical parameters such as ultraviolet (UV) light, ligands, and

hydrogen peroxide (H₂O₂) concentrations (**Figure 1.9**), pH and temperature. These affect the dFe(II)'s oxidation rate, concentrations, and Fe speciation in the ocean and will be discussed over the next few paragraphs.

1.4 Iron biochemistry & parameters influencing the dFe(II) and dFe(III) redox couple

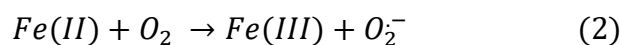
The oxidation of dFe(II) is often displayed as half-life time ($t_{1/2}$). This $t_{1/2}$ is the time for the respective concentration to reach half of its initial concentration. It is complex to predict oxidation reactions in natural waters as they depend on multiple parameters such as oxygen (O₂) and H₂O₂ concentrations (Millero and Sotolongo, 1989, Millero et al., 1987), temperature (Millero et al., 1987, Millero et al., 1995), pH (Millero et al., 2009), light (Miller et al., 1995) and biological uptake and/or complexation (Marschner et al., 1986, Sunda and Huntsman, 1995, Shaked and Lis, 2012).

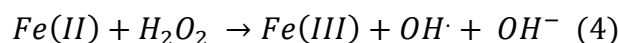
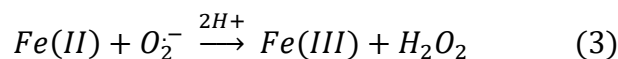
1.4.1 Kinetics of dFe(II) with oxygen & hydrogen peroxide

Amongst others, the main drivers of dFe(II) oxidation in surface water are O₂ and H₂O₂ (Millero and Sotolongo, 1989). A higher concentration of O₂ or H₂O₂ leads to a faster oxidation rate, thus a shorter dFe(II) half-life (equations 2-5) in water when these components are present. This leads to decreased dFe(II), more of the stable dFe(III) and other products such as superoxide (O₂⁻), hydroxide (OH⁻) and its neutral hydroxyl radical OH[•]. This process follows a pseudo first-order rate with respect to the concentration of dFe(II) and the dissolved O₂ concentration and is often expressed by the apparent oxidation rate constant k_{app} (eq. 1) (Davison and Seed, 1983, Santana-Casiano et al., 2005).

$$\frac{-dFe(II)}{dt} = k[Fe(II)](O_2) \quad (1)$$

The most cited and accepted reactions describing the oxidation process of dFe(II) with oxygen (O₂) in natural waters were defined by Haber and Weiss (1932) in the reactions 2-5 below.





Hydrogen peroxide (eq. 4) acts as both a reductant and as an oxidant in water (Winterbourn, 1995). Under natural conditions in seawater with a pH of 8.1, dFe(II) generally oxidizes within minutes when sufficient O_2 or H_2O_2 is present (Santana-Casiano et al., 2005, González-Dávila et al., 2006). For this case, and as described by González-Dávila et al. (2006), this means that a higher concentration of H_2O_2 leads to faster oxidation of dFe(II) (**Figure 1.6**).

For future oceans, it is hypothesised that O_2 concentrations will decrease as a result of increasing sea surface temperatures leading to a higher stratification and less mixing (Pörtner et al., 2019). Although the changes in O_2 are predicted to be small (3.9% decrease) by the end of the century (Pörtner et al., 2019), a retardation of dFe(II) oxidation time may occur when other factors are excluded, ultimately leading to extended half-lives for dFe(II).

1.4.2 Ocean acidification, pH changes & its effects on iron

Ocean acidification (OA) is induced by an uptake of anthropogenic CO_2 from the atmosphere

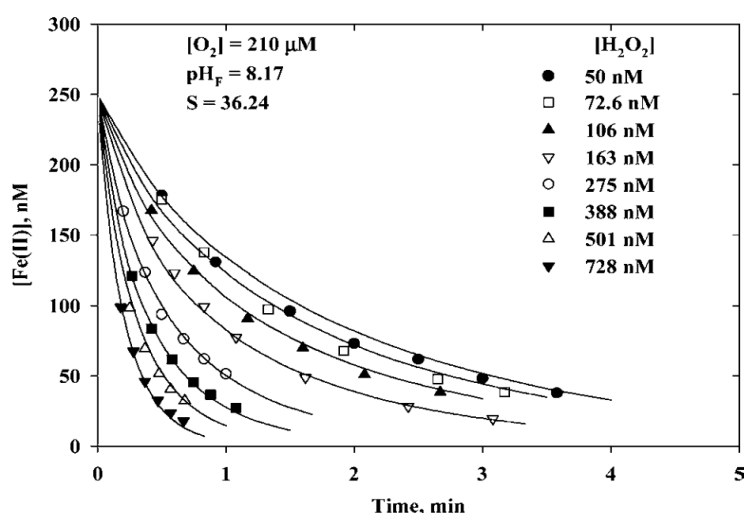
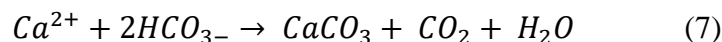
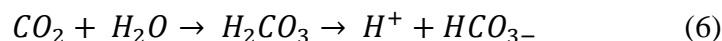


Figure 1.6 Modelled oxidation of dFe(II) in saline water ($S = 36.24$) at pH 8.17 at O_2 concentrations of $210 \mu M$ and varying H_2O_2 concentrations from 50 to 728 nM (González-Dávila et al., 2006).

from burning fossil fuels (Doney et al., 2009, Orr et al., 2005). The following equations define OA:



When CO_2 reacts with seawater (H_2O), carbonic acid (H_2CO_3) forms. This acid dissociates into hydrogen ions (H^+) and bicarbonate ions (HCO_3^- ; eq. 6). As a result, there is an increase in H_2CO_3 , HCO_3^- and H^+ ions, whereby an increase in H^+ reduces pH, and the ocean becomes more acidic as a result (Orr et al., 2005, Feely et al., 2004). In the reverse reaction, carbonate ions (CO_3^{2-}) decrease, and calcium carbonate ($CaCO_3$) dissolves (eq. 7). These 2 reactions impact the structural build-up of calcifying species (Guinotte and Fabry, 2008, Doney et al., 2009, Hallegraef, 2010).

The ocean currently has a pH of ~ 8.1 and it is predicted to drop by 0.072 to 0.108 units by 2050 and might have decreased by another 0.315 units by 2100 (RCP 8.5, high emission scenario; Pörtner et al., 2019). A reduction of surface pH by 0.1 units is equivalent to an increase of 30% of the hydrogen ions (Raven et al., 2005) in the water. As a result, a lowered pH leads to speciation changes of metals and more freely available metals (Millero, 1996, Millero et al., 2009, Hoffmann et al., 2012). The species of interest, $dFe(II)$, becomes more stable and stays in solution longer at lower pH (Millero et al., 2009). In terms of its $t_{1/2}$, **Figure 1.7, a)** displays that a pH decrease of seawater leads to an increase of the $dFe(II)$ half-life (Millero et al., 2009). Concerning future oceans, it is also suggested that the percentage concentrations of $dFe(II)$ are increasing with respect to other Fe species, when other factors such as temperature increase are not considered (Millero et al., 2009, Millero et al., 1995). This means that there will be an overall increase in the $dFe(II)$ concentration with ongoing acidification (**Figure 1.7, b)**. A decrease in pH also leads to an increase in its dissolved and more stable form of $dFe(III)$ (Liu and Millero, 2002, Millero et al., 1995), which could lead to extended availability of the unbound $dFe(II)$ species to phytoplankton.

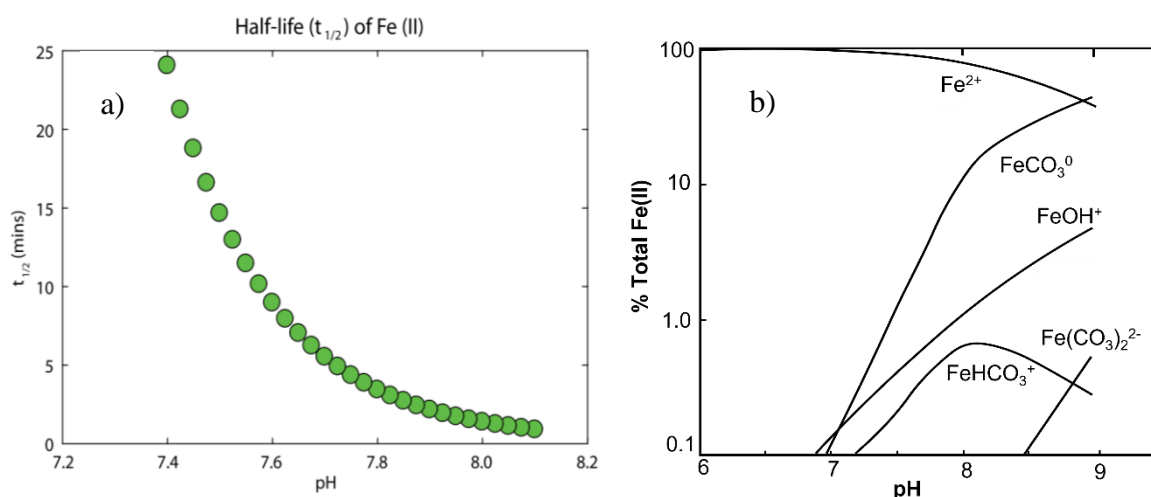


Figure 1.7 (a) The modelled dependance of the $t_{1/2}$ of dFe(II) to pH (Millero et al., 2009) and (b) the modelled pH dependent speciation of dFe(II) in seawater resulting in fractionation changes (Millero et al., 1995).

1.4.3 Ocean acidification & its effects on biology

Regarding biology, carbonate ions (CO_3^{2-}) are an essential building material of structures such as seashells, coral skeletons, and shells of calcifying phytoplankton (Riebesell et al., 2000, Fabry et al., 2008, Gattuso et al., 1999). A decrease in CO_3^{2-} complicates building and maintaining skeletons or other calcium carbonate-containing structures (Sabine and Feely, 2007, Doney et al., 2009). However, pH is also important in respect to growth of most plants since it affects the uptake mechanisms for Fe. While some terrestrial plants have developed systems to access Fe via acidification (e.g., the common soybean, Lindsay and Schwab (1982)), the uptake of Fe under future scenarios for non-rooting ‘drifting’ plants like phytoplankton is still a topic of debate. In a mesocosm study, Breitbarth et al. (2010) found that OA may lead to an enhanced Fe-bioavailability because of an increased fraction of dFe and higher dFe(II) concentrations. Due to a decreased pH, these fractions stay dissolved longer and are therefore better available for phytoplankton. Further, they support the idea of an increase in C export due to increased primary production. In another study, Shi et al. (2010) target Fe availability from a different angle: They did not assume that OA increases bioavailable Fe through a decreased pH. Instead, they proposed that OA increases the Fe stress for phytoplankton by upregulating processes requiring additional energy and Fe. Their results reveal that uptake of Fe by three different diatom species and one calcifying species was enhanced due to pH decreases, which

is not a physiological response of the organism itself. Therefore, it is suggested that OA may not only affect the marine biota on a physiological level but also alter the nutrient speciation and its availability to phytoplankton (Millero et al., 2009, Hoffmann et al., 2012).

1.4.4 Temperature, ocean warming & its effects on iron

Ocean warming has been an ongoing concern over the past 50 years (Levitus et al., 2000, Gleckler et al., 2016) and is increasing with the steady rise of greenhouse gas emissions. Observations of loss in polar sea ice, glacier retreat and a sea-level rise (Rignot et al., 2011) are caused by this increase in greenhouse gases, which in turn are warming up the ocean (Hansen, 1998, Levitus et al., 2000). In the past 100 years, global temperatures have increased by an average of 0.85°C (Change, 2018). Data collected exclusively from the upper 1000 m of the SO revealed an increase of 0.1°C to 0.2°C since the 1960s (Gille, 2002, Domingues et al., 2008). This increased temperature leads to a shorter time for ice sheets to grow over winter, changes the length of seasons (Steele et al., 2008) and leads to more extreme weather events like storms (Timmermann et al., 1999). From a physico-chemical point of view, there will be more stratification in the SO, which could slow the oceans' circulation, leading to less mixing of the water bodies (Toggweiler and Russell, 2008). This will further result in lower O₂ concentrations and shifts of nutrient composition in surface waters (Keeling et al., 2010).

Together with O₂ and pH, temperature is a key parameter affecting dFe(II) oxidation. At warmer temperatures, the kinetics of oxidation for dFe(II) increase while at lower temperatures, they are retarded. This means that at warmer temperatures, the oxidation happens faster (**Figure 1.8**), thus the $t_{1/2}$ is shorter (Millero et al., 1987, Millero et al., 1995). For the redox partner dFe(III), the solubility increases with a lower pH and a lower temperature (Liu and Millero, 2002). Therefore, there is more dFe(III) in solution in colder waters with a lower pH.

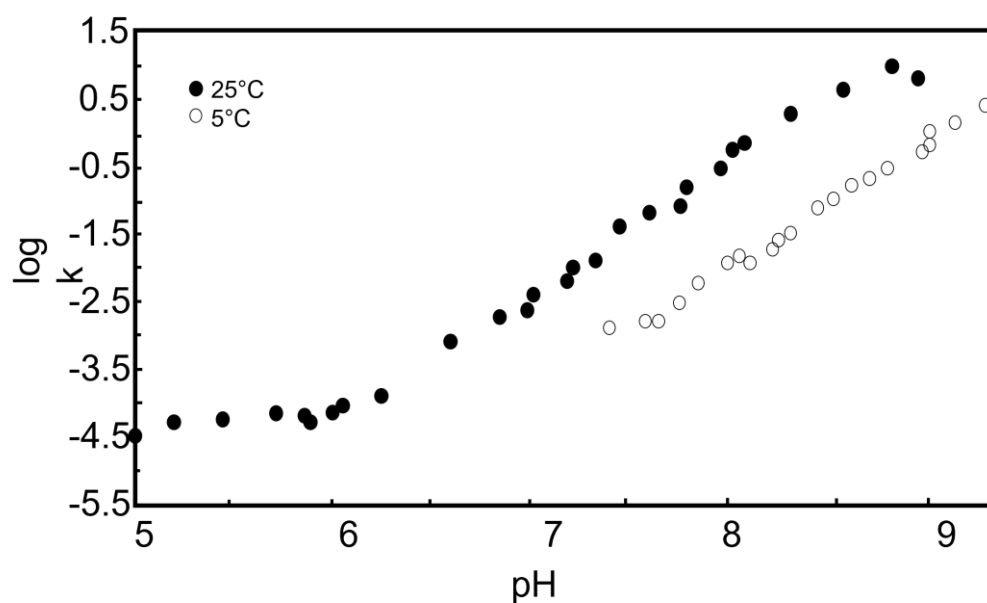


Figure 1.8 The oxidation rate constant k for $d\text{Fe(II)}$ in seawater at salinity of 35 as a function of pH (Millero et al., 1987).

1.4.5 Temperature & ocean warming & its effects on biology

Despite the uncertainty of the actual value for a global temperature increase, an increase will likely affect the availability and composition of nutrients for marine organisms (Van de Waal and Litchman, 2020). Temperature is also arguably the most critical parameter impacting phytoplankton species, leading to changes in physiology and migration processes (Kucera and Malmgren, 1998) and changes in growth or community structure shifts (Vilchis et al., 2005). Consequently, the species diversity of phytoplankton linked to specific ecological niches are at stake (Portner, 2008). An increase in temperature might also have physiological effects on the cell size. Sommer and Lewandowska (2011) found a tendency of phytoplankton to develop smaller cells with a higher density in warmer waters. A combination of changes in nutrient composition and changes in seawater properties (pH and temperature) could therefore result in combined impacts on phytoplankton physiology and ecology (see e.g. Petrou et al. (2016) and **Chapter 2**).

1.4.6 Impact of light for iron

Light is an important energy source for photosynthesis, but it also affects the dFe(II) to dFe(III) redox couple (e.g. Emmenegger et al., 2001, Croot and Heller, 2012). While dFe(II) is often unbound, 99% of dFe(III) is complexed by ligands (Gledhill and Buck, 2012), molecules that bind with and surround a central metal atom. Once sunlight is absorbed by such an Fe-ligand complex produced by phytoplankton (Fe(III)L), it splits into the ligand and the now freely available Fe species dFe(III). The dFe(III) released by a ligand through photoreduction can either be taken up by bacteria or phytoplankton or be reduced to dFe(II). This ‘free’ dFe(II) is transported into the phytoplankton cell or re-oxidised to dFe(III) by the processes described above. From there, dFe(III) can either form another Fe ligand again or aggregate into particulate form and sink (Barbeau *et al.*, 2001).

This photochemical cycle (**Figure 1.9**) enhances cellular Fe uptake by increasing the concentration of bioavailable Fe (dFe(II) and dFe(III)) for phytoplankton during daytime (Johnson et al., 1994). Hereby, light intensity and wavelength should be considered. Rich and Morel (1990) showed that dFe(III) is reduced faster under higher light intensities. This reductive process of Fe occurs at wavelengths below 560 nm. A study by Rijkenberg et al. (2005) revealed that UVB produces most of the dFe(II) followed by UVA and VIS (visible light, 400-700 nm). For phytoplankton however, increased light intensity could lead to photo-inhibition if exposed for extended periods (Powles, 1984) or photodamage in the case of high UV light (Smith et al., 1992). This conflict between cell damage and recycling of Fe through light adds one more layer of complexity to ocean Fe cycling.

The reduction of Fe to dFe(II) through light happens daily in surface water. Phytoplankton productivity in the SO is regulated by Fe, light and temperature and the mixed layer depth (Sunda and Huntsman, 1997). A lack of natural light in winter in the SO leads to less reduction of Fe through less phytoplankton uptake (Emmenegger et al., 1998, Emmenegger et al., 2001), resulting in light limiting conditions during that time. However, most SO phytoplankton species can grow under low light and Fe conditions, including the SO species *Phaeocystis antarctica*.

This species has shown the ability to shrink or decrease their chlorophyll concentrations upon limiting conditions and maintain their growth (Luxem et al., 2017, Trick et al., 1983).

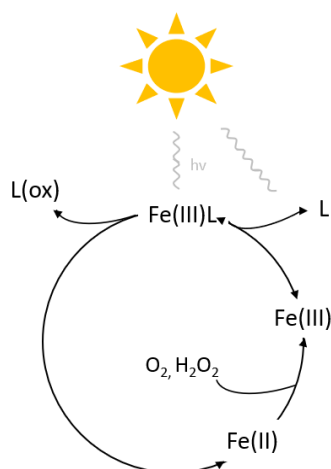


Figure 1.9 Photochemical cycle of Fe modified after (Turner and Hunter, 2001).

1.5 Importance of iron for phytoplankton

Phytoplankton growth accounts for approximately 40% of global C-fixation, which helps to regulate the earth's temperature (Falkowski, 1997). It is also vital for the ocean ecosystem as they form the base of the food chain. Iron has a crucial role within biosynthetic processes in plants such as phytoplankton, most notably in the reactions undertaken during photosynthesis and respiration. The redox partners dFe(II) and dFe(III) have allowed plants to develop various strategies for energy storage (Aisen and Listowsky, 1980), transfer mechanisms for O_2 (Cairo et al., 2006) and other biosynthetic processes.

Chlorophyll (**Figure 1.10**) is the primary green photoreceptor pigment in plants and most algae (Burke et al., 1993). It absorbs sunlight to generate energy via carbohydrates from CO_2 and water and has magnesium (Mg) as a central metal atom. Heme, another Fe-containing pigment in plants, helps with the assimilation of nitrogen (Hogle et al., 2014). It contains an Fe atom in the centre, similar to chlorophyll. Heme synthesises cytochromes (redox-active proteins), which function as electron transfer agents, especially during respiration (Römheld and Marschner, 1991). These cytochromes pass on an electron from one Fe species to another (dFe(III)) to

dFe(II)) in the NADH-Co enzyme Q reductase. In short, Fe is essential for the electron transport chain in photosynthesis. A lack of Fe inhibits the pigment synthesis in photosynthesis, which becomes visible when cells or leaves turn yellow (Brown, 1956).

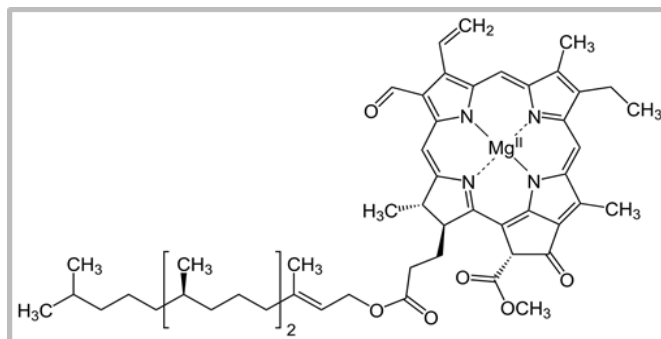


Figure 1.10 Chemical structure of photo pigment Chl-*a* with a porphyrin ring and a central magnesium atom; Scheer (1991).

1.5.1 Bioavailability and uptake

The majority of dFe(III) (> 99%) is organically bound by ligands (Gledhill and Buck, 2012), which keep Fe in solution and enhance its availability to phytoplankton for extended times relative to unbound Fe (Thuróczy et al., 2012). For dFe(II), no determination for ligands was established so far. Bioavailability is defined as the degree to which a particular nutrient can be accessed and utilised by an organism (Shaked and Lis, 2012), in this case, phytoplankton. The availability of Fe is influenced by its chemical forms (see 1.3.3), cycling (see section 1.3.1 and **Figure 1.9**) and uptake mechanisms by phytoplankton (Barbeau et al., 2001, Hutchins et al., 1999b, Strzepek et al., 2011).

For successful Fe acquisition, Fe has to pass through the cell membrane into the cytoplasm. One out of two major uptake mechanism theories suggests a ternary Fe-complex with a chelator and an Fe transporter (**Figure 1.11**), resulting in direct metal uptake (Mies et al., 2006, Harrington and Crumbliss, 2009). A second theory suggests an initial reduction of Fe and release from its ligand by photochemical activity (Maldonado et al., 2005, Turner and Hunter, 2001, Hunter and Boyd, 2007) or uptake through reductive release of dFe(II) from an Fe-organic ligand complex directly at the cell surface (Maldonado and Price, 2001, Yeala et al., 2005, Morel et al., 2008, Shaked and Lis, 2012, Shi et al., 2010).

While the actual uptake mechanisms are still under investigation, it is also thought that each phytoplankton species has a well-adapted uptake strategy. This again depends on the concentration of Fe, its form, particle size and environmental conditions (pH, temperature etc.; Hudson et al., 1990) with potential for environmental links. Sunda and Huntsman (1995) report that open ocean species grew smaller to increase their surface area or grew slower for a reduced Fe requirement (e.g. *Thalassiosira oceanica*) compared to their coastal relatives (e.g. *T. weissflogii*) to overcome Fe limitation. A study by Hassler and Twiss (2006) implies taxonomic differences where large diatoms have a weaker diffusive Fe supply than small cyanobacteria. Another suggested factor is that phytoplankton species excrete organic compounds interacting with Fe (Boye et al., 2001, Rijkenberg et al., 2008, Hassler et al., 2015). Phytoplankton is also known to compete for available Fe and potentially also sequester it from other species through the use of ligands (Völker and Wolf-Gladrow, 1999).

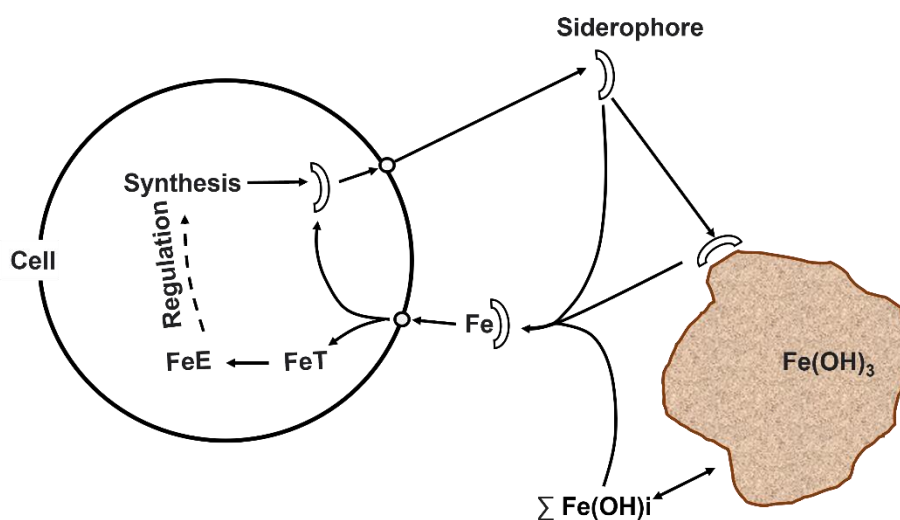


Figure 1.11 Iron uptake by siderophore exchange, after Braun et al. (1998) and Wilhelm (1995): Low intracellular Fe induces the synthesis of transporters such as siderophores and Fe-siderophore uptake at the outer cell membrane. Once the siderophore is outside the cell, it chelates and solubilizes Fe and iron hydroxide (Fe(OH)_3). The siderophore is transported (FeT) into the cell, where Fe is released, and an Fe protein (FeE) is synthesized. The free siderophore is then transported back outside the cell. Fe(OH)_3 is complexed by a siderophore, which enables transport into the cell where Fe is synthesized and the siderophore leaves the cell again.

1.6 Present knowledge gaps and aims

To summarize, a decrease in O_2 is likely to retard the dFe(II) oxidation, whereas an increase in temperature enhances dFe(II) oxidation (Millero et al., 1987, González-Davila et al., 2005). A lower pH will result in the dissolution of complex Fe structures; thus, there will be a higher solubility for dFe(II) and dFe(III) and a retardation of the dFe(II) oxidation (Millero et al., 2009). Future oceans are likely to observe shifts in Fe-demand by phytoplankton due to altered availability from these changes in physical parameters (Fung et al., 2000, van der Merwe et al., 2019). Phytoplankton additionally produces O_2 and organic material such as ligands, influencing the Fe cycle. The interaction of all these parameters makes it difficult to predict for altered dFe(II) oxidation rates, bioavailability, and overall concentrations of Fe in potential future ocean scenarios.

At present, no detailed study with extended run-time lengths of dFe(II) oxidation has been conducted, comparing coastal and open ocean systems under different climate change scenarios. Therefore, my primary goal for Chapter 2 was to explore dFe(II) oxidation during perturbations of pH, temperature and altered light schemes. Since coastal and open ocean water differ hugely in seawater chemistry, Fe sources and impacts by global climate change parameters were investigated for coastal and open ocean water. Therefore, I modified a flow injection analysis (FIA) system to observe the dFe(II) oxidation times in coastal and open ocean water at altered temperatures and shifting pH. Dissolved Fe(II) oxidations during dark, light and after UV exposure were observed. This experiment enabled us to compare the oxidation rate of dFe(II) in these two environments with implications for Fe bio-availabilities for SO phytoplankton species. Furthermore, a modelling approach was applied, to project for dFe(II) concentrations and half-lives times with temperature increases between 1-2°C and pH decreases by 0.2 units, as suggested by the scientific community (see 1.4.2 and 1.4.4).

This dFe(II) oxidation behaviour investigation laid the groundwork for the follow-up ‘biotic’ chapter (Chapter 3). The third chapter looks at the impacts of temperature, dFe(III), and freely available dFe(II) on phytoplankton growth. I therefore compared the growth of two common SO species *Phaeocystis antarctica* and *Fragilariopsis cylindrus* in open and coastal ocean water at 3°C, 5°C and 7°C. I observed growth changes in those species based on temperature changes in the distinct two environments. I also looked at how additions of dFe(II) would impact growth

of each species at each temperature in both water types. Through this approach, I could compare the growth of these two species and potential benefits from Fe additions.

Chapter 4 comprises of data collected during a voyage from the East Australian Current (EAC) into the Subantarctic Zone (SAZ) to the southeast of Australia. Samples were collected on the *RV Investigator* in 2018 to examine dFe(II) and H₂O₂ concentrations along the chosen transect. This was done to compare the Fe rich area east of the Australian main continent with the low Fe area in the SO and to look for potential processes and external sources of dFe(II) from the surface to greater depths in early spring. This study adds to the sparse data available on dFe(II) distributions and supply within the open and coastal oceans east and south of Australia. I also collected and analysed dFe(II) data during a rain event and from sediment porewater from 4000 m depth to directly measure sources of dFe(II) in the region. This chapter ties into the thesis as an additional input on dFe(II) sources and distribution.

The final chapter of this thesis summarises the main outcomes and interprets how my findings add to the current understanding of this topic. It further highlights questions that need further research in the future. A complete list of tasks regarding methodology for each chapter is given in **Appendix D**.

1.7 References

- ACHTERBERG, E. P., MOORE, C. M., HENSON, S. A., STEIGENBERGER, S., STOHL, A., ECKHARDT, S., AVENDANO, L. C., CASSIDY, M., HEMBURY, D., KLAR, J. K., LUCAS, M. I., MACEY, A. I., MARSAY, C. M. & RYAN-KEOGH, T. J. 2013. Natural iron fertilization by the Eyjafjallajökull volcanic eruption. *Geophysical Research Letters*, 40, 921-926.
- AISEN, P. & LISTOWSKY, I. 1980. Iron transport and storage proteins. *Annual review of biochemistry*, 49, 357-393.
- ARDYNA, M., LACOUR, L., SERGI, S., D'OVIDIO, F., SALLÉE, J.-B., REMBAUVILLE, M., BLAIN, S., TAGLIABUE, A., SCHLITZER, R. & JEANDEL, C. 2019. Hydrothermal vents trigger massive phytoplankton blooms in the Southern Ocean. *Nature communications*, 10, 1-8.

- ARRIGO, K. R., ROBINSON, D. H., WORTHEN, D. L., DUNBAR, R. B., DITULLIO, G. R., VANWOERT, M. & LIZOTTE, M. P. 1999. Phytoplankton community structure and the drawdown of nutrients and CO₂ in the Southern Ocean. *Science*, 283, 365-367.
- ARRIGO, K. R., VAN DIJKEN, G. L. & STRONG, A. L. 2015. Environmental controls of marine productivity hot spots around Antarctica. *Journal of Geophysical Research-Oceans*, 120, 5545-5565.
- BARBEAU, K., RUE, E., BRULAND, K. & BUTLER, A. 2001. Photochemical cycling of iron in the surface ocean mediated by microbial iron (III)-binding ligands. *Nature*, 413, 409-413.
- BINDOFF, N. & RINTOUL, S. 2011. *Position analysis: Climate change and the Southern Ocean*, The Antarctic Climate & Ecosystems Cooperative Research Centre.
- BIRKELAND, C. 2015. Geographic differences in ecological processes on coral reefs. *Coral Reefs in the Anthropocene*. Springer.
- BLAIN, S., SARTHOU, G. & LAAN, P. 2008. Distribution of dissolved iron during the natural iron-fertilization experiment KEOPS (Kerguelen Plateau, Southern Ocean). *Deep Sea Research Part II: Topical Studies in Oceanography*, 55, 594-605.
- BOWIE, A. R., ACHTERBERG, E. P., SEDWICK, P. N., USSHER, S. & WORSFOLD, P. J. 2002. Real-time monitoring of picomolar concentrations of iron (II) in marine waters using automated flow injection-chemiluminescence instrumentation. *Environmental science & technology*, 36, 4600-4607.
- BOWIE, A. R., LANNUZEL, D., REMENYI, T. A., WAGENER, T., LAM, P. J., BOYD, P. W., GUIEU, C., TOWNSEND, A. T. & TRULL, T. W. 2009. Biogeochemical iron budgets of the Southern Ocean south of Australia: Decoupling of iron and nutrient cycles in the subantarctic zone by the summertime supply. *Global Biogeochemical Cycles*, 23.
- BOWIE, A. R., MALDONADO, M. T., FREW, R. D., CROOT, P. L., ACHTERBERG, E. P., MANTOURA, R. F. C., WORSFOLD, P. J., LAW, C. S. & BOYD, P. W. 2001. The fate of added iron during a mesoscale fertilisation experiment in the Southern Ocean. *Deep Sea Research Part II: Topical Studies in Oceanography*, 48, 2703-2743.
- BOWMAN, J. P. & MCCUAIG, R. D. 2003. Biodiversity, community structural shifts, and biogeography of prokaryotes within Antarctic continental shelf sediment. *Applied and Environmental Microbiology*, 69, 2463-2483.
- BOYD, P. & ELLWOOD, M. 2010. The biogeochemical cycle of iron in the ocean. *Nature Geoscience*, 3, 675-682.
- BOYD, P. W., ELLWOOD, M. J., TAGLIABUE, A. & TWINING, B. S. 2017. Biotic and abiotic retention, recycling and remineralization of metals in the ocean. *Nature Geoscience*, 10, 167-173.
- BOYD, P. W., LAW, C. S., WONG, C., NOJIRI, Y., TSUDA, A., LEVASSEUR, M., TAKEDA, S., RIVKIN, R., HARRISON, P. J. & STRZEPEK, R. 2004. The decline and fate of an iron-induced subarctic phytoplankton bloom. *Nature*, 428, 549-553.

- BOYD, P. W., LENNARTZ, S. T., GLOVER, D. M. & DONEY, S. C. 2015. Biological ramifications of climate-change-mediated oceanic multi-stressors. *Nature Climate Change*, 5, 71.
- BOYD, R. W., WATSON, A. J., LAW, C. S. & ABRAHAM, E. R. 2000. A mesoscale phytoplankton bloom in the polar Southern Ocean stimulated by iron fertilization. *Nature*, 407, 695.
- BOYE, M., VAN DEN BERG, C. M., DE JONG, J. T., LEACH, H., CROOT, P. & DE BAAR, H. J. 2001. Organic complexation of iron in the Southern Ocean. *Deep Sea Research Part I: Oceanographic Research Papers*, 48, 1477-1497.
- BRAUN, V., HANTKE, K. & KOESTER, W. 1998. Bacterial iron transport: mechanisms, genetics, and regulation. *Metal ions in biological systems*, 35, 67-146.
- BREITBARTH, E., BELLERBY, R. J., NEILL, C. C., ARDELAN, M. V., MEYERHOFER, M., ZOLLNER, E., CROOT, P. L. & RIEBESELL, U. 2010. Ocean acidification affects iron speciation during a coastal seawater mesocosm experiment. *Biogeosciences*, 7, 1065-1073.
- BRITTON, D., CORNWALL, C. E., REVILL, A. T., HURD, C. L. & JOHNSON, C. R. 2016. Ocean acidification reverses the positive effects of seawater pH fluctuations on growth and photosynthesis of the habitat-forming kelp, *Ecklonia radiata*. *Scientific reports*, 6.
- BROWN, J. C. 1956. Iron chlorosis. *Annual Review of Plant Physiology*, 7, 171-190.
- BURKE, D. H., HEARST, J. E. & SIDOW, A. 1993. Early evolution of photosynthesis: clues from nitrogenase and chlorophyll iron proteins. *Proceedings of the National Academy of Sciences*, 90, 7134-7138.
- CAIRO, G., BERNUZZI, F. & RECALCATI, S. 2006. A precious metal: Iron, an essential nutrient for all cells. *Genes & nutrition*, 1, 25-39.
- CHANGE, I. P. O. C. 2018. Special Report on the Ocean and Cryosphere in a Changing Climate. IPCC Geneva.
- CHASE, Z., STRUTTON, P. G. & HALES, B. 2007. Iron links river runoff and shelf width to phytoplankton biomass along the U.S. West Coast. *Geophysical Research Letters*, 34, 4.
- CONKRIGHT, M. E., LOCARNINI, R. A., GARCIA, H. E., O'BRIEN, T. D., BOYER, T. P., STEPHENS, C. & ANTONOV, J. I. 2002. World Ocean Atlas 2001: Objective analyses, data statistics, and figures: CD-ROM documentation.
- CROOT, P. L. & HELLER, M. I. 2012. The importance of kinetics and redox in the biogeochemical cycling of iron in the surface ocean. *Frontiers in Microbiology*, 3.
- DAVISON, W. & SEED, G. 1983. The kinetics of the oxidation of ferrous iron in synthetic and natural waters. *Geochimica et Cosmochimica Acta*, 47, 67-79.
- DE BAAR, H. J. & DE JONG, J. T. 2001. Distributions, sources and sinks of iron in seawater. *IUPAC series on analytical and physical chemistry of environmental systems*, 7, 123-254.

- DOMINGUES, C. M., CHURCH, J. A., WHITE, N. J., GLECKLER, P. J., WIJFFELS, S. E., BARKER, P. M. & DUNN, J. R. 2008. Improved estimates of upper-ocean warming and multi-decadal sea-level rise. *Nature*, 453, 1090.
- DONEY, S. C., FABRY, V. J., FEELY, R. A. & KLEYPAS, J. A. 2009. Ocean acidification: the other CO₂ problem. *Ann Rev Mar Sci*, 1, 169-92.
- DUARTE, C. M. & CEBRIAN, J. 1996. The fate of marine autotrophic production. *Limnology and Oceanography*, 41, 1758-1766.
- DUGGEN, S., CROOT, P., SCHACHT, U. & HOFFMANN, L. 2007. Subduction zone volcanic ash can fertilize the surface ocean and stimulate phytoplankton growth: Evidence from biogeochemical experiments and satellite data. *Geophysical Research Letters*, 34, n/a-n/a.
- EMMENEGGER, L., KING, D. W., SIGG, L. & SULZBERGER, B. 1998. Oxidation kinetics of Fe (II) in a eutrophic Swiss lake. *Environmental Science & Technology*, 32, 2990-2996.
- EMMENEGGER, L., SCHÖNENBERGER, R., SIGG, L. & SULZBERGER, B. 2001. Light-induced redox cycling of iron in circumneutral lakes. *Limnology and Oceanography*, 46, 49-61.
- FABRY, V. J., SEIBEL, B. A., FEELY, R. A. & ORR, J. C. 2008. Impacts of ocean acidification on marine fauna and ecosystem processes. *Ices Journal of Marine Science*, 65, 414-432.
- FALKOWSKI, P., SCHOLLES, R., BOYLE, E., CANADELL, J., CANFIELD, D., ELSER, J., GRUBER, N., HIBBARD, K., HÖGBERG, P. & LINDER, S. 2000. The global carbon cycle: a test of our knowledge of earth as a system. *science*, 290, 291-296.
- FALKOWSKI, P. G. 1997. Photosynthesis: the paradox of carbon dioxide efflux. *Current Biology*, 7, R637-R639.
- FEELY, R. A., SABINE, C. L., LEE, K., BERELSON, W., KLEYPAS, J., FABRY, V. J. & MILLERO, F. J. 2004. Impact of anthropogenic CO₂ on the CaCO₃ system in the oceans. *Science*, 305, 362-366.
- FITZSIMMONS, J. N. & BOYLE, E. A. 2014. Both soluble and colloidal iron phases control dissolved iron variability in the tropical North Atlantic Ocean. *Geochimica et Cosmochimica Acta*, 125, 539-550.
- FUNG, I. Y., MEYN, S. K., TEGEN, I., DONEY, S. C., JOHN, J. G. & BISHOP, J. K. 2000. Iron supply and demand in the upper ocean. *Global Biogeochem. Cycles*, 14, 281-295.
- GABRIC, A. J., CROPP, R., MCTAINSH, G., BUTLER, H., JOHNSTON, B. M., O'LOINGSIGH, T. & VAN TRAN, D. 2016. Tasman Sea biological response to dust storm events during the austral spring of 2009. *Marine and Freshwater Research*, 67, 1090-1102.
- GATTUSO, J. P., ALLEMAND, D. & FRANKIGNOULLE, M. 1999. Photosynthesis and calcification at cellular, organismal and community levels in coral reefs: A review on interactions and control by carbonate chemistry. *American Zoologist*, 39, 160-183.

- GILLE, S. T. 2002. Warming of the Southern Ocean Since the 1950s. *Science*, 295, 1275-1277.
- GLECKLER, P. J., DURACK, P. J., STOUFFER, R. J., JOHNSON, G. C. & FOREST, C. E. 2016. Industrial-era global ocean heat uptake doubles in recent decades. *Nature Climate Change*, 6, 394-398.
- GLEDHILL, M. & BUCK, K. N. 2012. The organic complexation of iron in the marine environment: a review. *Frontiers in Microbiology*, 3, 69.
- GLOOR, M., GRUBER, N., SARMIENTO, J., SABINE, C., FEELY, R. & RÖDENBECK, C. 2003. A first estimate of present and preindustrial air-sea CO₂ flux patterns based on ocean interior carbon measurements and models. *Geophysical Research Letters*, 30.
- GONZÁLEZ-DAVILA, M., SANTANA-CASIANO, J. M. & MILLERO, F. J. 2005. Oxidation of iron (II) nanomolar with H₂O₂ in seawater. *Geochimica et Cosmochimica Acta*, 69, 83-93.
- GONZÁLEZ-DÁVILA, M., SANTANA-CASIANO, J. M. & MILLERO, F. J. 2006. Competition between O₂ and H₂O₂ in the oxidation of Fe (II) in natural waters. *Journal of solution chemistry*, 35, 95-111.
- GONZALEZ, A. G., SANTANA-CASIANO, J. M., PEREZ, N. & GONZALEZ-DAVILA, M. 2010. Oxidation of Fe(II) in Natural Waters at High Nutrient Concentrations. *Environmental Science & Technology*, 44, 8095-8101.
- GRAN, H. H. 1931. On the conditions for the production of plankton in the sea. *Conseil Perm. Internat. pour l'Explor. de la Mer. Rapp. et Proces-Verb.*, 75, 37-46.
- GRUBER, N., LANDSCHÜTZER, P. & LOVENDUSKI, N. S. 2019. The variable Southern Ocean carbon sink. *Annual review of marine science*, 11, 159-186.
- GUINOTTE, J. M. & FABRY, V. J. 2008. Ocean acidification and its potential effects on marine ecosystems. *Annals of the New York Academy of Sciences*, 1134, 320-342.
- HABER, F. & WEISS, J. 1932. Über die katalyse des hydroperoxydes. *Naturwissenschaften*, 20, 948-950.
- HALLEGRAEFF, G. M. 2010. OCEAN CLIMATE CHANGE, PHYTOPLANKTON COMMUNITY RESPONSES, AND HARMFUL ALGAL BLOOMS: A FORMIDABLE PREDICTIVE CHALLENGE¹. *Journal of Phycology*, 46, 220-235.
- HANSEN, J. E. 1998. Sir John Houghton: Global Warming: The Complete Briefing. *Journal of Atmospheric Chemistry*, 30, 409-412.
- HARRINGTON, J. M. & CRUMBLISS, A. L. 2009. The redox hypothesis in siderophore-mediated iron uptake. *Biometals*, 22, 679-689.
- HARVEY, H. 1940. Nitrogen and phosphorus required for the growth of phytoplankton. *Journal of The Marine Biological Association of the United Kingdom*, 24, 115-123.
- HASSLER, C. S., NORMAN, L., MANCUSO NICHOLS, C. A., CLEMENTSON, L. A., ROBINSON, C., SCHOEMANN, V., WATSON, R. J. & DOBLIN, M. A. 2015. Iron associated with exopolymeric substances is highly bioavailable to oceanic phytoplankton. *Marine Chemistry*, 173, 136-147.

- HASSLER, C. S. & TWISS, M. R. 2006. Bioavailability of iron sensed by a phytoplanktonic Fe-bioreporter. *Environmental science & technology*, 40, 2544-2551.
- HAWKINGS, J. R., BENNING, L. G., BAKER, A. R., KROM, M. D. & POULTON, S. W. 2016. Potentially bioavailable iron delivery by iceberg-hosted sediments and atmospheric dust to the polar oceans. *Biogeosciences*, 13, 3887.
- HODSON, A., NOWAK, A., SABACKA, M., JUNGBLUT, A., NAVARRO, F., PEARCE, D., ÁVILA-JIMÉNEZ, M. L., CONVEY, P. & VIEIRA, G. 2017. Climatically sensitive transfer of iron to maritime Antarctic ecosystems by surface runoff. *Nature communications*, 8, 1-7.
- HOFFMANN, L. J., BREITBARTH, E., BOYD, P. W. & HUNTER, K. A. 2012. Influence of ocean warming and acidification on trace metal biogeochemistry. *Marine Ecology Progress Series*, 470, 191-205.
- HOGLE, S. L., BARBEAU, K. A. & GLEDHILL, M. 2014. Heme in the marine environment: from cells to the iron cycle. *Metallomics*, 6, 1107-1120.
- HOLMES, T. M., WUTTIG, K., CHASE, Z., VAN DER MERWE, P., TOWNSEND, A. T., SCHALLENBERG, C., TONNARD, M. & BOWIE, A. R. 2019. Iron availability influences nutrient drawdown in the Heard and McDonald Islands region, Southern Ocean. *Marine Chemistry*, 211, 1-14.
- HUDSON, R. J., MOREL, F. M. & MOREL, F. 1990. Iron transport in marine phytoplankton: Kinetics of cellular and medium coordination reactions. *Limnol. Oceanogr*, 35, 1002-1020.
- HUNTER, K. A. & BOYD, P. W. 2007. Iron-binding ligands and their role in the ocean biogeochemistry of iron. *Environmental Chemistry*, 4, 221-232.
- HUTCHINS, D. A., DITULLIO, G. R. & BURLAND, K. W. 1993. Iron and regenerated production: Evidence for biological iron recycling in two marine environments. *Limnology and Oceanography*, 38, 1242-1255.
- HUTCHINS, D. A., FRANCK, V. M., BRZEZINSKI, M. A. & BRULAND, K. W. 1999a. Inducing phytoplankton iron limitation in iron-replete coastal waters with a strong chelating ligand. *Limnology and Oceanography*, 44, 1009-1018.
- HUTCHINS, D. A., WITTER, A. E., BUTLER, A. & LUTHER, G. W. 1999b. Competition among marine phytoplankton for different chelated iron species. *Nature*, 400, 858-861.
- IMRAN, M. & GURMANI, Z. A. 2011. Role of macro and micro nutrients in the plant growth and development. *Science Technology and Development (Pakistan)*.
- IPCC 2007. *Climate Change 2007: Working Group I: The Physical Science Basis*. Cambridge University Press Cambridge and New York.
- IPCC 2014. *IPCC, 2014: Climate change 2014: synthesis report. Contribution of Working Groups I, II and III to the fifth assessment report of the Intergovernmental Panel on Climate Change [Core Writing Team, R.K. Pachauri and L.A. Meyer (eds.)]. IPCC, Geneva, Switzerland, 151 pp., IPCC*.

- ITO, A., PERRON, M. M., PROEMSE, B. C., STRZELEC, M., GAULT-RINGOLD, M., BOYD, P. W. & BOWIE, A. R. 2020. Evaluation of aerosol iron solubility over Australian coastal regions based on inverse modeling: implications of bushfires on bioaccessible iron concentrations in the Southern Hemisphere. *Progress in Earth and Planetary Science*, 7, 1-17.
- JIAO, N., HERNDL, G. J., HANSELL, D. A., BENNER, R., KATTNER, G., WILHELM, S. W., KIRCHMAN, D. L., WEINBAUER, M. G., LUO, T., CHEN, F. & AZAM, F. 2010. Microbial production of recalcitrant dissolved organic matter: long-term carbon storage in the global ocean. *Nat Rev Micro*, 8, 593-599.
- JICKELLS, T., BAKER, A. & CHANCE, R. 2016. Atmospheric transport of trace elements and nutrients to the oceans. *Phil. Trans. R. Soc. A*, 374, 20150286.
- JICKELLS, T. D. & SPOKES, L. J. 2001. Atmospheric iron inputs to the oceans.
- JOHNSON, K. S., CHAVEZ, F. P. & FRIEDERICH, G. E. 1999. Continental-shelf sediment as a primary source of iron for coastal phytoplankton. *Nature*, 398, 697.
- JOHNSON, K. S., COALE, K. H., ELROD, V. A. & TINDALE, N. W. 1994. Iron photochemistry in seawater from the equatorial Pacific. *Marine Chemistry*, 46, 319-334.
- JOHNSON, K. S., GORDON, R. M. & COALE, K. H. 1997. What controls dissolved iron concentrations in the world ocean? *Marine Chemistry*, 57, 137-161.
- KEELING, R. F., KÖRTZINGER, A. & GRUBER, N. 2010. Ocean deoxygenation in a warming world. *Annual review of marine science*, 2, 199-229.
- KÖNIG, I., HAECKEL, M., DRODT, M., SUESS, E. & TRAUTWEIN, A. X. 1999. Reactive Fe (II) layers in deep-sea sediments. *Geochimica et Cosmochimica Acta*, 63, 1517-1526.
- KUCERA, M. & MALMGREN, B. A. 1998. Terminal Cretaceous warming event in the mid-latitude South Atlantic Ocean: evidence from poleward migration of *Contusotruncana contusa* (planktonic foraminifera) morphotypes. *Palaeogeography, Palaeoclimatology, Palaeoecology*, 138, 1-15.
- KUFFNER, I. B. & PAUL, V. J. 2001. Effects of nitrate, phosphate and iron on the growth of macroalgae and benthic cyanobacteria from Cocos Lagoon, Guam. *Marine Ecology Progress Series*, 222, 63-72.
- LANGMANN, B., ZAKŠEK, K., HORT, M. & DUGGEN, S. 2010. Volcanic ash as fertiliser for the surface ocean. *Atmospheric Chemistry and Physics*, 10, 3891-3899.
- LANNUZEL, D., BOWIE, A. R., REMENYI, T., LAM, P., TOWNSEND, A., IBISANMI, E., BUTLER, E., WAGENER, T. & SCHOEMANN, V. 2011. Distributions of dissolved and particulate iron in the sub-Antarctic and Polar Frontal Southern Ocean (Australian sector). *Deep Sea Research Part II: Topical Studies in Oceanography*, 58, 2094-2112.
- LANNUZEL, D., SCHOEMANN, V., DE JONG, J., TISON, J.-L. & CHOU, L. 2007. Distribution and biogeochemical behaviour of iron in the East Antarctic sea ice. *Marine Chemistry*, 106, 18-32.

-
- LAWS, E. A., FALKOWSKI, P. G., SMITH, W. O., DUCKLOW, H. & MCCARTHY, J. J. 2000. Temperature effects on export production in the open ocean. *Global Biogeochemical Cycles*, 14, 1231-1246.
- LEGENDRE, L., RIVKIN, R. B., WEINBAUER, M. G., GUIDI, L., & UITZ, J. (2015). The microbial carbon pump concept: Potential biogeochemical significance in the globally changing ocean. *Progress in Oceanography*, 134, 432-450.
- LEVITUS, S., ANTONOV, J. I., BOYER, T. P. & STEPHENS, C. 2000. Warming of the World Ocean. *Science*, 287, 2225-2229.
- LINDSAY, W. & SCHWAB, A. 1982. The chemistry of iron in soils and its availability to plants. *Journal of Plant Nutrition*, 5, 821-840.
- LIU, X. & MILLERO, F. J. 2002. The solubility of iron in seawater. *Marine Chemistry*, 77, 43-54.
- LOHAN, M.C. & TAGLIABUE, A., 2018. Oceanic micronutrients: Trace metals that are essential for marine life. *Elements: An International Magazine of Mineralogy, Geochemistry, and Petrology*, 14(6), pp.385-390.
- LUXEM, K. E., ELLWOOD, M. J. & STRZEPEK, R. F. 2017. Intraspecific variability in *Phaeocystis antarctica*'s response to iron and light stress. *PloS one*, 12, e0179751.
- MALDONADO, M. T., BOYD, P. W., LAROCHE, J., STRZEPEK, R., WAITE, A., BOWIE, A. R., CROOT, P. L., FREW, R. D. & PRICE, N. M. 2001. Iron uptake and physiological response of phytoplankton during a mesoscale Southern Ocean iron enrichment. *Limnology and oceanography*, 46, 1802-1808.
- MALDONADO, M. T. & PRICE, N. M. 2000. Nitrate regulation of Fe reduction and transport by Fe-limited *Thalassiosira oceanica*. *Limnology and Oceanography*, 45, 814-826.
- MALDONADO, M. T. & PRICE, N. M. 2001. Reduction and transport of organically bound iron by *Thalassiosira oceanica* (Bacillariophyceae). *Journal of Phycology*, 37, 298-310.
- MALDONADO, M. T., STRZEPEK, R. F., SANDER, S. & BOYD, P. W. 2005. Acquisition of iron bound to strong organic complexes, with different Fe binding groups and photochemical reactivities, by plankton communities in Fe-limited subantarctic waters. *Global Biogeochemical Cycles*, 19.
- MALDONADO, M. T., SURMA, S. & PAKHOMOV, E. A. 2016. Southern Ocean biological iron cycling in the pre-whaling and present ecosystems. *Phil. Trans. R. Soc. A*, 374, 20150292.
- MARSCHNER, H., RÖMHELD, V. & KISSEL, M. 1986. Different strategies in higher plants in mobilization and uptake of iron. *Journal of Plant Nutrition*, 9, 695-713.
- MARTIN, J. H. 1990. Glacial-interglacial CO₂ change: The iron hypothesis. *Paleoceanography*, 5, 1-13.
- MARTIN, J. H. & FITZWATER, S. 1988. Iron deficiency limits phytoplankton growth in the north-east Pacific subarctic. *Nature*, 331, 947-975.

- MARTIN, J. H., GORDON, R. M. & FITZWATER, S. E. 1990. Iron in Antarctic Waters. *Nature*, 345, 156-158.
- MIES, K. A., WIRGAU, J. I. & CRUMBLISS, A. L. 2006. Ternary complex formation facilitates a redox mechanism for iron release from a siderophore. *Biometals*, 19, 115-126.
- MILLER, W. L., KING, D. W., LIN, J. & KESTER, D. R. 1995. Photochemical redox cycling of iron in coastal seawater. *Marine Chemistry*, 50, 63-77.
- MILLERO, F. J. 1996. *Chemical Oceanography, Second Edition*, Taylor & Francis.
- MILLERO, F. J. & SOTOLONGO, S. 1989. The oxidation of Fe (II) with H₂O₂ in seawater. *Geochimica et Cosmochimica Acta*, 53, 1867-1873.
- MILLERO, F. J., SOTOLONGO, S. & IZAGUIRRE, M. 1987. The oxidation kinetics of Fe(II) in seawater. *Geochimica et Cosmochimica Acta*, 51, 793-801.
- MILLERO, F. J., WOOSLEY, R., DITROLIO, B. & WATERS, J. 2009. Effect of Ocean Acidification on the Speciation of Metals in Seawater. *Oceanography*, 22, 72-85.
- MILLERO, F. J., YAO, W. & AICHER, J. 1995. The speciation of Fe (II) and Fe (III) in natural waters. *Marine Chemistry*, 50, 21-39.
- MOORE, C., MILLS, M., ARRIGO, K., BERMAN-FRANK, I., BOPP, L., BOYD, P., GALBRAITH, E., GEIDER, R., GUIEU, C. & JACCARD, S. 2013. Processes and patterns of oceanic nutrient limitation. *Nature geoscience*, 6, 701.
- MOORE, J. K., DONEY, S. C., GLOVER, D. M. & FUNG, I. Y. 2001. Iron cycling and nutrient-limitation patterns in surface waters of the World Ocean. *Deep Sea Research Part II: Topical Studies in Oceanography*, 49, 463-507.
- MOREL, F. M. M., KUSTKA, A. B. & SHAKED, Y. 2008. The role of unchelated Fe in the iron nutrition of phytoplankton. *Limnology and Oceanography*, 53, 400-404.
- PLANAVSKY, N. J., MCGOLDRICK, P., SCOTT, C. T., LI, C., REINHARD, C. T., KELLY, A. E., CHU, X., BEKKER, A., LOVE, G. D., & LYONS, T. W. (2011). Widespread iron-rich conditions in the mid-Proterozoic ocean. *Nature*, 477(7365), 448-451.
- OKIN, G. S., BAKER, A. R., TEGEN, I., MAHOWALD, N. M., DENTENER, F. J., DUCE, R. A., GALLOWAY, J. N., HUNTER, K., KANAKIDOU, M. & KUBILAY, N. 2011. Impacts of atmospheric nutrient deposition on marine productivity: Roles of nitrogen, phosphorus, and iron. *Global Biogeochemical Cycles*, 25.
- ORR, J. C., FABRY, V. J., AUMONT, O., BOPP, L., DONEY, S. C., FEELY, R. A., GNANADESIKAN, A., GRUBER, N., ISHIDA, A., JOOS, F., KEY, R. M., LINDSAY, K., MAIER-REIMER, E., MATEAR, R., MONFRAY, P., MOUCHET, A., NAJJAR, R. G., PLATTNER, G. K., RODGERS, K. B., SABINE, C. L., SARMIENTO, J. L., SCHLITZER, R., SLATER, R. D., TOTTERDELL, I. J., WEIRIG, M. F., YAMANAKA, Y. & YOOL, A. 2005. Anthropogenic ocean acidification over the twenty-first century and its impact on calcifying organisms. *Nature*, 437, 681-686.

- PASSOW, U. & CARLSON, C. A. 2012. The biological pump in a high CO₂ world. *Marine Ecology Progress Series*, 470, 249-271.
- PEEKEN, I., HOFFMANN, L., ASSMY, P., BATHMANN, U., CROOT, P., VON HARBOU, L., HENJES, J., JANSEN, S., KRÄGEFSKY, S. & LOCHTE, K. Effect of in situ iron fertilisation during contrasting seasons comparison between EisenEx and EIFEX. 2006.
- PERRON, M. M., PROEMSE, B. C., STRZELEC, M., GAULT-RINGOLD, M., BOYD, P. W., RODRIGUEZ, E. S., PAULL, B. & BOWIE, A. R. 2020. Origin, transport and deposition of aerosol iron to Australian coastal waters. *Atmospheric Environment*, 117432.
- PETROU, K., KRANZ, S. A., TRIMBORN, S., HASSLER, C. S., AMEIJERAS, S. B., SACKETT, O., RALPH, P. J. & DAVIDSON, A. T. 2016. Southern Ocean phytoplankton physiology in a changing climate. *Journal of plant physiology*, 203, 135-150.
- PÖRTNER, H.-O., ROBERTS, D., MASSON-DELMOTTE, V., ZHAI, P., POLOCZANSKA, E., MINTENBECK, K., TIGNOR, M., ALEGRÍA, A., NICOLAI, M. & OKEM, A. 2019. IPCC, 2019: Technical Summary. *IPCC Special Report on the Ocean and Cryosphere in a Changing Climate*.
- PORTNER, H. O. 2008. Ecosystem effects of ocean acidification in times of ocean warming: a physiologist's view. *Marine Ecology Progress Series*, 373, 203-217.
- POWLES, S. B. 1984. Photoinhibition of photosynthesis induced by visible light. *Annual Review of Plant Physiology*, 35, 15-44.
- PRICE, N. M. & MOREL, F. M. 1998. Biological cycling of iron in the ocean. *Metal ions in biological systems*, 35, 1-36.
- RAISWELL, R. & CANFIELD, D. E. 2012. The iron biogeochemical cycle past and present. *Geochemical perspectives*, 1, 1-2.
- RAVEN, J., CALDEIRA, K., ELDERFIELD, H., HOEGH-GULDBERG, O., LISS, P., RIEBESELL, U., SHEPHERD, J., TURLEY, C. & WATSON, A. 2005. *Ocean acidification due to increasing atmospheric carbon dioxide*, The Royal Society.
- RAVEN, J. A., EVANS, M. C. & KORB, R. E. 1999. The role of trace metals in photosynthetic electron transport in O₂-evolving organisms. *Photosynthesis research*, 60, 111-150.
- RAVEN, J. A. & FALKOWSKI, P. G. 1999. Oceanic sinks for atmospheric CO₂. *Plant, Cell & Environment*, 22, 741-755.
- RICH, H. W. & MOREL, F. M. 1990. Availability of well-defined iron colloids to the marine diatom *Thalassiosira weissflogii*. *Limnology and Oceanography*, 35, 652-662.
- RIEBESELL, U., SCHULZ, K. G., BELLERBY, R., BOTROS, M., FRITSCH, P., MEYERHÖFER, M., NEILL, C., NONDAL, G., OSCHLIES, A. & WOHLERS, J. 2007. Enhanced biological carbon consumption in a high CO₂ ocean. *Nature*, 450, 545.
- RIEBESELL, U., ZONDERVAN, I., ROST, B., TORTELL, P. D., ZEEBE, R. E. & MOREL, F. M. 2000. Reduced calcification of marine plankton in response to increased atmospheric CO₂. *Nature*, 407, 364-367.

- RIES, J. B., COHEN, A. L. & MCCORKLE, D. C. 2009. Marine calcifiers exhibit mixed responses to CO₂-induced ocean acidification. *Geology*, 37, 1131-1134.
- RIGNOT, E., VELICOGNA, I., VAN DEN BROEKE, M. R., MONAGHAN, A. & LENAERTS, J. T. 2011. Acceleration of the contribution of the Greenland and Antarctic ice sheets to sea level rise. *Geophysical Research Letters*, 38.
- RIJKENBERG, M. J., GERRINGA, L. J., TIMMERMANS, K. R., FISCHER, A. C., KROON, K. J., BUMA, A. G., WOLTERBEEK, B. T. & DE BAAR, H. J. 2008. Enhancement of the reactive iron pool by marine diatoms. *Marine Chemistry*, 109, 29-44.
- RIJKENBERG, M. J. A., FISCHER, A. C., KROON, J., GERRINGA, L., TIMMERMANS, K., WOLTERBEEK, H. T. & DE BAAR, H. 2005. The influence of UV irradiation on the photoreduction of iron in the Southern Ocean. *Marine Chemistry*, 93, 119-129.
- RÖMHELD, V. & MARSCHNER, H. 1991. Function of micronutrients in plants. *Micronutrients in agriculture*, 297-328.
- ROST, B. & RIEBESELL, U. 2004. Coccolithophores and the biological pump: responses to environmental changes. In: THIERSTEIN, H. R. & YOUNG, J. R. (eds.) *Coccolithophores: From Molecular Processes to Global Impact*. Berlin, Heidelberg: Springer Berlin Heidelberg.
- SABINE, C. L. & FEELY, R. A. 2007. 3 The Oceanic Sink for Carbon Dioxide. *Greenhouse Gas Sinks*, 31.
- SANTANA-CASIANO, J. M., GONZÁLEZ-DÁVILA, M. & MILLERO, F. J. 2005. Oxidation of nanomolar levels of Fe (II) with oxygen in natural waters. *Environmental science & technology*, 39, 2073-2079.
- SARMIENTO, J. L. 2013. *Ocean biogeochemical dynamics*, Princeton university press.
- SARMIENTO, J. L., HUGHES, T. M., STOUFFER, R. J. & MANABE, S. 1998. Simulated response of the ocean carbon cycle to anthropogenic climate warming. *Nature*, 393, 245.
- SCHALLENBERG, C., BESTLEY, S., KLOCKER, A., TRULL, T. W., DAVIES, D. M., GAULT-RINGOLD, M., ERIKSEN, R., RODEN, N. P., SANDER, S. G. & SUMNER, M. 2018. Sustained upwelling of subsurface iron supplies seasonally persistent phytoplankton blooms around the southern Kerguelen plateau, Southern Ocean. *Journal of Geophysical Research: Oceans*, 123, 5986-6003.
- SCHALLENBERG, C., VAN DER MERWE, P., CHEVER, F., CULLEN, J. T., LANNUZEL, D. & BOWIE, A. R. 2016. Dissolved iron and iron (II) distributions beneath the pack ice in the East Antarctic (120 E) during the winter/spring transition. *Deep Sea Research Part II: Topical Studies in Oceanography*, 131, 96-110.
- SCHEER, H. 1991. Structure and occurrence of chlorophylls.
- SEDWICK, P. N. & DITULLIO, G. R. 1997. Regulation of algal blooms in Antarctic shelf waters by the release of iron from melting sea ice. *Geophysical Research Letters*, 24, 2515-2518.
- SHAKED, Y. & LIS, H. 2012. Disassembling iron availability to phytoplankton. *Frontiers in microbiology*, 3.

- SHI, D., XU, Y., HOPKINSON, B. M. & MOREL, F. M. M. 2010. Effect of Ocean Acidification on Iron Availability to Marine Phytoplankton. *Science*, 327, 676-679.
- SMITH, R., PREZELIN, B., BAKER, K., BIDIGARE, R., BOUCHER, N., COLEY, T., KARENTZ, D., MACINTYRE, S., MATLICK, H. & MENZIES, D. 1992. Ozone depletion-Ultraviolet radiation and phytoplankton biology in Antarctic waters.
- SOMMER, U. & LEWANDOWSKA, A. 2011. Climate change and the phytoplankton spring bloom: warming and overwintering zooplankton have similar effects on phytoplankton. *Global Change Biology*, 17, 154-162.
- STEELE, M., ERMOLD, W. & ZHANG, J. 2008. Arctic Ocean surface warming trends over the past 100 years. *Geophysical Research Letters*, 35.
- STRZELEC, M., PROEMSE, B. C., GAULT-RINGOLD, M., BOYD, P. W., PERRON, M. M., SCHOFIELD, R., RYAN, R. G., RISTOVSKI, Z. D., ALROE, J. & HUMPHRIES, R. S. 2020. Atmospheric trace metal deposition near the Great Barrier Reef, Australia. *Atmosphere*, 11, 390.
- STRZEPEK, R. F., BOYD, P. W. & SUNDA, W. G. 2019. Photosynthetic adaptation to low iron, light, and temperature in Southern Ocean phytoplankton. *Proceedings of the National Academy of Sciences*, 201810886.
- STRZEPEK, R. F., MALDONADO, M. T., HUNTER, K. A., FREW, R. D. & BOYD, P. W. 2011. Adaptive strategies by Southern Ocean phytoplankton to lessen iron limitation: Uptake of organically complexed iron and reduced cellular iron requirements. *Limnology and Oceanography*, 56, 1983-2002.
- SUNDA, W. G. & HUNTSMAN, S. A. 1995. Iron Uptake and Growth Limitation in Oceanic and Coastal Phytoplankton. *Marine Chemistry*, 50, 189-206.
- SUNDA, W. G. & HUNTSMAN, S. A. 1997. Interrelated influence of iron, light and cell size on marine phytoplankton growth. *Nature*, 390, 389-392.
- TAGLIABUE, A., BOWIE, A. R., BOYD, P. W., BUCK, K. N., JOHNSON, K. S. & SAITO, M. A. 2017. The integral role of iron in ocean biogeochemistry. *Nature*, 543, 51-59.
- TAKAHASHI, T., SUTHERLAND, S. C., SWEENEY, C., POISSON, A., METZL, N., TILBROOK, B., BATES, N., WANNINKHOF, R., FEELY, R. A. & SABINE, C. 2002. Global sea-air CO₂ flux based on climatological surface ocean pCO₂, and seasonal biological and temperature effects. *Deep Sea Research Part II: Topical Studies in Oceanography*, 49, 1601-1622.
- TAUCHER, J., JONES, J., JAMES, A., BRZEZINSKI, M. A., CARLSON, C. A., RIEBESELL, U. & PASSOW, U. 2015. Combined effects of CO₂ and temperature on carbon uptake and partitioning by the marine diatoms *Thalassiosira weissflogii* and *Dactyliosolen fragilissimus*. *Limnology and Oceanography*, 60, 901-919.
- THURÓCZY, C.-E., ALDERKAMP, A.-C., LAAN, P., GERRINGA, L. J. A., MILLS, M. M., VAN DIJKEN, G. L., DE BAAR, H. J. W. & ARRIGO, K. R. 2012. Key role of organic complexation of iron in sustaining phytoplankton blooms in the Pine Island and Amundsen Polynyas (Southern Ocean). *Deep Sea Research Part II: Topical Studies in Oceanography*, 71-76, 49-60.

- TIMMERMANN, A., OBERHUBER, J., BACHER, A., ESCH, M., LATIF, M. & ROECKNER, E. 1999. Increased El Niño frequency in a climate model forced by future greenhouse warming. *Nature*, 398, 694-697.
- TOGGWEILER, J. R. & RUSSELL, J. 2008. Ocean circulation in a warming climate. *Nature*, 451, 286-288.
- TRÉGUER, P. & JACQUES, G. 1992. Review Dynamics of nutrients and phytoplankton, and fluxes of carbon, nitrogen and silicon in the Antarctic Ocean. *Weddell Sea Ecology*. Springer.
- TRICK, C. G., ANDERSEN, R. J., GILLAM, A. & HARRISON, P. J. 1983. Prorocentrin: an extracellular siderophore produced by the marine dinoflagellate *Prorocentrum minimum*. *Science*, 219, 306-308.
- TURNER, D. R. & HUNTER, K. A. 2001. *The biogeochemistry of iron in seawater*, Wiley Chichester.
- UCHIDA, R. 2000. Essential nutrients for plant growth: nutrient functions and deficiency symptoms. *Plant nutrient management in Hawaii's soils*, 31-55.
- USSHER, S. J., ACHTERBERG, E. P. & WORSFOLD, P. J. 2004. Marine biogeochemistry of iron. *Environmental Chemistry*, 1, 67-80.
- VAN DE WAAL, D. B. & LITCHMAN, E. 2020. Multiple global change stressor effects on phytoplankton nutrient acquisition in a future ocean. *Philosophical Transactions of the Royal Society B*, 375, 20190706.
- VAN DER MERWE, P. C., WUTTIG, K., HOLMES, T., TRULL, T., CHASE, Z., TOWNSEND, A., GOEMANN, K. & BOWIE, A. R. 2019. High lability Fe particles sourced from glacial erosion can meet previously unaccounted biological demand: Heard Island, Southern Ocean. *Frontiers in Marine Science*, 6, 332.
- VILCHIS, L. I., TEGNER, M. J., MOORE, J. D., FRIEDMAN, C. S., RISER, K. L., ROBBINS, T. T. & DAYTON, P. K. 2005. Ocean warming effects on growth, reproduction, and survivorship of southern California abalone. *Ecological Applications*, 15, 469-480.
- VOLK, T. & HOFFERT, M. I. 2013. Ocean Carbon Pumps: Analysis of Relative Strengths and Efficiencies in Ocean-Driven Atmospheric CO₂ Changes. *The Carbon Cycle and Atmospheric CO₂: Natural Variations Archean to Present*. American Geophysical Union.
- VÖLKER, C. & WOLF-GLADROW, D. A. 1999. Physical limits on iron uptake mediated by siderophores or surface reductases. *Marine Chemistry*, 65, 227-244.
- WATSON, A. J. & LISS, P. S. 1998. Marine biological controls on climate via the carbon and sulphur geochemical cycles. *Philosophical Transactions of the Royal Society of London B: Biological Sciences*, 353, 41-51.
- WHEELER, P. A. 1983. Phytoplankton nitrogen metabolism. *Nitrogen in the marine environment*, 9, 309-346.

-
- WILHELM, S. W. 1995. Ecology of iron-limited cyanobacteria: a review of physiological responses and implications for aquatic systems. *Aquatic Microbial Ecology*, 9, 295-303.
- WINTERBOURN, C. C. 1995. Toxicity of iron and hydrogen peroxide: the Fenton reaction. *Toxicology letters*, 82, 969-974.
- YEALA, S., B., K. A. & M., M. F. M. 2005. A general kinetic model for iron acquisition by eukaryotic phytoplankton. *Limnology and Oceanography*, 50, 872-882.
- ZEEBE, R. E. & WOLF-GLADROW, D. A. 2001. *CO₂ in seawater: equilibrium, kinetics, isotopes*, Amsterdam ; New York : Elsevier, 2001.

Chapter 2: Dissolved iron(II) oxidation in coastal and open ocean waters under future scenarios

Helene Aflenzer^{a,b,c}, Kathrin Wuttig^a, Andrew Bowie^{a,b}

Affiliations

^a Antarctic Climate and Ecosystems Cooperative Research Centre (ACE CRC), University of Tasmania, Private Bag 80, Hobart, Tasmania 7001, Australia

^b Institute for Marine and Antarctic Studies (IMAS), University of Tasmania, Private Bag 129, Hobart, Tasmania, Australia

^c Australian Research Council Gateway Partnership, University of Tasmania, Private Bag 80, Hobart, Tasmania 7001, Australia

Abstract

The Southern Ocean is essential for marine biogeochemical cycles and global air-sea carbon dioxide fluxes. While this region is rich in nitrogen and phosphorus, primary production is often limited by iron (Fe) which is vital for various cell functions. Of the two redox species of dissolved (d) Fe available for phytoplankton uptake [dFe(II) and dFe(III)], dFe(III) is thermodynamically favoured in oxygenated oceans. Dissolved Fe(II), on the other hand, is more accessible to phytoplankton. Yet, the oxidation rate of dFe(II), and thus its half-life, is dependent on several parameters such as pH and temperature. Therefore, ocean acidification and global warming will modify half-life times dramatically in the future oceans. A projected increase in the sea surface temperature by 1°C promotes the oxidation of dFe(II), shortening its half-life, whereas a shift from pH 8.1 to 7.9 extends its half-life. This study presents data obtained during laboratory-controlled experiments observing the oxidation of dFe(II).

Further examinations were done for differing light regimes and differences in filtered vs. unfiltered samples. For the parameters of interest (temperature and pH), the results demonstrate an extended half-life of dFe(II) in future ocean scenarios under acidified conditions and a varying half-life time when exposed to three different temperatures (5°C, 10°C, 15°C), which were chosen to facilitate observations during the experiment. Using this experimental procedure in combination with modelled oxidation rates, we show that the dFe(II) half-life is shortened by an increase in temperature by just 1°C and extended by a pH decrease of 0.2 units in coastal and oligotrophic Southern Ocean waters, with an overall net increase in dFe(II) half-life due to the pH decrease. The results further revealed that acidification and an increase in temperature will be crucial for the availability of dFe(II) to phytoplankton and thus for ocean productivity.

Keywords: dFe(II), ocean acidification, temperature increase, Southern Ocean

2.1 Introduction

The Southern Ocean (SO) is defined by high nutrient concentrations combined with low chlorophyll contents, also called a High Nutrient – Low Chlorophyll (HNLC) area. This has the result that there is low phytoplankton abundance, despite sufficient macronutrient supply linked to scarce amounts of iron (Fe) (Martin et al., 1994, Boyd et al., 2000). Phytoplankton is crucial as it forms the base of the food chain and plays a leading role in carbon (C) sequestration by converting carbon dioxide (CO_2) into organic biomass through photosynthesis (Riebesell et al., 1993), followed by exporting it to the deep ocean floor (Ducklow et al., 2001, Schlitzer, 2002, Smetacek et al., 2012). One known factor limiting primary production in the open SO is the lack of Fe (Martin, 1990). This essential element is used during photosynthesis, respiration, and nitrogen-fixing processes by phytoplankton (Geider and La Roche, 1994). Major sources of Fe in the SO (**Figure 2.1**) are atmospheric deposition, continental runoff, shelf sediments, hydrothermal vents, and cryospheric sources closer to polar regions (de Baar and de Jong, 2001, Blain and Tagliabue, 2016). Oceanic Fe concentrations are usually lower at the surface due to phytoplankton uptake, which contributes to the Fe sink. Low Fe concentrations are especially found in remote areas of the SO ($< 0.3 \text{ nM}$).

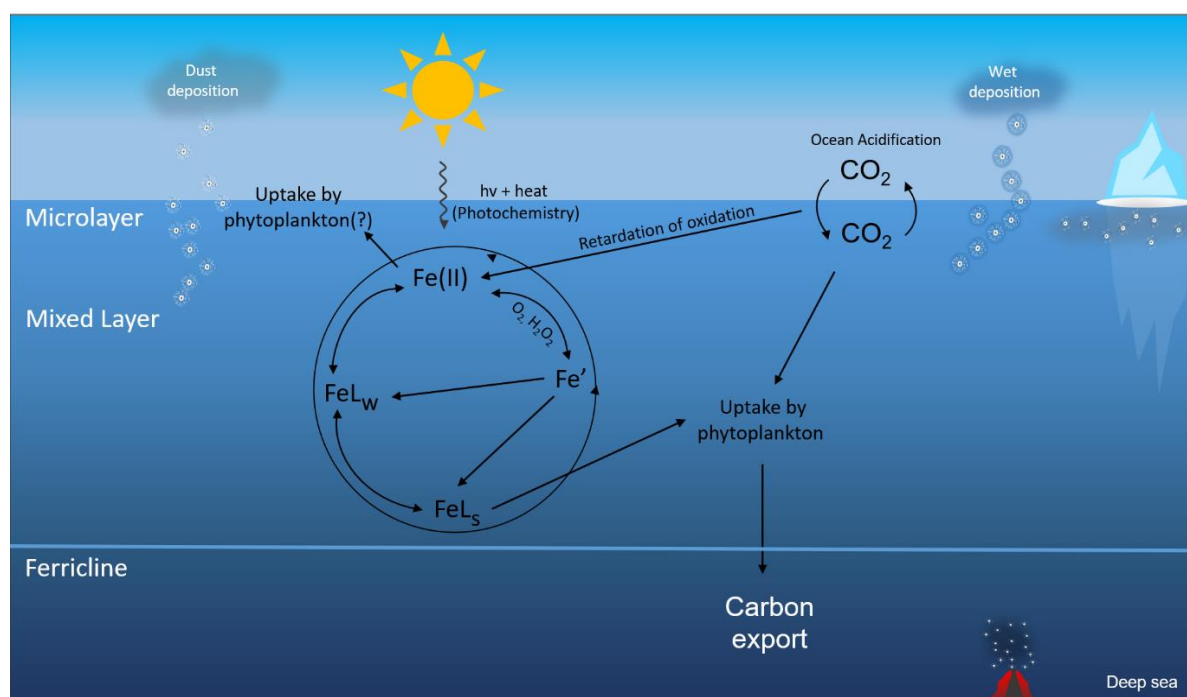


Figure 2.1 Schematic of processes in the cycling of surface dissolved Fe. Abbreviations: FeL_s , Fe complexed by strong ligand; FeL_w , Fe complexed by weak ligand; dFe(II) , sum of all dFe(II) species; Fe' , sum of all inorganic dFe(III) species; $h\nu$ (photon flux); O_2 , CO_2 and H_2O_2 . Schematic modified for the SO after Croot and Heller (2012).

Oceanic Fe chemistry has been of interest for the scientific community for the past 40 years for many reasons, with the major reason being that Fe could potentially be used to fertilise the ocean, promoting phytoplankton growth and thus absorbing CO₂ from the atmosphere (e.g. Landry et al., 2000, Boyd et al., 2000, Blain et al., 2007). Another aspect that started to emerge is the idea that in areas of low Fe concentrations, multiple forms of Fe could be important for phytoplankton, depending on the Fe sources, fractionation and particle size, redox state and complexation (Hutchins et al., 1999, van der Merwe et al., 2019). In this study, the focus was on the thermodynamically stable dissolved Fe (III) [dFe(III)] and its reduced partner dissolved (d) Fe(II). This redox couple is relevant because phytoplankton can use both through differing uptake mechanisms (Lis et al., 2015). Another advantage is that both can be analysed by highly developed, inexpensive methods (e.g. Bowie et al., 1998, King et al., 1995, Hansard and Landing, 2009, Stookey, 1970).

Dissolved Fe(III) is most often found in a complexed form. At the same time, dFe(II) is thought to be more easily accessible for phytoplankton as it is unbound and therefore freely available (Strzepek et al., 2011, Lis et al., 2015). However, dFe(II) is a reactive species under current natural oceanic conditions (e.g. pH 8.1, oxic) and therefore oxidised back to dFe(III) rapidly within minutes to hours (Millero et al., 1987) above the oxygenated ferricline. This oxidative process is strongly affected by several parameters of chemical, physical or biological origin (**Figure 2.1**).

First, the overall concentration of Fe(III) within seawater impacts the concentration and oxidation of dFe(II). This means if there is substantial Fe present to begin with (e.g., above 1 nM), the redox process can be retarded (Roy and Wells, 2011, Santana-González et al., 2018). Secondly, light and specifically ultraviolet (UV) light increases the reactivity of Fe, thus photoreduces Fe(III) in the surface and thus decreases the oxidation time (Johnson et al., 1994). As a third parameter, an increased concentration of hydrogen peroxide (H₂O₂) together with oxygen (O₂) has been proven to decrease the half-life time ($t_{1/2}$) of dFe(II) immensely (Haber and Weiss, 1932, Emmenegger et al., 2001). Additionally, it has been shown that ligands, nutrients and chromophoric dissolved material (CDOM) with interlinked biotic activity in the upper photic zones alter the speciation of freely available Fe (Fe') (Roy and Wells, 2011, Gonzalez et al., 2010, Kuma and Matsunaga, 1995). While these parameters are of natural

origin, anthropogenic perturbations such as ocean acidification (OA) and ocean warming are becoming more significant in respect to dFe(II) oxidation.

Ocean acidification is defined by a decrease in pH in the ocean due to CO₂ uptake from fossil fuel burning (Doney et al., 2009). This excess CO₂ is emitted into the atmosphere, which dissolves into the ocean, leading to a lower pH in the seawater, making it more acidic. While OA is often linked to calcifying organisms, it is rarely thought to affect the nutrient compositions in the ocean. In the case of dFe(II), it has been shown in laboratory experiments to have a $t_{1/2}$ of only a few minutes at its current pH of ~8.1 (Millero et al., 1987). A modelled decline of pH by 0.77 until the year 2300 in surface ocean water as suggested by Caldeira and Wickett (2003), could increase the persistence of dFe(II). An extension of the $t_{1/2}$ could mean that phytoplankton species preferring dFe(II) are in favour of a decreased pH, while others might be disadvantaged (Breitbarth et al., 2010a). Dissolved Fe(III) on the other hand, occurs in greater concentrations in seawater than dFe(II) due to its thermodynamical stability (Millero, 1998). Regarding OA, a decreased pH means that dFe(III) stays in solution and is less complexed in an acidic matrix (Millero et al., 1995). Both OA-linked processes suggest higher Fe availability, promoting microbiological productivity. Temperature, however, is also often a key driver for physiological processes (Pörtner, 2002). Therefore, a suggested increase in the seawater surface temperature of 1.5 to 2°C by 2100 (IPCC, 2014, Bindoff et al., 2019) could accelerate the oxidation of dFe(II) but as a result have negative effects for microbiological growth (Samperio-Ramos et al., 2016).

It is not yet fully understood whether OA or ocean warming will have a more significant impact on the $t_{1/2}$ of dFe(II) in the ocean and to which extent this impacts availability to phytoplankton. Understanding the impact of the coupled processes OA and ocean warming on the Fe redox cycle is crucial for interpreting how ecological processes will impact future coastal and open oceans. Coastal oceans tend to be rich in microbiological activity due to high nutrient and trace-metal concentrations, while the open SO covers a larger area but is scarce in phytoplankton due to Fe limitations. Therefore, both settings must be considered in assessing OA and warming impacts on microbes and the dFe(II) oxidation.

Since there will likely be lower pH and higher temperatures in the future, in this study I explored two different matrices from coastal and open ocean regarding the dFe(II) oxidation behaviour with implications for future climate scenarios. I used a modified direct flow injection analysis

(FIA) technique within a custom-made tank setup for temperature and CO₂ control to address the current and future dFe(II) oxidation scenarios. I further addressed impacts on dFe(II) oxidations by considering macronutrients, ligands, trace metals and CDOM together with UV-light-dark and filtered and unfiltered treatments for open and coastal water.

My first hypothesis (1) was that a potentially Fe-limited water matrix from the open SO would have short oxidation times of dFe(II) due to less impact by parameters potentially extending it (e.g. ligands, CDOM, macronutrients (Gonzalez et al., 2010, Millero et al., 1987)). In contrast, nutrient-rich coastal water would have increased the oxidation times. My second objective (2) was to observe and determine the influence of combined temperature and pH on dFe(II) oxidation. Thirdly (3), I addressed several other parameters for dFe(II) oxidations in open and coastal water oxidations such as CDOM, ligands and other trace metals. Last but not least (4), I employed calculations after Millero et al. (1987) and Santana-González et al. (2018) to compare the theoretical findings with the laboratory observations and look for ways to improve models.

2.2 Material and Methods

2.2.1 Cleaning and sample handling

All bottles (low density polyethylene (LDPE), Nalgene), carboys (high density polyethylene (HDPE), Nalgene) and other materials were initially cleaned in a 2 % Decon bath for two days and acid cleaned in 6 M hydrochloric acid (HCl; in-house distilled acid using a Savillex perfluoroalkoxy-polymer still, DST-1000) for one week, followed by thorough rinses with ultra-pure water (UPW, Barnstead, 18.2 M Ω). Each bottle was preconditioned by double rinsing with the seawater also used for the experiments. The sample seawater was filled into the bottles gravimetrically. Filtered (0.2 μ m) macronutrient samples were sampled into 15 mL (polypropylene) vials before the experiments and frozen at -80°C immediately. Similarly, samples for the analysis of dFe(III) were taken at the beginning of the experiment (additionally acid cleaned in 1 M HCl for one month 10 mL polycarbonate (PC) vials, 0.2 μ m filtered, following the GEOTRACES sampling protocol from Cutter et al. (2017)) and acidified to pH 1.8 directly, using ultrapure HCl (Baseline, Seastar). To reduce airborne contamination, all experimental work was carried out under a ISO class-5 laminar flow bench. All reagents were prepared under an ISO class-5 laminar flow hood (LMFH) in an ISO class-6 clean air laboratory. All chemicals were of trace metal grade unless stated otherwise.

2.2.2 Seawater collection

Two pre-cleaned 25 L carboys (Nalgene) were manually filled with coastal surface water from the east coast of Tasmania (Kingston Beach, 42° 98'S, 147° 32'E), collected from the jetty directly in February 2017 and 0.2 μm filtered (Acropak, Pall) under clean conditions and is further referred to as 'coastal seawater'. Two 25 L carboys of 0.2 μm filtered surface seawater were collected in 2016 on *RV Investigator* during the GEOTRACES Process study ('HEOBI – Heard Earth-Ocean Biosphere Interactions'), using a trace metal rosette at an open-ocean reference station, approximately 100 km to the south of Heard Island and off the Kerguelen plateau (van der Merwe et al., 2019, Holmes et al., 2020) in HNLC waters (54° 10'S, 73° 40'E) between 48 and 83 m depths, referred to hereafter as 'open ocean water'. Both water types were stored in the dark at 4°C for at least one month before use.

2.2.3 Analysis of dFe(II)

Dissolved Fe(II) stock and standard solutions

Dissolved Fe(II) stock solutions were prepared monthly in UPW using ferrous ammonium Fe(II) sulphate hexahydrate (Sigma-Aldrich) in 0.1 M HCl (Seastar, Baseline). An intermediate 50 μM dFe(II) standard was prepared monthly from this stock in 0.05 M HCl (Seastar, Baseline). Working solutions of 1 μM and 100 nM were prepared daily via serial dilution from this intermediate stock in UPW. All dFe(II) stock solutions contained sodium sulphite (Na_2SO_3 , 0.01 mM final conc.) as a reducing agent and were kept in the fridge in the dark when not in use.

Luminol

A 0.75 mM luminol (Sigma) solution was prepared in large batches of 2 L (HDPE, opaque, Nalgene), containing 3.2 mM sodium carbonate (Na_2CO_3 , Merck) to facilitate dissolution and buffering of luminol. The reagent was adjusted to pH ~10 with 40 mL concentrated ammonium hydroxide (NH_4OH , Seastar, Baseline) and 11 mL distilled HCl (Seastar, Baseline). The luminol solution was prepared at least two days before use in opaque bottles to ensure optimal reactivity.

Calibrations

Calibrations for dFe(II) were completed daily before the experiments. Low Fe seawater was used for the calibration, kept at the same temperature as the experimental water. This calibration seawater was acidified to 0.4 mM with HCl, which retarded the dFe(II) oxidation but minimally decreased the pH (0.01 ± 0.01 , $n=10$). To delay the oxidation for the calibration further, 75 μL of a 0.04 M Na_2SO_3 (Sigma) stock were added to the calibration matrix. To obtain a calibration curve, addition steps for dFe(II) of 1 nM, 2.5 nM, and 5 nM were used. The detection limit, defined as the analyte concentration equivalent to three times the standard deviation of the blank (Bowie et al., 2004), was 0.017 nM ($n = 42$).

Dissolved Fe(II) instrumentation

A direct (non-column) method, similar to that described by Croot and Laan (2002) and Schallenberg et al. (2015), was used to obtain continuous measurements for dFe(II) oxidation (**Figure 2.2**). This method incorporates a flexible PVC tube (yellow-blue, 1.52 mm i.d., Choice Analytical) clamped into a peristaltic pump (Gilson, Inc, MINIPULS 3, France) at the end of the setup. One new feature was to pull the solutions instead of pushing them through the system. Using this newly modified method, the pump pulled the mixed luminol and seawater at a flow rate of 4.5 mL/min and allowed us to keep the black PVC tubing (1/16" Global FIA, INC) as short as possible and therein prevent warming of the sample. The actual outflow was measured gravimetrically (4.37 ± 0.26 mL/min, $n = 12$). The reagents were constantly pulled into a mirrored spiral flow cell (Tygon™ tubing, i.d. 0.7 mm) placed above a photon multiplying tube (PMT, Hamamatsu 8259, Japan), inside a custom-made light-proof box. The PMT gave ten readings per second, recorded continuously on a laptop running LabVIEW 6.1 (National Instruments). The output was then processed using MATLAB (Version 2018, 9), which slightly smoothed the output by averaging 100 points.

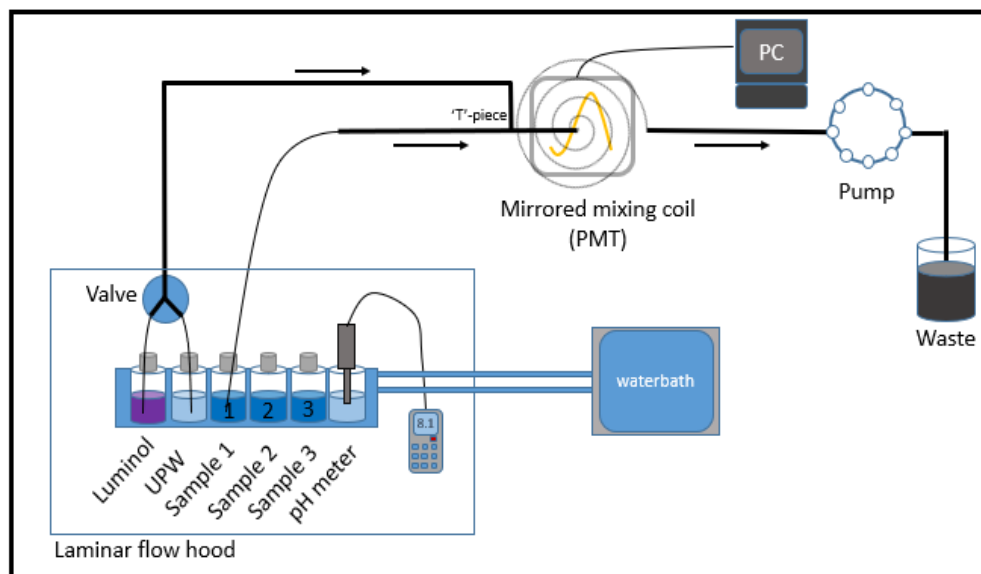


Figure 2.2 Flow injection analysis for dFe(II) sampling from a temperature cooled tank system, placed inside an ISO class-5 laminar flow hood (LMFH): Luminol or ultrapure water (UPW), switched by a 3-port valve, and a sample are pulled from the bottles placed in the cooled tanks located inside a LMFH. Once the reagent and the sample are mixed in the y-piece, they are drawn into a mirrored coil and detected through a photon multiplying tube (PMT). The pH-electrode and buffers were kept at the same temperature as the experimental bottles.

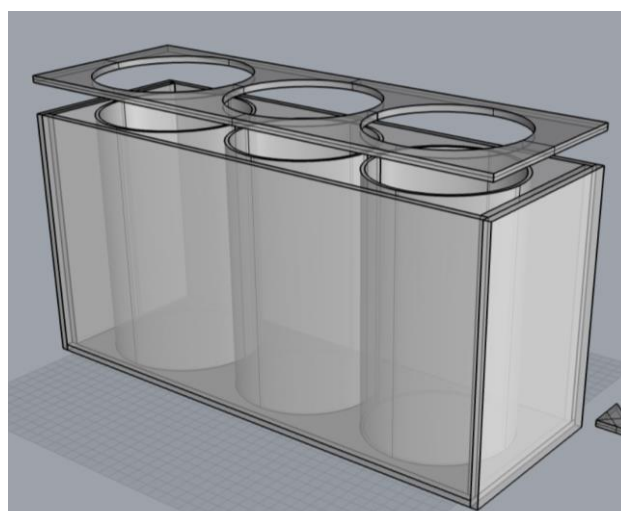


Figure 2.3 Schematic for one of the two custom-made acrylic tanks (inlet and outlet not shown).

Temperature control

Custom-made acrylic tanks were integrated into the setup to store reagents and sample bottles (**Figure 2.3**) at a constant temperature. They were placed into an ISO class-5 LMFH and connected to an immersion heater circulator (Ratek TH8000) and a cooler (Ratek RC1). The inbuilt pump of the water bath was set to a pump rate of 14 L per minute, which ensured a complete exchange of water in both tanks within one minute. The temperature was set to $5.00 \pm 0.50^\circ\text{C}$, $10.00 \pm 0.7^\circ\text{C}$ and $15 \pm 0.3^\circ\text{C}$ ($n=14$). This temperature range was used because they fall into the range of the natural surface seawater around the Tasmanian coast. While an approach to use lower temperatures $0\text{-}5^\circ\text{C}$ would have been beneficial for cold water such as the SO, the luminol reactivity was highly decreased at low temperatures, and changes in temperature or pH were difficult to observe. Additionally, having steps of 5°C from 5°C to 15°C enabled us to observe the kinetics under almost natural temperature conditions, while this was problematic when just elevating the temperature by, for example, 1°C . Using this system, the temperature could be accurately controlled, and the samples were kept free from contamination.

Procedure and timing

The two temperature-controlled tanks (**Figure 2.3**) held up to six bottles. Three slots were used to cool sample replicates. Two slots were used to cool the luminol and UPW-wash bottles and to ensure the temperature would not be altered during the mixing of reagent and sample. The last slot was used to store the plastic bagged pH electrode (Hach, HQ40C, probe PHC10101), the respective calibration buffers and a 60 mL LDPE bottle with seawater to measure temperature before the analysis. The pH probe was also kept in the cooled conditions with the buffers to calibrate for pH at the same temperature as the samples and reagents. All bottles were placed into the tanks for at least 4 hours before the experiment to ensure the targeted temperature was reached. After calibration of the dFe(II) setup, a 20-second UPW wash cycle was initiated, after which a three-port valve (Part no. 075T3MP12-32, Biochem Inc, Boonton, NJ) switched to the sample line. These 20 seconds were sufficient to spike, cap and gently mix the sample with 5 nM dFe(II) inside acid washed bottles (Nalgene, LDPE).

Setup for artificial light, dark (control) and UV light

To determine whether light impacted the photochemical cycle of dFe(II), the samples were exposed to artificial light or kept in the dark, which was considered the control. For the dark experiments, the LMFH was covered, and the lights in the laboratory were turned off. The samples and the calibration water were kept in the dark before analysis for 24 hours for lit and darkened conditions. To test for the effect of artificial light, a lamp (F18T8/840, 600mm, 4000 kelvin, cool white, Crompton, Australia) was placed above the water tanks inside the LMFH. Fluorescent light (550 nm - 600 nm) with $200 \pm 10 \mu\text{mol quanta m}^{-2} \text{s}^{-1}$ was measured in seawater filled LDPE bottles inside the tanks by a spherical quantum sensor (Li-193, Li-Cor). The dFe(II) oxidation rate was measured for at least 20 to 30 minutes for each sample during darkened and light temperature experiments (see **Figure 2.5**). To observe whether UV light affected the dFe(II) oxidation rate constant, a two-time 15-minute UV treatment was carried out in acid cleaned quartz bottles using 2 UV-light tubes, with an output of 30 mW s cm^{-2} each (Atlantic Ultraviolet, NY, USA). Afterwards, the water was stored in the dark at the same temperature as the experimental set up for 24 hours to ensure enough time had passed for the water to cool again.

Setup of CO₂ experiments & adjustments

The CO₂ experiments (**Figure 2.4**) were all done in PC bottles (Nalgene) to overcome CO₂ outgassing, as suggested in the ‘Guide to best practice for OA research and data reporting’ by Riebesell et al. (2011). A 1:10 filtered (0.2 μm PTFE, Choice Analytical, Australia) mix of CO₂ (Food quality, BOC, Australia) and air controlled by an electrical air pump (ACO-9610, Hailea) was delivered to the water using non-permeable LDPE tubing (1/8” ID x 1/4” OD, Tygon). Two litre PC bottles of seawater were then directly bubbled to adjust the seawater pH to 6, 7, 7.5 and 7.9, respectively, using a custom-made lid connected to the gas mixture in a simplified version of Hoffmann et al. (2013). The pH stayed constant in the 2 L bottles even with headspace and stayed constant for at least three following days (± 0.3 , $n = 5$). The lid had two ports for the CO₂ distribution (inlet and outlet). To prepare samples for dFe(II) oxidation, 300 mL of the pre-bubbled seawater was gently filled gravimetrically into PC bottles before a 5 nM dFe(II) spike.

Open ocean water was bubbled to pH 6 and 7.5, while the third point was kept natural at 8.1. In coastal water, the pH was adjusted to 7.5, 7.9 and 8.1 (natural). Each pH treatment was further combined with temperatures of 5°C, 10°C, 15°C to observe the oxidation of dFe(II) (**Figure 2.4** and **Table 2.1** for an overview). All CO₂ linked experiments were performed under artificial light as described above.

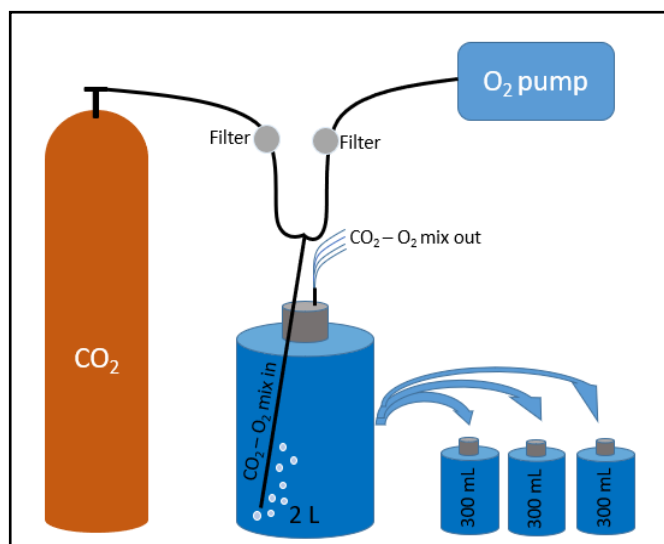


Figure 2.4 Filtered CO₂ from a cylinder and filtered O₂ from a pump get mixed together. This mix is used to bubble seawater to a pH of 6, 7, 7.5 and 7.9 through a lid with one inlet and one outlet port.

2.2.4 Analysis of sub-parameters

pH, dissolved oxygen, temperature, and salinity

Temperature and pH (NBS scale) were both measured with an electrode (PHC10101), using a pH meter (Hach HQ40C). The pH probe was calibrated daily by three-point measurements. Dissolved oxygen (DO) was measured with the same instrument using another probe (LDO10101) which was calibrated monthly. Salinity was measured with a portable refractometer (Imbros, Australia). To avoid contamination for dFe(II), 25 mL were subsampled into a cooled LDPE vessel, from which the measurements of pH and DO were taken once immediately before the experiment.

Macronutrients

The 0.2 μm filtered samples for macronutrients were frozen at -80°C in 15 mL PC vials and stored until analysis. Macronutrient (Ammonia (NH⁴⁺), phosphate (PO₄³⁻), nitrate (NO₃⁻),

silicate (SiO_4^{2-}) analyses were done within 12 months from the sampling in the laboratory, using a 4 channel LACHAT Quick-Chem 8500 auto analyser following the Quick-Chem methods by Diamond (2008a), Diamond (2008b) and Liao (2008).

Dissolved Fe(III) analysis

EAs as a background and to check for contamination of dFe(III), analyses with pH 1.8 acidified samples were done a week after the oxidation experiment. No re-analysis of the samples after six months as suggested was performed. A flow injection approach with an in-line preconcentration onto a 8-hydroxyquinoline (8-HQ) resin was used (Obata et al., 1993; De Jong et al. (1998). In short, during the dFe(III) determination, Fe was eluted in 0.3 M HCl (Seastar, Baseline), which mixed with 0.1 mM luminol (Sigma)/0.3mM TETA (Sigma), 0.2 M NH_4^+ (Seastar, Baseline) and 0.1 M H_2O_2 (Sigma), causing a luminescent reaction before it was detected on a photon multiplying head (PMT, Hamamatsu). A dFe(III) stock (Sigma) was prepared monthly. Calibrations were done before analysis in low Fe seawater, which was acidified to pH 1.8. The acidification of calibration and sample water was done at least 24 hours prior to analysis.

SF-ICP-MS analysis

Samples for dissolved trace metals from open and coastal water were taken in 125 mL LDPE bottles (Nalgene; 0.2 μm filtered, Millex, GP), acidified with distilled HCl to pH 1.8, and stored for a month. An offline configuration of a seaFAST S2 pico (ESI, Elemental Scientific, USA) multi-element extraction system was used with a Nobias Chelate-PA1 column, followed by analysis on a sector field inductively coupled plasma mass spectrometer (SF-ICP-MS, Element 2 Thermo Fisher Scientific, Inc.; Wuttig et al., 2019). Using this approach, a preconcentration factor of 53.33 was obtained. The detection limit for Fe was determined as three times the average of the blank concentration. Mixed multi-element standards were used for SF-ICP-MS tuning and calibrations (MISA Solutions, 100 μg , VHG Labs, USA; solution 6 containing Fe amongst others (Wuttig et al., 2019). In-house seawater collected during a voyage in the SO was used as an internal standard during SF-ICP-MS analysis. It was added in-line to standards and samples via the elution acid at a final concentration of 10 $\mu\text{g/L}$.

Chromophoric dissolved organic matter (CDOM) analysis

The open and coastal seawater CDOM samples were 0.2 μm filtered using a 10 mL Teflon syringe and were frozen until the analysis. For detecting CDOM, a 10 cm liquid waveguide capillary cell (LWCC, LWCC-2100 World Precision Instruments, Sarasota, FL, USA) and an Ocean Optics USB4000 UV-VIS spectrophotometer in combination with an Ocean Optics DT-Mini-2-GS light sources similar to Heller et al. (2016) were used. In short, to measure the absorbance, the first 10 mL of sample were discarded, and the following sample volume was injected directly into the LWCC. This was done relative to UPW and corrected for the refractive index of seawater (Nelson et al., 2007). The obtained optical spectra were converted to an absorption coefficient (m^{-1}) using a CDOM (λ) = 2.303 λ/l , whereby 2.303 converts decadal logarithmic absorbance to the base of e, and l is the effective optical pathlength of the waveguide. The CDOM absorbance spectra measured here ranged between the wavelength (λ) of 280 to 800 nm.

2.2.5 Calculations & modelling

To calculate oxidation rates, the highest dFe(II) concentration from the continuous FIA-dFe(II) measurements was used as a starting point ([dFe(II)]). The concentration from the time (dt), where half of the amount had oxidised, was used as the endpoint [dFe(II)] to obtain the $t_{1/2}$ value. To calculate the decay constant k' , equation 1 was used (e.g. González-Davila et al., 2005).

$$\frac{d[Fe(II)]}{dt} = -k'[Fe(II)] \quad (1)$$

From that, O_2 data for the temperature experiments was integrated using equation 2 to derive k_{app} , an apparent constant of the decay rate.

$$\frac{dFe(II)}{dt} = -k_{app, \text{O}_2} [Fe(II)] [\text{O}_2] \quad (2)$$

By using equation 3, the $t_{1/2}$ was obtained, which was compared to the experimental observations with results using equation 1.

$$t_{1/2} = \frac{\ln 2}{k'} \quad (3)$$

A slightly modified equation suggested recently by Santana-González et al. (2018) was used to also calculate k' (equation 4) by using physico-chemical parameters temperature (T), pH and salinity (S). Therefore, ionic strength (I) was obtained following the calculation presented in Millero et al. (1987).

$$k'(\text{min}^{-1}) = I - 0.0004T + 0.0003T^2 + 0.0389\text{pH} - 0.0287S \quad (4)$$

From that, equation 3 was reapplied to obtain the $t_{1/2}$, compared to the observations here. During the temperature experiments, the oxidation rate until after the 2nd $t_{1/2}$ had passed was observed. During the CO₂ experiments, however, the oxidation was so slow at low pH that the sample volume was used up before the 1st $t_{1/2}$ was fully recorded. Therefore, initial concentrations combined with the concentration at a set time for each replicate were used and integrated into equation 1. A Pearson correlation approach was used to gain insight into which parameter (temperature or OA) has a stronger effect in each environment (coastal or open ocean). The entire $t_{1/2}$ from each sample was observed, including filtered and unfiltered water with the dark, light and UV treatments and the complete set from the CO₂ experiments. For the statistical analysis, SPSS (Version 27) was used (see **Supplementary tables 1-9**).

2.2.6 Experimental overview

The kinetic oxidation experiments were carried out under three different conditions: (1) dark (control), (2) light, and (3) UV treatment. All three treatments were performed on open and coastal waters at 5°C, 10°C and 15°C (**Table 2.1**). Coastal water was used in its filtered stage; open ocean water was tested filtered (0.2 μm) and unfiltered. Once the oxidation experiments for temperature were completed, the CO₂ experiments were started. For this, coastal water at 10°C and 15°C was used, which was acidified to pH 7.5, 7.9 and 8.1 and open ocean water at 5°C, 10°C and 15°C was used acidified to pH 6, 7 and 8.1. Afterwards, the calculations as outlined in section **2.2.5** were applied.

Table 2.1 Overview of experimental treatments from temperature and CO₂ experiments in coastal and open ocean water.

	Coastal	Open ocean water
Temperature experiment	<ul style="list-style-type: none"> • pH – unchanged (natural, 8.04) • Temperature: 5°C, 10°C, 15°C • Filtered (0.2 μm) • Dark, light, UV treatment 	<ul style="list-style-type: none"> • pH – unchanged (natural, 8.01) • Temperature: 5°C, 10°C, 15°C • Filtered (0.2 μm) and unfiltered • Dark, light, UV treatment
CO ₂ experiment	<ul style="list-style-type: none"> • pH 8.1, 7.9, 7.5 • Temperature: 10°C, 15°C • Filtered (0.2 μm) 	<ul style="list-style-type: none"> • pH 8.1, 7, 6 • Temperature: 5°C, 10°C, 15°C • Filtered (0.2 μm)

2.2.7 Methodological caveats

The current guide to best practices for ocean CO₂ measurements Riebesell et al. (2011) suggest diffusive bubbling of CO₂ via silicone tubing while using living organisms. We found that the bubbling with diffusive tubes is slowed immensely in 5°C water (2 - 3 hours) compared to 39 minutes at 10°C. An explanation for the slowed time of bubbling may lie in the reduction of the pore sizes from the silicone tubes in colder conditions (verbal conversation with Stacy Deppeler). Since the experiments in Chapter 2 are abiotic, a direct bubbling approach was applied for all treatments during the CO₂ experiments.

Another approach that could be improved, is having a uniform O₂ concentration at the start of the experiment. Unlike Roy & Wells (2011) and Gonzalez et al. (2010), the samples were not aerated initially. Therefore, the O₂ concentrations were measured but not controlled. This resulted in differing O₂ concentrations between samples. To overcome this, dissolved oxygen DO measurements were integrated into the calculations.

During the CO₂ experiments, it was expected that a lower pH would retard the oxidation times compared to samples with natural pH. The 300 mL of the dFe(II)-spiked samples were used up rapidly during the continuous approach, and eventually, the sample was used up. Therefore, only part of the 1st t_{1/2} could be logged for some samples. This became a greater issue at low pH with extended run-time lengths. To overcome this issue, the obtained parameters from these specific experiments were applied to a theoretical calculation (equation 2 in section 2.2.5) to obtain the 1st t_{1/2} of open ocean water. To overcome this during the experimental run in coastal water, where the oxidation times were even longer, pausing the otherwise continuous inline

measurement for 10-15 minutes several times helped with extending the observation time, despite the low volume of only 300 mL (see **Figure 2.6**, a & b). Dissolved Fe(II) oxidation sample points were obtained through this later approach, which was sufficient for receiving an oxidation rate.

2.3 Results

2.3.1 Temperature Experiments

Impact of temperature on the dFe(II) oxidation: first half-lives

The $t_{1/2}$ is the time that passes for a certain analyte, in this case dFe(II), to reduce to half of its initial value. The 2nd $t_{1/2}$ life follows the 1st $t_{1/2}$ and defines when only 25% of the initial value is left.

Coastal water

As expected, dFe(II) had the slowest oxidation rate at the coldest temperature (5°C), increasing with temperature to 15°C (**Figure 2.5** and the correlating input parameters, k , k_{app} and $t_{1/2}$ in **Table 2.2**). This was also true for the 1st $t_{1/2}$ in the control of filtered coastal water in the dark: A spike of 5 nM dFe(II) took longest to decay at 5°C (**Figure 2.5** a, blue data points, 41 ± 8 min), followed by 10°C (**Figure 2.5** a, yellow datapoints, 21 ± 3 min) and was fastest at 15°C (**Figure 2.5** a, red datapoints, 20.33 ± 4.15 min). The $t_{1/2}$ during artificial light exposure in coastal water (**Figure 2.5** b) was slightly faster with 33 ± 5 min at 5°C, 14 ± 4 min at 10°C and 15 ± 3 min at 15°C. ExWhile the dark and the light treatment were not significantly different from each other (Tukey's HSD test for multiple comparison; $p = 0.145$, see **Supplementary Table 1** and **Figure 2.5** a and b), the treatment with UV light **Figure 2.5** c) was significantly different to the light treatment ($p = 0.001$) with a $t_{1/2}$ of 2.3 ± 0.0 min at 5°C, 1.1 ± 0.1 min at 10°C and 1.34 ± 0.5 at 15°C. As described in **Table 2.2**, salinity and I vary between coastal and open ocean seawater. While coastal ocean water has a salinity of 35.51 with an I of 0.73, open ocean water has 35.81 and an I of 0.74.

Open ocean water

Oxidation times were generally 25 % faster in ocean water compared to coastal water. The unfiltered open ocean water followed similar oxidation trends to the coastal water, with the

slowest oxidation at 5°C and fastest at 15°C (**Figure 2.5** d-f). It took 8 ± 2 min at 5°C, 10 ± 3 min at 10°C and 4 ± 0.5 min at 15°C for 5 nM dFe(II) to reach half its concentration in the dark (**Figure 2.5** d). These dark treatment results were not significantly different from the light (7 min at 5°C, 9 ± 3 at 10°C and 2 ± 0.5 at 15°C) treatment ($p = 0.894$, **Supplementary Table 2** and **Figure 2.5** e). There was a significant difference when comparing the oxidation of dark and UV treatment ($p = 0.044$) and also significantly different when comparing light and UV ($p = 0.004$, **Supplementary Table 2**, **Figure 2.5**, and **Table 2.2**) in open ocean water. In open ocean water, the oxidation in filtered vs. unfiltered water was significantly different ($p < 0.001$, ANOVA, **Supplementary Table 3**, **Figure 2.5**).

A significant difference in the 1st $t_{1/2}$ was detected between dark and light in the filtered water ($p < 0.001$) and between light and UV ($p < 0.001$). Dark and UV light, however, were non significantly different (**Supplementary Table 4**). A faster oxidation in the filtered open ocean water compared to the unfiltered samples was observed. No significant difference in the oxidation rate was detected ($p = 0.11$) between dark and light treatments in the unfiltered open ocean water. In contrast, light and dark treatments were significantly different to UV ($p = 0.011$ and 0.010 respectively, **Supplementary Table 5**). The UV treatment increased the short-term variability and signal to noise ratio of the oxidation reaction (**Figure 2.5** g-I).

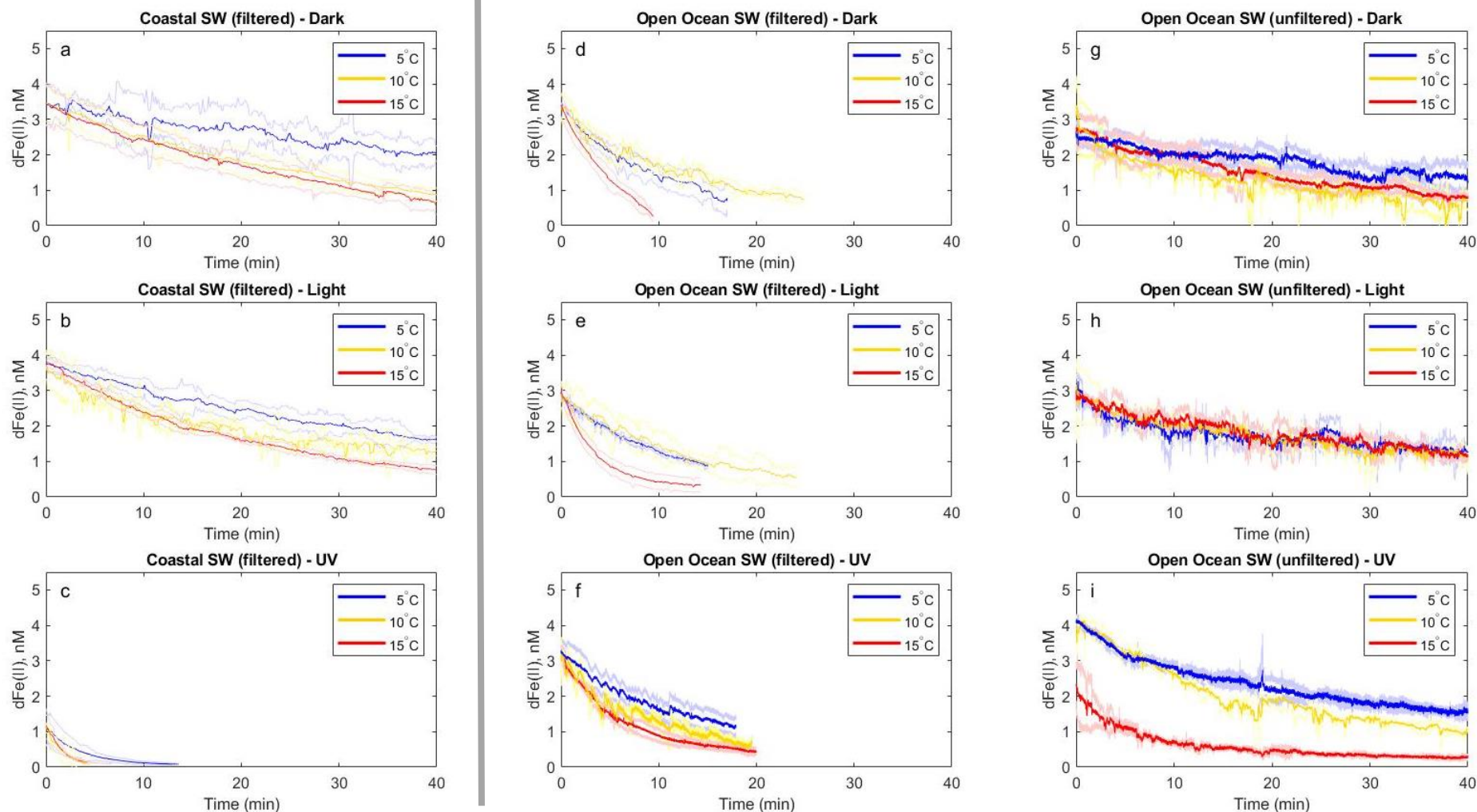


Figure 2.5 Oxidation curves of dFe(II) over time (minutes) at natural pH at temperatures of 15°C (red), 10°C (yellow) and 5°C (blue) in 0.2 μm filtered coastal water (a-c), filtered open ocean water (d-f), and unfiltered open ocean water (g-h). sw = seawater. Thick datapoints denote replicate averages ($n=3$), transparent datapoints in the respective colours display the standard deviation for the three replicates. For each water 53 type, dark (a, d, g), light (b, e, h) and UV (c, f, i) treatments were applied.

Table 2.2 Temperature based dFe(II) oxidations in coastal and open ocean water for 0.2 μm filtered (f.) and unfiltered (unf.) treatments. A dark (control, grey), light (yellow) and a UV treatment (purple) was considered at 5°C (blue), 10°C (orange) and 15°C (red). In the left columns are the general parameters temperature (T), pH, salinity (S), dissolved oxygen (DO) and ionic strength (*I*), followed by the 1st and 2nd $t_{1/2}$, with $t_{1/2}$, k' and $\text{Log } K_{app}$ reported from each experiment. The calculated values for $t_{1/2}$ and k' are also shown.

							1 st $t_{1/2}$			2 nd $t_{1/2}$			Calculated values	
		T (°C)	pH	S	DO (mg/L)	<i>I</i>	$t_{1/2}$ (a) (min)	k' (b) (min ⁻¹)	Log k_{app} (c) (M ⁻¹ min ⁻¹)	$t_{1/2}$ (a) (min)	k' (b) (min ⁻¹)	Log k_{app} (c) (M ⁻¹ min ⁻¹)	$t_{1/2}$ (d) (min ⁻¹)	k' (d) (min ⁻¹)
Open Ocean (f.)	Dark	5.66 ± 0.49	8.01 ± 0.01	35.81	10.78 ± 0.26	0.74	8.12 ± 1.98	0.062 ± 0.016	2.25 ± 0.09	8.04 ± 1.49	0.061 ± 0.01	2.25 ± 0.06	21.58 ± 0.99	0.031 ± 0.001
		10.03 ± 0.28	7.96 ± 0.01	35.81	9.72 ± 0.01	0.74	10.4 ± 3.23	0.048 ± 0.013	2.19 ± 0.12	12.19 ± 1.73	0.04 ± 0.006	2.12 ± 0.06	11.43 ± 0.53	0.058 ± 0.002
		15.8 ± 0.87	7.77 ± 0.01	35.81	9.42 ± 0.17	0.74	4.03 ± 0.47	0.116 ± 0.011	2.59 ± 0.04	4.21 ± 1.82	0.12 ± 0.043	2.58 ± 0.16	8.06 ± 0.68	0.083 ± 0.008
	Light	5.66 ± 0.57	7.90 ± 0.01	35.81	9.71 ± 0.13	0.74	7.24 ± 0.13	0.065 ± 0.001	2.33 ± 0.05	9.37 ± 1.66	0.051 ± 0.008	2.22 ± 0.07	25.19 ± 1.13	0.027 ± 0.001
		10.87 ± 0.63	7.89 ± 0.02	35.81	9.75 ± 0.14	0.74	9.07 ± 3.05	0.056 ± 0.017	2.25 ± 0.13	9.58 ± 1.55	0.049 ± 0.008	2.2 ± 0.06	13.37 ± 1.51	0.051 ± 0.005
		15.23 ± 0.47	7.95 ± 0.09	35.81	9.56 ± 0.59	0.74	2.37 ± 0.46	0.18 ± 0.026	2.77 ± 0.07	3.09 ± 0.91	0.16 ± 0.041	2.72 ± 0.11	9.19 ± 1.46	0.073 ± 0.009
	UV	5.23 ± 0.17	7.93 ± 0.04	35.81	10.34 ± 0.23	0.74	9.01 ± 1.19	0.054 ± 0.006	2.22 ± 0.06	-	-	-	22.57 ± 0.78	0.030 ± 0.001
		10.15 ± 0.77	7.87 ± 0.01	35.81	9.14 ± 0.20	0.74	3.46 ± 3.33	0.087 ± 0.015	2.48 ± 0.06	7.16 ± 0.64	0.044 ± 0.002	2.19 ± 0.01	10.09 ± 1.84	0.045 ± 0.040
		15.63 ± 0.11	7.79 ± 0.01	35.81	9.83 ± 0.10	0.74	4.05 ± 0.66	0.116 ± 0.02	2.57 ± 0.07	6.29 ± 1.53	0.105 ± 0.049	2.50 ± 0.20	8.148 ± 0.09	0.082 ± 0.001
Open Ocean (unf.)	Dark	5.32 ± 0.00	7.71 ± 0.01	35.81	10.74 ± 0.36	0.74	62.57 ± 1.41	0.009 ± 0.001	1.46 ± 0.06	-	-	-	32.02 ± 0.83	0.021 ± 0.001
		11.23 ± 0.51	7.67 ± 0.05	35.81	9.70 ± 0.54	0.74	38.00 ± 9.63	0.013 ± 0.003	1.64 ± 0.13	-	-	-	15.33 ± 0.51	0.044 ± 0.002
		15.80 ± 0.50	7.72 ± 0.07	35.81	9.92 ± 0.16	0.74	20.39 ± 3.18	0.024 ± 0.004	1.89 ± 0.07	25.04 ± 7.67	0.02 ± 0.006	1.81 ± 0.13	8.20 ± 0.88	0.081 ± 0.007
	Light	5.60 ± 0.00	7.66 ± 0.13	35.81	10.04 ± 0.23	0.74	43.58 ± 7.42	0.011 ± 0.002	1.56 ± 0.08	-	-	-	41.16 ± 9.40	0.002 ± 0.005
		10.16 ± 0.05	7.91 ± 0.03	35.81	9.71 ± 0.13	0.74	51.05 ± 9.16	0.009 ± 0.001	1.51 ± 0.08	-	-	-	14.36 ± 0.43	0.047 ± 0.001
		15.30 ± 0.50	7.73 ± 0.08	35.81	9.83 ± 0.13	0.74	26.38 ± 8.10	0.019 ± 0.005	1.79 ± 0.13	-	-	-	8.2 ± 0.54	0.082 ± 0.008
	UV	5.15 ± 0.40	7.63 ± 0.08	35.81	9.48 ± 0.07	0.74	18.27 ± 6.60	0.029 ± 0.01	1.97 ± 0.16	31.18 ± 2.14	0.015 ± 0.001	1.72 ± 0.03	43.49 ± 6.40	0.016 ± 0.002
		10.40 ± 0.14	7.65 ± 0.08	35.81	9.88 ± 0.05	0.74	8.58 ± 7.82	0.036 ± 0.003	2.07 ± 0.03	21.17 ± 1.86	0.016 ± 0.005	1.71 ± 0.14	15.34 ± 0.79	0.045 ± 0.002
		15.07 ± 0.15	7.75 ± 0.01	35.81	10.76 ± 0.05	0.74	13.12 ± 9.00	0.025 ± 0.006	1.87 ± 0.11	-	-	-	8.09 ± 0.00	0.084 ± 0.000
Coastal Ocean (f.)	Dark	4.95 ± 0.45	8.04 ± 0.02	35.51	8.24 ± 0.71	0.73	41.03 ± 7.82	0.012 ± 0.002	1.68 ± 0.11	48.02 ± 7.39	0.01 ± 0.001	1.60 ± 0.10	20.57 ± 0.57	0.033 ± 0.001
		10.35 ± 0.15	7.99 ± 0.07	35.51	8.69 ± 0.12	0.73	21.22 ± 2.93	0.023 ± 0.003	1.93 ± 0.05	19.35 ± 1.09	0.025 ± 0.001	1.96 ± 0.02	13.20 ± 0.86	0.051 ± 0.003
		15.03 ± 0.04	8.00 ± 0.01	35.51	9.48 ± 0.30	0.73	20.33 ± 4.15	0.024 ± 0.005	1.91 ± 0.1	17.57 ± 1.86	0.027 ± 0.002	1.96 ± 0.05	7.33 ± 0.03	0.087 ± 0.001
	Light	4.96 ± 0.05	7.89 ± 0.10	35.51	8.32 ± 0.25	0.73	33.12 ± 5.27	0.015 ± 0.002	1.76 ± 0.08	38.32 ± 5.5	0.013 ± 0.002	1.69 ± 0.06	25.53 ± 1.55	0.027 ± 0.004
		10.00 ± 0.34	8.08 ± 0.00	35.51	9.04 ± 0.55	0.73	15.40 ± 4.33	0.032 ± 0.008	2.05 ± 0.10	34.13 ± 0.2	0.014 ± 0.001	1.71 ± 0.02	12.23 ± 0.03	0.055 ± 0.000
		14.98 ± 0.43	8.07 ± 0.06	35.51	8.67 ± 0.29	0.73	15.22 ± 2.64	0.032 ± 0.005	2.07 ± 0.07	19.13 ± 0.72	0.025 ± 0.001	1.97 ± 0.02	7.42 ± 0.13	0.090 ± 0.003
	UV	5.00 ± 0.11	8.01 ± 0.02	35.51	8.69 ± 0.62	0.73	2.28 ± 0.01	0.178 ± 0.001	2.81 ± 0.03	2.14 ± 0.05	0.208 ± 0.008	2.88 ± 0.04	21.49 ± 0.62	0.032 ± 0.001
		10.02 ± 0.23	7.91 ± 0.19	35.51	9.30 ± 0.21	0.73	1.13 ± 0.05	0.359 ± 0.026	3.09 ± 0.03	1.06 ± 0.09	0.429 ± 0.053	3.16 ± 0.05	14.21 ± 1.96	0.048 ± 0.008
		15.05 ± 0.12	7.96 ± 0.02	35.51	9.95 ± 0.59	0.73	1.39 ± 0.53	0.278 ± 0.064	2.94 ± 0.08	1.14 ± 0.11	0.362 ± 0.052	3.06 ± 0.05	8.04 ± 0.01	0.085 ± 0.000

a) Observed or measured values from the experiment

b) k' values derived from equation 1

c) K_{app} values derived from integrating measured O₂ concentrations (equation 2)

d) Based on the modified calculation from Santana-González et al. (2018): $k' \text{ (min}^{-1}\text{)} = I - 0.0004T + 0.0003T^2 + 0.0389\text{pH} - 0.0287S$, their equation (7).

- no values could be derived due to either fast oxidation or insufficient sample volume

Impact of temperature on the dFe(II) oxidation: 2nd half-lives

Coastal water

In the case of sufficient water, the 2nd $t_{1/2}$ curves were also observed (**Table 2.2** and **Figure 2.5**). The 2nd $t_{1/2}$ of dFe(II) when comparing temperature for the filtered coastal water also followed the trend of 5°C being the slowest, increasing with temperature. This was true for all treatments (dark, light UV; see **Table 2.2**). A post hoc test did not reveal significant differences between the dark and the light treatment ($p = 0.904$) for the 2nd $t_{1/2}$. In contrast, UV light did display significant differences ($p = 0.01$) in coastal water to light and the dark treatment (**Supplementary Table 6**).

Open ocean water

The filtered open ocean water also displayed a similar trend for the 2nd $t_{1/2}$ compared to the 1st $t_{1/2}$. The oxidation at 10°C here was still slightly slower than the one at 5°C. However, all treatments had similar trends from the 1st and the 2nd $t_{1/2}$ and were non-significant for the light treatments (**Supplementary Table 7**). Fewer results for 2nd $t_{1/2}$ were observed in unfiltered open ocean water due to retarded oxidation rates in unfiltered water, resulting insufficient sample volume (see **Table 2.2**). Therefore, no statistical observation based on measurements could be performed.

2.3.2 CO₂ Experiment

Half-life times in open ocean water

In the open ocean water at 5°C, the 1st $t_{1/2}$ was 24 ± 1.5 min at and unchanged, natural pH (pH 8.1) and increased to 208 ± 123 min at pH 6 (**Table 2.3**). At 10°C, the 1st $t_{1/2}$ lasted 15 ± 1 min at pH 8.1; 85 ± 8 min at pH 7; and 258 ± 17 min at pH 6. At 15°C, the oxidation was 5 to 20 times faster with a 1st $t_{1/2}$ of 9 ± 2 min at natural pH; 51 ± 15 min at pH 7; and 111 ± 15 min at pH 6. The difference of the 1st $t_{1/2}$ between pH 6 and 7 was non-significant, while the difference in pH 6 to pH 8.1 and 7 to 8.1 was significant (**Supplementary Table 8**) and is also displayed in **Figure 2.6**.

Half-life times in coastal water

In coastal water, the oxidation at 10°C had times ranging from 4 ± 2 min at natural pH to 28 ± 3 min at the lowest pH of 7.5 (**Table 2.3**). At 15°C, this time was reduced to 1.7 ± 1.01 min for the oxidation of dFe(II) at the natural pH of 8.1, which increased to 73 ± 8 min at the lowest pH (pH 7). Statistically speaking, pH 7.5 to 7.8 were not significant, while all other relations were significant (**Supplementary Table 9**). This is also summarised in **Figure 2.6**. The uncertainties for $t_{1/2}$ (**Table 2.3**) increase 10 to 15-fold when comparing calculated values of pH 8.1 to pH 6. These major changes come from small differences in the actual temperature or pH for each replicate.

Table 2.3 Oxidation of dFe(II) at altering pH via CO₂ manipulation and varying temperatures of 5°C (blue), 10°C (orange) and 15°C (red). Measured parameters include temperature (T°C), pH, salinity (S) and ionic strength (I). Calculated values of k' and $t_{1/2}$ are also included.

Treatments		General parameters				Calculated values ^{a)}		
T (°C) *	pH*	T (°C)**	pH**	S	I	k' (min ⁻¹)	$t_{1/2}$ (min ⁻¹)	
Open Ocean, filtered	5°C	8.1	5.83 ± 0.40	8.09 ± 0.08	35.81	0.74	0.029 ± 0.001	23.71 ± 1.51
		7	6.13 ± 0.80	7.15 ± 0.10	35.81	0.74	0.004 ± 0.000	149.63 ± 9.86
		6	5.96 ± 0.15	6.00 ± 0.00	35.81	0.74	0.002 ± 0.002	208.10 ± 123.05
	10°C	8.1	10.80 ± 0.00	8.04 ± 0.01	35.81	0.74	0.047 ± 0.003	14.57 ± 0.93
		7	10.70 ± 0.01	6.82 ± 0.15	35.81	0.74	0.008 ± 0.001	85.07 ± 7.92
		6	10.20 ± 0.02	6.12 ± 0.14	35.81	0.74	0.002 ± 0.001	258.44 ± 16.91
	15°C	8.1	15.06 ± 0.05	8.00 ± 0.04	35.81	0.74	0.083 ± 0.022	8.73 ± 2.13
		7	15.10 ± 0.01	7.06 ± 0.07	35.81	0.74	0.014 ± 0.004	50.75 ± 13.48
		6	15.40 ± 0.34	5.98 ± 0.03	35.81	0.74	0.006 ± 0.001	110.7 ± 15.09
Coastal, filtered	10°C	8.1	10.00 ± 0.01	8.19 ± 0.00	35.51	0.73	0.247 ± 0.178	3.70 ± 1.90
		7.9	10.10 ± 0.17	7.83 ± 0.02	35.51	0.73	0.025 ± 0.005	27.69 ± 6.61
		7.5	10.00 ± 0.09	7.56 ± 0.03	35.51	0.73	0.025 ± 0.002	27.90 ± 2.93
	15°C	8.1	15.16 ± 0.20	8.20 ± 0.01	35.51	0.73	0.504 ± 0.227	1.68 ± 1.01
		7.9	15.00 ± 0.07	7.87 ± 0.02	35.51	0.73	0.030 ± 0.004	22.85 ± 3.59
		7.5	15.26 ± 0.46	7.48 ± 0.01	35.51	0.73	0.009 ± 0.000	73.35 ± 7.52

a) These values were calculated by using equation (1)

* Experimentally pre-defined values

** Actual value (measured)

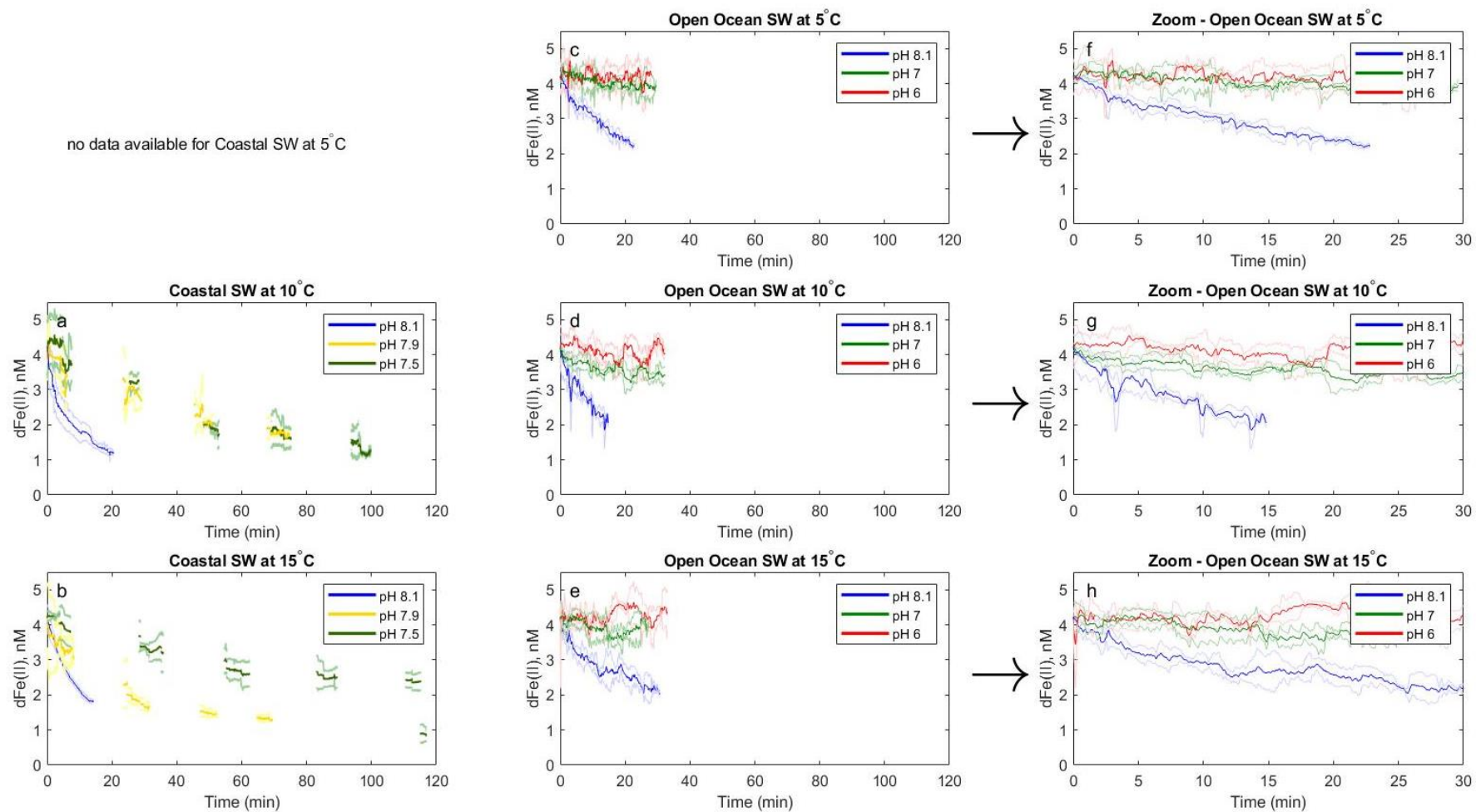


Figure 2.6 Filtered (0.2) dFe(II) oxidation under varying pH in coastal water at 10°C and 15°C (a & b) and in open ocean water at 5°C, 10°C and 15°C (c, d, & e). Panels f, g and h display enlarged data from the oxidation in open ocean water. Thick datapoints represent averaged values ($n = 3$), transparent datapoints represent the standard deviation ($n = 3$).

2.3.3 Comparison of actual observations vs. calculated values

Data obtained from the temperature experiments were used to compare it to results obtained by using equation 4 (**Table 2.4**), introduced by Santana-González et al. (2018). The results from using equation 4 can be found in the right hand two columns in **Table 2.2** (footnote d). The statistical results using a paired t-test revealed significant differences between the observed values (1st t½ in **Table 2.2**) and the calculated values of 1st t½ and k' of open ocean water ($p < 0.001$, $n = 27$, **Supplementary Table 8**) and coastal water ($p < 0.001$; $n = 18$, **Supplementary Table 9**). The 1st t½ varied by at least 5 min for all treatments and temperatures for the calculations compared to the observed values. Modelled values below a certain threshold of pH and temperature could not be obtained.

Table 2.4 Modelled approach of CO₂ experiment: Input parameters were obtained from observations T, (°C), pH, salinity and ionic strength (I) from Table 2.2) from which k' and t½ were calculated using equation 4. ‘-’ denotes that no value was derived through the calculation.

		Input parameters				Output parameters	
		T (°C)	pH	Salinity	Ionic Strength	k' (min ⁻¹)	t½ (min ⁻¹)
Coastal water, 0.2 µM filtered	5°C	8.1	35.81	0.74	0.035	19.81	
		7.9	35.81	0.74	0.027	25.47	
		7.5	35.81	0.74	0.012	59.49	
		7	35.81	0.74	-	-	
		6	35.81	0.74	-	-	
	10°C	8.1	35.81	0.74	0.055	12.49	
		7.9	35.81	0.74	0.048	14.53	
		7.5	35.81	0.74	0.032	21.56	
		7	35.81	0.74	0.013	54.58	
		6	35.81	0.74	-	-	
	15°C	8.1	35.81	0.74	0.091	7.62	
		7.9	35.81	0.74	0.083	8.33	
		7.5	35.81	0.74	0.068	10.25	
		7	35.81	0.74	0.048	14.38	
		6	35.81	0.74	0.009	74.53	
Open Ocean water, 0.2 µM filtered	5°C	8.1	35.51	0.73	0.033	21.13	
		7.9	35.51	0.73	0.025	27.69	
		7.5	35.51	0.73	0.009	73.20	
		7	35.51	0.73	-	-	
		6	35.51	0.73	-	-	
	10°C	8.1	35.51	0.73	0.053	13.00	
		7.9	35.51	0.73	0.46	15.22	
		7.5	35.51	0.73	0.030	23.13	
		7	35.51	0.73	0.011	65.89	
		6	35.51	0.73	-	-	
	15°C	8.1	35.51	0.73	0.089	7.80	
		7.9	35.51	0.73	0.810	8.55	
		7.5	35.51	0.73	0.065	10.59	
		7	35.51	0.73	0.046	15.06	
		6	35.51	0.73	0.007	97.36	

2.4 Discussion

A distinct aim of this study was to obtain further insights into the longevity and availability of dFe(II) in a more acidic, warmer SO. While calculations and coherent kinetic relationships of dFe(II) have been described (Millero et al., 1987, Santana-Casiano et al., 2006, Shaked, 2008, Gonzalez et al., 2010, Breitbarth et al., 2010b, Hopwood et al., 2018), actual experiments lack runtime lengths to observe complete trends. Experiments also often lack background analysis of the used natural seawater such as nutrients, Fe(III) ligand data, macronutrients etc. to exclude potential interferences from these components. Collecting as much information on the seawater composition combined with running the oxidation experiments at extended lengths allowed to compare the oxidation curves of dFe(II) in oligotrophic and eutrophic SO water as a means to improve the understanding of the dFe(II) kinetics in future oceans.

Besides those effects from background parameters, there are several controlling factors for dFe(II) oxidation, including temperature, pH, light and nutrients, which were used to compare measurements and calculations.

2.4.1 Role of temperature for the dFe(II) oxidation in open and coastal water in combination with trace metals, ligands, and nutrients

Temperature is often the main driver for oxidation. In the mentioned setup, the temperature was kept constant at 5°C, 10°C and 15°C for the coastal and the open ocean water, respectively. The observed oxidations in this study were faster at 15°C than at 5°C. This follows the same trend as the calculated decay rate k' . The k' increased in all cases with an increase of temperature and was previously reported in numerous studies (Santana-González et al., 2018, Millero et al., 1987, Millero and Izaguirre, 1989). While the trend of the oxidations was the same within each water type, filtered open ocean water vs. filtered coastal water were very different. The decay in open ocean water was four to five times faster than in coastal water. This contrasts with the oxidation rate in the unfiltered water, which was retarded two to three-fold comparatively (**Figure 2.5** and **Table 2.1**). A potential reason can be found in the contrasting seawater compounds such as trace metals, ligands, or nutrients, elaborated below (Johnson et al., 1999, Martin and Gordon, 1988, Wu and Luther III, 1996).

2.4.2 Trace metals

Some trace metals such as Fe or copper (Cu) are observed in higher concentrations in coastal waters due to proximity to landmass and a greater variety of sources (Bruland and Lohan, 2003, Johnson et al., 1999). In this specific case, the concentrations of Cu were found to be five times higher in the coastal water and eight times higher for Zinc (Zn) than in open ocean samples (**Table 2.5**). While both Cu and Zn are toxic for phytoplankton above a certain threshold (Wells et al., 1995), no correlation of Zn for impacting dFe(II) oxidation is known. Studies with Cu however, have shown that Cu(I) behaves similarly to dFe(II) species by oxidising slower at colder temperatures (Sharma and Millero, 1988). More importantly, it has also been shown that the presence of Cu(II) increases the dFe(II) oxidation rates especially when exposed to UV light shortening the $t_{1/2}$ of dFe(II) (Sharma and Millero, 1989, Pérez-Almeida et al., 2019).

Table 2.5 Trace metal concentrations for open and coastal seawater obtained through ICP-MS analysis (n = 1).

Seawater type	Fe (nM)	Cu (nM)	Zn (nM)	Cd (nM)	Pb (nM)	Ti (nM)	V (nM)	Mn (nM)	Co (nM)	Ni (nM)	Ga (nM)
Coastal	1.15	9.64	72.05	0.23	0.35	0.07	31.20	0.89	0.04	4.89	0.05
Open Ocean	0.96	1.94	8.74	0.73	0.03	0.15	34.2	0.25	0.03	6.47	0.03

Another factor impacting the overall decay rate is the initial concentration of Fe in seawater (**Table 2.5**). Several dFe(II) addition experiments showed that the starting concentration of Fe influences the oxidation rate of dFe(II), leading to retarded oxidation of dFe(II) in cases of high Fe concentrations (Santana-González et al., 2018, Roy and Wells, 2011). In this case, the starting concentrations of Fe were relatively low to begin with but also only differed minimally between open (0.96 nM, **Table 2.5**) and coastal water (1.15 nM). While these high open ocean concentrations may be the result of contamination during filtration or handling other samples, an interference of the starting Fe concentrations is therefore unlikely to impact the oxidation curves.

2.4.3 Ligands

The oxidation of dFe(II) is expected to be faster at higher temperatures (Millero et al., 1987, Hopwood et al., 2018). For the observations of the temperature experiments in open ocean water, however, we observed during multiple experiments (light and dark treatment) that dFe(II) at 10°C oxidised slower or at a similar pace as at 5°C.

By measuring ligand concentrations, we found that open ocean water had 6.15 nM ligands and therein a ratio of ligand: dFe of 6.39. To explain these oxidation time similarities between temperature treatments (10°C being as slow as 5°C), looking at ligand modelling as described by Völker and Tagliabue (2015) helped the observations. They set one model in their study to a uniform stability constant for ligands with changing temperatures, while another model varies once temperature changes. Their modelled results indicate that a temperature dependant ligand system can bind Fe easier in colder water. In contrast, these results indicate a stable constant regarding temperature when considering 5°C and 10°C in coastal water. Generally, it is suggested that the ligand stability constant for Fe is higher at warmer temperatures, which might lead to reduced scavenging in warmer water such as 15°C warm surface water (Völker and Tagliabue, 2015).

A medical study by Arsenault et al. (2007) tried to incite a temperature-dependent ligand-receptor contact point, which are supposedly specifically designed to retard dFe(II) oxidation within a temperature threshold. While the results leave many unanswered questions regarding the oxidation time, if ligands act similarly in a marine system, this could mean that Fe is kept longer in solution longer within a specific temperature range, which could explain our observations and thus Fe is kept from binding to larger complexes. Other studies suggest that dFe(II) oxidation rates can be balanced, accelerated, or retarded under aerobic conditions in the presence of organic species since they can act as a ligand but also as a source of H₂O₂ (Theis and Singer, 1974, Santana-González et al., 2019). In this case, a five-fold higher concentration of CDOM (see **Table 2.6**) in coastal water compared to open ocean water was found. These high concentrations in coastal water may further explain the retarded oxidation times compared to the open ocean water in general. Additionally, they may also hold the answer for similar oxidation times in filtered open ocean water at 10°C and 5°C (dark & light) because these concentrations of CDOM may act as a source of ligands that are most effective at complexing within a certain temperature range.

Table 2.6 Chromophoric dissolved organic matter (CDOM) concentrations for open and coastal water (n = 1).

Seawater type	CDOM (m ⁻¹)
Coastal	1.1515
Open Ocean	0.2303

* Measurements and calculations are based on Andrew et al. (2013) using a 10 cm liquid wavelength capillary cell.

2.4.4 Nutrients

A study by Gonzalez et al. (2010) describes the impacts of macronutrients such as NO₃⁻, PO₄³⁻ and SiO₄²⁻, where the dFe(II) oxidation rate was increased upon adding these nutrients. Their findings further indicate that SiO₄²⁻ was the nutrient with the most significant impact on the oxidation rate. The measured macronutrient concentrations (**Table 2.7**) resemble conditions for oligotrophic surface waters for coastal and open ocean water and were very low compared to previous studies in the region, such as Bowie et al. (2009) or Lannuzel et al. (2011). Furthermore, Gonzalez et al. (2010) used concentrations of 10 to 2000 μmol for their additions which is substantially higher than the values observed here (**Table 2.7**). It is unlikely that macronutrients at those relatively low concentrations influence the t^{1/2}; further laboratory experiments would be required for confirmation.

Table 2.7 Nutrient concentrations in coastal and open ocean water (n = 1).

Seawater type	NO ₃ ⁻ (μmol)	PO ₄ ³⁻ (μmol)	SiO ₄ ²⁻ (μmol)	NH ₄ ⁺ (μmol)
Coastal	1.51	0.15	-*	1.57
Open Ocean	23.57	1.73	60.92	1.94

* Values were below the detection limit

2.4.5 Role of UV and visible light for the dFe(II) oxidation in open and coastal water

When comparing the dFe(II) oxidation rates in the control (dark) setup to the visible light setup in open ocean and coastal water, no significant differences were found (p = 0.894 in open ocean water; p = 0.145 in coastal water; **Supplementary Table 1** and **Supplementary Table 2**). This

was similarly described by Rijkenberg et al. (2005), where visible light (400 – 700 nm) had the least effect on dFe(II) oxidation. However, the findings after the UV treatment showed that the oxidation rate in coastal water was ten times faster and also significantly different to the treatment with visible light ($p = 0.001$ in coastal water and 0.004 in open ocean water; **Supplementary Table 1** and **Supplementary Table 2**). A potential reason may be that the UV exposure destroyed certain complexing ligands with the effect that they could not bind Fe any longer, leading to faster oxidation times (Gledhill and van den Berg, 1994, Pérez-Almeida et al., 2019). Another effect could have been the development of H_2O_2 during UV exposure (Millero and Sotolongo, 1989).

In open ocean water, the dFe(II) oxidation after the UV treatment happened at almost the same rate as under visible light conditions. This may be explained due to generally stronger binding ligands in open ocean water (Maldonado and Price, 1999). Additionally, it is also likely that there was less organic material such as CDOM (see **Table 2.6**) in the open ocean water. In the former case, it might have been that the ligands in the open ocean were not affected in the same way by a UV based degradation as coastal ligands, as shown by Rijkenberg et al. (2006). Higher spikes of a greater magnitude in dFe(II) concentrations after the UV treatment were recorded. These higher fluctuations could result from H_2O_2 production during UV radiation, which would have increased the dFe(II) oxidation rate as reported earlier (Millero and Sotolongo, 1989, Santana-Casiano et al., 2006).

2.4.6 Filtered vs. non-filtered open ocean water

The overall trend for effect of temperature on oxidation rate was the same in the filtered vs. non-filtered open ocean seawater, with the fastest oxidation rates again at 15°C and the lowest at 5°C . However, the overall $t_{1/2}$ of dFe(II) in the filtered water was seven times shorter than in the unfiltered water. Roy and Wells (2011) also compared filtered and unfiltered open ocean water from the subarctic Pacific Ocean but found little difference in the oxidation rate. For example, at 5 minutes, their calculated decay rate constant $\log k_{ox}$ was 2.44 in the filtered sample and 2.42 in the unfiltered samples. This is substantially different from the findings here, with a $\log k_{app}$ of 2.25 in the filtered seawater and 1.46 in the unfiltered seawater. These values may result from removed CDOM due to filtration and other particles leading to different compounds

in the sample water after filtration, which may not have been present in the water samples analysed by (Roy and Wells, 2011).

2.4.7 Role of pH in combination with temperature on the oxidation rate of dFe(II) in coastal and open ocean water

While temperature increased the oxidation rate of dFe(II), decreasing pH retarded oxidation during the acidification experiment in both mentioned water types. A Pearson's correlation between pH and temperature (see **Figure 2.7**) was computed to assess the relationship between pH and $t_{1/2}$ and temperature and $t_{1/2}$, respectively. For this test, the measured values of the 1st $t_{1/2}$ were used, including all dark, light and UV-light, filtered and unfiltered treatments and the CO₂ treatments (see **Table 2.3** and **Table 2.4**).

The results of the linear and Pearson correlations (**Figure 2.7**) suggest that pH in both water types had a greater impact on the $t_{1/2}$ compared to temperature. In open ocean water, the Pearson correlation coefficient had a strong significant negative correlation ($r = -0.80$, $p = 0.001$, $n = 78$). Coastal water also had a strong significant negative correlation for pH ($r = -0.669$, $p = 0.001$, $n = 45$). On the other hand, temperature showed weak correlations in both water types but was also negatively correlated. Therefore, we suggest that pH is the stronger driver for dFe(II) oxidation in the study region, considering various parameters as described above.

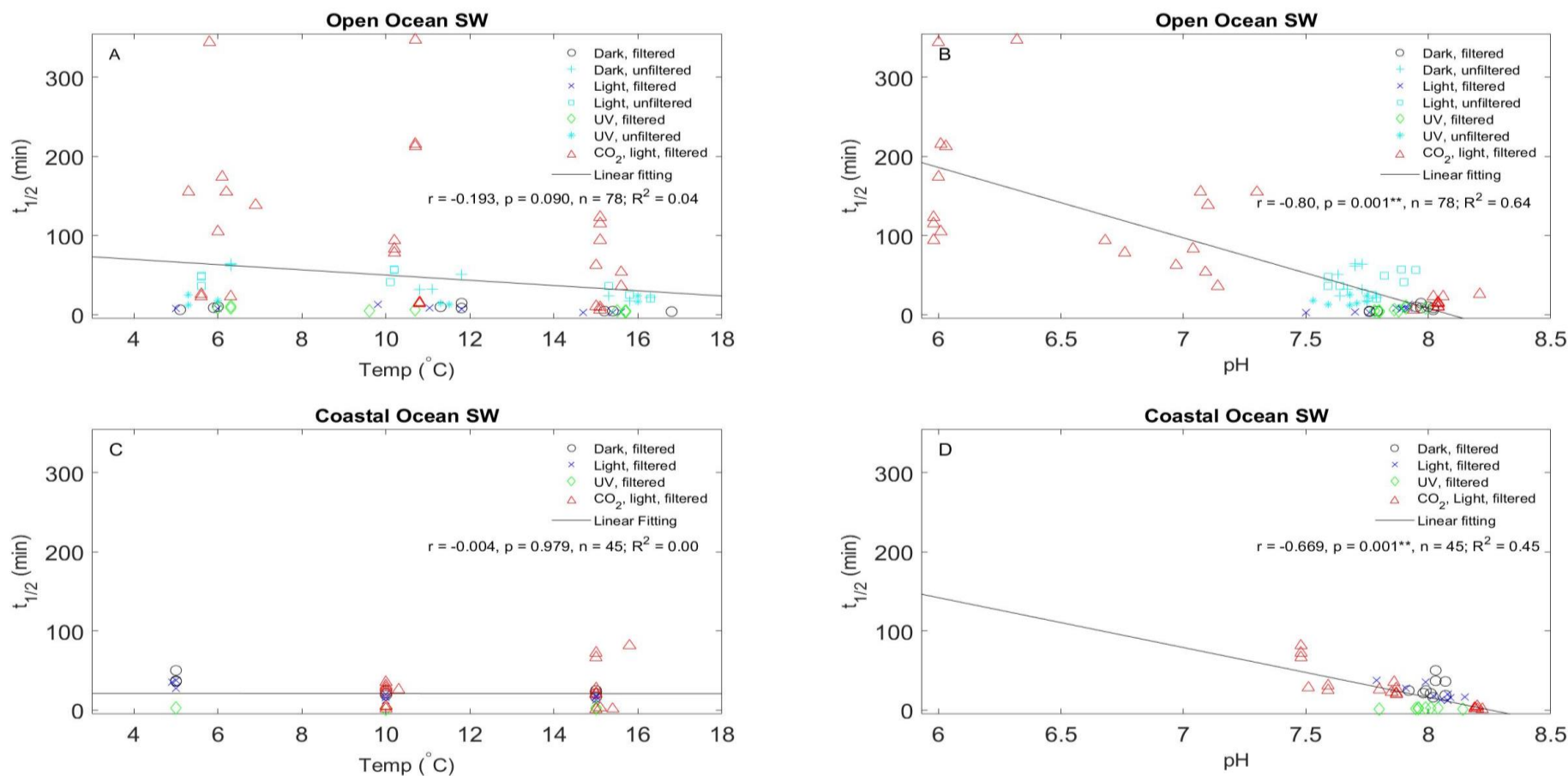


Figure 2.7 Scatterplots with Pearson correlation comparison of measured values from open (A, B) and coastal (C, D) seawater for temperature and $t_{1/2}$ (A, C) and pH and $t_{1/2}$ (B, D). In open ocean water dark (black), light (blue), UV (green), filtered, unfiltered (cyan) and CO₂ (red) treatments are considered. In coastal water no values for unfiltered water were assessed. The black line displays the linear fit for all values in each plot including the R^2 . The correlation coefficient r and its p -value and respective sample numbers n are also shown. P – values are significant at 0.01 level (2-tailed) and are marked with **.

2.4.8 Modelling and suggestions for future models

A continuously running, column-free setup allowed to trace dFe(II) oxidation in open and coastal water based on extended run-time lengths. A calculation suggested by Santana-González et al. (2018) (here equation 4) was utilised to compare whether the observations match the calculated data. Ionic strength, temperature, pH and salinity from **Table 2.2** and **Table 2.3** were used to compute k' . These values were then further applied to calculate the $t_{1/2}$ using equation 3. A second scatter plot was generated from those, and the Pearson correlation between the measured pH and temperature and their corresponding $t_{1/2}$ were computed (see **Figure 2.8**). Results show that the correlation trend for pH is also strong and significant in open ($r = -0.394$, $p = 0.002$, $n = 62$) and coastal water ($r = -0.749$, $p = 0.002$, $n = 39$) and temperature is also negative and significantly linked (open ocean $r = -0.718$, $p = 0.001$, $n = 62$; coastal ocean $r = -0.357$, $p = 0.026$, $n = 39$). Results using equation 4 however, do not compare to the observed natural values in some cases. For instance, filtered vs. unfiltered treatments displayed similar results when calculated using equation 4, while these results are significantly different to the measured values. Also, the data for dark, light, UV etc., are very similar from coastal to the open ocean water when modelled. This suggests that the calculation may be a good approach but does not take parameters such as particulates, CDOM, ligands or nutrients into consideration. For future approaches, incorporating these parameters for a realistic reflection of seawater conditions would be ideal.

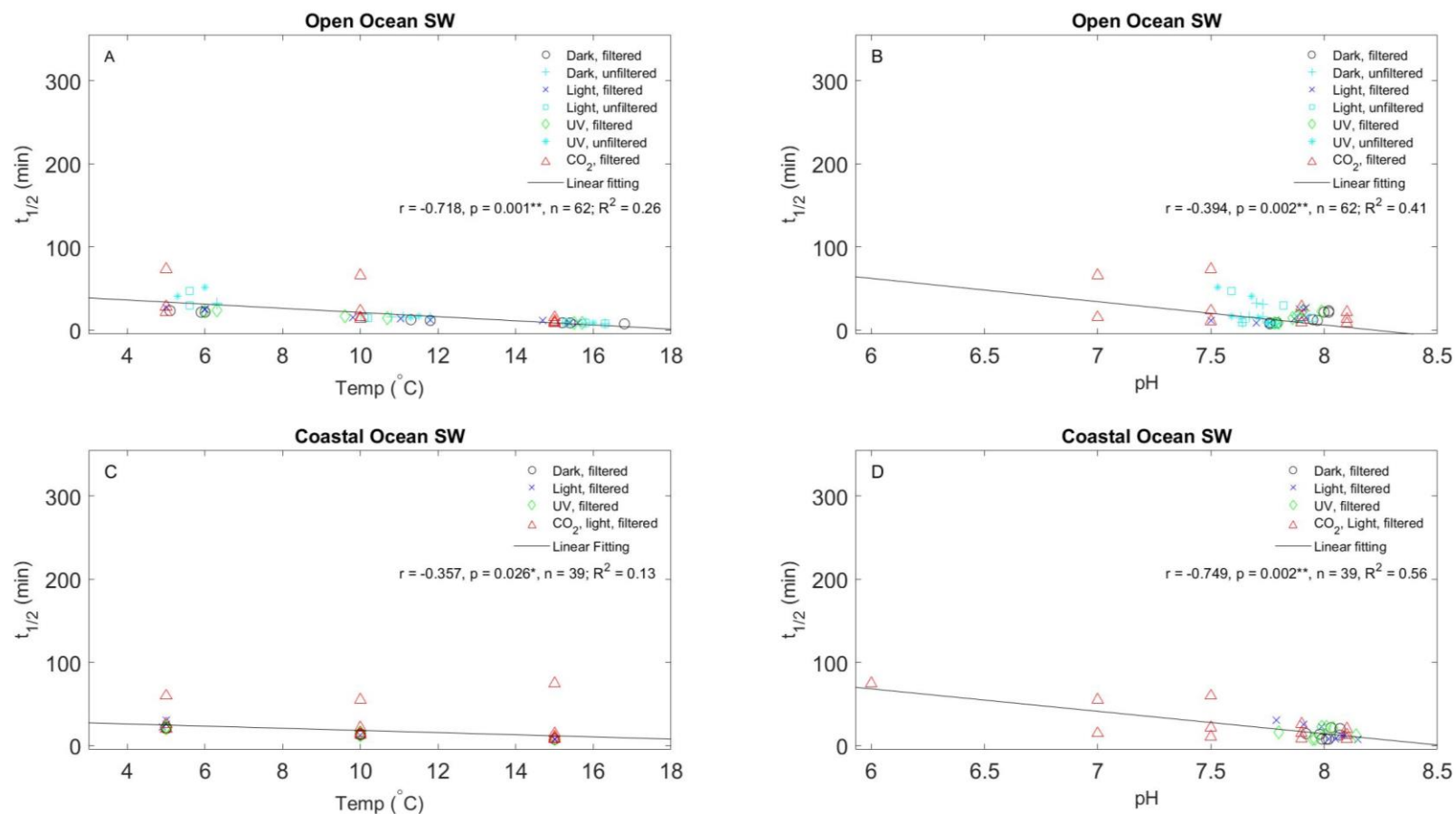


Figure 2.8 Scatterplots with Pearson correlation comparison of modelled values from open (A, B) and coastal (C, D) seawater for temperature and $t_{1/2}$ (A, C) and pH and $t_{1/2}$ (B, D). In open ocean water dark (black), light (blue), UV (green), filtered, unfiltered (cyan) and CO_2 (red) treatments are considered whereas in coastal water no values for unfiltered water were assessed. The black line displays the linear fitting for all values in each plot including the respective R^2 . The correlation coefficient r and its p -value and respective sample numbers n are also given below the legend. P – values are significant at 0.05 level (2-tailed) and are marked with * or ** for $p = 0.01$.

2.4.9 Results for the oxidation of dFe(II) at realistic values of pH and temperature

Since neither a temperature increase from 5°C to 15°C nor the pH decline from 8.1 to 6 is realistic under future climate change scenarios. Intermediate values for a temperature increase by 1°C and a pH decline of 0.2 units were chosen. This was based on the data obtained during the CO₂ experiment (**Table 2.3**). A change in temperature by 1°C in temperature and 0.2 for pH is also well within the proposed changes of sea surface temperature increase, and pH decrease suggested in model RCP8.5 by the latest ocean related IPCC report (Bindoff et al., 2019). By plotting the data (**Table 2.3**), the data for these realistic values were interpolated from measured data points (**Table 2.8**) for each temperature and targeted pH, as displayed in **Figure 2.9**.

Table 2.8 Summary of read out data obtained by using data from Table 2.3.

	pH	Temperature (°C)	t _{1/2} (min)
Coastal water	8.1	5	9.56
		10	3.7
		15	1.68
	8	5	21.4
		10	15.8
		15	11.7
	7.9	5	34.1
		10	27.9
		15	22.9
Open ocean water	8.1	5	23.7
		10	14.6
		15	8.73
	8	5	35.4
		10	20.6
		15	12.5
	7.9	5	49.6
		10	26.3
		15	18.3

Once all three variables from **Table 2.8** were plotted, a line was fitted, which was exponential for all data, except coastal ocean pH 7.9, which was polynomial (see **Figure 2.9**). The obtained functions were then used to calculate oxidation rates at temperatures between 0°C and 15°C. A complete list of the t_{1/2} from pH 8.1, 8 and 7.9 for the calculation input and output parameters with further detail can be found in **Supplementary Table 10**.

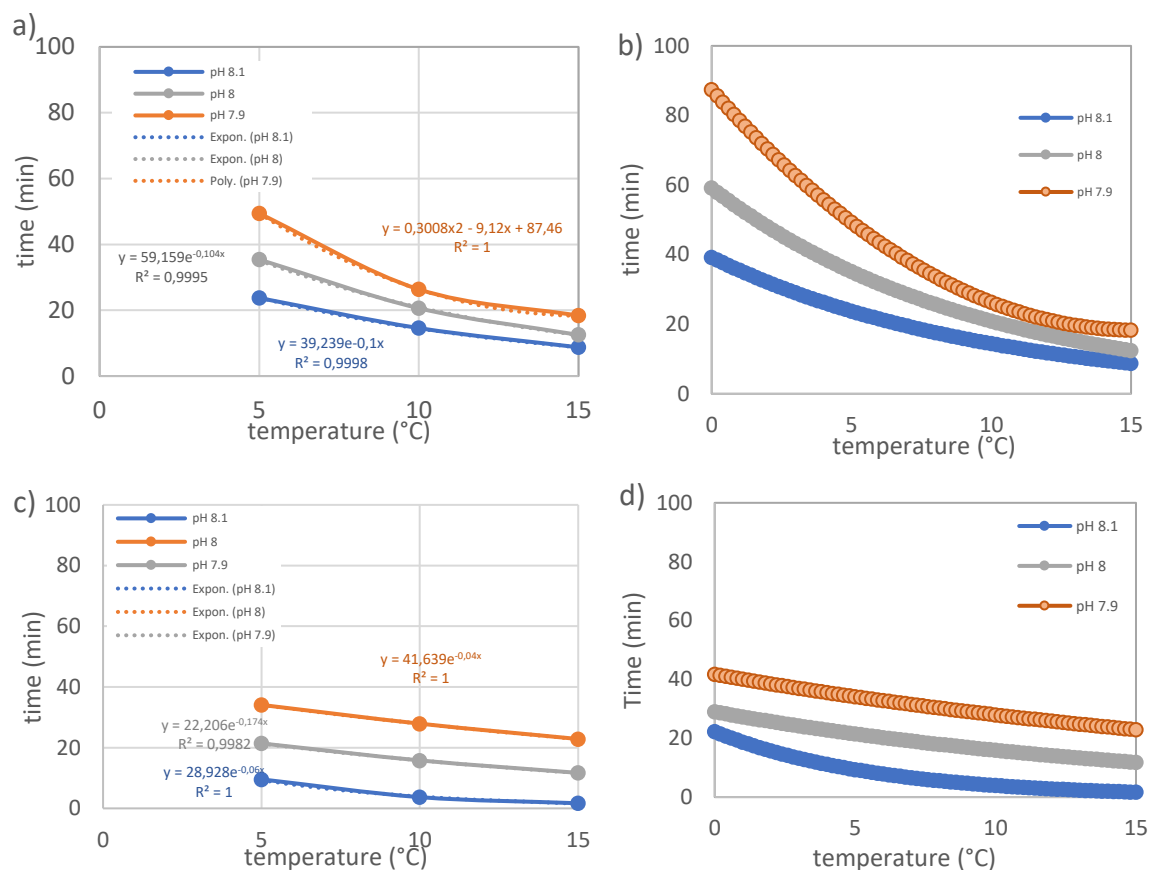


Figure 2.9 Coastal (a) and open ocean water (c) oxidation rates based on **Table 2.8** are displayed in the two left figures. Through these three points in a) and c), an exponential or polynomial function was obtained. This was applied and displayed in b) (open ocean) and d) (coastal).

These functions allowed for approximations of the $t_{1/2}$ based on the sampled seawater. The oxidation of $dFe(II)$ is two minutes faster for open ocean water (see **Figure 2.10**, ‘Open ocean’) when the temperature was raised by $1^\circ C$ from $5^\circ C$ to $6^\circ C$, but overall retarded by ~ 23 minutes once the pH was lowered from 8.1 to 7.9. In the coastal water, an increase by $1^\circ C$ from $5^\circ C$ to $6^\circ C$ shortened the $t_{1/2}$ by ~ 1 minute but increased it by 26 minutes when the pH was lowered to 7.9 (see **Figure 2.10**, ‘Coastal ocean’). In summary, when considering realistic values, $dFe(II)$ oxidations are more influenced by a change in pH than a temperature change.

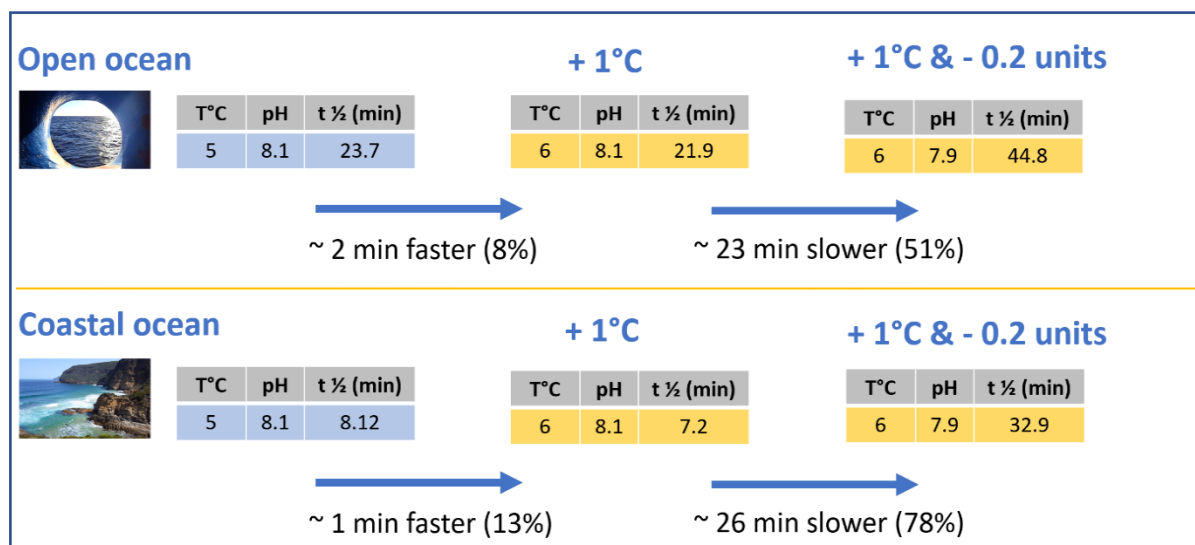


Figure 2.10 Summary of the oxidation of dFe(II) with an increase of 1°C and a decrease in pH by 0.2 units (right) based on measured values (**Supplementary Table 10**).

2.5 Conclusion

This study suggests that the dFe(II) oxidation in coastal areas is retarded due to higher concentrations of ligands and other trace elements than in the open ocean, as proposed in my first hypothesis. The second hypothesis dealt with whether pH or temperature changes will have a more significant impact on the dFe(II) oxidation. The findings indicate that a change in pH by 0.2 units will more significantly impact the oxidation of dFe(II) compared to impacts due to temperature changes for changes of 2°C and 0.2 units, respectively. Similar experiments were performed using filtered and unfiltered seawater and differing light schemes, to test the third hypothesis. The results revealed that filtered vs. unfiltered open ocean water was significantly different. Due to potentially removing larger particles and altering the oxygen concentration through filtration, it can be suggested that future studies should use unfiltered samples throughout if possible. This approach would also resemble natural conditions. Differences between light and UV exposure were observed and compared to the dark control. It was found that artificial light does not impact oxidation substantially. However, UV light led to a shortened $t_{1/2}$ in both tested environments (70% less in open ocean water, 10% less and elevated spikes in open ocean water), suggesting that organic matter plays some role in stabilising dFe(II). To

test hypothesis four, experimentally assessed data was compared to oxidation calculations developed in previous studies. The calculated results do not compare to the measurements, and an adjustment to incorporate other parameters might be necessary for future modelled approaches.

Overall, it can be concluded that changes in pH will have a greater impact in coastal areas on the dFe(II) oxidation rates in future climate scenarios, which could result in impacts of dFe(II) availability to phytoplankton. Extended half-lives for dFe(II) could theoretically make dFe(II) more accessible with likely benefits for certain phytoplankton species, which will be further discussed in Chapter 3.

2.6 Suggested improvements

Several steps would have been required to improve the FIA method after its modification for this chapter. For one, dimethylglyoxime (DMG) would have been added to my luminol solution when analysing for dFe(II), in order to exclude potential Co(II) interferences. Ideally, one would consider the observation of nanopyrite, which is a large portion of the dissolved Fe pool, which was not done here.

As for the larger setup, it would have been ideal to monitor temperature continuously, monitor & adjust O₂ continuously and adjust the pH to keep it constant. Through this, it would have been possible to compare oxidation rates in coastal and open water better. Also, a TRIS buffer instead of an NBS buffer would have been the better choice.

When considering UV treated water, it was brought to my attention that waiting for a minimum of 30 days is required for the sample to be in the dark in order for the ROS and created H₂O₂ to degenerate completely. In that respect, adding a H₂O₂-FIA system would have at this early stage would have helped as well.

As a last point, the choices of acidifying the pH of my two water samples (coastal and open ocean) were either 6, 7 and 8.1 or 7, 7.5 and 8.1. Ideally, these would have had the same pH, but I was limited with low Fe seawater, so I continued and thought of a way to calculate for more representative values of 7 and 7.5.

Acknowledgment

I would like to thank Nils Jansen for the analysis of the macronutrients in this study. Thank you also to Thomas Holmes, Pier van der Merwe, Manon Tonnard, Lavenia Ratnarajah, who helped sample ‘open ocean water’ during HEOBI (‘Heard-Earth-Ocean-Biosphere Interactions’). Thank you to Ashley Townsend, Melanie Gault-Ringold and Pauline Latour for their effort of doing the ICP-MS analysis.

This research was supported under Australian Research Council's Special Research Initiative for Antarctic Gateway Partnership (Project ID SR140300001). The Antarctic Climate & Ecosystems Cooperative Research Centre (ACE - CRC) and the Institute for Marine and Antarctic Studies (IMAS) provided additional funding and logistics.

2.7 References

- ANDREW, A. A., DEL VECCHIO, R., SUBRAMANIAM, A. & BLOUGH, N. V. 2013. Chromophoric dissolved organic matter (CDOM) in the Equatorial Atlantic Ocean: Optical properties and their relation to CDOM structure and source. *Marine Chemistry*, 148, 33-43.
- ARSENAULT, J., RENAUD, M. L. H., CLEMENT, M., FILLION, D., GUILLEMETTE, G., LEDUC, R., LAVIGNE, P. & ESCHER, E. 2007. Temperature-dependent variations of ligand-receptor contact points in hAT1. *Journal of peptide science: an official publication of the European Peptide Society*, 13, 575-580.
- BINDOFF, N., CHEUNG, W., KAIRO, J., ARÍSTEGUI, J., GUINDER, V., HALLBERG, R., HILMI, N., JIAO, N., KARIM, M., LEVIN, L. & ODONOGHUE 2019. Changing Ocean, Marine Ecosystems, and Dependent Communities. *IPCC Special Report on the Ocean and Cryosphere in a Changing Climate*.
- BLAIN, S., QUEGUINER, B., ARMAND, L., BELVISO, S., BOMBLED, B., BOPP, L., BOWIE, A., BRUNET, C., BRUSSAARD, C., CARLOTTI, F., CHRISTAKI, U., CORBIERE, A., DURAND, I., EBERSBACH, F., FUDA, J. L., GARCIA, N., GERRINGA, L., GRIFFITHS, B., GUIGUE, C., GUILLERM, C., JACQUET, S.,

- JEANDEL, C., LAAN, P., LEFEVRE, D., LO MONACO, C., MALITS, A., MOSSERI, J., OBERNOSTERER, I., PARK, Y. H., PICHERAL, M., PONDAVEN, P., REMENYI, T., SANDRONI, V., SARTHOU, G., SAVOYE, N., SCOUARNEC, L., SOUHOUT, M., THUILLER, D., TIMMERMANS, K., TRULL, T., UITZ, J., VAN BEEK, P., VELDHUIS, M., VINCENT, D., VIOLLIER, E., VONG, L. & WAGENER, T. 2007. Effect of natural iron fertilization on carbon sequestration in the Southern Ocean. *Nature*, 446, 1070-4.
- BLAIN, S. & TAGLIABUE, A. 2016. *Iron Cycle in Oceans*, John Wiley & Sons.
- BOWIE, A. R., ACHTERBERG, E. P., MANTOURA, R. F. C. & WORSFOLD, P. J. 1998. Determination of sub-nanomolar levels of iron in seawater using flow injection with chemiluminescence detection. *Analytica Chimica Acta*, 361, 189-200.
- BOWIE, A. R., LANNUZEL, D., REMENYI, T. A., WAGENER, T., LAM, P. J., BOYD, P. W., GUIEU, C., TOWNSEND, A. T. & TRULL, T. W. 2009. Biogeochemical iron budgets of the Southern Ocean south of Australia: Decoupling of iron and nutrient cycles in the subantarctic zone by the summertime supply. *Global Biogeochemical Cycles*, 23.
- BOWIE, A. R., SEDWICK, P. N. & WORSFOLD, P. J. 2004. Analytical intercomparison between flow injection-chemiluminescence and flow injection-spectrophotometry for the determination of picomolar concentrations of iron in seawater. *Limnology and Oceanography-Methods*, 2, 42-54.
- BOYD, R. W., WATSON, A. J., LAW, C. S. & ABRAHAM, E. R. 2000. A mesoscale phytoplankton bloom in the polar Southern Ocean stimulated by iron fertilization. *Nature*, 407, 695.
- BREITBARTH, E., BELLERBY, R., NEILL, C., ARDELAN, M. & MEYERH, M. 2010a. Ocean acidification affects iron speciation in seawater.
- BREITBARTH, E., BELLERBY, R. J., NEILL, C. C., ARDELAN, M. V., MEYERHOFER, M., ZOLLNER, E., CROOT, P. L. & RIEBESELL, U. 2010b. Ocean acidification affects iron speciation during a coastal seawater mesocosm experiment. *Biogeosciences*, 7, 1065-1073.
- BRULAND, K. W. & LOHAN, M. C. 2003. 6.02 - Controls of Trace Metals in Seawater. In: HOLLAND, H. D. & TUREKIAN, K. K. (eds.) *Treatise on Geochemistry*. Oxford: Pergamon.
- CALDEIRA, K. & WICKETT, M. E. 2003. Anthropogenic carbon and ocean pH. *Nature*, 425, 365-365.
- CROOT, P. L. & HELLER, M. I. 2012. The importance of kinetics and redox in the biogeochemical cycling of iron in the surface ocean. *Frontiers in Microbiology*, 3.
- CROOT, P. L. & LAAN, P. 2002. Continuous shipboard determination of Fe (II) in polar waters using flow injection analysis with chemiluminescence detection. *Analytica Chimica Acta*, 466, 261-273.
- CUTTER, G., CASCIOTTI, K., CROOT, P., GEIBERT, W., HEIMBUERGER, L. E., LOHAN, M. C., PLANQUETTE, H. & FLIERDT, T. 2017. Sampling and Sample-

- handling Protocols for GEOTRACES Cruises (Version 3).
<http://www.geotraces.org/images/stories/documents/intercalibration/Cookbook.pdf>.
- DE BAAR, H. J. & DE JONG, J. T. 2001. Distributions, sources and sinks of iron in seawater. *IUPAC series on analytical and physical chemistry of environmental systems*, 7, 123-254.
- DE JONG, J., DEN DAS, J., BATHMANN, U., STOLL, M., KATTNER, G., NOLTING, R. & DE BAAR, H. 1998. Dissolved iron at subnanomolar levels in the Southern Ocean as determined by ship-board analysis. *Analytica Chimica Acta*, 377, 113-124.
- DIAMOND, D. 2008a. Determination of nitrate/nitrite in brackish or seawater by flow injection analysis. *LaChat Instruments, Loveland, USA*, pp. 19.
- DIAMOND, D. 2008b. Determination of orthophosphate in brackish or seawater by flow injection analysis. *LaChat Instruments, Loveland, USA*, pp. 19.
- DONEY, S. C., FABRY, V. J., FEELY, R. A. & KLEYPAS, J. A. 2009. Ocean acidification: the other CO₂ problem. *Ann Rev Mar Sci*, 1, 169-92.
- DUCKLOW, H. W., STEINBERG, D. K. & BUESSELER, K. O. 2001. Upper ocean carbon export and the biological pump. *OCEANOGRAPHY - WASHINGTON DC - OCEANOGRAPHY SOCIETY*-, 14, 50-58.
- EMMENEGGER, L., SCHÖNENBERGER, R., SIGG, L. & SULZBERGER, B. 2001. Light-induced redox cycling of iron in circumneutral lakes. *Limnology and Oceanography*, 46, 49-61.
- GEIDER, R. J. & LA ROCHE, J. 1994. The role of iron in phytoplankton photosynthesis, and the potential for iron-limitation of primary productivity in the sea. *Photosynthesis research*, 39, 275-301.
- GLEDHILL, M. & VAN DEN BERG, C. M. 1994. Determination of complexation of iron (III) with natural organic complexing ligands in seawater using cathodic stripping voltammetry. *Marine Chemistry*, 47, 41-54.
- GONZÁLEZ-DAVILA, M., SANTANA-CASIANO, J. M. & MILLERO, F. J. 2005. Oxidation of iron (II) nanomolar with H₂O₂ in seawater. *Geochimica et Cosmochimica Acta*, 69, 83-93.
- GONZALEZ, A. G., SANTANA-CASIANO, J. M., PEREZ, N. & GONZALEZ-DAVILA, M. 2010. Oxidation of Fe(II) in Natural Waters at High Nutrient Concentrations. *Environmental Science & Technology*, 44, 8095-8101.
- HABER, F. & WEISS, J. 1932. Über die katalyse des hydroperoxydes. *Naturwissenschaften*, 20, 948-950.
- HANSARD, S. P. & LANDING, W. M. 2009. Determination of iron (II) in acidified seawater samples by luminol chemiluminescence. *Limnology and Oceanography: Methods*, 7, 222-234.
- HELLER, M. I., WUTTIG, K. & CROOT, P. L. 2016. Identifying the Sources and Sinks of CDOM/FDOM across the Mauritanian Shelf and Their Potential Role in the Decomposition of Superoxide (O₂⁻). *Frontiers in Marine Science*, 3.

- HOFFMANN, L. J., BREITBARTH, E., MCGRAW, C. M., LAW, C. S., CURRIE, K. I. & HUNTER, K. A. 2013. A trace-metal clean, pH-controlled incubator system for ocean acidification incubation studies. *Limnology and Oceanography: Methods*, 11, 53-61.
- HOLMES, T. M., WUTTIG, K., CHASE, Z., SCHALLENBERG, C., VAN DER MERWE, P., TOWNSEND, A. T. & BOWIE, A. R. 2020. Glacial and Hydrothermal Sources of Dissolved Iron (II) in Southern Ocean Waters Surrounding Heard and McDonald Islands. *Journal of Geophysical Research: Oceans*, 125, e2020JC016286.
- HOPWOOD, M. J., SANTANA-GONZÁLEZ, C., GALLEGU-URREA, J., SANCHEZ, N., ACHTERBERG, E. P., ARDELAN, M. V., GLEDHILL, M., GONZÁLEZ-DÁVILA, M., HOFFMANN, L., LEIKNES, Ø., SANTANA-CASIANO, J. M., TSAGARAKI, T. M. & TURNER, D. 2018. Fe(II) stability in seawater. *Biogeosciences Discuss.*, 2018, 1-29.
- HUTCHINS, D. A., WITTER, A. E., BUTLER, A. & LUTHER, G. W. 1999. Competition among marine phytoplankton for different chelated iron species. *Nature*, 400, 858-861.
- IPCC 2014. *IPCC, 2014: Climate change 2014: synthesis report. Contribution of Working Groups I, II and III to the fifth assessment report of the Intergovernmental Panel on Climate Change [Core Writing Team, R.K. Pachauri and L.A. Meyer (eds.)]. IPCC, Geneva, Switzerland, 151 pp.*, IPCC.
- JOHNSON, K. S., CHAVEZ, F. P. & FRIEDERICH, G. E. 1999. Continental-shelf sediment as a primary source of iron for coastal phytoplankton. *Nature*, 398, 697.
- JOHNSON, K. S., COALE, K. H., ELROD, V. A. & TINDALE, N. W. 1994. Iron photochemistry in seawater from the equatorial Pacific. *Marine Chemistry*, 46, 319-334.
- KING, D. W., LOUNSBURY, H. A. & MILLERO, F. J. 1995. Rates and mechanism of Fe (II) oxidation at nanomolar total iron concentrations. *Environmental science & technology*, 29, 818-824.
- KUMA, K. & MATSUNAGA, K. 1995. Availability of colloidal ferric oxides to coastal marine phytoplankton. *Marine Biology*, 122, 1-11.
- LANDRY, M., CONSTANTINOU, J., LATASA, M., BROWN, S., BIDIGARE, R. & ONDRUSEK, M. 2000. Biological response to iron fertilization in the eastern equatorial Pacific (IronEx II). III. Dynamics of phytoplankton growth and microzooplankton grazing. *Marine Ecology Progress Series*, 201, 57-72.
- LANNUZEL, D., BOWIE, A. R., REMENYI, T., LAM, P., TOWNSEND, A., IBISANMI, E., BUTLER, E., WAGENER, T. & SCHOEMANN, V. 2011. Distributions of dissolved and particulate iron in the sub-Antarctic and Polar Frontal Southern Ocean (Australian sector). *Deep Sea Research Part II: Topical Studies in Oceanography*, 58, 2094-2112.
- LIAO, N. 2008. Determination of ammonia in brackish or seawater by flow injection analysis. *LaChat Instruments Loveland, USA*, pp. 20.
- LIS, H., SHAKED, Y., KRANZLER, C., KEREN, N. & MOREL, F. M. 2015. Iron bioavailability to phytoplankton: an empirical approach. *The ISME journal*, 9, 1003-1013.

- MALDONADO, M. T. & PRICE, N. M. 1999. Utilization of iron bound to strong organic ligands by plankton communities in the subarctic Pacific Ocean. *Deep Sea Research Part II: Topical Studies in Oceanography*, 46, 2447-2473.
- MARTIN, J. H. 1990. Glacial-interglacial CO₂ change: The iron hypothesis. *Paleoceanography*, 5, 1-13.
- MARTIN, J. H., COALE, K., JOHNSON, K., FITZWATER, S., GORDON, R., TANNER, S., HUNTER, C., ELROD, V., NOWICKI, J. & COLEY, T. 1994. Testing the iron hypothesis in ecosystems of the equatorial Pacific Ocean. *Nature*, 371, 123-129.
- MARTIN, J. H. & GORDON, R. M. 1988. Northeast Pacific iron distributions in relation to phytoplankton productivity. *Deep Sea Research Part A. Oceanographic Research Papers*, 35, 177-196.
- MILLERO, F. J. 1989. Effect of ionic interactions on the oxidation of Fe(II) and Cu(I) in natural waters. *Marine Chemistry*, 28, 1-18.
- MILLERO, F. J. 1998. Solubility of Fe(III) in seawater. *Earth and Planetary Science Letters*, 154, 323-329.
- MILLERO, F. J. & IZAGUIRRE, M. 1989. Effect of ionic strength and ionic interactions on the oxidation of Fe (II). *Journal of Solution Chemistry*, 18, 585-599.
- MILLERO, F. J. & SOTOLONGO, S. 1989. The oxidation of Fe (II) with H₂O₂ in seawater. *Geochimica et Cosmochimica Acta*, 53, 1867-1873.
- MILLERO, F. J., SOTOLONGO, S. & IZAGUIRRE, M. 1987. The oxidation kinetics of Fe(II) in seawater. *Geochimica et Cosmochimica Acta*, 51, 793-801.
- MILLERO, F. J., YAO, W. & AICHER, J. 1995. The speciation of Fe (II) and Fe (III) in natural waters. *Marine Chemistry*, 50, 21-39.
- NELSON, N. B., SIEGEL, D. A., CARLSON, C. A., SWAN, C., SMETHIE JR, W. M. & KHATIWALA, S. 2007. Hydrography of chromophoric dissolved organic matter in the North Atlantic. *Deep Sea Research Part I: Oceanographic Research Papers*, 54, 710-731.
- OBATA, H., KARATANI, H. & NAKAYAMA, E. 1993. Automated determination of iron in seawater by chelating resin concentration and chemiluminescence detection. *Analytical Chemistry*, 65, 1524-1528.
- PÉREZ-ALMEIDA, N., GONZÁLEZ, A. G., SANTANA-CASIANO, J. M. & GONZÁLEZ-DÁVILA, M. 2019. Iron and copper redox interactions in UV-seawater: A kinetic model approach. *Chemical Geology*, 506, 149-161.
- PÖRTNER, H. O. 2002. Climate variations and the physiological basis of temperature dependent biogeography: systemic to molecular hierarchy of thermal tolerance in animals. *Comparative Biochemistry and Physiology Part A: Molecular & Integrative Physiology*, 132, 739-761.
- RIEBESELL, U., FABRY, V. J., HANSSON, L. & GATTUSO, J.-P. 2011. *Guide to best practices for ocean acidification research and data reporting*, Office for Official Publications of the European Communities.

- RIEBESELL, U., WOLF-GLADROW, D. & SMETACEK, V. 1993. Carbon dioxide limitation of marine phytoplankton growth rates. *Nature*, 361, 249-251.
- RIJKENBERG, M. J., GERRINGA, L. J., VELZEBOER, I., TIMMERMANS, K. R., BUMA, A. G. & DE BAAR, H. J. 2006. Iron-binding ligands in Dutch estuaries are not affected by UV induced photochemical degradation. *Marine Chemistry*, 100, 11-23.
- RIJKENBERG, M. J. A. 2005. Photochemistry and organic complexation of iron: Interactions in the Southern Ocean.
- RIJKENBERG, M. J. A., FISCHER, A. C., KROON, J., GERRINGA, L., TIMMERMANS, K., WOLTERBEEK, H. T. & DE BAAR, H. 2005. The influence of UV irradiation on the photoreduction of iron in the Southern Ocean. *Marine Chemistry*, 93, 119-129.
- ROY, E. G. & WELLS, M. L. 2011. Evidence for regulation of Fe(II) oxidation by organic complexing ligands in the Eastern Subarctic Pacific. *Marine Chemistry*, 127, 115-122.
- SAMPERIO-RAMOS, G., CASIANO, J. M. S. & DÁVILA, M. G. 2016. Effect of ocean warming and acidification on the Fe (II) oxidation rate in oligotrophic and eutrophic natural waters. *Biogeochemistry*, 128, 19-34.
- SANTANA-CASIANO, J., GONZALEZ-DAVILA, M. & MILLERO, F. 2006. The role of Fe (II) species on the oxidation of Fe (II) in natural waters in the presence of O₂ and H₂O₂. *Marine Chemistry*, 99, 70-82.
- SANTANA-GONZÁLEZ, C., GONZÁLEZ-DÁVILA, M., SANTANA-CASIANO, J. M., GLADYSHEV, S. & SOKOV, A. 2019. Organic matter effect on Fe (II) oxidation kinetics in the Labrador Sea. *Chemical Geology*, 511, 238-255.
- SANTANA-GONZÁLEZ, C., SANTANA-CASIANO, J. M., GONZÁLEZ-DÁVILA, M., SANTANA-DEL PINO, A., GLADYSHEV, S. & SOKOV, A. 2018. Fe(II) oxidation kinetics in the North Atlantic along the 59.5° N during 2016. *Marine Chemistry*.
- SCHALLENBERG, C., DAVIDSON, A. B., SIMPSON, K. G., MILLER, L. A. & CULLEN, J. T. 2015. Iron (II) variability in the northeast subarctic Pacific Ocean. *Marine Chemistry*, 177, 33-44.
- SCHLITZER, R. 2002. Carbon export fluxes in the Southern Ocean: results from inverse modeling and comparison with satellite-based estimates. *Deep Sea Research Part II: Topical Studies in Oceanography*, 49, 1623-1644.
- SHAKED, Y. 2008. Iron redox dynamics in the surface waters of the Gulf of Aqaba, Red Sea. *Geochimica Et Cosmochimica Acta*, 72, 1540-1554.
- SHARMA, V. K. & MILLERO, F. J. 1988. Oxidation of copper (I) in seawater. *Environmental science & technology*, 22, 768-771.
- SHARMA, V. K. & MILLERO, F. J. 1989. The oxidation of Cu(I) with H₂O₂ in natural waters. *Geochimica et Cosmochimica Acta*, 53, 2269-2276.
- SMETACEK, V., KLAAS, C., STRASS, V. H., ASSMY, P., MONTRESOR, M., CISEWSKI, B., SAVOYE, N., WEBB, A., D'OVIDIO, F. & ARRIETA, J. M. 2012. Deep carbon export from a Southern Ocean iron-fertilized diatom bloom. *Nature*, 487, 313-319.

-
- STOOKEY, L. L. 1970. Ferrozine-a new spectrophotometric reagent for iron.
- STRZEPEK, R. F., MALDONADO, M. T., HUNTER, K. A., FREW, R. D. & BOYD, P. W. 2011. Adaptive strategies by Southern Ocean phytoplankton to lessen iron limitation: Uptake of organically complexed iron and reduced cellular iron requirements. *Limnology and Oceanography*, 56, 1983-2002.
- THEIS, T. L. & SINGER, P. C. 1974. Complexation of iron (II) by organic matter and its effect on iron (II) oxygenation. *Environmental Science & Technology*, 8, 569-573.
- VAN DER MERWE, P. C., WUTTIG, K., HOLMES, T., TRULL, T., CHASE, Z., TOWNSEND, A., GOEMANN, K. & BOWIE, A. R. 2019. High lability Fe particles sourced from glacial erosion can meet previously unaccounted biological demand: Heard Island, Southern Ocean. *Frontiers in Marine Science*, 6, 332.
- VÖLKER, C. & TAGLIABUE, A. 2015. Modeling organic iron-binding ligands in a three-dimensional biogeochemical ocean model. *Marine Chemistry*, 173, 67-77.
- WELLS, M. L., PRICE, N. M. & BRULAND, K. W. 1995. Iron chemistry in seawater and its relationship to phytoplankton: a workshop report. *Marine Chemistry*, 48, 157-182.
- WU, J. & LUTHER III, G. W. 1996. Spatial and temporal distribution of iron in the surface water of the northwestern Atlantic Ocean. *Geochimica et Cosmochimica Acta*, 60, 2729-2741.
- WUTTIG, K., TOWNSEND, A. T., VAN DER MERWE, P., GAULT-RINGOLD, M., HOLMES, T., SCHALLENBERG, C., LATOUR, P., TONNARD, M., RIJKENBERG, M. J. & LANNUZEL, D. 2019. Critical evaluation of a seaFAST system for the analysis of trace metals in marine samples. *Talanta*.

Chapter 3: Effect of dissolved iron (II) and temperature on the growth of the Southern Ocean species *Fragilariopsis cylindrus* and *Phaeocystis antarctica*

This chapter was prepared to be published in the Journal *Polar Biology* after thesis submission.

Author list

Helene Aflenzer^{a,b,c*}, Linn Hoffmann^d, Kathrin Wuttig^a, Cristina Genovese^b, Andrew Bowie^{a,b}

Affiliations

^a Antarctic Climate and Ecosystems Cooperative Research Centre (ACE CRC), University of Tasmania, Private Bag 80, Hobart, Tasmania 7001, Australia

^b Institute for Marine and Antarctic Studies (IMAS), University of Tasmania, Private Bag 129, Hobart, Tasmania, Australia

^c Australian Research Council Gateway Partnership, University of Tasmania, Private Bag 80, Hobart, Tasmania 7001, Australia

^d Department of Botany, University of Otago, Dunedin 9054, New Zealand

***Corresponding Author.** E-mail: helene.aflenzer@utas.edu.au

Abstract

Iron (Fe) is a vital yet limiting element for phytoplankton growth in the Southern Ocean. Phytoplankton utilises Fe for essential processes such as the transport chain reaction during photosynthesis. Low concentrations of Fe limit primary production in large regions of the ocean and impact phytoplankton community structures. This has further implications for carbon export as phytoplankton converts atmospheric carbon dioxide into organic carbon and exports it to greater depths. This study investigated the impacts of temperature (3°C, 5°C and 7°C) and Fe(II) additions on growth of two Southern Ocean phytoplankton species *Fragilariopsis cylindrus* and *Phaeocystis antarctica* in coastal and open ocean water.

The growth rates for *P. antarctica* were significantly higher in the incubations with added iron compared to the ones without added iron in both waters (coastal and open ocean) at all temperatures tested. An increase in temperature from 3°C to 5°C did not significantly affect growth of this species, however a further increase to 7°C significantly increased the growth rates compared to the respective treatments at lower temperatures. For *F. cylindrus*, growth rates were also higher in the incubations with Fe(II) added, but the difference was only significant in the incubations at 7°C in both waters. Temperature did not affect the growth rate of *F. cylindrus* except for a significant decrease in coastal waters without iron added at 7°C.

Keywords: *Fragilariopsis cylindrus*, Iron, Ocean Warming, *Phaeocystis antarctica*, Southern Ocean

3.1 Introduction

The Southern Ocean (SO) contributes ~ 33 % of global carbon (C) export from the atmosphere to the deep ocean (Arrigo et al., 1999, Schlitzer, 2002). It is characterised by its richness in macronutrients such as nitrate (NO_3^-) and phosphate (PO_4^{3-}) and its growth limiting iron (Fe) concentrations, leading to the definition of a High Nutrient Low Chlorophyll area (HNLC). Concentrations of Fe in the SO are usually < 1 nM (Sedwick et al., 1997, Bowie et al., 2002) and can range from 0.7 nM in deeper waters (Boye et al., 2001) to < 0.2 nM in surface open ocean water (Schallenberg et al., 2018). In contrast, coastal areas, which extend from landmasses to the continental shelf, may be rich in Fe due to higher flux from a greater variety of sources (e.g. atmospheric supply, sea ice melt or sediment leaching (Tagliabue et al., 2017)).

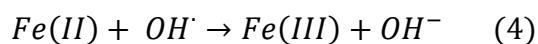
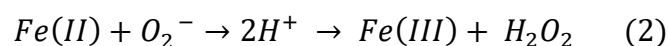
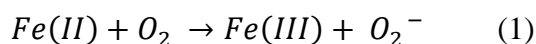
Iron is crucial for phytoplankton growth in the oceans due to its essential role in photosynthesis and respiration. Phytoplankton growth is controlled by Fe bioavailability, which is especially low in the SO (Martin et al., 1990). Most of the Fe in seawater is bound to strong ligands (L), which aids in keeping Fe from forming particles and sinking to depth, therefore allowing a more consistent supply of Fe to phytoplankton (Hunter and Boyd, 2007, Maldonado and Price, 1999, Shaked and Lis, 2012).

The uptake of Fe by phytoplankton is described as a two-step process of Fe reduction from dFe(III) to Fe(II) followed by transport across the cell membrane (Maldonado and Price, 2001). This can be further distinguished into the use of transporter compounds like siderophores, the use of Fe(II) transporters which carry Fe(II) across the membrane through oxidation, and a third option in which dFe(III) is initially reduced to Fe(II) at the cell surface before it can be transported into the cell via transporters using oxidation (Morel et al., 2008, Yeala et al., 2005, Salmon et al., 2006).

Iron is not available for phytoplankton in all chemical forms. Dissolved Fe (dFe) is often considered a proxy for the 'bioavailable' form (Hassler and Schoemann, 2009, Trimborn et al., 2017a, Lis et al., 2015, Shi et al., 2010, Kuma and Matsunaga, 1995, Rich and Morel, 1990, Shaked and Lis, 2012). Of the two main Fe redox species (dFe(II) and dFe(III)), dFe(III) is generally more thermodynamically stable in seawater at its current pH of ~ 8.1. In contrast, dFe(II) is transitory due to its rapid oxidation to dFe(III), which makes it challenging to measure (Croot and Laan, 2002, Bowie et al., 2002, King et al., 1995, Hansard and Landing, 2009).

Besides this, it is assumed that freely available dFe(II) is the favoured Fe species used by phytoplankton, reflected in its preferred form during uptake described above.

The oxidation rate of dFe(II), and therefore the period it is available to phytoplankton, is linked to parameters such as oxygen (O₂) and hydrogen peroxide (H₂O₂) concentrations, temperature and pH (equations 1 - 4; Millero et al., 1987, Millero and Sotolongo, 1989, Millero and Izaguirre, 1989, Moffett and Zika, 1987, Haber and Weiss, 1932). In seawater, most Fe exists in the oxidized form dFe(III) when there is O₂ present (Noffke et al., 2012). In contrast, dFe(II) occurs in sub-nanomolar ranges, which is equal to only 4-13% of the Fe in open ocean surface waters (Bowie et al., 2002) but can be much higher in coastal areas (>1 nM) due to leaching from sediments (Kuma et al., 1992).



To summarise, seawater temperature and pH have direct impacts on Fe chemistry and Fe bioavailability. For this study however, the focus was temperature, as there remain important unanswered questions around temperature impacts on SO phytoplankton species.

Seawater temperatures have already increased by 0.85°C since the industrial revolution due to the enhanced emission of greenhouse gases into the atmosphere and are predicted to rise a further 1.5 – 3°C by the end of the century (Bindoff et al., 2019). This significant increase will impact many marine organisms, including phytoplankton. Each species of these single-celled organisms has its own thermal tolerance window (Pörtner, 2002, Boyd, 2019). Ocean warming will directly impact species composition (Lacour et al., 2017; Noiri et al., 2005), extending to different ocean environments such as the coastal and open ocean.

Here, the growth of two SO phytoplankton species in open ocean and coastal seawater were compared to see if a change in temperature affects growth under the two assumptions that growth itself is affected by temperature (1), and there is less Fe available in the form of dFe(II) upon increasing temperatures due to increased oxidation rates (2). Therefore, two important SO

species, *Phaeocystis antarctica* and *Fragilariopsis cylindrus* at 3°C, 5°C and 7°C, were cultured for two weeks in Fe-rich coastal water and Fe-poor open ocean water (**Figure 3.1**).

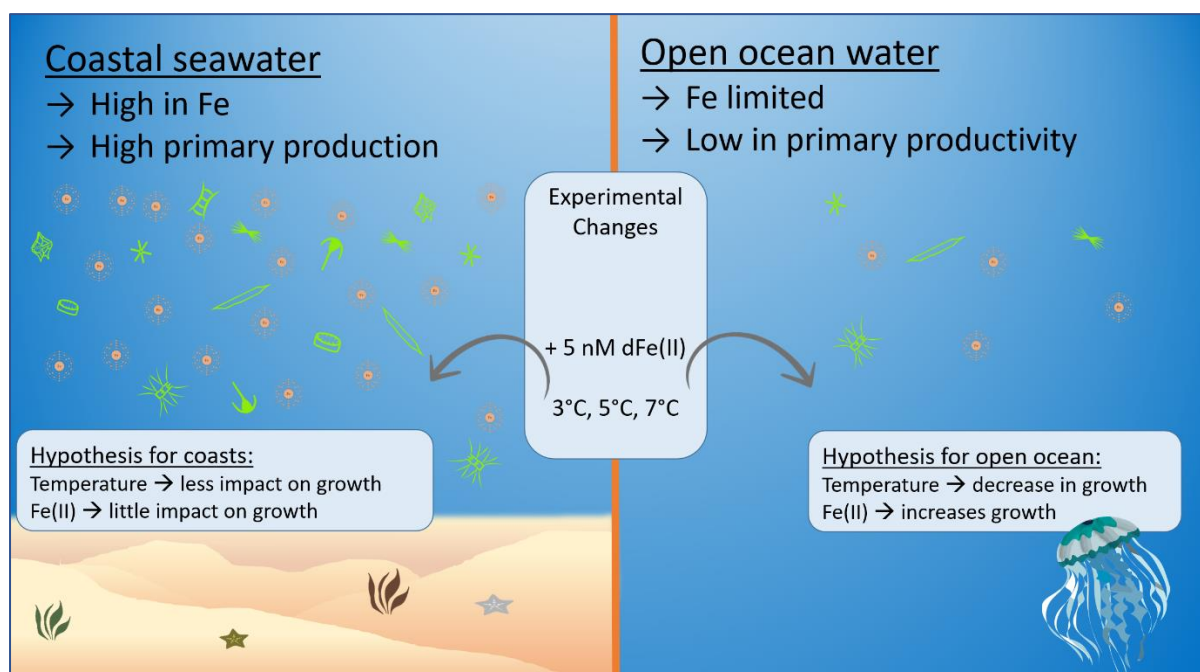


Figure 3.1 Experimental hypothesis for coastal and open ocean water from the SO, showing respective Fe concentrations and resulting primary production.

Antarctic phytoplankton increases its photosynthetic rates over a wide range of temperatures (-0.8°C to 7°C; Neori and Holm-Hansen, 1982). However, these rates are not transferable to growth rates and the increase in photosynthetic activity also only holds true when species are acclimated slowly and enough time for adaptation is given. In this study, growth rates were observed and how these changed from the starting temperature of 3°C, to which the species were acclimated. The temperatures were then increased to 5°C and 7°C, without a slow adjustment of temperature. *Phaeocystis antarctica* is known to have its best growth performance between 5°C and 6°C (Boyd, 2019, Andrew et al., 2019). The optimum temperature for *Fragilariopsis cylindrus* is 5°C (Fiala and Oriol, 1990) unless acclimated for an extended time (3 months or longer; e.g. Mock and Hoch, 2005). During these experiments, the cultures were only acclimated for 5 days. However, this was not deemed as detrimental to the experiments as they intended to look at the combined effects of temperature and dFe(II) addition between the two environments.

In open ocean water, it is expected that an increase in temperature would lead to a decrease in growth for both species because of a combination of a direct negative effect of warmer temperatures crossing outside the optimal thermal window, combined with lower dFe(II) availability, in the already low Fe waters. It was further expected that dFe(II) additions in this water would reduce the negative effect of increasing temperatures on growth. In contrast, it was expected that there would be less impact on growth from increased temperatures in coastal water due to high Fe concentrations, and therefore also no further enhancement of growth upon the addition of freely available dFe(II).

This experiment provides an insight into phytoplankton dFe(II) utilization and changes to Fe speciation under future ocean warming scenarios, with implications for community assemblages in a warmer SO.

3.2 Methods

3.2.1 Experimental overview

Fragilariopsis cylindrus and *Phaeocystis antarctica* were grown in coastal and in open ocean seawater under differing temperature and Fe conditions in 28 mL polycarbonate (PC) screw-capped vials (Thermo Fisher). This closed small-vessel system allowed us to measure growth rates without opening the sample vials during the experiment and limit Fe contamination. This was enabled due to the perfect fit of these vials into the Turner instrument (Model 10-AU), measuring *in vivo* chlorophyll-*a* (Chl-*a*) fluorescence (Designs Model 10-AU, also see section 3.3.2). Another advantage of this closed system is, that the overall Fe concentrations were not altered, allowing us to observe the Fe addition effect directly. After inoculating 600 μ L of either *P. antarctica* or *F. cylindrus* cultures into the vials, they were placed into a rack in a cold room at 3.2 ± 0.6 °C for 16 days and in two temperature blocks for $5^\circ\text{C} \pm 0.5^\circ\text{C}$ and $7^\circ\text{C} \pm 0.5^\circ\text{C}$ ($n = 5$), respectively (see **Figure 3.2**). To three vials from each treatment, 5 nM dFe(II) was added while the remaining three were incubated in the unaltered coastal and open ocean water.

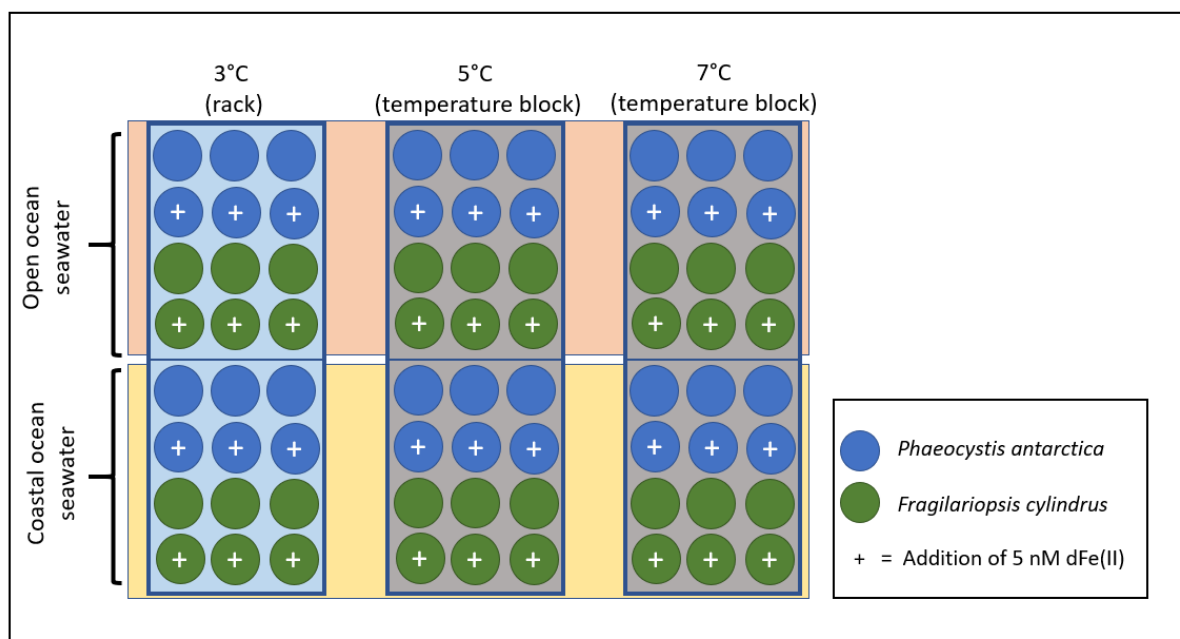


Figure 3.2 Experimental overview: Growth rate experiment at 3°C (left), 5°C (middle) and 7°C (right) for *Phaeocystis cylindrus* (blue) and *Fragilariopsis cylindrus* (green); with and without an addition (+) of 5 nM dFe(II) in coastal (shaded in yellow) and open ocean water (shaded in red).

3.2.2 Cleaning

All processing and sampling was carried out under an ISO class-5 laminar airflow hood in a 3°C cold room. Trace metal clean protocols (Cutter *et al.*, 2017) were used to prevent trace metal contamination. This included initial 2% Decon baths, followed by thorough rinses with ultra-high pure water (UHP, Barnstead, 18.2 MΩ). After washing all equipment in a 6 M hydrochloric acid (HCl; in-house distilled acid using a Savillex perfluoroalkoxy-polymer (PFA) still, DST-1000) bath for one month, everything was rinsed seven times with UHP water. Three initial preconditioning rinsing steps were done with the respective seawater used for the experiments for each vial. The pipette tips were sterile microwaved for five minutes in UHP water to prevent bacterial contamination for further culture work. This was followed by three HCl acid (distilled) and seven UHP water rinses.

3.2.3 Seawater

The coastal seawater was collected from Kingston beach (Kingston seawater, KISW, 42° 98'S, 147° 32'E directly from the jetty), Tasmania in January 2018. An acid cleaned 400 μm mesh was used to prefilter any large grazers and particles before 0.2 μm filtration (PALL, Acropak 200) under an ISO class-5 laminar flow hood into a trace metal clean carboy (Nalgene, 20 L, low density polyethylene (LDPE)). The open ocean water was collected along the SR3-GEOTRACES voyage in the SO on board of the *RV Investigator* in January/February 2018, using a trace metal rosette as described in Holmes et al. (2019) at an open ocean station (55.93° S, 140.41°E, from between 100 and 700 m depths). The open ocean water was 0.2 μm filtered (PALL, Acropak 200) directly on board. Both water types were stored for aging in large containers (Nalgene, 20 L, LDPE) in the dark at 4°C for at least a month prior to the experiments to ensure the complete oxidation of dFe(II), which usually happens within minutes to hours (Millero *et al.*, 1987).

3.2.4 Study organisms

The haptophyte *Phaeocystis antarctica* and the diatom *Fragilariopsis cylindrus* were collected and isolated from Antarctic pack ice (Davis station, East Antarctica) in 2015. Both cultures were grown under cool white fluorescent light (50 $\mu\text{mol photon m}^{-2} \text{s}^{-1}$, 12:12 D/L cycle, Osram) at 2°C \pm 1°C prior to the experiment. *Phaeocystis antarctica* was cultured in L1 (Guillard and Hargraves, 1993) medium, while the diatom *F. cylindrus* was kept in Aquil (Morel et al., 1979; Price et al., 1989) medium before they were inoculated into two distinct seawaters (coastal and open ocean). Both species were washed in either coastal or open ocean seawater three times to reduce the amount of ethylenediaminetetraacetic acid (EDTA) left from either L1 or Aquil. The final residual concentrations of EDTA for the experiments using *P. antarctica* was calculated to be 0.8 nM and 0.7 nM for *F. cylindrus*, respectively.

3.2.5 Temperature, pH and salinity

The seawater temperatures in the rack and the temperature block were measured daily using a built-in pH meter probe (Hach HQ40D, probe no. PHC10101). The seawater's salinity and pH were measured initially at 20°C using a conductivity probe (Orion 013005MD, Thermo scientific) and the same pH meter.

3.2.6 Macronutrients

Before the experiment, samples from coastal and open ocean water were filtered through a 0.2 μm syringe filter (PES, Millex GP) into PC vials (15 mL) and frozen at -80°C until analysis. PO_4^{3-} , NO_3^- and silicate (SiO_4^{2-}) concentrations were measured within 12 months of sampling, using a 4 channel LACHAT Quick-Chem 8500 auto analyzer, following the Quick-Chem-methods by Diamond (2008a), Diamond (2008b) and Liao (2008).

3.2.7 Trace elements

Samples for dissolved trace metals (cadmium (Cd), cobalt (Co), copper (Cu), Fe, gallium (Ga), manganese (Mn), nickel (Ni), lead (Pb), titanium (Ti), vanadium (V), and zinc (Zn)) were taken in 125 mL LDPE bottles (Nalgene; 0.2 μm filtered, Millex, GP), acidified with distilled HCl to pH 1.8 and stored for a month. The dissolved trace metal concentrations were determined using an offline combination of a seaFAST S2 pico (ESI, Elemental Scientific, USA) multi-element extraction system with a Nobias Chelate-PA1 column, followed by analysis on a sector field inductively coupled plasma mass spectrometer (SF-ICPMS, Element 2 Thermo Fisher Scientific, Inc.; Wuttig et al., 2019). The preconcentration factor 53.33 was achieved by preconcentrating 40 mL of inline buffered sample onto a Nobias PA1 column. Afterwards, the column was eluted with 750 μL of 1.7 M distilled nitric acid (HNO_3). The data was blank corrected by subtracting three acidified (2%, HCl) UHP water blanks treated the same way as the samples. The blank was corrected by subtracting one blank from acidified UPW water. The detection limit for Fe was three times (Σ) of the blank. Mixed multi-element standards were used for SF-ICP-MS tuning and calibrations (MISA Solutions, 100 μg , VHG Labs, USA; solutions 1 and 6 (Wuttig et al., 2019). In-house seawater collected during a voyage in the SO was used as an internal standard during SF-ICP-MS analysis. This in house seawater was added to standards and samples via the elution acid to obtain a final concentration of 10 $\mu\text{g/L}$.

3.2.8 Voltammetry

A voltammetric technique for the determination of Fe binding organic ligand concentration in two oceanic water types (Competitive Ligand Exchange-Adsorptive Cathodic Stripping voltammetry, CLW-AdCSV) was applied. The system (757 VA Computrace, Metrohm, Switzerland) is characterized by a hanging mercury drop electrode, a glassy carbon counter

electrode, and a silver/silver chloride reference electrode (provided with an inner electrode submerged in a 3 M KCl solution, Metrohm) which acts as bridge electrolyte. A 2-(2-Tiazolylazo)-p-cresol (TAC) solution was used as the competing ligand (Croot and Johansson, 2000). A buffered seawater solution was mixed using 100 μ L of a 1 M stock EPPS buffer solution added to 20 mL seawater. Additions of Fe were made from a 10 mM Fe(III) stock in 1% Q-HCl ranging from 0 to 20.4 nM. After equilibrating for 3 hours, 100 μ l of a 0.01 M TAC solution was added into each Teflon vessel. After overnight equilibration, all vessels were analysed following procedures outlined in Croot and Johansson (2000).

Data (dFe concentrations and relative peak height (intensity, nA)) were measured using the software ProMCC (Omanović et al., 2015). The values of $\alpha'_{Fe'TAC2}$ and $K'_{Fe'TAC2}$ were obtained from seawater salinity (Croot and Johansson, 2000). The Langmuir/Gerringa (Gerringa et al., 1995) and Ruzic/van den Berg (Ružić, 1982, Van den Berg, 1982) methods were used for the simultaneous calculations of total concentration and conditional stability constants to determine the natural Fe-binding organic ligand fraction. DFe values derived from earlier SF-ICP-MS analysis were used for the calculations. Ancillary parameters were further calculated: The excess ligand concentration (L') is calculated as the difference between L and dFe concentrations. The inorganic Fe concentration (Fe') was calculated according to equation 5.

$$K'_{Fe'L}(Fe')^2 + (1 + K'_{Fe'L}(L)) - K'_{Fe'L}(dFe)(Fe') - (dFe) = 0 \quad (5)$$

The concentration of organically-bound Fe, expressed as percentage, was calculated as %FeL = 100 ([dFe]-[Fe'])/[dFe]. The side reaction coefficient for Fe complexation with the natural ligand ($\log \alpha'_{Fe'L}$) was obtained as the logarithmic sum between $K'_{Fe'L}$ and L.

3.2.9 Growth rates

Growth rates were derived by using *in vivo* Chl-*a* fluorescence (Turner Designs Model 10-AU). The 28 mL vials were dark-adapted for 10 minutes and cooled on ice during the time of measurement. The specific growth rates (μ ; d^{-1}) were calculated from linear regressions of each replica of the Ln *in vivo* fluorescence or cell counts versus time (t) for exponentially growing cultures, where N_0 and N_1 are the densities at the beginning and end of an exponential growth phase (equation 6).

$$\ln N_1 = \ln N_0 + \mu(t_1 - t_0) \quad (6)$$

Irradiance was $50 \pm 5 \mu\text{mol photons m}^{-2}\text{s}^{-1}$, measured with a 4π quantum sensor (model QSL2100, Biospherical Instruments) in a 12:12 Dark/Light cycle.

3.2.10 Statistical analysis

All statistical analyses were conducted using IBM SPSS (version 27). ANOVAs were used to assess the impacts of different Fe sources on the growth rate (natural vs. additions of 5 nM dFe(II)) and the impact of temperature between the different environments. For specific information on each temperature and natural or dFe(II) additions, a pairwise comparison of variables was undertaken using a Tukey post hoc test derived from a MANOVA. All testing was done at the 95% confidence level and is summarised in **Supplementary table 11**.

3.3 Results

3.3.1 Seawater

Salinity in coastal seawater was 35.5 ± 0.05 and 36.2 ± 0.04 for open ocean water. At 20°C , pH in coastal water was 8.01 ± 0.0 and 7.9 ± 0.0 in open ocean water (**Table 3.1**). The nutrient concentrations in the open ocean seawater were $19.6 \mu\text{M}$ for NO_3^- and $1.3 \mu\text{M}$ for PO_4^{3-} . This corresponds to a nitrogen (N) : phosphate (P) ratio of 15.2:1, which is close to the Redfield ratio of 16:1. The coastal concentrations for NO_3^- were $0.37 \mu\text{M}$ and $0.32 \mu\text{M}$ for PO_4^{3-} (ratio: 1.15:1). Silicate concentrations were $22.5 \mu\text{M}$ in open ocean water. No values of SiO_4^{2-} were assessed for coastal waters. High ammonia (NH_4^+) values were measured in the open ocean water ($3.06 \mu\text{M}$) compared to $0.25 \mu\text{M}$ in the coastal water. Except for Cd, V and Ni, all trace metals analysed were higher in the coastal water when compared to the open ocean water. This is especially accentuated for Fe, Mn, Pb, and Zn (**Table 3.1**).

Table 3.1 Salinity (n = 3), pH (n = 3), dissolved trace metal and nutrient composition of surface (0 -15 m) coastal and open ocean water.

		Coastal ocean	Open ocean	Ratio
Salinity		35.50 ± 0.05	36.2 ± 0.04	1:1
pH		8.01 ± 0.00	7.90 ± 0.01	1:1
Tracemetals (nM/L, n = 1)	Cd	0.18	0.90	0.2:1
	Co	0.11	0.04	2.9:1
	Cu	6.45	1.31	5:1
	Fe	12.18	0.15	81.2:1
	Ga	0.05	0.01	10.8:1
	Mn	6.20	0.29	34.2:1
	Ni	3.53	7.26	0.5:1
	Pb	0.87	0.01	79:1
	Ti	0.20	0.03	6.6:1
	V	35.10	33.70	1:1
Zn	41.85	4.91	8.5:1	
dFe(II)	Fe ²⁺ *	5.00	5.00	1:1
Macronutrients	NO ₃ ⁻	0.37	19.64	0.02:1
	PO ₄ ³⁻	0.32	1.29	0.25:1
	SiO ₄ ²⁻	-	22.47	-
	NH ₄ ⁺	3.06	0.25	12.25:1

* 5 nM ammonium Fe(II) sulphate hexahydrate [(NH₄)₂Fe(SO₄)₂·6H₂O] was added to the +Fe treatment

3.3.2 Growth rates

Growth response to different temperatures and dFe(II) in coastal and open ocean water

Phaeocystis antarctica had its highest growth rates in coastal water at 7°C (0.31 ± 0.01; n = 3) when no Fe was added (**Figure 3.3**). This is significantly higher compared to growth at 3°C (0.26 ± 0.01, n = 3; p = 0.05) but not significantly different from growth at 5°C (0.25 ± 0.02, n = 3; p = 0.679) (**Supplementary Table 11**). In open ocean water without the addition of Fe, *P. antarctica* grew best at 7°C (0.29 ± 0.04) which was not significantly different to growth at 3°C (0.24 ± 0.01, n = 3; p = 0.164) but significantly different to growth at 5°C (0.18 ± 0.01, n = 3, p = 0.005, **Figure 3.3**). The highest growth rates of *F. cylindrus* in coastal water without Fe added was found at 3°C (0.20 ± 0.03, n = 3), which did not differ significantly from 5°C (0.20 ± 0.03, n = 3; p = 0.99) and decreased significantly to 0.05 ± 0.06 when incubated at 7°C compared to 3°C (p = 0.010). In open ocean water without Fe added, *F. cylindrus* also grew best at 3°C (0.25 ± 0.02, n = 3) and did not change significantly when grown at 5°C and 7°C (0.22 ± 0.02 and 0.22 ± 0.04, respectively). For *P. antarctica*, the growth rates in coastal water at 3°C and 5°C with the dFe(II) addition were the same at 0.31 ± 0.02. However, there was a

significant increase from 3°C to 7°C with rates of 0.43 ± 0.04 ($n = 3$; $p = 0.040$) in coastal water. In open ocean waters, the growth improved even more with the addition of dFe(II) at 7°C (0.48 ± 0.04), which was significantly higher compared to the growth rates at 3°C (0.33 ± 0.03 , $p = 0.005$) but not significantly different when comparing growth between 3°C and 5°C (0.35 ± 0.02 , $p = 0.775$).

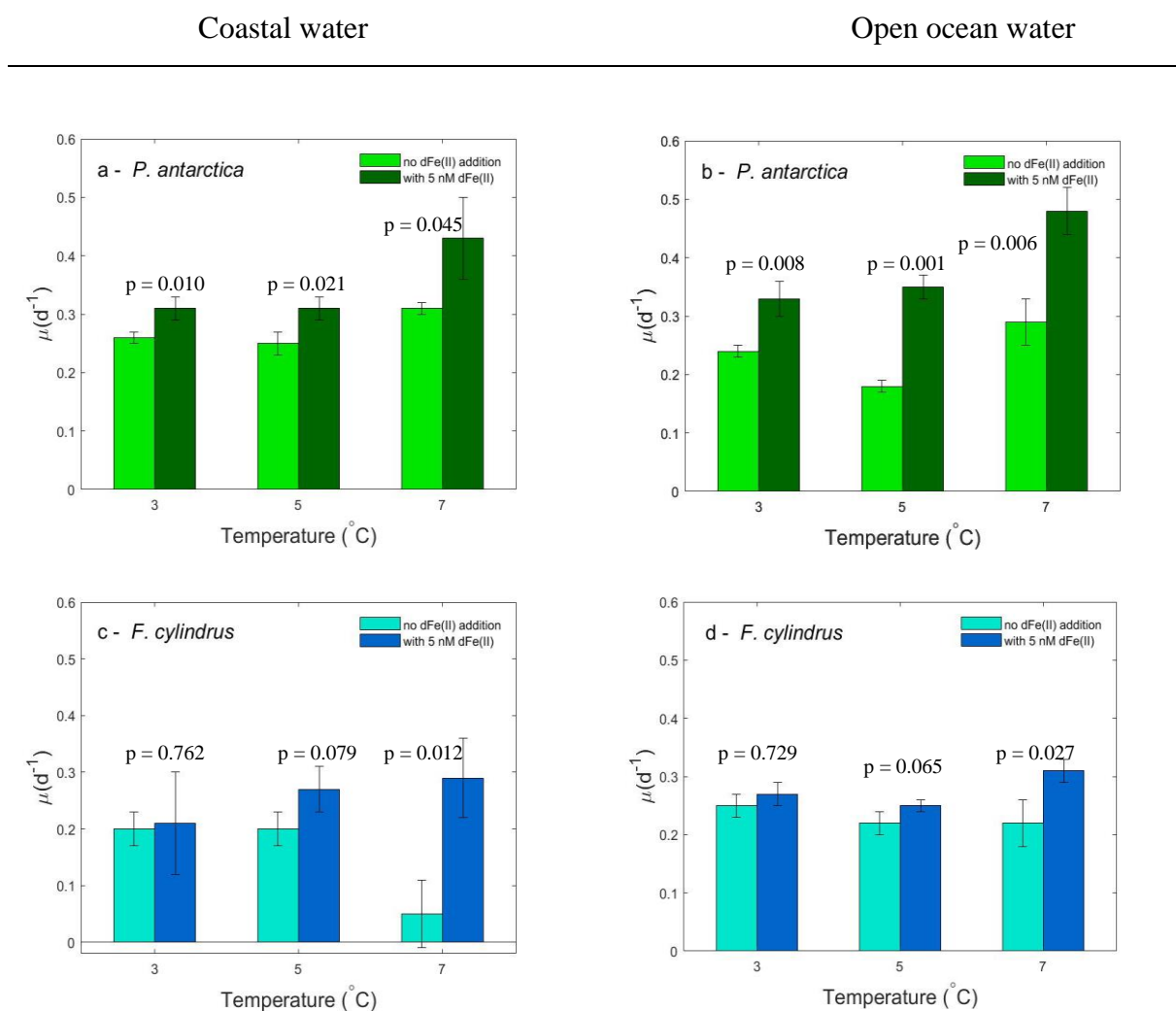


Figure 3.3 Specific growth rate (μ , d^{-1}) of *Phaeocystis antarctica* (a, b) and *Fragilariopsis cylindrus* (c, d) grown in coastal (a, c) and open ocean (b, d) water, with the addition (dark colour) and without the addition (light colour) of 5 nM dFe(II). Error bars are standard deviation, $n = 3$, p-values derived through one-way ANOVAs (**Supplementary Table 11**) comparing for with and without dFe(II) additions are given above the respective bars.

Fragilariopsis cylindrus also grew better when 5 nM dFe(II) was added. Its growth in coastal water displayed a steady but non-significant increase from 3°C (0.21 ± 0.09) to 5°C (0.27 ± 0.04 , $n = 3$; $p = 0.665$), and was also non-significant from 5 to 7°C (0.29 ± 0.07 , $p = 0.910$). In open ocean water, a slight non-significant decline in growth from 3°C (0.27 ± 0.02) to 5°C (0.25 ± 0.1 , $n = 3$, $p = 0.654$) was observed with a significant increase again when incubated at 7°C (0.31 ± 0.02) and compared to growth at 5°C ($p = 0.019$).

Combined impacts of temperature and Fe additions on growth

In coastal water, *P. antarctica* grew significantly better when Fe was added (ANOVAs at 3°C with $p = 0.010$, $p = 0.021$ at 5°C and $p = 0.045$ at 7°C (**Figure 3.3**). In open ocean, the significant difference of growth when Fe was added at 3°C was $p = 0.008$, $p = 0.001$ at 5°C and $p = 0.006$ at 7°C. In contrast to this, *F. cylindrus* only had significant differences in coastal water upon the Fe addition at 7°C ($p = 0.012$) while the Fe additions at 3°C and 5°C were non-significant ($p = 0.762$ and $p = 0.079$). In open ocean water, *F. cylindrus* showed similar trends where additions at 7°C were significant ($p = 0.027$) and non-significant at 3°C ($p = 0.729$) and at 5°C ($p = 0.065$).

A two-way ANOVA for the combined treatments revealed that for *P. antarctica* there was no significant interaction between Fe additions and temperature on growth in coastal water ($p = 0.269$), whereas the interaction of Fe addition and temperature changes had a significant interactive impact on growth in open ocean water ($p = 0.029$). For *F. cylindrus*, the combined treatments of Fe additions and temperature increases were significant for growth in both water types (open ($p = 0.025$) and coastal water ($p = 0.013$)).

3.3.3 Iron-binding organic ligands

The dFe concentrations in open ocean water were low at 0.15 nM. In comparison, the coastal water had concentrations of 12.18 nM. The ligand start concentrations (L) for open ocean water were 19.30 ± 1.1 nM and 15.0 ± 0.5 nM for coastal water. The ligand to Fe (L/dFe) ratio was very high for the open ocean water with 128.67 but low for coastal water with 1.29. The binding strength value $\log K'_{\text{Fe}^{\text{L}}}$ for open water was 11.21 ± 0.05 and 11.86 ± 0.08 for coastal water. The freely available Fe' was 0.05 pM in open ocean water and 4.72 pM in coastal water. For both samples, > 99% of dFe was complexed by organic ligands. The $\log \alpha'_{\text{Fe}^{\text{L}}}$, the side reaction

coefficient (Gerringa et al., 2014) revealed a lower reactivity for open ocean water with 3.49 and a higher reactivity (4.06) for coastal water.

Table 3.2 Dissolved (d) Fe is the concentration of Fe, L (nM) is the ligand concentration in the respective seawater samples, $\text{Log}K'_{\text{Fe}'\text{L}}$ is the ligand-binding strength or complexation capacity, L' the freely available ligand, $L/d\text{Fe}$ displays the ratio of ligand to dFe concentrations, Fe' (pM) the freely available Fe, %FeL is the percentage concentration of dFe organically complexed, and $\text{log}\alpha'_{\text{Fe}'\text{L}}$ is a parameter describing the reactivity for new binding capacities.

	dFe (nM)	L (nM)	$\text{log}K'_{\text{Fe}'\text{L}}$	L' (nM)	$L/d\text{Fe}$	Fe' (pM)	%FeL	$\text{log}\alpha'_{\text{Fe}'\text{L}}$
Open ocean	0.15	19.30 ± 1.1	11.21 ± 0.05	19.15	128.67	0.05	99.97	3.49
Coastal water	12.18	15.70 ± 0.5	11.86 ± 0.08	3.52	1.29	4.72	99.96	4.06

3.4 Discussion

3.4.1 Growth rates

For more than thirty years, it has been known that temperature is a major factor influencing growth for phytoplankton and their metabolic processes (Raven and Geider, 1988). For an extended period, research looked at Fe and temperature and their impacts on phytoplankton individually. With John Martin's Fe hypothesis (Martin, 1990) and ongoing observations of temperature increases due to anthropogenic impacts, the need for combined experiments was recognized. Rose et al. (2009) revealed that the combination of Fe and temperature in phytoplankton do not have merely additive effects but are much greater than when looking at temperature and Fe individually. They further observed synergistic effects on abundance, physiology and nutrient drawdown once the parameters were combined. Recently, Boyd (2019) showed that many SO species have a temperature range with functional performance curves. Future studies should also combine Fe and temperature treatments to improve our understanding of how phytoplankton physiological processes will change under future ocean conditions. Here, the reduced form of Fe (dFe(II)) is combined with two distinct environments from the SO. The main aim was to investigate how changing seawater temperature affects Fe bioavailability and thus the growth of two representative phytoplankton species of the SO in open ocean and coastal waters (Kropuenske et al., 2009). This research has important implications for phytoplankton species composition under future global climate change conditions and further contributes to this field of research by examining Fe supply changes with

increasing temperature. Therefore, it is hypothesized that increasing temperature in open ocean water would lead to decreased phytoplankton growth and that growth would be enhanced once dFe(II) was added. In coastal water, it was assumed there would be fewer impacts on growth from temperature due to high Fe concentrations and a small to no effect upon the addition of dFe(II).

This hypothesis is not supported by findings for *P. antarctica*. In this study in open ocean water without the addition of dFe(II), a decrease in growth was found from 3°C to 5°C, but an increase of growth was observed again once the temperatures were elevated to 7°C. Similar trends in coastal water were found where *P. antarctica* without the addition of Fe also grew slightly less at 5°C compared to 3°C but had an increase in growth again at 7°C and grew evidently better once dFe(II) was added. The growth of *F. cylindrus* followed the hypothesis partially: Growth in open ocean water declined once the temperature was increased. However, an addition of dFe(II) led to the predicted increase in growth from 0.02 to 0.2 μ d⁻¹. In coastal water, a strong decrease in growth of *F. cylindrus* was found with increasing temperature at 7°C. Here, the addition of dFe(II) led to a 3-fold increase in growth at 7°C.

Phaeocystis antarctica is a bloom-forming and highly abundant prymnesiophyte in the SO. Its thermal window ranges from -1°C to +8 °C with its optimum growth around 6°C to 7°C, which makes it quite an adaptive organism (Alderkamp et al., 2012, Kennedy et al., 2012, Boyd, 2019). Many studies have been performed under controlled conditions using artificial seawater such as Aquil (e.g. Strzepek et al., 2019) combined with trace metal clean handling (Cutter et al., 2017). Despite the differences in media, the growth here compares with such studies (Luxem et al., 2017, Andrew et al., 2019, Strzepek et al., 2019). When Fe was added at 2°C and 3°C, respectively, a 2-fold increase of growth was observed for *P. antarctica* (Strzepek et al., 2019, Alderkamp et al., 2012). While this two-fold increase was not found in this study, an improvement when dFe(II) was added was also observed.

Based on the findings and documented growth within its thermal window of - 1°C to + 8°C, it can be concluded that *P. antarctica* is able to overcome temperature changes at least in coastal waters due to sufficiently available Fe. However, in open ocean water, *P. antarctica* did not grow as well, regardless of the dFe(II) addition. Repeating the study at temperatures higher than 7°C might be beneficial but may also exceed the expected temperature changes within the foreseen future.

Growth values for *P. antarctica* compared well to what was reported earlier. At 3°C, growth rates of 0.33 $\mu^{\text{d}^{-1}}$ in high Fe and 0.15 $\mu^{\text{d}^{-1}}$ in low Fe conditions were reported (Strzepek et al., 2019), whereas our results of growth at 3°C are between 0.26 \pm 0.01 (low Fe) and 0.32 \pm 0.02 $\mu^{\text{d}^{-1}}$ (dFe(II) addition). An explanation for varying growth may be that no vitamins or other trace metals were added to open ocean water in this study, in contrast to e.g. Trimborn et al. (2017b), in which they also used natural Antarctic seawater with a salinity of 33.2 but added a trace metal and vitamin cocktail.

Fragilariopsis cylindrus is also a common diatom from the SO. Pančić et al. (2015) report growth rates at temperatures of 1°C (0.69 \pm 0.00 $\mu^{\text{d}^{-1}}$ to 0.22 \pm 0.00 $\mu^{\text{d}^{-1}}$), 5°C (0.72 \pm 0.01 $\mu^{\text{d}^{-1}}$ to 0.20 \pm 0.01 $\mu^{\text{d}^{-1}}$) and 8°C (0.90 \pm 0.00 $\mu^{\text{d}^{-1}}$ to 0.41 \pm 0.00 $\mu^{\text{d}^{-1}}$) for several different strains of *F. cylindrus* in artificial seawater. The growth rates obtained in this study lie within these windows for both water types. Alderkamp et al. (2012) report growth rates of 0.05 $\mu^{\text{d}^{-1}}$ in Fe-limited conditions (1 nM Fe) and 0.16 $\mu^{\text{d}^{-1}}$ in Fe replete (1 μM Fe) culture at 2°C. These results do not compare to our findings for open or coastal water as the growth rates observed in this study were always higher (e.g., open ocean water 3°C: - Fe: 0.25 \pm 0.02 $\mu^{\text{d}^{-1}}$, + Fe: 0.27 \pm 0.02 $\mu^{\text{d}^{-1}}$; coastal water 3°C: - Fe: 0.20 \pm 0.03 $\mu^{\text{d}^{-1}}$, + Fe: 0.21 \pm 0.09 $\mu^{\text{d}^{-1}}$), independent of the Fe addition. This was especially noticeable in open ocean water, where we suggest that *F. cylindrus* was likely adapted to low Fe concentrations. Although Fe concentrations were low (dFe: 0.150 nM, **Table 3.1**) they still had a boosting effect upon the 5 nM dFe(II) addition.

Interestingly, *F. cylindrus* did not grow well (0.05 \pm 0.06 $\mu^{\text{d}^{-1}}$) in coastal water at 7°C when no additional Fe was added. Since it can also grow at 7°C, further physiological investigations are required to explain its low growth in these conditions. One potential factor for decreased growth in open ocean could be toxicity of Cu or other metals there (Chu et al., 2019). In future oceans, the results presented here could mean that *F. cylindrus* may be outcompeted by other species at increased temperatures, with unknown ecosystem impacts and unknown impacts on the C sequestration capacity of the SO.

3.4.2 Iron binding organic ligands

Both water types had high concentrations of Fe(III) ligands (**Table 3.2**), which bound most of the Fe(III) (> 99%). Therefore, it is questionable how much Fe(II) is bound. However, an

addition of 5 nM dFe(II) may have created an dFe(II) ‘saturated’ condition, meaning that there was more dFe(II) than unbound ligands in both water types. This boost of dFe(II) could have led to an increase in growth in both water types, despite an increase in temperature. Furthermore, a higher dFe(II) to ligand concentrations (‘saturation’) could have slowed the oxidation process of dFe(II), as suggested by Roy et al. (2008).

The ratio of ligands to the overall Fe concentration may also have been an important factor in the availability of dFe(II) and therefore the resulting growth: The open ocean sample had a very high ligand to Fe ratio (128:1), whereas the ratio in coastal water was lower at 1.29:1, implying that less Fe was available in open ocean water (0.15 nM in open ocean vs. 12.18 nM in coastal water). This may be linked to differences in physical or biological parameters such as salinity and pH (e.g., Buck, 2007, Genovese et al., 2022), which define the side reaction coefficient $\log \alpha'_{\text{Fe}\cdot\text{L}}$. Our $\log \alpha'_{\text{Fe}\cdot\text{L}}$ was 3.49 in open ocean water and 4.06 in coastal water. That could mean that, the open ocean water had low concentrations of Fe and high, but potentially unused or less reactive ligands compared to coastal water, where there was a balanced ratio and the reactivity was higher. These inert ligands in open ocean water might result from little ligand to Fe concentrations and could further lead to greater bioavailability of Fe for phytoplankton. In coastal water on the other hand, both the Fe concentrations and Fe-ligand concentrations were high and more reactive compared to open ocean water. The addition of 5 nM dFe(II) in both water types may therefore have led to facilitated growth. Additionally, the binding strength of ligands comes into play: open ocean water had a slightly lower binding strength (11.21 ± 0.05) compared to the coastal water (11.86 ± 0.08), which facilitated availability in open ocean water compared to coastal water. See **Figure 3.4** for a visual summary.

Many SO phytoplankton studies use cold water species with a temperature-based optimum for growth at temperatures between 0°C and 5°C. *Phaeocystis antarctica* and *F. cylindrus* were chosen based on their greater temperature range combined with the parameters Fe and temperature. Future studies are encouraged to look at entire communities, including Fe or other nutrient effects, to provide better insight into species composition changes from warming effects. Another suggestion for future studies is to measure dFe(II) throughout the experiment, which was impossible in this instance due to limited seawater volumes.

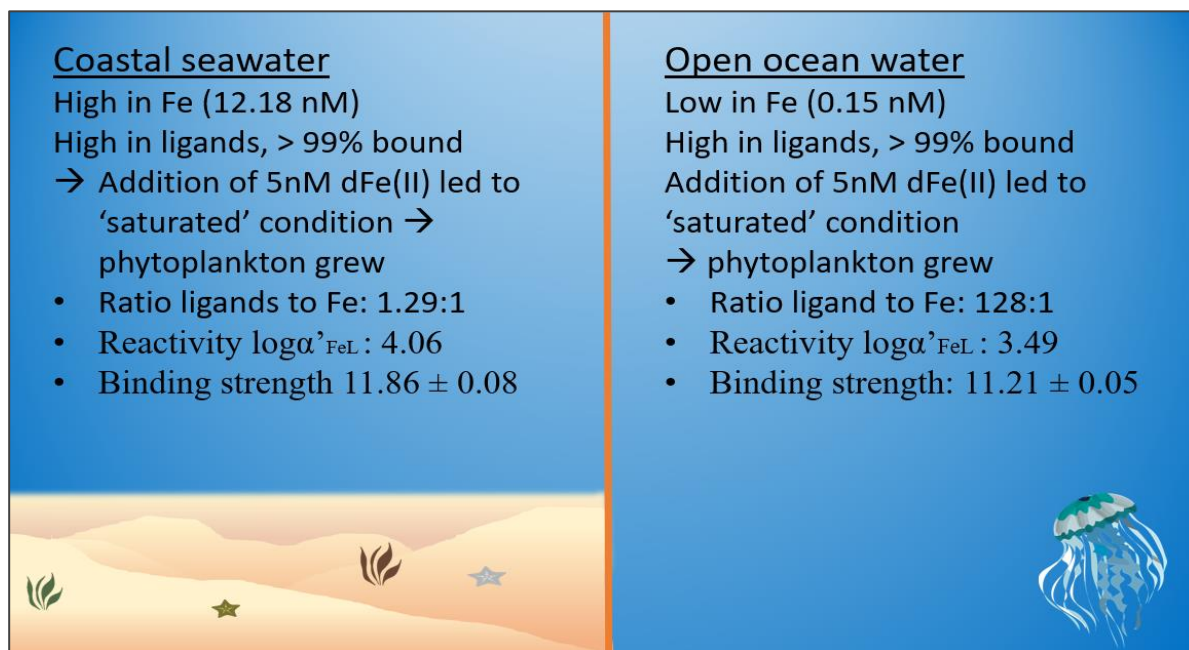


Figure 3.4 Visual summary of Fe : Ligand ratio and their states in coastal and open ocean water.

3.5 Conclusions

The findings show that dFe(II) additions resulted in a direct biological response but may have had the underlying effect that all ligands were bound to Fe, leaving the added dFe(II) 'ready to use' and freely available for phytoplankton. Temperature led to a great difference in growth for *Phaeocystis antarctica*. This could not be related to the effects of an accelerated oxidation of dFe(II) from increased temperature. However, the addition of 5 nM dFe(II), may have led to increased growth. For *Fragilariopsis cylindrus*, no increased growth was observed at higher temperatures with implications for a shift in species composition due to being outcompeted, especially in coastal systems, where increased temperature had a negative effect on growth. For the SO, changes in the phytoplankton composition have unknown consequences with further unknown implications for carbon cycling and future scenarios. Using a greater range of temperatures in combination with dFe(II) measurements, a wider range of SO phytoplankton species, and multiple natural-seawater background analyses to define the composition better in future studies may offer new insights into nutrient and ligand complexing processes in combination with in-situ ocean observations of ecological processes. This would help to better

understand and outline effects of iron on phytoplankton growth and their ability to sequester carbon.

HA, KW and ARB designed the research. HA conducted the experiments. CG analysed and partially interpreted the ligand data (voltammetry). KW analysed the trace metal data (ICP-MS). HA and LH analysed the data. HA wrote the manuscript. All authors read and approved the manuscript.

Acknowledgement

I am grateful to the scientists onboard the SR3 expedition (IN2018_V01) of the *R.V Investigator*: For the collection and filtration of seawater, I would like to thank Pauline Latour, Pier van der Merwe, Melanie Gault-Ringold, Thomas Holmes, Christine Weldrick and Matt Corkill. I would also like to thank Damon Britton and Catriona Hurd for the use and analysis of the macronutrient concentrations. Thank you also to Pier van der Merwe, Melanie Gault-Ringold and Pauline Latour for their assistance with preparing samples for the analyses in the SF-ICP-MS and thank you to Ashley Townsend for analysing them. Further thank you to Andrew McMinn for providing the phytoplankton cultures and to Fraser Kennedy for insights into culturing techniques. I would also like to thank Thomas Holmes and Robert Strzepek for providing comments on the manuscript. This research was supported under Australian Research Council's Special Research Initiative for Antarctic Gateway Partnership (Project ID SR140300001). Further support was given by the Australian Government's Cooperative Research Centres Program through the Antarctic Climate and Ecosystems Cooperative Research Centre (ACE CRC). Funding for the nutrient analysis was provided by the ACE CRC. The analysis of the trace metal samples using SF-ICP-MS was made possible through Australian Research Council funding of the instrumentation LIEF scheme (LEO989539).

3.6 References

- ALDERKAMP, A. C., KULK, G., BUMA, A. G., VISSER, R. J., VAN DIJKEN, G. L., MILLS, M. M. & ARRIGO, K. R. 2012. The effect of iron limitation on the photophysiology of *Phaeocystis antarctica* (prymnesiophyceae) and *Fragilariopsis cylindrus* (bacillariophyceae) under dynamic irradiance. *Journal of Phycology*, 48, 45-59.
- ANDREW, S. M., MORELL, H. T., STRZEPEK, R. F., BOYD, P. W. & ELLWOOD, M. J. 2019. Iron Availability Influences the Tolerance of Southern Ocean Phytoplankton to Warming and Elevated Irradiance. *Frontiers in Marine Science*, 6.
- ARRIGO, K. R., ROBINSON, D. H., WORTHEN, D. L., DUNBAR, R. B., DITULLIO, G. R., VANWOERT, M. & LIZOTTE, M. P. 1999. Phytoplankton community structure and the drawdown of nutrients and CO₂ in the Southern Ocean. *Science*, 283, 365-367.
- BINDOFF, N., CHEUNG, W., KAIRO, J., ARÍSTEGUI, J., GUINDER, V., HALLBERG, R., HILMI, N., JIAO, N., KARIM, M., LEVIN, L. & ODOGNOGUE 2019. Changing Ocean, Marine Ecosystems, and Dependent Communities. *IPCC Special Report on the Ocean and Cryosphere in a Changing Climate*.
- BOWIE, A. R., ACHTERBERG, E. P., SEDWICK, P. N., USSHER, S. & WORSFOLD, P. J. 2002. Real-time monitoring of picomolar concentrations of iron (II) in marine waters using automated flow injection-chemiluminescence instrumentation. *Environmental science & technology*, 36, 4600-4607.
- BOYD, P. W. 2019. Physiology and iron modulate diverse responses of diatoms to a warming Southern Ocean. *Nature Climate Change*, 9, 148-152.
- BOYE, M., VAN DEN BERG, C. M., DE JONG, J. T., LEACH, H., CROOT, P. & DE BAAR, H. J. 2001. Organic complexation of iron in the Southern Ocean. *Deep Sea Research Part I: Oceanographic Research Papers*, 48, 1477-1497.
- BUCK, K.N., LOHAN, M.C., BERGER, C.J. AND BRULAND, K.W., 2007. Dissolved iron speciation in two distinct river plumes and an estuary: Implications for riverine iron supply. *Limnology and Oceanography*, 52(2), pp.843-855.
- CHU, W.L., DANG, N.L., KOK, Y.Y., YAP, K.S.I., PHANG, S.M. AND CONVEY, P., 2019. Heavy metal pollution in Antarctica and its potential impacts on algae. *Polar Science*, 20, pp.75-83.
- CROOT, P. L. & JOHANSSON, M. 2000. Determination of Iron Speciation by Cathodic Stripping Voltammetry in Seawater Using the Competing Ligand 2-(2-Thiazolylazo)-p-cresol (TAC). *Electroanalysis*, 12, 565-576.
- CROOT, P. L. & LAAN, P. 2002. Continuous shipboard determination of Fe (II) in polar waters using flow injection analysis with chemiluminescence detection. *Analytica Chimica Acta*, 466, 261-273.
- CUTTER, G., CASCIOTTI, K., CROOT, P., GEIBERT, W., HEIMBUERGER, L. E., LOHAN, M. C., PLANQUETTE, H. & FLIERDT, T. 2017. Sampling and Sample-

- handling Protocols for GEOTRACES Cruises (Version 3). <http://www.geotraces.org/images/stories/documents/intercalibration/Cookbook.pdf>.
- DIAMOND, D. 2008a. Determination of nitrate/nitrite in brackish or seawater by flow injection analysis. *LaChat Instruments, Loveland, USA*, pp. 19.
- DIAMOND, D. 2008b. Determination of orthophosphate in brackish or seawater by flow injection analysis. *LaChat Instruments, Loveland, USA*, pp. 19.
- FIALA, M. & ORIOL, L. 1990. Light-temperature interactions on the growth of Antarctic diatoms. *Polar Biology*, 10, 629-636.
- GENOVESE, C., GROTTI, M., ARDINI, F., WUTTIG, K., VIVADO, D., CABANES, D., TOWNSEND, A., HASSLER, C. AND LANNUZEL, D., 2021. Effect of salinity and temperature on the determination of dissolved iron-binding organic ligands in the polar marine environment. *Marine Chemistry*, p.104051.
- GERRINGA, L., HERMAN, P. & POORTVLIET, T. 1995. Comparison of the linear van den Berg/Ružić transformation and a non-linear fit of the Langmuir isotherm applied to Cu speciation data in the estuarine environment. *Marine Chemistry*, 48, 131-142.
- GERRINGA, L.J., RIJKENBERG, M.J., THURÓCZY, C.E. AND MAAS, L.R., 2014. A critical look at the calculation of the binding characteristics and concentration of iron complexing ligands in seawater with suggested improvements. *Environmental Chemistry*, 11(2), pp.114-136.
- GUILLARD, R.R.L. & HARGRAVES, P.E., 1993. *Stichochrysis immobilis* is a diatom, not a chrysophyte. *Phycologia*, 32(3), pp.234-236.
- HABER, F. & WEISS, J. 1932. Über die katalyse des hydroperoxydes. *Naturwissenschaften*, 20, 948-950.
- HANSARD, S. P. & LANDING, W. M. 2009. Determination of iron (II) in acidified seawater samples by luminol chemiluminescence. *Limnology and Oceanography: Methods*, 7, 222-234.
- HASSLER, C. & SCHOEMANN, V. 2009. Bioavailability of organically bound Fe to model phytoplankton of the Southern Ocean. *Biogeosciences*, 6, 2281-2296.
- HOLMES, T. M., WUTTIG, K., CHASE, Z., VAN DER MERWE, P., TOWNSEND, A. T., SCHALLENBERG, C., TONNARD, M. & BOWIE, A. R. 2019. Iron availability influences nutrient drawdown in the Heard and McDonald Islands region, Southern Ocean. *Marine Chemistry*, 211, 1-14.
- HUNTER, K. A. & BOYD, P. W. 2007. Iron-binding ligands and their role in the ocean biogeochemistry of iron. *Environmental Chemistry*, 4, 221-232.
- KENNEDY, F., MCMINN, A. & MARTIN, A. 2012. Effect of temperature on the photosynthetic efficiency and morphotype of *Phaeocystis antarctica*. *Journal of Experimental Marine Biology and Ecology*, 429, 7-14.
- KING, D. W., LOUNSBURY, H. A. & MILLERO, F. J. 1995. Rates and mechanism of Fe (II) oxidation at nanomolar total iron concentrations. *Environmental science & technology*, 29, 818-824.

- KROPUENSKE, L. R., MILLS, M. M., VAN DIJKEN, G. L., BAILEY, S., ROBINSON, D. H., WELSCHMEYER, N. A. & ARRIGO, K. R. 2009. Photophysiology in two major Southern Ocean phytoplankton taxa: photoprotection in *Phaeocystis antarctica* and *Fragilariopsis cylindrus*. *Limnology and Oceanography*, 54, 1176-1196.
- KUMA, K. & MATSUNAGA, K. 1995. Availability of colloidal ferric oxides to coastal marine phytoplankton. *Marine Biology*, 122, 1-11.
- KUMA, K., NAKABAYASHI, S., SUZUKI, Y., KUDO, I. & MATSUNAGA, K. 1992. Photo-reduction of Fe (III) by dissolved organic substances and existence of Fe (II) in seawater during spring blooms. *Marine Chemistry*, 37, 15-27.
- LIAO, N. 2008. Determination of ammonia in brackish or seawater by flow injection analysis. *LaChat Instruments Loveland, USA*, pp. 20.
- LIS, H., SHAKED, Y., KRANZLER, C., KEREN, N. & MOREL, F. M. 2015. Iron bioavailability to phytoplankton: an empirical approach. *The ISME journal*, 9, 1003-1013.
- LUXEM, K. E., ELLWOOD, M. J. & STRZEPEK, R. F. 2017. Intraspecific variability in *Phaeocystis antarctica*'s response to iron and light stress. *PloS one*, 12, e0179751.
- MALDONADO, M. T. & PRICE, N. M. 1999. Utilization of iron bound to strong organic ligands by plankton communities in the subarctic Pacific Ocean. *Deep Sea Research Part II: Topical Studies in Oceanography*, 46, 2447-2473.
- MALDONADO, M. T. & PRICE, N. M. 2001. Reduction and transport of organically bound iron by *Thalassiosira oceanica* (Bacillariophyceae). *Journal of Phycology*, 37, 298-310.
- MARTIN, J. H. 1990. Glacial-interglacial CO₂ change: The iron hypothesis. *Paleoceanography*, 5, 1-13.
- MARTIN, J. H., GORDON, R. M. & FITZWATER, S. E. 1990. Iron in Antarctic Waters. *Nature*, 345, 156-158.
- MILLERO, F. J. & IZAGUIRRE, M. 1989. Effect of ionic strength and ionic interactions on the oxidation of Fe (II). *Journal of Solution Chemistry*, 18, 585-599.
- MILLERO, F. J. & SOTOLONGO, S. 1989. The oxidation of Fe (II) with H₂O₂ in seawater. *Geochimica et Cosmochimica Acta*, 53, 1867-1873.
- MILLERO, F. J., SOTOLONGO, S. & IZAGUIRRE, M. 1987. The oxidation kinetics of Fe(II) in seawater. *Geochimica et Cosmochimica Acta*, 51, 793-801.
- MOCK, T. & HOCH, N. 2005. Long-term temperature acclimation of photosynthesis in steady-state cultures of the polar diatom *Fragilariopsis cylindrus*. *Photosynthesis Research*, 85, 307-317.
- MOFFETT, J. W. & ZIKA, R. G. 1987. Reaction kinetics of hydrogen peroxide with copper and iron in seawater. *Environmental Science & Technology*, 21, 804-810.
- MOREL, F.M., RUETER, J.G., ANDERSON, D.M. AND GUILLARD, R.R.L., 1979. Aquil:Aa chemically defined phytoplankton culture medium for trace metal studies 1 2. *Journal of Phycology*, 15(2), pp.135-141.

- MOREL, F. M. M., KUSTKA, A. B. & SHAKED, Y. 2008. The role of unchelated Fe in the iron nutrition of phytoplankton. *Limnology and Oceanography*, 53, 400-404.
- NEORI, A. & HOLM-HANSEN, O. 1982. Effect of temperature on rate of photosynthesis in Antarctic phytoplankton. *Polar Biology*, 1, 33-38.
- NOFFKE, A., HENSEN, C., SOMMER, S., SCHOLZ, F., BOHLEN, L., MOSCH, T., GRACO, M. & WALLMANN, K. 2012. Benthic iron and phosphorus fluxes across the Peruvian oxygen minimum zone. *Limnology and Oceanography*, 57, 851-867.
- OMANOVIĆ, D., GARNIER, C. & PIŽETA, I. 2015. ProMCC: an all-in-one tool for trace metal complexation studies. *Marine Chemistry*, 173, 25-39.
- PANČIĆ, M., HANSEN, P. J., TAMMILEHTO, A. & LUNDHOLM, N. 2015. Resilience to temperature and pH changes in a future climate change scenario in six strains of the polar diatom *Fragilariopsis cylindrus*. *Biogeosciences*, 12, 4235-4244.
- PÖRTNER, H. O. 2002. Climate variations and the physiological basis of temperature dependent biogeography: systemic to molecular hierarchy of thermal tolerance in animals. *Comparative Biochemistry and Physiology Part A: Molecular & Integrative Physiology*, 132, 739-761.
- PRICE, N.M., HARRISON, G.I., HERING, J.G., HUDSON, R.J., NIREL, P.M., PALENIK, B. AND MOREL, F.M., 1989. Preparation and chemistry of the artificial algal culture medium Aquil. *Biological oceanography*, 6(5-6), pp.443-461.
- RAVEN, J. A. & GEIDER, R. J. 1988. Temperature and algal growth. *New phytologist*, 110, 441-461.
- RICH, H. W. & MOREL, F. M. 1990. Availability of well-defined iron colloids to the marine diatom *Thalassiosira weissflogii*. *Limnology and Oceanography*, 35, 652-662.
- ROSE, J., FENG, Y., DITULLIO, G. R., DUNBAR, R. B., HARE, C., LEE, P., LOHAN, M., LONG, M., SMITH JR, W. & SOHST, B. 2009. Synergistic effects of iron and temperature on Antarctic phytoplankton and microzooplankton assemblages. *Biogeosciences*, 6.
- ROY, E. G., WELLS, M. L. & KING, D. W. 2008. Persistence of iron (II) in surface waters of the western subarctic Pacific. *Limnology and Oceanography*, 53, 89-98.
- RUŽIĆ, I. 1982. Theoretical aspects of the direct titration of natural waters and its information yield for trace metal speciation. *Analytica Chimica Acta*, 140, 99-113.
- SALMON, T. P., ROSE, A. L., NEILAN, B. A. & WAITE, T. D. 2006. The FeL model of iron acquisition: Nondissociative reduction of ferric complexes in the marine environment. *Limnology and Oceanography*, 51, 1744-1754.
- SCHALLENBERG, C., BESTLEY, S., KLOCKER, A., TRULL, T. W., DAVIES, D. M., GAULT-RINGOLD, M., ERIKSEN, R., RODEN, N. P., SANDER, S. G. & SUMNER, M. 2018. Sustained upwelling of subsurface iron supplies seasonally persistent phytoplankton blooms around the southern Kerguelen plateau, Southern Ocean. *Journal of Geophysical Research: Oceans*, 123, 5986-6003.

- SCHLITZER, R. 2002. Carbon export fluxes in the Southern Ocean: results from inverse modeling and comparison with satellite-based estimates. *Deep Sea Research Part II: Topical Studies in Oceanography*, 49, 1623-1644.
- SEDWICK, P., EDWARDS, P., MACKEY, D., GRIFFITHS, F. & PARSLow, J. 1997. Iron and manganese in surface waters of the Australian subantarctic region. *Deep Sea Research Part I: Oceanographic Research Papers*, 44, 1239-1253.
- SHAKED, Y. & LIS, H. 2012. Disassembling iron availability to phytoplankton. *Frontiers in microbiology*, 3.
- SHI, D., XU, Y., HOPKINSON, B. M. & MOREL, F. M. M. 2010. Effect of Ocean Acidification on Iron Availability to Marine Phytoplankton. *Science*, 327, 676-679.
- STRZEPEK, R. F., BOYD, P. W. & SUNDA, W. G. 2019. Photosynthetic adaptation to low iron, light, and temperature in Southern Ocean phytoplankton. *Proceedings of the National Academy of Sciences*, 201810886.
- TAGLIABUE, A., BOWIE, A. R., BOYD, P. W., BUCK, K. N., JOHNSON, K. S. & SAITO, M. A. 2017. The integral role of iron in ocean biogeochemistry. *Nature*, 543, 51-59.
- TRIMBORN, S., BRENNEIS, T., HOPPE, C. J., LAGLERA, L. M., NORMAN, L., SANTOS-EICHEANDÍA, J., VÖLKNER, C., WOLF-GLADROW, D. & HASSLER, C. S. 2017a. Iron sources alter the response of Southern Ocean phytoplankton to ocean acidification. *Marine Ecology Progress Series*, 578, 35-50.
- TRIMBORN, S., THOMS, S., BRENNEIS, T., HEIDEN, J. P., BESZTERI, S. & BISCHOF, K. 2017b. Two Southern Ocean diatoms are more sensitive to ocean acidification and changes in irradiance than the prymnesiophyte *Phaeocystis antarctica*. *Physiologia plantarum*, 160, 155-170.
- VAN DEN BERG, C. 1982. Determination of copper complexation with natural organic ligands in seawater by equilibration with MnO₂ I. Theory. *Marine Chemistry*, 11, 307-322.
- WUTTIG, K., TOWNSEND, A. T., VAN DER MERWE, P., GAULT-RINGOLD, M., HOLMES, T., SCHALLENBERG, C., LATOUR, P., TONNARD, M., RIJKENBERG, M. J. & LANNUZEL, D. 2019. Critical evaluation of a seaFAST system for the analysis of trace metals in marine samples. *Talanta*.
- YEALA, S., B., K. A. & M., M. F. M. 2005. A general kinetic model for iron acquisition by eukaryotic phytoplankton. *Limnology and Oceanography*, 50, 872-882.

Chapter 4: Processes governing distribution and cycling of Fe(II) and H₂O₂ in the South Tasman Sea and northern subantarctic zone

Helene Aflenzer^{a,b,c,*}, Thomas Holmes^b, Kathrin Wuttig^a, Pauline Latour^{a,b}, Andrew Bowie^{a,b}

Affiliations

^a Antarctic Climate and Ecosystems Cooperative Research Centre (ACE CRC), University of Tasmania, Private Bag 80, Hobart, Tasmania 7001, Australia

^b Institute for Marine and Antarctic Studies (IMAS), University of Tasmania, Private Bag 129, Hobart, Tasmania, Australia

^c Australian Research Council Gateway Partnership, University of Tasmania, Private Bag 80, Hobart, Tasmania 7001, Australia

*Corresponding Author. E-mail: helene.aflenzer@utas.edu.au

Abstract

Iron (Fe) is one of the most important elements involved in the photosynthetic processes of marine-based plants such as phytoplankton. However, it is scarce in the Southern Ocean (SO). Its dissolved (d) form (Fe(II)) is a rapidly oxidising iron-species, considered easily available to primary producers. A major current linked to the SO is the East Australian Current (EAC) which flows south along the eastern Australian mainland. It is thought to transport Fe-rich water from the north into Fe poor High Nutrient Low Chlorophyll waters in the SO with the potential to induce phytoplankton blooms.

This study compares 12 stations from two transects for dFe(II) and hydrogen peroxide (H₂O₂) concentrations collected on a north-to-south transect along the EAC and an east-west transect in the northern subantarctic zone, south of Tasmania (~155°E and 40°S) in early spring. By using dFe(II) and H₂O₂, additional sources of Fe linked to several parameters that affect its oxidation were defined. Dissolved Fe(II) concentrations were highest (0.5 nM) at the surface of transit station (TS) 8. It was also high (> 0.3 nM) at the surface and depths below 1000 m in the most southern station (process station 1). At greater depths, dFe(II) concentrations were higher (> 0.2 nM) close to seamounts such as the South Tasman Rise or deep-sea sediments, while it was below 0.2 nM otherwise. Hydrogen peroxide was overall higher at greater depths of southern stations (~15 nM) compared to stations north of 40°S (< 15 nM) and was highest in the upper 200 m (~ 60 nM) in the mixing zone. The dFe(II): dFe ratios presented here are 10 % higher than what was reported for previous Southern Ocean studies further away from the Australian mainland. High concentrations of primary production in the surface waters down to the frontal mixing zone could be the reason for low dFe concentrations and high H₂O₂ concentrations. Occasional local higher peaks of dFe(II) may have come from aerosols or other external sources such as rain or vertical transport from the seamount.

Keywords: Fe(II), H₂O₂, Southern Ocean, East Australian Current, external Fe sources

4.1 Introduction

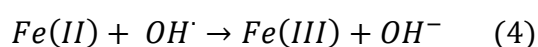
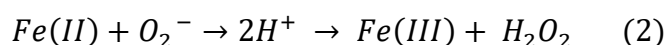
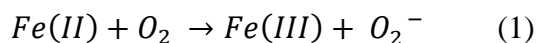
The Southern Ocean (SO) is the largest High Nutrient Low Chlorophyll (HNLC) area of the oceans, where phytoplankton growth is limited due to low concentrations of iron (Fe) (Martin, 1990). This region is also one of the largest areas where primary production drives the biological pump and carbon dioxide (CO₂) is taken up by phytoplankton from the atmosphere resulting in carbon (C) export to greater depths (Sarmiento and Orr, 1991, Smetacek et al., 2012, Ducklow et al., 2001). However, changes in pH from ocean acidification (OA) and ocean warming are thought to have major impacts on calcifying SO species, which could impact this pump (McNeil and Matear, 2008, Trimborn et al., 2017, Hoppe et al., 2013).

Many of the laboratory Fe incubation experiments previously conducted used the more thermodynamically stable, oxidized state of Fe, dFe(III) (e.g. Hutchins and Boyd, 2016, Strzepek et al., 2019, Andrew et al., 2019). This is Fe's most common and stable redox state form in the oxygenated ocean, which facilitates its analytical assay under aerobic conditions (Bowie et al., 1998). However, its reduced redox partner dissolved (d) Fe(II) is more soluble and energetically active due to its unbound state (Millero et al., 1987). Therefore, it is thought to be more easily accessible to phytoplankton (Shaked and Lis, 2012, Yeala et al., 2005). Concentrations of dFe(III) in the open-ocean are very low (typically 0.1-1.0 nM) (Lannuzel et al., 2011), with dFe(II) representing only a small fraction of that (pico to nanomolar; e.g. Bowie et al., 1998).

Several sources and processes are known to influence dFe(II) concentrations in surface ocean waters, such as photoreduction of dFe(III), atmospheric input from wet and dry deposition, (e.g. sandstorms or rain; Kieber et al., 2001a, Perron et al., 2020, Gabric et al., 2016). Other input of Fe includes river runoff and benthic flux (de Jong et al., 2012, Chase et al., 2007) with decreasing concentrations away from continents and towards open ocean waters. These water masses often contain low dFe(II) (< 0.2 nM) concentrations due to distance from sources (Duce and Tindale, 1991, Bowie et al., 2009, Perron et al., 2020, Tagliabue et al., 2017). Deeper waters, on the other hand, are often characterized by lower (<0.1 nM) concentrations (Holmes et al., 2019, Schallenberg et al., 2016) increasing again near ocean sediments (Laufer et al., 2016, Azzoni et al., 2005, Coleman et al., 1993).

The availability of dFe(II) to phytoplankton is time-limited, as it oxidises within minutes in surface waters (Millero et al., 1987). This oxidative process underlies several biological and

physico-chemical parameters. Phytoplankton cells, for instance, reduce dFe(III) to dFe(II) for facilitated uptake (Yeala et al., 2005, Morel et al., 2008). Parameters such as pH, temperature, oxygen (O₂), and hydrogen peroxide (H₂O₂) influence the oxidation rate of dFe(II). Decreasing seawater pH retards the oxidation of dFe(II) while increasing temperature speeds up oxidation rate (Millero et al., 1987).



As per equations 1-4 (Haber and Weiss, 1932), O₂ and H₂O₂ act as both oxidising and reducing agents, with the most important oxidant depending on H₂O₂ and dFe(II) concentrations (Millero and Sotolongo, 1989, Santana-Casiano et al., 2006). In seawater, H₂O₂ concentrations are mainly produced by biological activity and seawater exposure to sunlight, but external sources such as rainwater can also increase concentrations locally (Sharma and Millero, 1989, Kieber et al., 2001a). Because H₂O₂ is also produced through photooxidation of dissolved organic matter, it can act as an oxidant or reductant for the dFe(II) oxidation in regions with strong sources of dissolved organic matter (Moffett and Zika, 1987).

The study location is set where the East Australian current (EAC) meets the most northern part of the Antarctic Circumpolar Current (ACC), called the Sub-Tropical Front (STF), south of Tasmania, Australia (**Figure 4.1**). The EAC is a westward flowing eddy-dominated current system (Oke et al., 2019). Driven by westerly winds, the ACC is the major current of the SO flowing eastward around the Antarctic continent, marking rapid changes in temperature and salinity along latitudinal boundaries (Rintoul et al., 2001). In contrast, the EAC delivers warm, saline water from the north, where it mixes with the colder water from the STF (Tracey et al., 2006, Belkin and Gordon, 1996, Morrow et al., 2004, Phillips and Rintoul, 2002). The importance of the EAC lies within the removal of heat from the tropics in the north into the mid-latitude atmosphere (Roemmich et al., 2007).

This study is part of a 28-day voyage (IN2018-V04; GEOTRACES Process Study GPpr13) onboard the *RV Investigator* from 11th of September to 8th October 2018, starting and ending in

Hobart, Australia. This voyage aimed to examine the external Fe sources and distribution in the southern extension of the EAC and the STF. Due to the character and potential importance of dFe(II) for phytoplankton, depth profiles from 12 stations for dFe(II) and H₂O₂ were sampled and analysed onboard. A comparison of the distribution of dFe(II) and H₂O₂ was made through the contrasting biogeochemistry of EAC waters with HNLC waters located south of Tasmania. The motivation was to better understand contemporary processes impacting Fe bioavailability in this oceanographically important region and how these two different regions (EAC and SO incl. HNLC) may change under future changing climate scenarios. Through observations from satellite data, potential dFe(II) impacts on phytoplankton growth at this time of the year (early spring) were targeted.

The dFe(II) and H₂O₂ concentrations from rainwater at one station were also analysed together with dFe(II) concentrations from sediment porewater collected during the same voyage. Using this data, we gain insight into the external sources and impacts of dFe(II) on biogeochemistry in this region.

4.2 Methods

4.2.1 Oceanographic setting

The STF runs from west to east along the southern coast of Australia into the south Tasman Sea (**Figure 4.1**). It is a dynamic frontal boundary separating cooler, fresher SO surface waters from the warmer, saltier waters of the EAC. The STF is further defined by sea surface temperatures (SST) ranging from 12°C to 16°C in summer, and 7°C to 12°C in winter and by its salinity (Belkin and Gordon, 1996, Rintoul et al., 1997). The STF merges with the EAC south of Tasmania, a highly dynamic system in the Southwestern Pacific. The EAC has a relatively weak southward flow between 18° and 35°S of 25 to 37 Sverdrup (Sv), which is greater in summer (Ridgway and Godfrey, 1997). The EAC is further associated with large mesoscale eddies meandering away from the east coast of Australia (Bowen et al., 2005, Mata et al., 2006). It has an SST of at least 18°C all year round in the north (around 35°S) from where warm and nutrient-poor, but Fe-rich water is transported southwards (Ridgway and Hill, 2009).

4.2.2 Study area

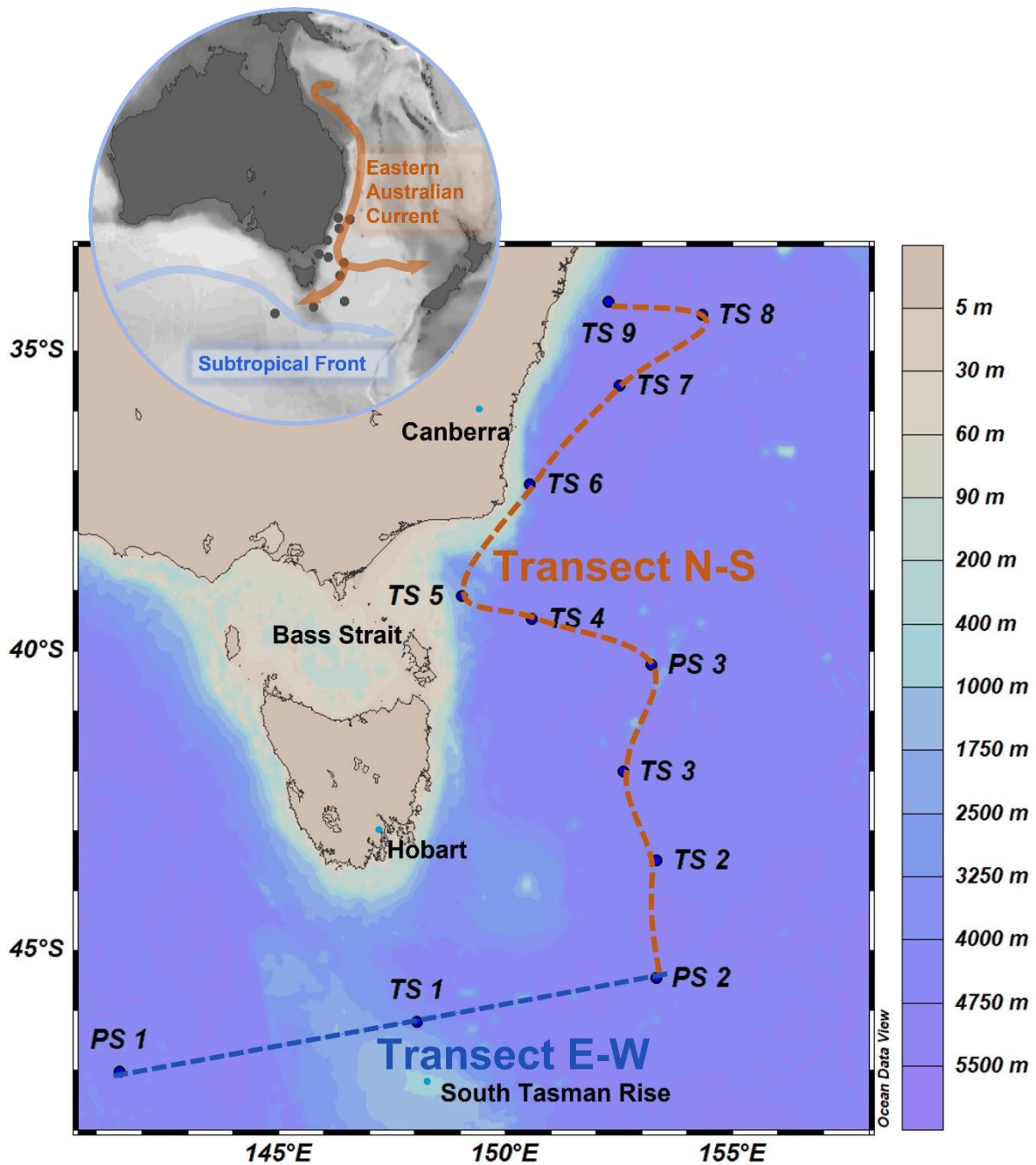


Figure 4.1 Inset: The locations of the East Australian Current (EAC, orange) and the Sub-Tropical Front (STF, blue) with respect to the Australian continent. Main: the 12 sampling stations and 2 transects (E-W and N-S) sampled during IN2018-V04 on the R/V *Investigator* during September and October 2018. PS = Process station; TS = Transit station. The colour bar indicates depth.

From Hobart, the voyage headed north along the EAC via transit stations (TS) 5, 6, 7, 8 and 9 (34.92°S , 152.27°E) before heading south via station TS 4, process station (PS) 3, TS 3, and TS 2. Transit station 5 is close to the Bass Strait and therefore shallow, with a bottom depth of 1674 m (**Figure 4.1** for bathymetry). Although TS 6 and 9 are closer to the continental margin, their bottom depths are 4667 m and 4866 m, similar to the other stations from the N-S transect. These stations form the north-south transect (N-S, coloured in orange, **Figure 4.1**) run 1280 km along the eastern Australian coastline with depths down to 4500 m. The voyage then headed west (south of Tasmania) via stations PS 2, TS 1, and PS 1 located within currents associated with the ACC (**Figure 4.1**). This forms the east-west transect (E-W, blue, **Figure 4.1**), extending 900 km from PS 2 to PS 1 south of Tasmania into HNLC water. Process station 1 and PS 2 have bottom depths of 4551 m and 4546 m, respectively. In contrast, TS 1 is shallow (2614 m bottom depth) compared to the other two stations (**Supplementary Table 14**) due to the South Tasman Rise indicated in **Figure 4.1** and **Figure 4.2, c**.

4.2.3 Sample collection and preparation

Water column

All trace metal sampling and analytical procedures followed internationally accepted trace metal clean protocols as recommended by the GEOTRACES program (Cutter et al., 2017). At each of the 12 stations sampled, a polyurethane powder-coated aluminium rosette (TMR, Seabird) fitted with 12 acid-cleaned externally sprung Teflon-coated Niskin bottles (12 L) was deployed attached to a Dyneema rope, collecting water sampled from 1250 m to surface. At TS 5, 7, 3, 2, 1, and PS 3, an additional deep cast to 4500 m depth was taken. Once the Niskin bottles were retrieved, they were transferred into a trace metal clean container on deck for subsampling under ISO class-5 HEPA clean conditions following GEOTRACES guidelines (Cutter et al., 2017). Due to rapid oxidation, the surface samples for dFe(II) were collected first and analysed directly. All dFe(II) samples were filtered through acid-washed filters (Acropak, $0.2\ \mu\text{m}$), while samples for H_2O_2 were analysed without filtration. Both samples for dFe(II) and H_2O_2 were subsampled into acid cleaned (10% hydrochloric acid (HCl)) 125 mL dark (low-light transmittance), high-density polyethylene bottles (Nalgene) without any headspace. Prior, these bottles were thoroughly rinsed with ultra-high purity water (UHP, Mili-Q, Merck) and

conditioned with low Fe seawater rinses. Once the samples for dFe(II) and H₂O₂ were collected, they were double bagged on ice until analysis.

Rainwater

The overall rainwater volumes (mm) were recorded using two RM Young Rain Gauge sensors (type 50202) mounted to the foremast port and starboard of the ship. Rainwater was collected once during a rain event at TS 4 via a Teflon funnel, mounted at an elevated position at the ship's bow. Before sampling, the funnel was acid cleaned and covered twice in plastic. A subsample of the rainwater (pH 6.5, salinity 0-1) was filtered (0.2 μ m acid-washed Millex filter) and analysed for dFe(II) within one hour after the rainfall.

Sediment

The sediment samples were collected via a KC Multicorer provided by the Marine National Facility (MNF) close to PS 3 at 3349 m depth (*40.17° S; 153.30° E*). Once the core was recovered, 2.5 mL subsamples of seawater for dFe(II) analysis were taken from several depths of this core and seawater respectively (see **Table 4.1**). These were 25 cm above the undisturbed seabed (watercolumn), 1 cm above the seabed, and approximately every 1 cm until 10 cm depth of the core (porewater samples). Each sample was centrifuged without a headspace and 0.2 μ m filtered (Millex). Once the samples were centrifuged, they were kept in 2.5 mL centrifuge tubes without a headspace, in the dark on ice and were analysed 16 hours later. No calculations to project for the concentrations directly after sampling were considered here.

4.2.4 Analysis

Dissolved Fe(II) in the water column

The analysis of dFe(II) was started 20-30 minutes after collection. Due to the analysis time of 800 s (~13 min) for one run (including 3 technical replicates), it took us approximately 2.7 hours (~160 minutes) to measure all samples starting from surface to bottom. A chemiluminescence based Flow Injection Analysis (CL-FIA) system was used with a preconcentration step using an 8-hydroxy quinoline column (Bowie et al., 2002, Bowie et al.,

2005, Sedwick et al., 2015, Holmes et al., 2019). No dimethylglyoxime (DMG) to prevent Co(II) interference was used. A 0.02 M stock solution of Fe(II) ammonium sulphate hexahydrate was prepared in 0.1 M HCl, which was kept under dark and cold conditions for the duration of the voyage. Serial dilutions of 200 μ M and 200 nM were prepared in UHP water for daily calibrations. All dFe(II) standard solutions were spiked with sodium sulphite (Na_2SO_3), acting as a reducing and stabilizing agent. To keep the calibration matrix similar to the sampled water, low dFe(II) deep-water was used, collected the day before, kept on ice in the dark without a headspace. The calibration seawater was buffered to a pH of 6.4 with ammonium acetate during the flow injection procedure. Aged seawater was run three times before and after the sample run to correct for instrumental drift over time. The aged seawater was collected in the SO between Tasmania and Antarctica in February 2018 during the GEOTRACES SR3 voyage. It was aged in the dark and kept in the cold for more than six months before use. The limit of detection (LOD) was defined as three times the standard deviation of the blank peak ($n=3$) (Bowie et al., 2004). During this voyage, the LOD was determined for each TMR cast and ranged from 0.02 to 0.18 nM with a mean of 0.06 nM ($n = 18$).

Dissolved Fe(II) in rainwater

To dilute the high concentrations of dFe(II) in rainwater and to obtain values for pH and salinity closer to sea surface values (necessary for the chemiluminescent Flow Injection Analysis (CL-FIA) method, see below), the filtered rainwater was mixed with low dFe(II) seawater from the previous cast from TS 5 (0.08 nM Fe, measured 24 hours prior). The calibration was also done in water collected from the cast of TS 5 to mix and dilute with the rainwater. A 1:1 mixture of sea to rainwater was used for the dilution, resulting in a pH of 7.48 and a salinity of 18, and a 3:1 mixture, resulting in a pH of 7.73 and a salinity of 34. The initial pH and salinity of the low dFe(II) seawater were 7.83 ± 0.03 ($n = 3$) and 36, respectively. For the analysis of H_2O_2 , a 50-x dilution in aged low Fe and low H_2O_2 seawater was used. The measurement was performed as stated in the 'Dissolved Fe(II) in the water column' section above.

Dissolved Fe(II) in sediments

Dilutions from 1:60 to 1:6 were done empirically with seawater samples (**Supplementary Table 12**). The seawater used for dilutions was previously collected from the deepest cast at the same station (0.24 nM of dFe(II) 24 hours prior to the sediment analysis) and kept at approximately 3°C prior to use, to resemble temperatures close to the ocean floor. Once the samples were diluted, they were analysed immediately (CL-FIA) as described above. No time correction was considered for further data processing to account for the time loss between the core sampling/centrifugation until actual analysis.

Hydrogen peroxide

Unfiltered samples for the measurement of H₂O₂ were analysed within 30 minutes post sample collection, starting with the surface samples and ending with the deepest. A flow injection system based on the approach by Yuan and Shiller (1999) was used. This method also uses the chemiluminescent reagent luminol, which catalyses H₂O₂ in the presence of cobalt (Co²⁺). Calibration standards were prepared weekly by serial dilution from a 30% stock solution (Seastar Baseline) and were determined by spectrophotometric measurements using a 10 cm Liquid Waveguide Capillary Flow Cell (LWCC, World Precision Instruments, $\epsilon = 40.9 \text{ M cm}^{-1}$; Hwang and Dasgupta, 1985). Each sample was analysed 4-5 times with a 3-5% precision and a concentration ranging from 0.5 nM to 55 nM. The LOD here was 0.5 nM (n = 18), defined as three times the standard deviation of the blank peak.

Dissolved Fe

Samples for the analysis of dissolved Fe (dFe) were also collected from the TMR as described in 4.2.3 and methods and data were published in Barret et al., 2021. All bottles used for this trace metal sampling were cleaned for one week in 1% w/w nitric acid (HNO₃) and filled with 0.1% w/w HNO₃ until use. After thorough rinsing with UHP, the seawater was filtered (0.2 μm , Acropak) into 250 mL low-density polyethylene bottles, acidified to pH < 1.8 using distilled HNO₃ and stored until analysis at the Australian National University (ANU) facilities. The samples were preconcentrated, and the seawater matrix was removed offline using an automated preconcentration system (Ellwood et al., 2018). Afterwards, the samples were spiked

with isotopes (^{57}Fe , ^{206}Pb , ^{65}Cu , ^{61}Ni , ^{67}Zn) and buffered to pH 5 with an ammonium acetate buffer. The samples were analysed via isotope dilution inductively coupled plasma mass spectrometry (ICP-MS, Thermo Scientific). See Barrett et al. (2021) for detailed methods.

Hydrographic data and Chlorophyll-*a*

At all 12 stations, the Conductivity-Temperature-Depth (CTD) rosette was also deployed to assess hydrochemistry parameters. Samples for salinity and O_2 were analysed from water samples collected using the CTD Niskin bottles and through rosette mounted Sea-Bird Electronics sensors SBE3T, SBE4C, SBE9plus, and SBE43, respectively (see Holmes et al., 2019 for more detail). Macronutrients (nitrate (NO_3^-), silicate (SiO_4^{2-}), and phosphate (PO_4^{3-})) were determined onboard using a SEAL AA3 HR AutoAnalyzer (Rees et al., 2019). Samples for chlorophyll-*a* (Chl-*a*), collected from CTD casts, were assessed with an acetone extraction method (Wright et al., 2005) using a Turner Designs model 10-AU fluorometer on board (see suppl. Table 2). Neutral density (γ^n) and the apparent oxygen utilisation (AOU, μM) were calculated using Ocean Data View (ODV; Schlitzer, 2015).

4.3 Results

4.3.1 Hydrography

Along the two transects (N-S & E-W), the distribution of temperature, salinity, and oxygen displays a typical gradual change in the upper 500 m from north to south (**Figure 4.2** & **Figure 4.3** Depth profiles of temperature ($^{\circ}\text{C}$; green), salinity (orange) and O_2 (μM ; purple) for stations TS 9 to TS 2 (N-S transect) and stations PS 2 to PS 1 (E-W transect)). The temperature-salinity sections and profiles show a warm and saline layer in the northern stations (N-S transect) and a colder, less saline surface layer in the southern subantarctic waters (E-W transect, **Figure 4.2** and **Figure 4.3**). Temperature (**Figure 4.2**, a) was highest in the north at stations 7, 8, and 9, with values between 18°C and 19.3°C in the upper 200 m. In the southern stations between 46°S and 47°S , the SST was found to be between 9.4°C (PS 1, 40 m depth) and 9.1°C (TS 1, 15 m deep). A higher SST of 12°C characterized PS 2 (45.4°S) within the first 100 m, which may be due to the mixing of the EAC and STF currents. The southern stations (E-W; PS 1, PS 2, TS 1) had a temperature of 9°C from surface to 500 m depth and decreased to 4°C below

1500 m. Salinity (**Figure 4.2**, b) was highest in the surface (0-200 m) water masses in the northern stations (TS 4 to TS 9), with values from 35.44 to 35.76. In the stations south of 40°S (PS 3 to PS 1), salinity was between 34.64 and 35.42 in the upper 200 m. A water mass with homogeneously low salinities of ~ 34.2 to 34.5 between 700 and 1000 m depth was found. This stretched laterally throughout the sampling transect. This water mass was defined as the minimum-salinity Pacific Antarctic Intermediate Water just above the actual Antarctic intermediate water (AAIW), which originates in the thick surface layer of the Subantarctic Mode Water (SAMW) in the southeast Pacific (Talley, 2011). Below 2000 m, salinity was more homogeneous (34.44 to 34.60) without a north-south gradient. Oxygen concentrations in the surface also followed a north-south gradient with increasing concentrations towards the pole (**Figure 4.2**, c and **Figure 4.3**). These concentrations ranged between ~230 μM in the upper 200 m in the north to ~280 μM in the southern stations. Oxygen concentrations decreased from the surface layer to ~ 1500 m and increased from 175 μM at 1500 m depth to 200 μM at depths below 4000 m. Between 1000 and 2000 m depth, a water mass band stretching from north to south matching the descriptions for Upper Circumpolar Deep Water (UCDW; **Figure 4.2**, c) with Lower Circumpolar Deep Water (LCDW) beneath it (Rintoul et al., 2001, Orsi et al., 1999) was found. Considering the profiles of all stations (**Figure 4.3**), they all show lower O_2 concentrations at depths between 1000 and 2000 m with a salinity minimum above it. As described earlier (Oke et al., 2019) and based on findings by Barrett et al., 2021, an anticyclonic eddy at 31-34°S (TS 7 and 8) was defined and linked to low concentrations of dFe and the anomalously deep mixed layer (> 200 m vs. 125 m in other locations, also see macronutrient sections in **Fig. 4.2**).

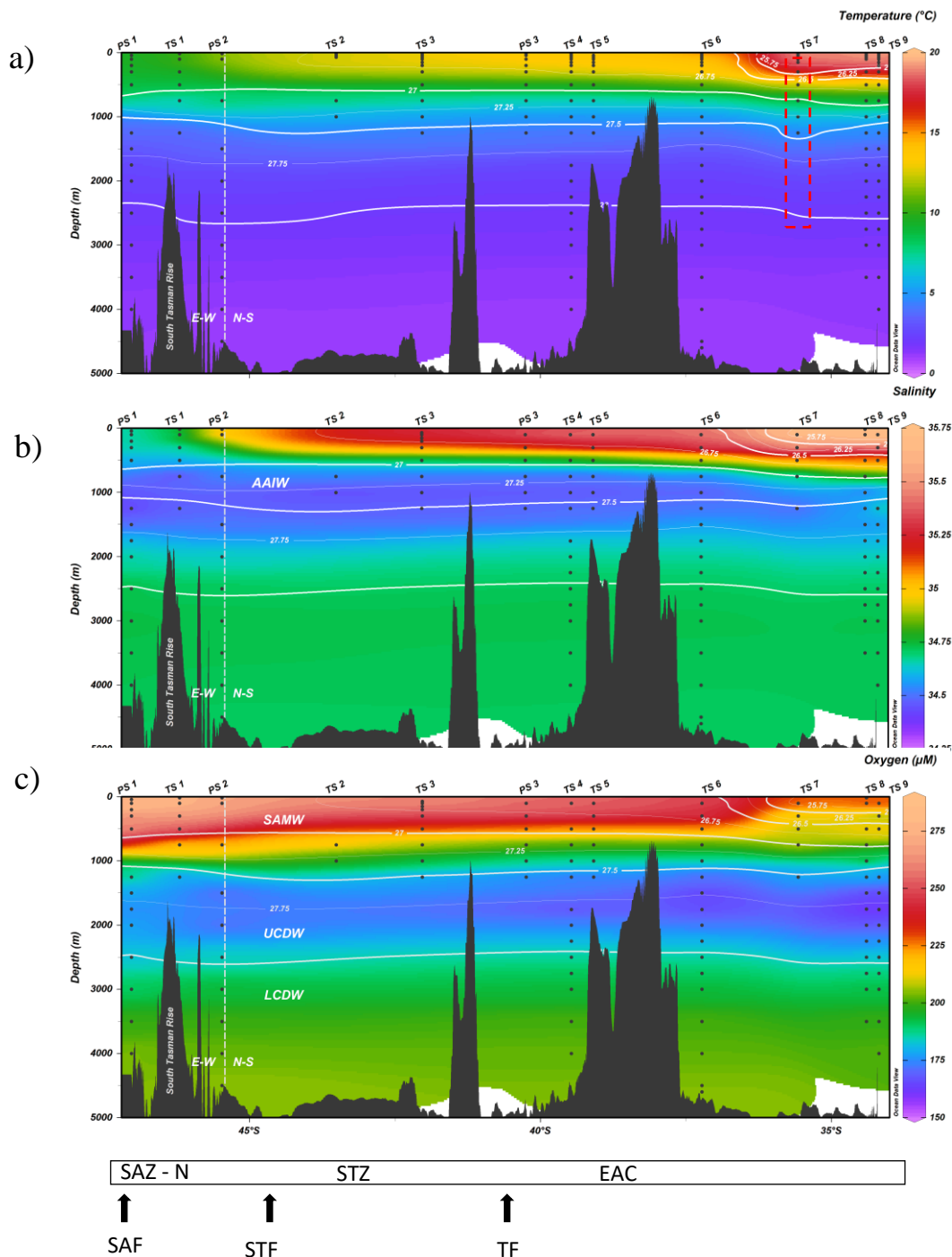


Figure 4.2 Temperature (a), salinity (b) and oxygen (c) along transects N-S and E-W from 0 to 5000 m. The colour bar indicates concentrations, black dots indicate sampling depths for each station, including neutral density contours (γ^n ; kg m^{-2} , white lines). Antarctic Intermediate Water (AAIW, b) and Subantarctic Mode water (SAMW, c) was defined in the surface and followed by upper (U) and lower (L) Circumpolar Deep Water (CDW) below. Below section (c) the northern Subantarctic Front (SAF) is displayed followed by the northern Subantarctic Zone (SAZ-N) and the Subtropical Front (STF). This figure also outlines the Subtropical Zone (STZ) and the Tasman Front (TF), followed by the East Australian Current (EAC). The red rectangle displayed in a) indicates the position of a cyclonic eddy observed during this voyage.

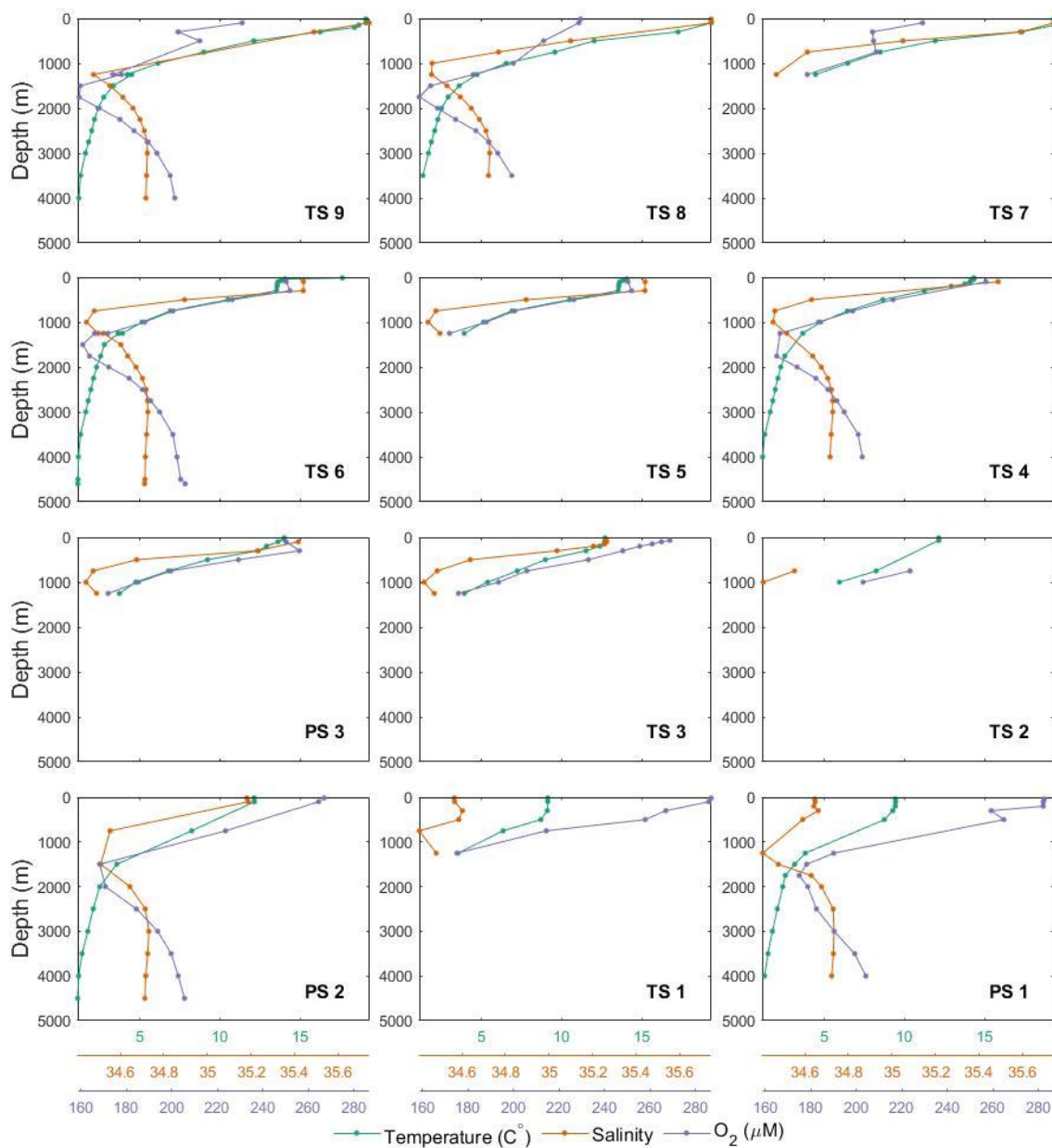


Figure 4.3 Depth profiles of temperature (°C; green), salinity (orange) and O₂ (μM; purple) for stations TS 9 to TS 2 (N-S transect) and stations PS 2 to PS 1 (E-W transect).

4.3.2 Macronutrients

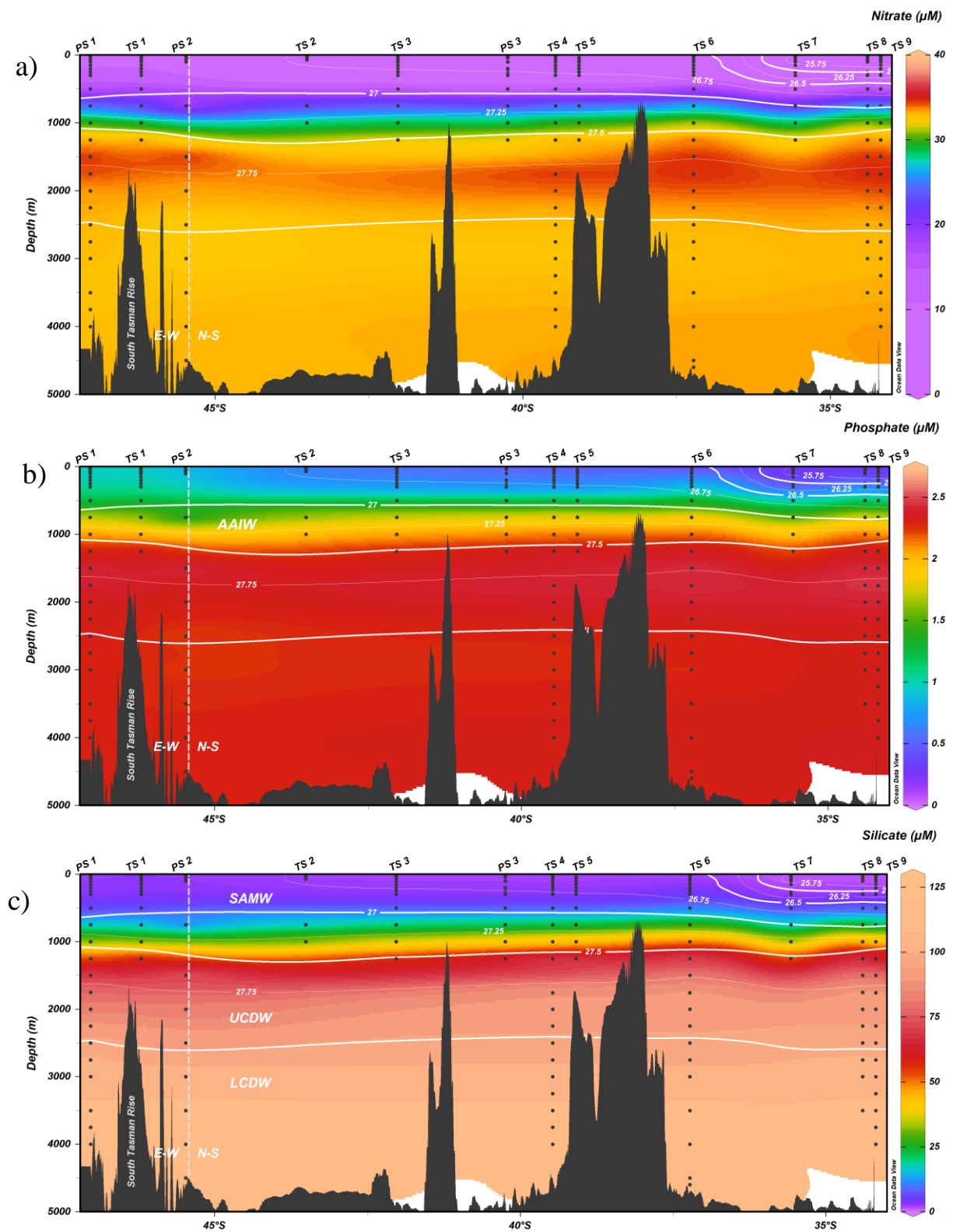


Figure 4.4 Macronutrient concentrations in the water column along the transects E-W and N-S: a) NO_3^- , b) PO_4^{3-} and c) SiO_4^{2-} including neutral density contours (γ^n ; kg m⁻², white lines).

Sampled NO_3^- values (**Figure 4.4 a** and **Figure 4.5** for all stations) ranged between 0 and $35 \mu\text{M}$ in the upper 1000 m, with the highest values between 1000 m and 2000 m. Phosphate (**Figure 4.4, b**) had concentrations of $0.5 \mu\text{M}$ in surface waters, with concentrations increasing to $2.5 \mu\text{M}$ below 1000 m in the LDCW layer. Silicate values (**Figure 4.4, c**) were lower in the first 1000 m and increased to $125 \mu\text{M}$ at depths below 3000 m. All three nutrients were significantly correlated (Pearson correlation $r \geq 0.84$, $n = 185$) for all stations (see **Figure 4.5**).

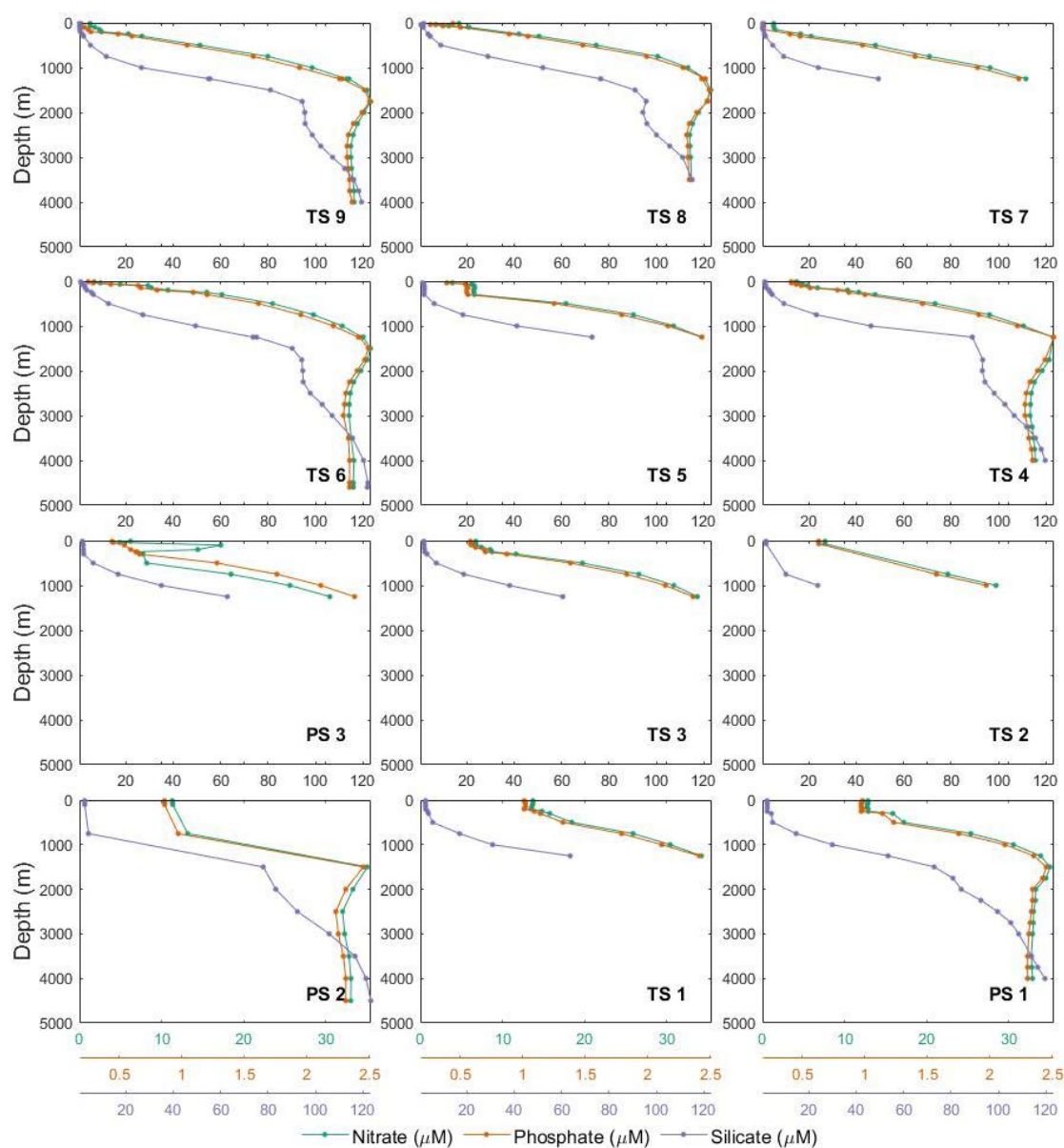


Figure 4.5 Depth profiles of macronutrients NO_3^- (μM , green), PO_4^{3-} (μM , orange) and SiO_4^{2-} (μM , purple) for all stations. Stations TS 9 to TS 2 are summarised as the N-S transect and stations PS 2 to PS 1 as the E-W transect.

4.3.3 Chlorophyll-*a*

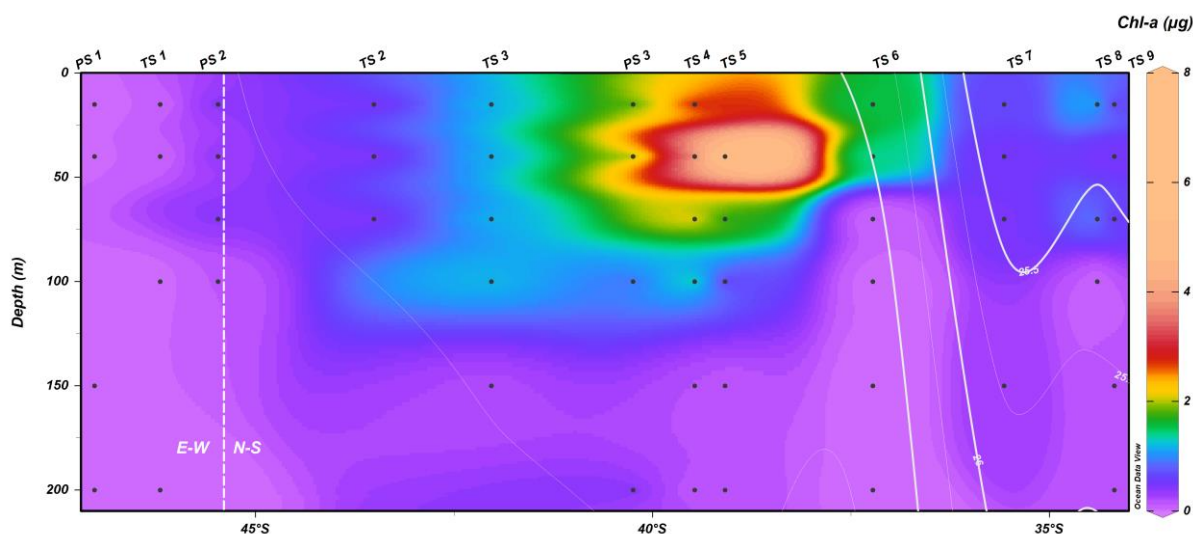


Figure 4.6 Chl-*a* concentrations (μg) along both transects in the upper 200 m of the water column. White lines denote neutral density contours (γ^n ; kg m^{-2}).

Chlorophyll-*a* (**Figure 4.6**) was found to be highest in the upper 100 m close to the Bass Strait and the Australian main continent. The highest values from the first 70 m of stations TS 4, TS 5 and TS 6 were 2.6 ± 0.32 , 3.2 ± 4.1 and $1 \pm 0.81 \mu\text{g}$ respectively. The average at the other stations in the upper 70 m were 0.5 ± 0.01 (TS 9), 1.07 ± 0.2 (TS 8), 0.54 ± 0.08 (TS 7), 1.26 ± 0.43 (PS 3), 1.18 ± 0.02 (TS 3), 0.36 ± 0.02 (TS 2), 0.368 ± 0.02 (PS 2), 0.05 ± 0.01 (TS 1) and 0.054 ± 0.01 (PS 1; also see **Supplementary Table 13**).

4.3.4 Dissolved Fe(II) distribution

Overall, the dFe(II) concentrations (**Supplementary Table 13**) varied greatly, with the highest concentrations in the upper 500 m east of the most northern Stations (TS 7 and 8) with peaks between 0.4 nM and 0.5 nM (**Figure 4.7, a**). The highest overall concentration was found at 500 m depth at TS 4 with a value of 0.53 nM. Concentrations from the southern stations (PS 1, TS 1, PS 2) were generally lower, with concentrations peaking at 0.30 nM at the surface. At depths below 500 m, concentrations were below 0.2 nM except for PS 1, PS 3, TS 4, TS 7 and TS 9, where the highest concentrations ranged from 0.2 to 0.34 nM.

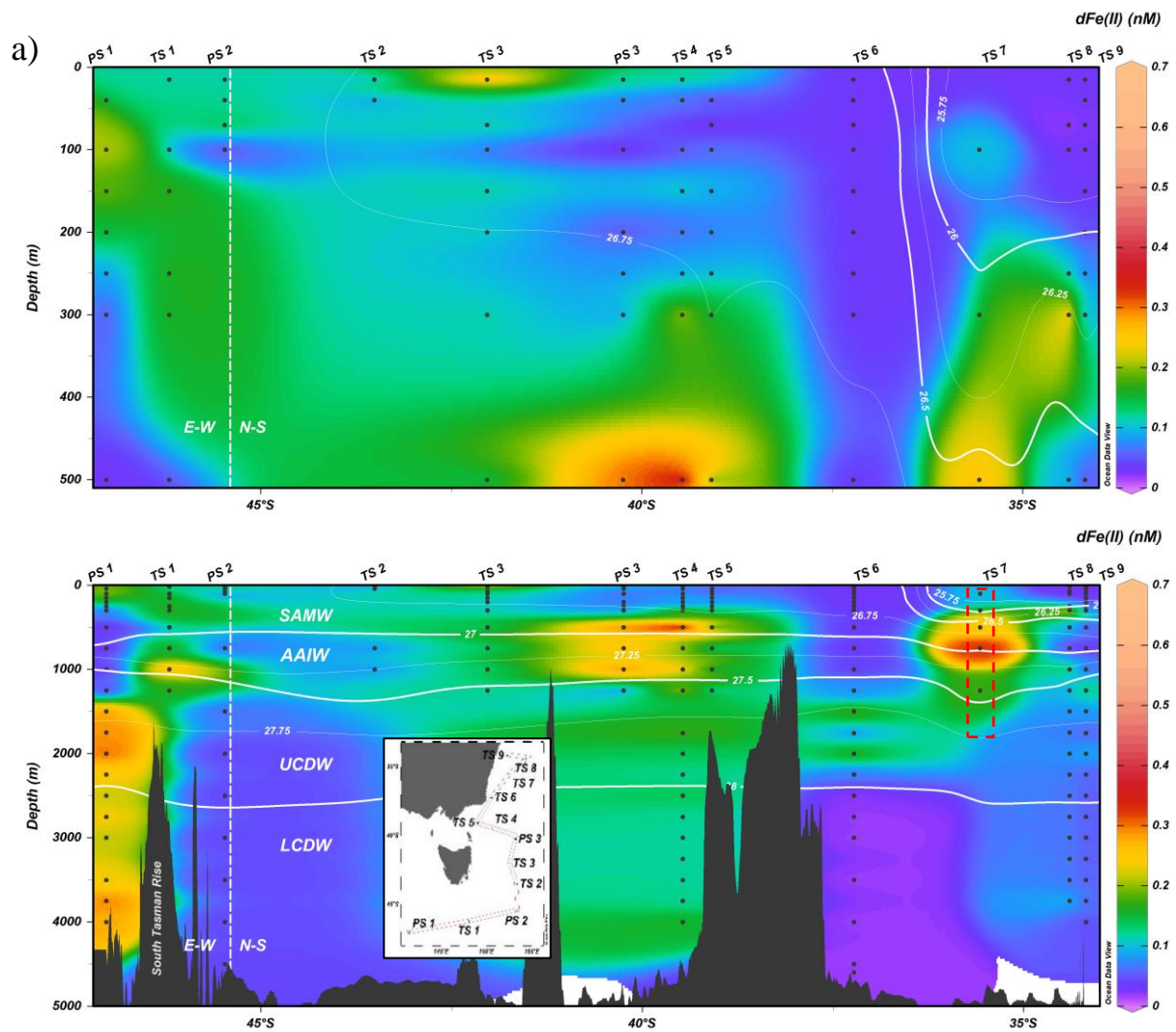


Figure 4.7 Dissolved Fe(II) concentrations (nM) along the transect into depths in the upper 500 m (a) and below 4000 m (b) with neutral density contours (σ^{θ} ; kg m⁻², white lines). The colour bar indicates concentrations of dFe(II), black dots display stations labelled at the top. The full data set can be found in **Supplementary Table 13**. The red rectangle displayed in a) indicates the position of a cyclonic eddy observed during this voyage.

4.3.5 Dissolved iron distributions

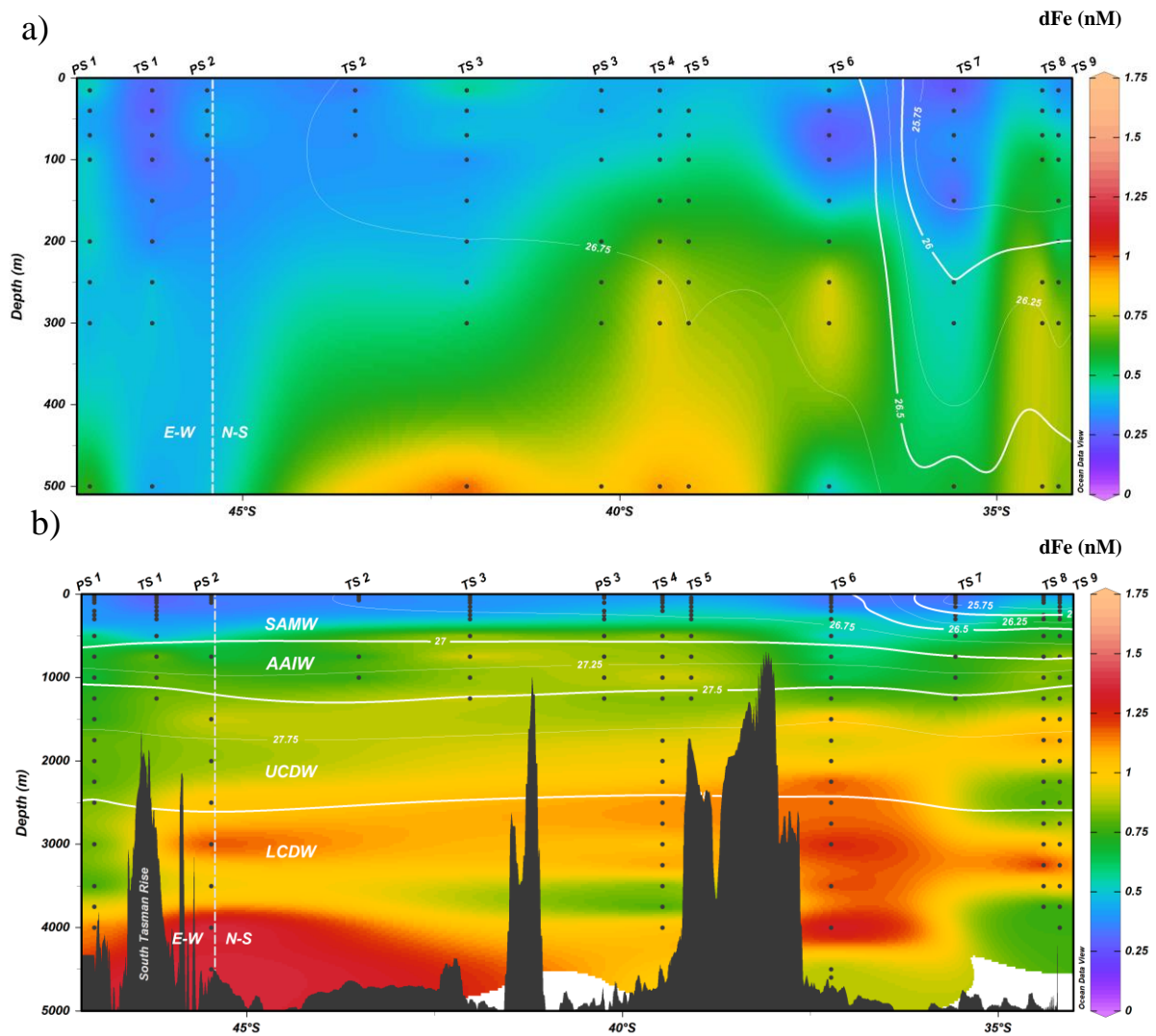


Figure 4.8 DFe (nM) following N-S and E-W transects of (a) concentration from surface to 500 m depth, and (b) concentration from surface to below 4000 m with neutral density contours (σ^{θ} ; kg m^{-2} , white lines). DFe values presented were used from Barrett et al., (2021).

DFe (nM), as described for this voyage by Barrett *et al.*, (2021), was lowest in surface waters at all stations, with concentrations below 0.5 nM (**Figure 4.8** and **Figure 4.9**). In comparison, concentrations increased to 1.5 nM closer to the South Tasman Rise at PS 2 and increased closer to the landmass at TS 6 and TS 7. When comparing profiles of dFe(II) and dFe (**Figure 4.9**), most stations show surface maxima of dFe(II) with decreasing concentrations at greater depths, except for PS 1, where high dFe(II) concentrations are likely due to proximity to the South Tasman Rise. DFe, on the other hand, often had low concentrations in the surface 200 m with increasing values below the photic zone, which explains why the ratio of dFe(II) to dFe is often higher in the upper 200 m.

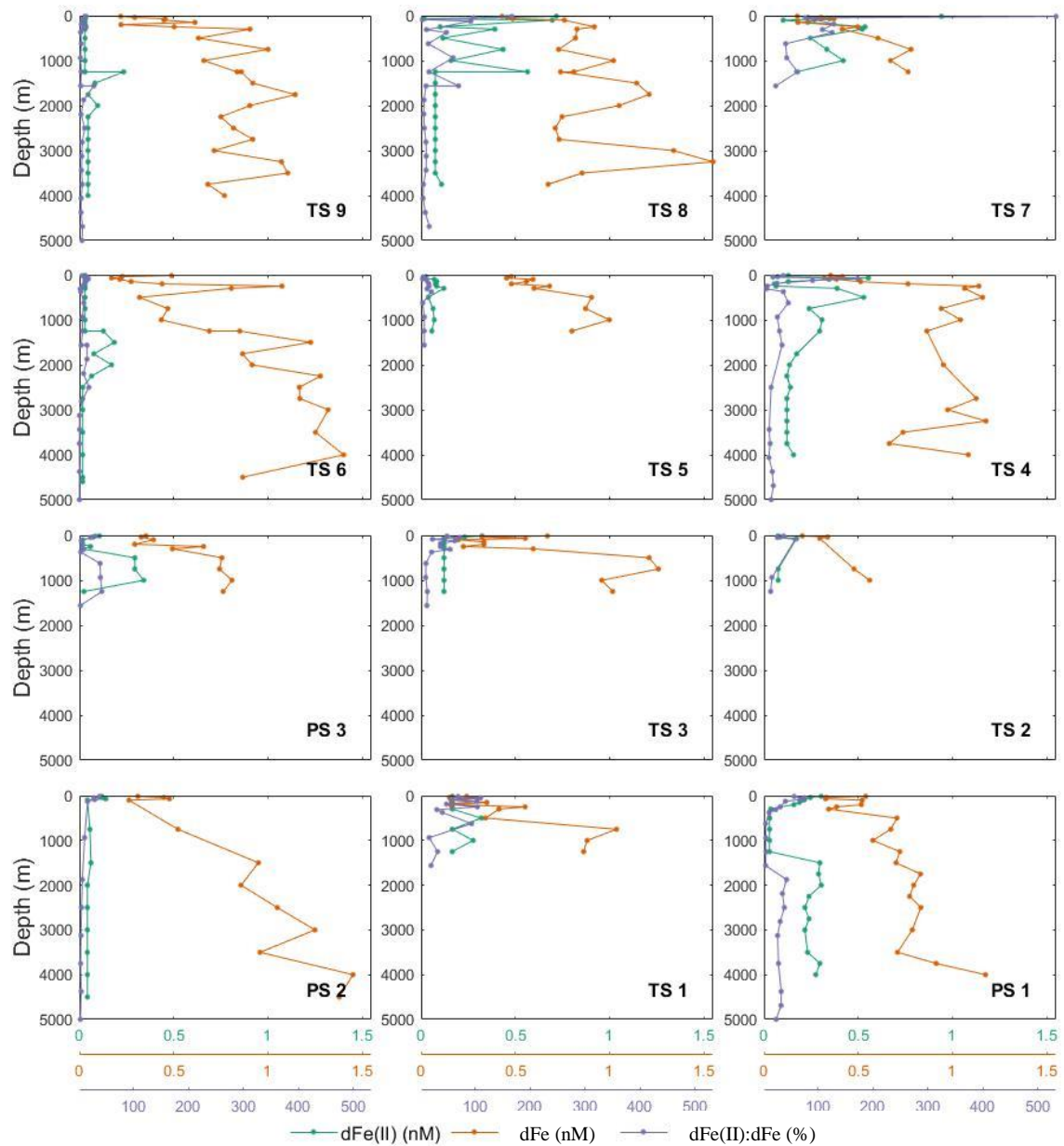


Figure 4.9 Concentrations of dFe(II) (nM, green) and dFe (nM, orange) and the ratio of dFe(II) to dFe (blue) for all 12 stations. Stations TS 9 to TS 2 (N-S transect) is followed by stations PS 2 to PS 1 (E-W transect). The dFe data was used from Barrett et al., (2021).

4.3.6 Dissolved H₂O₂ distribution

Surface concentrations decreased gradually from south to north, where the concentration ranged between 11.4 nM and 27.9 nM for TS 5, TS 6, TS 7, TS 8, and TS 9. Dissolved H₂O₂ concentrations were highest at the southern stations PS 1, TS1, PS 2, TS 3, and PS 3 with a peak concentration at TS 2 (55.72 nM at 15 m, (**Figure 4.10**, a)). At depths below 500 m (**Figure 4.10**, b), concentrations ranged from 0 to 20 nM. The concentration below 500 m was more homogenous at the northern stations, ranging from 0 nM to 10 nM. Higher concentrations in the first 100 m at TS 2 (46 ± 2.9 nM) were observed. **Figure 4.10** visualises combined concentrations of dFe(II) and H₂O₂ with O₂ concentrations. Concentrations of H₂O₂ and dFe(II) (**Figure 4.11**) were not correlated for all sampling stations ($r = 0.021$, $p = 0.78$, $n = 179$, see **Supplementary Table 14**) while H₂O₂ and O₂ had a moderate and significant correlation ($r = 0.660$, $p < 0.01$, $n = 110$).

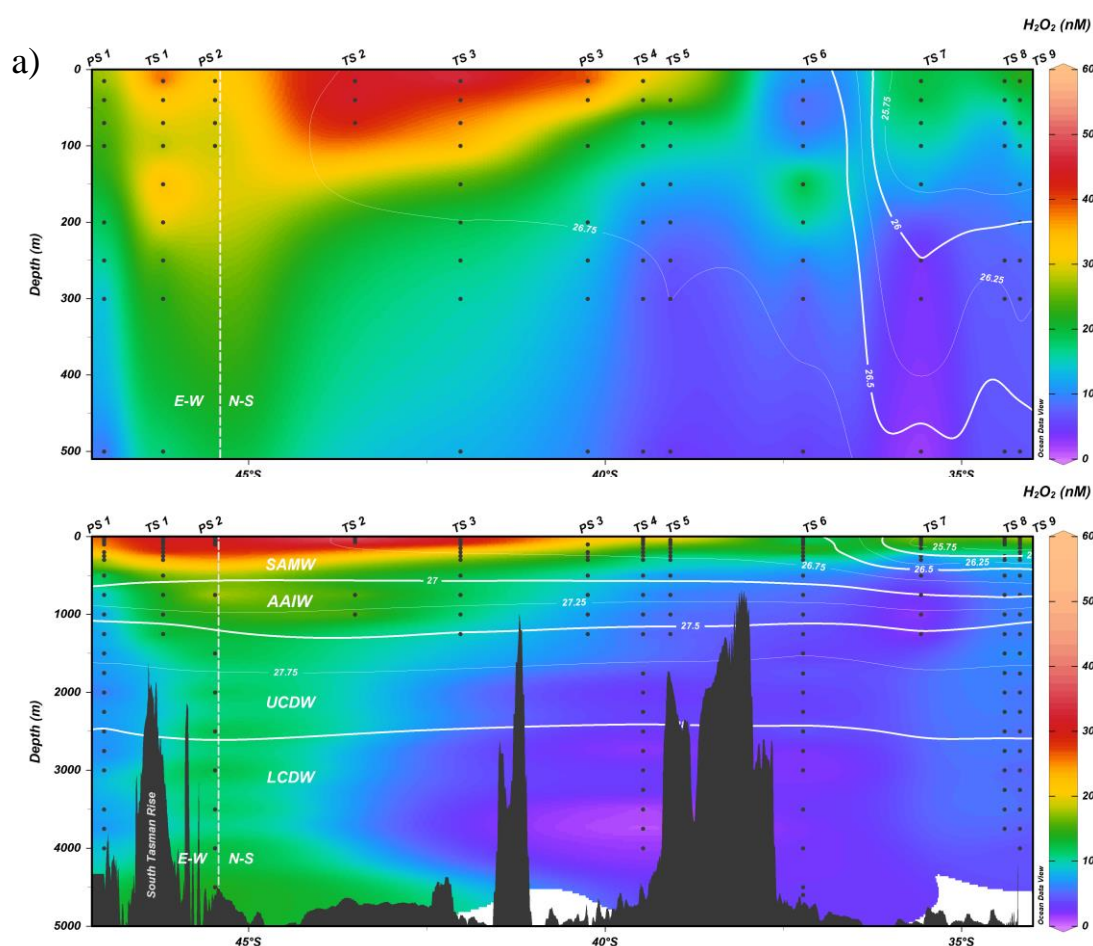


Figure 4.10 Dissolved H₂O₂ concentrations (nM) along the transect in the upper 500 m (a) and below 4000 m (b) with neutral density contours (γ^n ; kg m⁻², white lines). Colour bar indicates concentrations of H₂O₂ (nM), black dots display stations, labelled at the top. The full data set can be found in the appendix.

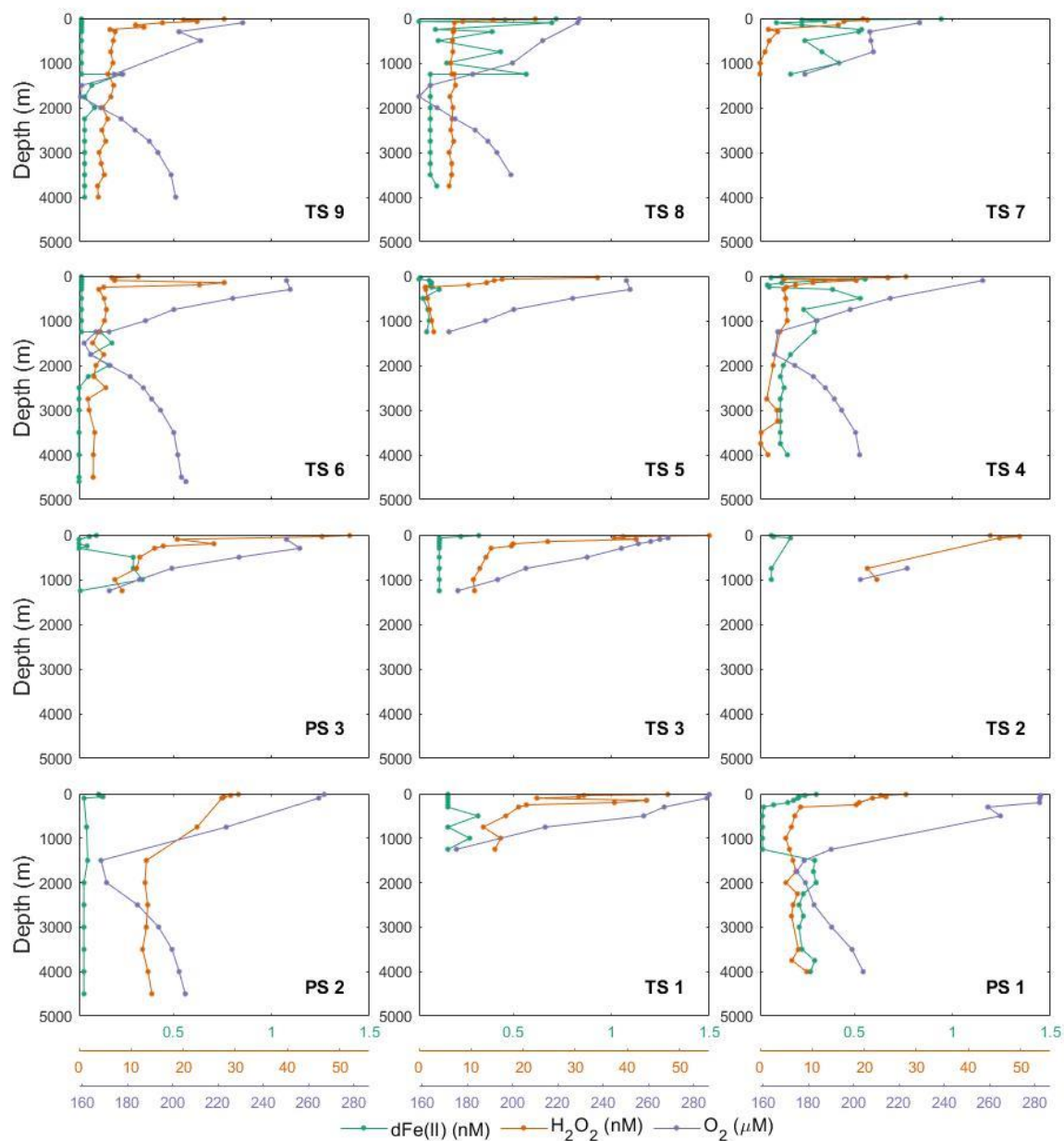
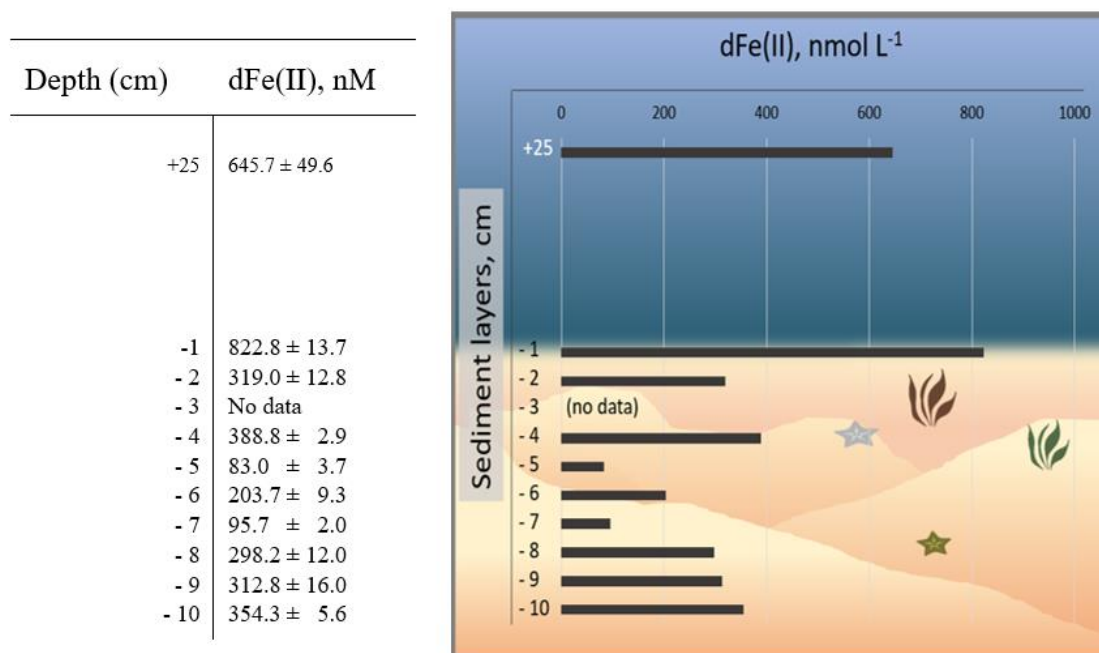


Figure 4.11 Deep profiles from surface to below 4000 m. Samples taken for dFe(II) (green), H₂O₂ (orange) and O₂ (blue) in the N-S transect (TS 9 to TS 2) following the E-W transect (PS 2 to PS 1). The full data set is displayed in the appendix (**Supplementary Table 13**).

4.3.7 Rainwater and sediment pore water

The concentration of dFe(II) for the sampled rainwater was 30.2 ± 0.3 nM ($n = 3$) when using a 1:1 dilution (see method section) and 37.4 ± 0.5 nM ($n = 3$) for the 1:3 dilution. A value of 3.2 nM ($n = 1$) for H_2O_2 in the analysed rainwater was measured. The dFe(II) concentrations in sediment 16 hours post collection were highest at 1 cm depth with 823 nM, followed by a concentration of 645 nM at 25 cm above the sediment floor. Below the sediment surface, the concentrations followed an irregular pattern (see **Table 4.1**) ranging from 822.8 ± 13.7 nM at 1 cm depth to 354.3 ± 5.6 nM at 10 cm depth.

Table 4.1 Left: Concentrations of dFe(II) 16 hours after collection from 25 cm above the seafloor, followed by concentrations below the surface from approximately -1 cm to -10 cm. Each concentration was analysed 3 times ($n = 3$). Right: Figure of the measured concentrations of dFe(II) nM.



4.4 Discussion

4.4.1 Dissolved Fe(II), H₂O₂ and dFe concentrations in the Southern Ocean

The concentrations of H₂O₂ in the upper 500 m of the northern stations of the EAC voyage ranged from 20 to 30 nM and were up to 60 nM in the south. Conversely, the highest values of dFe(II) were in the surface layers of the northern stations (TS 4 and TS 8, up to 0.4 to 0.5 nM) and lower in the southern stations (> 0.2 nM). Although there is little data describing dFe(II) concentrations in the Tasman Sea, the data compares well to other findings from the SO. The observed dFe(II) values are higher (0.01 nM - 0.10 nM; Schallenberg et al., 2016, Sarthou et al., 2011) or comparable (0.1 nM - 0.5 nM; Holmes et al., 2020) to other data found close to continents or islands in the SO. The relatively high dFe(II) values in the upper 200 m of PS 1 (0.18 ± 0.0) and TS 3 (0.17 ± 0.1) may reflect dry or wet deposition from the continents, photochemical reduction paired with impacts from organic matter and phytoplankton activity especially at PS 1 and TS 3 (see sections below and Obernosterer et al., 2001, Perron et al., 2020). At TS 7 and 8, we suggest a high dFe(II) concentration due to the anticyclonic eddy there (**Figure 4.7, b**) (Oke et al., 2019 and Barrett et al., 2021), delivering nutrient rich water from the core of the EAC (Oke and Middleton, 2000). These high nutrients were further associated with high Chl-*a* concentrations due transport of nutrients from the EAC into western Tasmanian water (Tilburg et al; Everett et al., 2012). The dFe(II) values of TS 1 and PS 3 between 500 and 1000 m depth lie within the AAIW. They may be higher (> 0.2 nM) due to remineralisation at those depths, especially when considering the AOU rate, which is highest at 1000 m depth (**Figure 4.12**) (Sedwick et al., 2015).

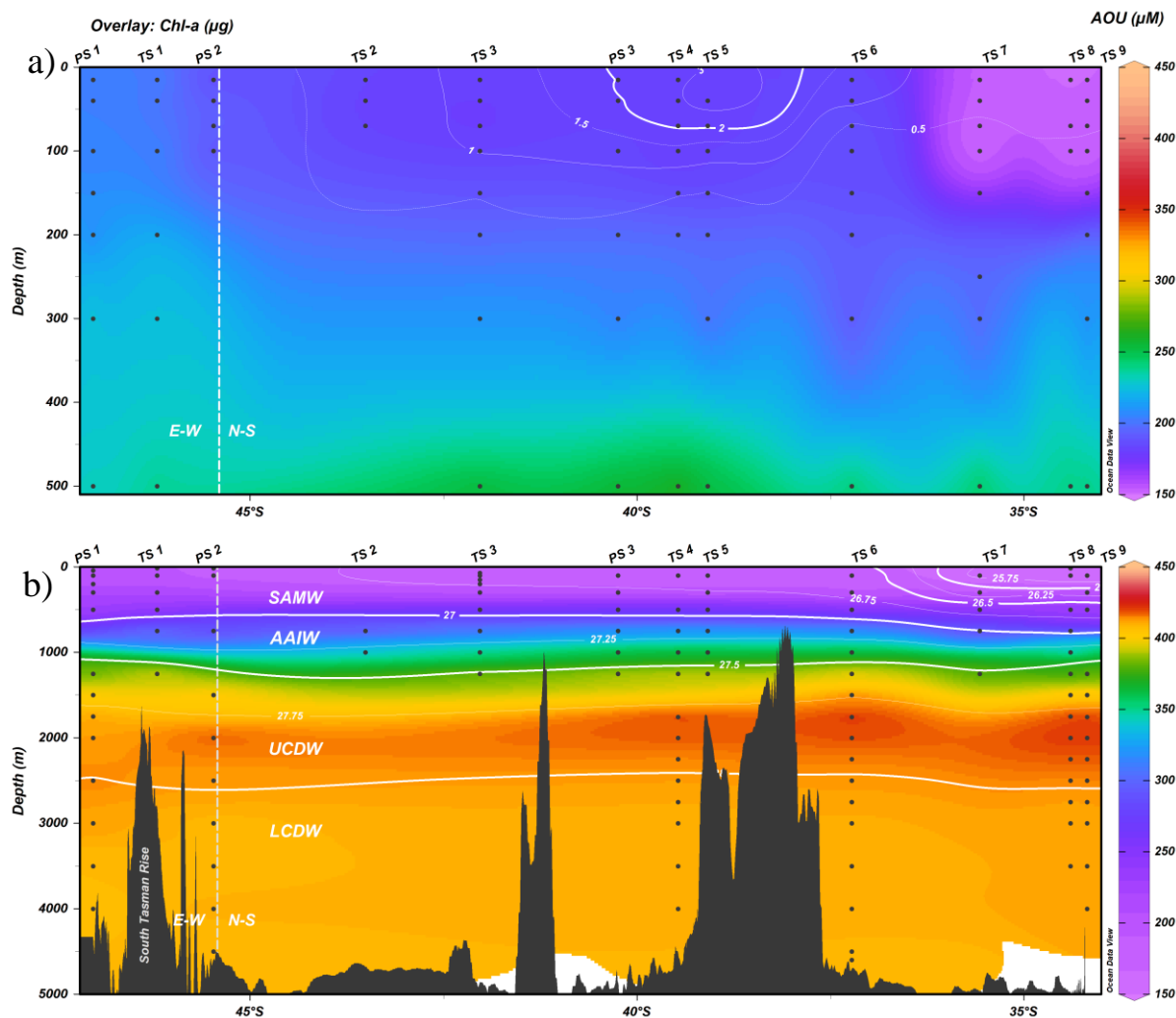


Figure 4.12 Apparent oxygen utilisation in the upper 500 m (a) and 5000 m (b). White lines in a) denote Chl-*a* contours. White lines in b) denote neutral density contours (γ^n ; kg m^{-2})

Similar to Holmes et al. (2020), the two variables dFe(II) and H_2O_2 are not correlated ($r = 0.021$, $p = 0.78$, $n = 179$; Pearson correlation **Supplementary Table 15**) in this study. However, both display significant positively correlated trends for temperature and salinity combined with a negative correlation for depth (see **Figure 4.13**). This also indicates facilitated oxidation of dFe(II) when the concentrations of H_2O_2 are high due to potential interactive processes (Croot et al., 2019, Millero and Sotolongo, 1989). Furthermore, when comparing dFe and H_2O_2 (**Figure 4.13**), they show similar patterns in the upper 1500 m with significant correlations for all stations ($r = -0.574$; $p < 0.001$, $n = 178$; Pearson correlation **Supplementary Table 15**). This correlation of H_2O_2 and dFe combined with dFe(II) and H_2O_2 not being correlated may be due

are relatively low compared to some of the ratios found in this study (e.g. TS 3, 48%) but we could not see a clear pattern regarding our ratios related to depth, sources or proximity to landmass.

4.4.2 Impact of physico-chemical parameters for the H₂O₂ and dFe(II) concentration

Dissolved Fe(II) is often highest (> 0.2 nM) in surface waters despite its rapid oxidation due to several impacting parameters such as photo-reductive processes and impacts from ROS such as H₂O₂. The first influencing parameters highlighted here are based on depth/pressure, temperature and salinity, followed by the impact of macronutrients, other trace metals, Chl-*a*, *PAR* and O₂.

Depth, pressure, salinity and temperature

Although pressure/depth influences the activity coefficients in seawater compounds (Millero, 1979), it has not been shown experimentally how depth/pressure impacts the concentrations of H₂O₂ or dFe(II) in situ at depths below the surface. Overall, one would expect lower dFe(II) concentrations at high temperatures due to rapid oxidation (Millero et al., 1987, González-Davila et al., 2005). However, in the northern surface samples (~20°C), the highest dFe(II) concentrations (0.5 nM at TS 4, 0.4 nM at TS 8) from this dataset were observed. Apart from that, the trend of less dFe(II) in warmer water and more dFe(II) in cold water holds true. Although depth and temperature are highly correlated in this study ($r = -0.829$, $p < 0.001$, $n = 155$; **Supplementary Table 15**), one can suggest that the high concentrations of dFe(II) at station TS 1 in the surface layer are likely results of external sources such as aerosol-based mineral dust (verbal communication with M. Perron) and other inputs from the continent. Also, the area of TS 7 was subject to an anticyclonic eddy, as described by Barrett et al. (2021). These upwelling water masses transported from the north through the EAC often contain high macro nutrient and Fe concentrations which may explain high dFe and dFe(II) concentrations.

At greater depths below 1000 m, however, temperatures below 5°C and high dFe(II) concentrations (> 0.2 nM) at TS 4, 5 and 6 and PS 1 (**Figure 4.7**) were observed. While the

major explanation for these concentrations is likely proximity to landmasses and seamounts, a retarded oxidation from slower kinetics at 5°C (Millero et al., 1987) combined with low O₂ concentrations could also be considered to have led to extended half-lives of dFe(II) there. For PS 1, high dFe values also could have led to higher values of dFe(II) from 2000 m to 3500 m depth in combination with lowered oxidation rates due to colder water with lower O₂ concentrations such as the UCDW.

While it is known that shifts in salinity alter the ionic strength and the linked oxidation of dFe(II) (Millero, 1989), the differences from north to south presented here are likely too small to reveal an impact due to changed salinity. Therefore, impacts due to shifts in salinity can be excluded when comparing surface water from the north (N-S transect) to the south (E-W transect) where salinity was higher in the north (surface salinity of TS 7, TS 8, and TS 9: 35.75 ± 0.01) and lower in the southern stations (surface salinity of PS 1, TS 1, and PS 2: 34.79 ± 0.33). This range in salinity only led to a small change in ionic strength, I (north: $I = 0.739$, south $I = 0.718$), revealing that salinity had an insignificant impact on the dFe(II) oxidation rate (Millero, 1985, Millero and Izaguirre, 1989).

On the contrary, higher O₂ concentrations in the upper 1000 m of the southern stations (transect E-W: $262.4 \pm 22.7 \mu\text{M}$) compared to northern stations (N-S: $223.3 \pm 25.01 \mu\text{M}$) could have led to accelerated oxidation of dFe(II) (Millero et al., 1987). Additionally, decreasing temperatures (N-S: $12.78^\circ\text{C} \pm 4.36$ vs. E-W: 9.33 ± 1.5) in the south could have retarded the oxidation of dFe(II) (Millero et al., 1987), which might explain the higher concentrations observed at the surface of PS 1.

Macronutrient impacts

It has been shown that high concentrations of Si can extend the half-life of dFe(II) (Gonzalez et al., 2010). Silicate concentrations were low in surface waters ($1.78 \pm 0.71 \mu\text{M}$) and overall, no correlations were found for dFe(II) with SiO₄²⁻ ($r = -0.17$, $p = 0.02$, $n = 184$) or any other macronutrients (see **Supplementary Table 15**) throughout the voyage. Therefore, SiO₄²⁻ can be excluded as a major contributor to dFe(II) oxidation and thus half-lives in surface layers.

Other Sources: Distance to landmass & photosynthetic activity

Considering that the longest distance between a station and the mainland or seamount respectively (PS 3 and TS 1) is 500 km, one would expect that the continental input of dFe(II) is the most important source for the observations in the upper 250 m. However, no significant correlations between dFe(II) or dFe to distance from landmass/seamount were observed (see **Supplementary Table 15**). Conversely, for H₂O₂ there was a moderate but significant correlation with distance to landmass/seamount ($r = 0.463$, $p < 0.001$, $n = 64$, also **Supplementary Table 15**).

When comparing photosynthetic active radiation (PAR) with H₂O₂, dFe(II) and dFe, a weak but significant correlation for H₂O₂ ($r = 0.265$, $p < 0.001$, $n = 179$), a weak negative but significant correlation with dFe (-0.155 , $p = 0.039$, $n = 179$), and no correlation for dFe(II) was found (see **Supplementary Table 15**). These low r values, however, speak for a high variance in this data set, related to other factors. Furthermore, the southern transect (E-W) had high H₂O₂ concentrations in the upper 250 m correlated with a high PAR, less dFe and similar concentrations of dFe(II) with low Chl-*a* concentrations, in comparison to the northern transect (N-S) (**Table 4.2**). Higher H₂O₂ concentrations with lower dFe concentrations were found in the south, with overall similar values for dFe(II), with high Chl-*a* vs. lower PAR values. This indicates an area in the south (E-W transect) with high primary production, and consequently low dFe values. The high concentrations of H₂O₂ may also be linked to high concentrations of organic matter, which could be directly related to the production of H₂O₂ through the photochemical reduction and oxidation of organic matter in this area (Heller et al., 2016, Wuttig et al., 2013, Price et al., 1992). High Chl-*a* concentrations at TS 4 and TS 5 and high phytoplankton biomass might bias the section average, but the overall Chl-*a* concentration is still found to be higher in this section ($0.77 \mu\text{M}$ N-S vs. $0.11 \mu\text{M}$ E-W). While PAR values fall in range with previous findings for the southern transect (Cheah et al., 2013), the relevance of biology and proximity to landmass cannot be linked to the overall dFe(II) concentrations.

Table 4.2 Summary of N-S and E-W data for the main parameters H₂O₂, dFe, dFe(II) and the biological parameters PAR and Chl-*a* for from 0 to 250 m depth.

Transect	H ₂ O ₂ (nM)	dFe (nM)	dFe(II) (nM)	Chl- <i>a</i> (μM)	PAR (μE)
N-S	20.28 ± 14.14	0.44 ± 0.22	0.16 ± 0.2	0.93 ± 1.33	15.49 ± 65.12
E-W	28.45 ± 8.23	0.35 ± 0.14	0.17 ± 0.06	0.11 ± 0.13	31.27 ± 47.57

Phytoplankton consumes dFe(II), leading to low dFe(II) concentrations, but is also known to recycle dFe(II), maintaining low surface dFe(II) concentrations (Gonzalez et al., 2014, Samperio-Ramos et al., 2018). Dissolved Fe(II) sampling was undertaken in spring (September/October) when nutrients are well mixed, but primary production is still low/starting. Hence, dFe concentrations were expected to be relatively high in surface waters (0.35 ± 0.14 nM, upper 250 m, see **Table 2**) and non-limiting (Ryan-Keogh et al., 2018) in the E-W transect, which contradicts our findings. For the northern transect (N-S), it seems that sources and processes other than biology played a key role in the dFe(II) distribution.

Comparing apparent oxygen utilisation (AOU, see **Figure 4.12**, a) in the first 500 m with Chl-*a* gives a correlation of $r = -0.470$, $p = 0.21$, $n = 21$ (**Suppl. Table 15**), which more accurately describes the overall biological processes: the upper 500 m are low in AOU, due to high primary productivity compared to water masses below 500 m, where the AOU increases. Because of a low r and a p value not close to being significant, we suspect that other processes must be involved as well. The high Chl-*a* concentrations at TS 4, 5 and 6 can also be linked to exceptionally low values of AOU. These concentrations at TS 4, 5 and 6, however, are very likely induced from high dFe(II) linked to ligands, which is transported into this area via the Bass Strait (**Figure 4.14**) and has a slower oxidation time due to low O₂ concentrations, likely due to high organic matter and high O₂ consumption there.

The high dFe(II) observed in surface waters at PS 1, might be explained by fewer biological processes and colder temperatures. Further, this may also explain the high dFe(II) values at TS 7, 8 and 9 in the upper layer. These high dFe(II) concentrations are very likely due to input from the Australian mainland with stabilising organic matter or ligands and are not fully utilised as there is little to no primary production at these stations (**Figure 4.14**). The correlation of AOU to dFe(II) is negative and significant ($r = -0.228$, $p = 0.014$, $n = 116$, **Supplementary Table**

15). This trend contrasts with the observed dFe here ($r = 0.693$, $p < 0.001$, $n = 110$, **Suppl. Table 15**), but matches findings for the Indian ocean (Nishioka et al., 2013) and the North Atlantic (Fitzsimmons et al., 2013)

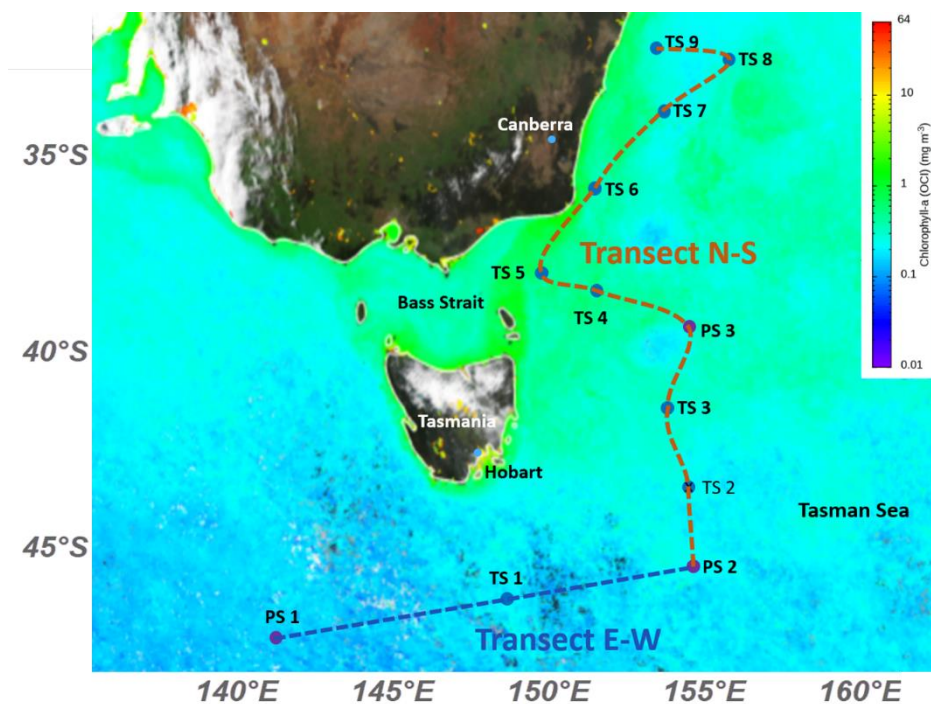


Figure 4.14 Chl-*a* concentrations averaged over the time of the voyage. (NOAA, VIIRS; Wang et al., 2017).

Other external sources

While seasonality can be invoked to explain high surface dFe(II) concentrations due to less uptake, dust originating from the Australian mainland and deposited over the Tasman Sea also occurs in the austral spring and summer (Gabric et al., 2016, Ekström et al., 2004) leading to elevated concentrations. In addition, the current movement from September 12th to September 22nd displayed eddies for the surface water at TS 7, 8 and 9, (**Figure 4.15**), where high dFe(II) concentrations were found. These eddies could upwell waters from greater depths (Oke et al., 2019), which can contain high dFe and also dFe(II) concentrations (Uchida et al., 2019, Laglera et al., 2020).

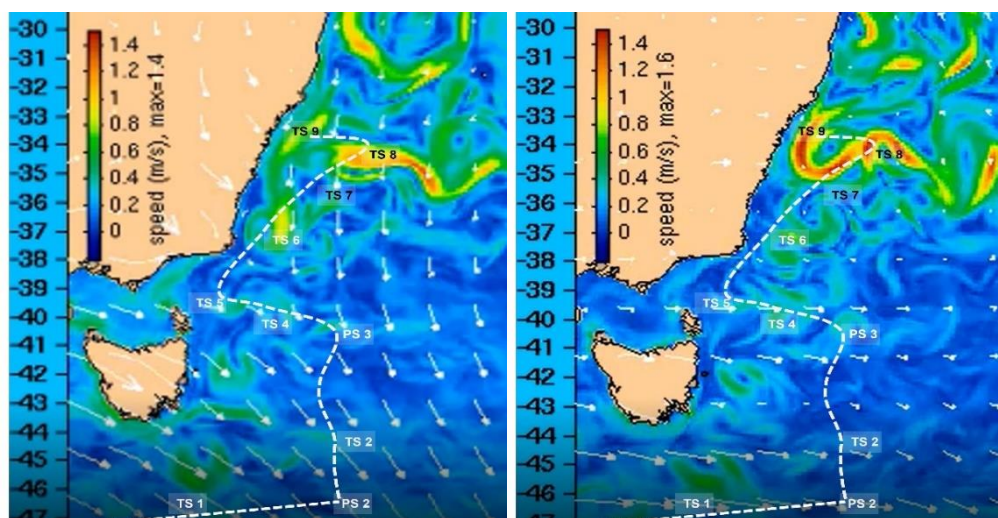


Figure 4.15 Current movement and speed from the surface (0-5m) from 12th of September (left) to 22nd of September (right) 2018.

Source: http://oceancurrent.imos.org.au/news/20181023/OM_af00_AuFiji_tp311p2.mp4

4.4.3 Dissolved Fe(II) from rain and sediment pore water sources

The measured rainwater dFe(II) concentrations of 37 nM were within the values described by previous studies conducted closer to the coast or directly on land (25 - 45 nM; Zhuang et al., 1995, Willey et al., 2000, Kieber et al., 2001b). Kieber et al. (2001b) suggested that approximately one-quarter of the total rainwater Fe-flux is found as dFe, half of which is available in the form of dFe(II). As shown in **Figure 4.16**, several rain events were registered during the time of the voyage. Major events with volumes higher than 10000 mm were observed at TS 7, TS 4, TS 3 and PS 2. For TS 4, where we collected the rainwater and analysed it for dFe(II), no extraordinarily high volumes of rain were recorded. For TS 7, the observed high dFe(II) concentrations are too deep (200 m) to link it to a rain event at that site.

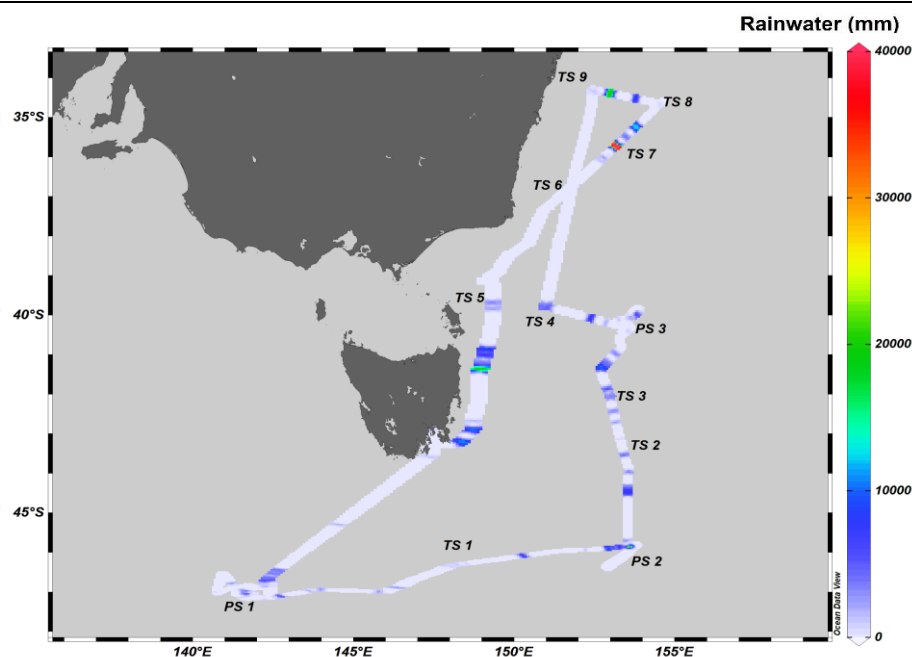


Figure 4.16 Rainwater data (mm) during the time of the voyage. The plot was generated using the averaged data (port and starboard) for the iso surface mode from ODV (Schlitzer, 2015).

Sediments are a major source of dFe(II) in coastal and deep waters (König et al., 1999, Croot et al., 2019). Coastal sediments often host bacteria that oxidise dFe(II) to dFe (Coleman et al., 1993, Rozan et al., 2002, Croot et al., 2019). Deep water sediments are often described as having a brown-green colour change (Lyle, 1983), which is linked to a reduction of dFe(III) into dFe(II). This oxidation horizon was described to be below 20 cm in the study by König et al. (1999). Since dFe(II) samples were only collected from the first 10 cm in this study, it is likely that this brown-green boundary was not crossed but that biological perturbation and geochemical impacts were observed. The decline of dFe(II) in the first 10 cm into the sediment might therefore be linked to Fe-reducing sulphate bacteria within these layers (Coleman et al., 1993, Azzoni et al., 2005). But a redox change from dFe(II) to Fe(III), resulting in lower concentrations of dFe(II), is more likely to have happened here during the time of sampling and analysis, when the sediment was exposed to atmospheric O₂ and temperatures. High values of dFe(II) in the sediments at PS 3 (3426 m depth) compare well with data from a study at 4000 m depth off the Peruvian coast (König et al., 1999). The dFe(II) concentrations were observed in the same range over the complete sediment profile (0-1 μ M). This data also compares to the shape of the profile described by König et al. (1999). Regarding the impact of sediment for the samples, high concentrations in the upper few cm of the sediment (\sim 800 nM) are observed with

higher values within the first 25 cm of the water column above the sediment (~600 nM) explaining the higher dFe(II) observed at depths as seen in PS 1 and TS 4. Low concentrations of dFe(II) were found in the deep-water column water of TS 6, where one would expect sediments and the seamount to impact the dFe(II) concentrations. The sample at this station might have been taken too far away from the seamount to observe impacts from the sediments or seamounts.

4.4.4 Ocean acidification and temperature impacts on dFe(II)

Due to anthropogenic impacts, warmer and more acidic conditions are predicted for future oceans. While this can have both positive effects and negative impacts for different organisms (e.g. Shi et al., 2010, Campbell et al., 2014, Britton et al., 2016, Hurd et al., 2018), it is still debated how OA and ocean warming will influence the overall nutritional composition of the ocean. For dFe(II), it is well established that dFe(II) oxidation kinetics are accelerated under warmer conditions (Millero et al., 1987). Therefore, an increase in the surface temperature by 2°C, as suggested for the end of the century (Change, 2018), would lead to faster dFe(II) oxidation rates. However, an increase in temperature also brings a decrease in the O₂ concentration (Keeling et al., 2010), which retards dFe(II) oxidation (Millero et al., 1987, González-Dávila et al., 2006). Additionally, a lowering in pH caused by OA, would retard the oxidative process from dFe(II) to dFe(III) (Millero et al., 2009).

However, as described in Chapter 2, a decrease in pH by 0.2 units has a stronger impact on dFe(II) concentrations than the projected temperature changes of 2°C. This holds true for coastal and open ocean water despite its compositional differences. Since the 0.2 units in pH change will have the strongest effect in coastal areas, the dFe(II) concentrations there might be higher due to slower oxidation rate but also due to more efficient leaching processes from riverine inputs, sediments and other continental sources.

At depths below 1000 m, a decrease in O₂ is likely to keep the dFe(II) concentrations more stable, which can already be seen at changes in concentrations of 10 μM (King et al., 1995). However, a timespan of 300-500 years are required for the upper 1000 m of the ocean to acidify by 0.2 (Caldeira & Wickett, 2003). Warmer water is also expected to slow the current movement and circulation processes, leading to stronger stratification and less mixing between the water masses (Dong et al., 2019). Overall, this might result in less mixing from mid and

deeper layers to the surface, leaving the airborne sources such as dust as the primary sources of Fe in surface waters of the open SO.

An elevated temperature and a lowered pH will likely cause a higher overall solubility of Fe in the water column (Millero, 1998) from sources such as sediments or continental margins. That is why the overall concentration of Fe might be higher in future coastal oceans compared to the concentrations today. Naturally, not only Fe becomes more soluble but also copper and other metals that are toxic to phytoplankton and other species above a certain level, which could lead to negative impacts on growth. Furthermore, phytoplankton can only withstand changes in pH and temperature until a certain threshold is reached. Therefore, it cannot be said if the adaptation time for phytoplankton is sufficiently long to physiologically adjust to those new conditions from warming or lowered pH to actually benefit from a Fe-rich ocean.

By using equations 1 and 2 (Millero et al., 1987, Millero and Izaguirre, 1989), a simplified model (see **Table 4.3**) was applied to compare current oxidation rates and concentrations of dFe(II) with future conditions comparing warmer water (TS 7) to colder water (PS 1). Therefore, the oxidation rate k' and half-life time ($t_{1/2}$) was calculated, using ionic strength I , temperature and pH. While salinity was kept constant, pH and temperature values measured during the voyage were used to represent current conditions.

$$k'(\text{min}^{-1}) = I - 0.0004T + 0.0003T^2 + 0.0389\text{pH} - 0.0287S \quad (1)$$

$$t_{1/2} = \frac{\ln 2}{k'} \quad (2)$$

While the overall $t_{1/2}$ of TS 7 is half the time calculated compared to PS 1 in the south (~5 vs. ~10 minutes; **Table 4.3**) the increase of 2°C in temperature lead to a 15.2 % faster oxidation rate in warmer conditions such as TS 7 (~20°C) and a 16.75 % faster oxidation in cold water such as for PS 1 (~10°C). On the other hand, a decrease in pH by 0.2 units leads to an extended $t_{1/2}$ by 0.006% (warm water, TS 7) and a 0.013 % (cold water, PS 1). When combining an increase of 2°C and a decrease of 0.2 in pH, a 14.77% faster oxidation was observed in warmer water from TS 7 and a 15.82% faster oxidation in colder water (PS 1). This simple model does not incorporate changes in O₂ or organic matter due to OA or OW. The results show that an increase in temperature by 2°C led to a faster oxidation rate of dFe(II), while a decrease in pH by 0.2 units might extend oxidation times which is insignificant compared to a temperature increase of 2°C. These modelled data contradict the experimental findings due to their use of

inorganic seawater, shown in chapter two. This is why it would be important to observe further continuous dFe(II) oxidation experiments rather than modelling them.

Table 4.3 Comparison of TS 7 and PS 1 for modelled dFe(II) changes, based on pH, temperature, and salinity.

Station	Condition	depth (m)	pH	Temp (°C)	Salinity	Ionic strength	k'	$t/2$ (min)	changes in time (%)	change compared to 'today's' values (%)
TS 7	V04_2018 (today)	15.00	8.09	19.31	35.750	0.7387	0.1315	5.16	100	0
	2°C warmer		8.09	21.31	35.750	0.7387	0.1551	4.27	84.8	15.20
	0.2 units more acidic		8.07	19.31	35.750	0.7387	0.1307	5.18	100.60	-00.60
	+2°C warmer & 0.2 units more acidic		8.07	21.31	35.750	0.7387	0.1543	4.29	85.23	14.77
PS 1	V04_2018 (today)	15.00	8.09	9.50	34.650	0.7151	0.0587	11.49	100	0
	2°C warmer		8.09	11.50	34.650	0.7151	0.0705	9.50	83.25	16.75
	0.2 units more acidic		8.07	9.50	34.650	0.7151	0.0579	11.58	101.34	-01.34
	2°C warmer & 0.2 units more acidic		8.07	11.50	34.650	0.7151	0.0697	9.57	84.18	15.82

4.5 Conclusions

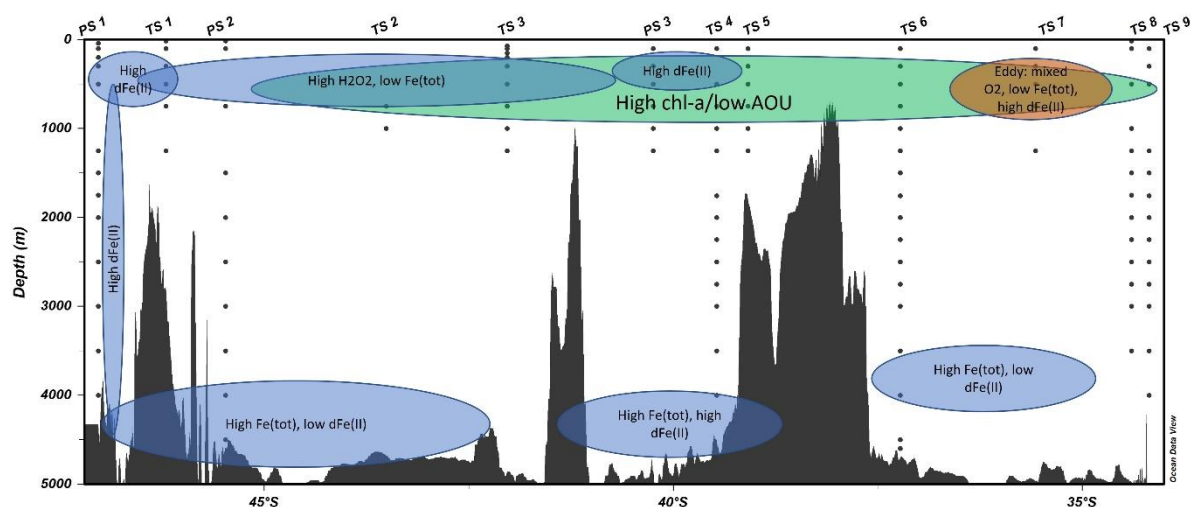


Figure 4.17 Schematic summary of the key findings of the for the V04_2018 voyage.

In the presented study, the dFe(II) concentrations are generally higher when the temperatures are lower and that the dFe(II): dFe ratios are 10 % higher than reported by previous Southern Ocean studies. However, dFe(II) concentrations in the upwelling eddy at TS 7 in the north of the study region were quite high. At the surface, dFe(II) concentrations are higher where airborne sources were stronger, while at the deeper sampling stations, proximity to landmasses and seamount are more dominant. Although temperature is a strong impacting factor on dFe(II) kinetics, it is not the only key driver for sources in this region, but it is a combination of external sources and biochemical processes.

Hydrogen peroxide is negatively correlated to dFe(II), especially in the surface layers. This could result from high primary production (high AOU, high Chl-*a*) in the N-S transect compared to the frontal mixing zone at the start of the E-W transect. This is also strengthened by a high negative correlation of H₂O₂ with dFe ($r = -0.574$, $p < 0.001$, $n = 178$; **Supplementary Table 15**), which is further linked to higher activity by primary producers and other kinetically linked processes in the surface area of the northern stations, whereas the concentrations of dFe(II) are low (see **Figure 4.17**). In future oceans, airborne and land-based sources might become more important due to increased solubility and elevated kinetic activity due to higher temperatures and a lowered pH. Dissolved Fe(II) in surface waters is likely higher due to those

increased source pools but might be less available to phytoplankton due to faster oxidation rates.

Acknowledgement

The authors would like to thank the officers and crew of the *RV Investigator* and the staff from the Marine National Facility for their help in preparing and organizing the cruise. I further thank the chief scientist Michael Ellwood for designing and managing this voyage. I also thank the voyage manager Max McGuire. The authors would like to thank the Australian National University (ANU) team for sampling and filtering water from the TMR and supplying us with Chl-*a* data: Rob Grun, Prayna Maharaj Riteshma Devi and Sarah Andrew. Thank you to April Abott, Dave Janssen, Hannah Kumar, Hannah Wilson, and Annabel Payne for collecting and processing the sediment samples from the KC Multicorer before the dFe(II) analysis. Thank you to Morgane Perron for her interpretation of the results from the rain event and potential aerosol data. All co-authors contributed and edited the manuscript.

I would like to thank the CSIRO team for their excellent hydrochemical analyses. I also thank the captain, officers and crew of the *RV Investigator*. Furthermore, I thank Chief Scientist Michael Ellwood and his team (Pamela Barrett, Sarah Andrews, Rob Grum) for their support during this 28-day voyage. This research was supported under Australian Research Council's Special Research Initiative for Antarctic Gateway Partnership (Project ID SR140300001). I would also like to thank Antarctic climate Ecosystems-CRC, IMAS, and UTAS for funding and PhD support.

4.6 References

- ANDREW, S. M., MORELL, H. T., STRZEPEK, R. F., BOYD, P. W. & ELLWOOD, M. J. 2019. Iron Availability Influences the Tolerance of Southern Ocean Phytoplankton to Warming and Elevated Irradiance. *Frontiers in Marine Science*, 6.
- AZZONI, R., GIORDANI, G. & VIAROLI, P. 2005. Iron-sulphur-phosphorus interactions: implications for sediment buffering capacity in a mediterranean eutrophic lagoon (Sacca di Goro, Italy). *Hydrobiologia*, 550, 131-148.
- BARRETT, P. M., GRUN, R. & ELLWOOD, M. J. 2021. Tracing iron along the flowpath of East Australian Current using iron stable isotopes. *Marine Chemistry*, 104039.
- BELKIN, I. M. & GORDON, A. L. 1996. Southern Ocean fronts from the Greenwich meridian to Tasmania. *Journal of Geophysical Research: Oceans*, 101, 3675-3696.
- BOWEN, M. M., WILKIN, J. L. & EMERY, W. J. 2005. Variability and forcing of the East Australian Current. *Journal of Geophysical Research: Oceans*, 110.
- BOWIE, A. R., ACHTERBERG, E. P., MANTOURA, R. F. C. & WORSFOLD, P. J. 1998. Determination of sub-nanomolar levels of iron in seawater using flow injection with chemiluminescence detection. *Analytica Chimica Acta*, 361, 189-200.
- BOWIE, A. R., ACHTERBERG, E. P., SEDWICK, P. N., USSHER, S. & WORSFOLD, P. J. 2002. Real-time monitoring of picomolar concentrations of iron (II) in marine waters using automated flow injection-chemiluminescence instrumentation. *Environmental science & technology*, 36, 4600-4607.
- BOWIE, A. R., ACHTERBERG, E. P., USSHER, S. & WORSFOLD, P. J. 2005. Design of an automated flow injection-chemiluminescence instrument incorporating a miniature photomultiplier tube for monitoring picomolar concentrations of iron in seawater. *Journal of Automated Methods & Management in Chemistry*, 37-43.
- BOWIE, A. R., LANNUZEL, D., REMENYI, T. A., WAGENER, T., LAM, P. J., BOYD, P. W., GUIEU, C., TOWNSEND, A. T. & TRULL, T. W. 2009. Biogeochemical iron budgets of the Southern Ocean south of Australia: Decoupling of iron and nutrient cycles in the subantarctic zone by the summertime supply. *Global Biogeochemical Cycles*, 23.
- BRITTON, D., CORNWALL, C. E., REVILL, A. T., HURD, C. L. & JOHNSON, C. R. 2016. Ocean acidification reverses the positive effects of seawater pH fluctuations on growth and photosynthesis of the habitat-forming kelp, *Ecklonia radiata*. *Scientific reports*, 6.
- CALDEIRA, K., & WICKETT, M. E. (2003). Anthropogenic carbon and ocean pH. *Nature*, 425(6956), 365-365. <https://doi.org/10.1038/425365a>
- CAMPBELL, A. L., MANGAN, S., ELLIS, R. P. & LEWIS, C. 2014. Ocean Acidification Increases Copper Toxicity to the Early Life History Stages of the Polychaete *Arenicola marina* in Artificial Seawater. *Environmental Science & Technology*, 48, 9745-9753.

- CHANGE, I. P. O. C. 2018. Special Report on the Ocean and Cryosphere in a Changing Climate. IPCC Geneva.
- CHASE, Z., STRUTTON, P. G. & HALES, B. 2007. Iron links river runoff and shelf width to phytoplankton biomass along the U.S. West Coast. *Geophysical Research Letters*, 34, 4.
- CHEAH, W., MCMINN, A., GRIFFITHS, F. B., WESTWOOD, K. J., WRIGHT, S. W. & CLEMENTSON, L. A. 2013. Response of phytoplankton photophysiology to varying environmental conditions in the sub-antarctic and polar frontal zone. *PloS one*, 8, e72165.
- COLEMAN, M. L., HEDRICK, D. B., LOVLEY, D. R., WHITE, D. C. & PYE, K. 1993. Reduction of Fe (III) in sediments by sulphate-reducing bacteria. *Nature*, 361, 436-438.
- CROOT, P. L., HELLER, M. I. & WUTTIG, K. 2019. Redox Processes impacting the flux of Fe (II) from shelf sediments to the OMZ along the Peruvian shelf. *ACS Earth and Space Chemistry*, 3(4), 537-549.
- CUTTER, G., CASCIOTTI, K., CROOT, P., GEIBERT, W., HEIMBUERGER, L. E., LOHAN, M. C., PLANQUETTE, H. & FLIERDT, T. 2017. Sampling and Sample-handling Protocols for GEOTRACES Cruises (Version 3). <http://www.geotraces.org/images/stories/documents/intercalibration/Cookbook.pdf>.
- DE JONG, J., SCHOEMANN, V., LANNUZEL, D., CROOT, P., DE BAAR, H. & TISON, J.-L. 2012. Natural iron fertilization of the Atlantic sector of the Southern Ocean by continental shelf sources of the Antarctic Peninsula. *Journal of Geophysical Research: Biogeosciences*, 117.
- DONG, S., BARINGER, M. O. & GONI, G. J. 2019. Slow down of the Gulf Stream during 1993–2016. *Scientific Reports*, 9, 1-10.
- DUCE, R. A. & TINDALE, N. W. 1991. Atmospheric transport of iron and its deposition in the ocean. *Limnology and Oceanography*, 36, 1715-1726.
- DUCKLOW, H. W., STEINBERG, D. K. & BUESSELER, K. O. 2001. Upper ocean carbon export and the biological pump. *OCEANOGRAPHY - WASHINGTON DC - OCEANOGRAPHY SOCIETY*, 14, 50-58.
- EKSTRÖM, M., MCTAINSH, G. H. & CHAPPELL, A. 2004. Australian dust storms: temporal trends and relationships with synoptic pressure distributions (1960–99). *International Journal of Climatology: A Journal of the Royal Meteorological Society*, 24, 1581-1599.
- ELLWOOD, M. J., BOWIE, A. R., BAKER, A., GAULT-RINGOLD, M., HASSLER, C., LAW, C. S., MAHER, W. A., MARRINER, A., NODDER, S., SANDER, S., STEVENS, C., TOWNSEND, A., VAN DER MERWE, P., WOODWARD, E. M. S., WUTTIG, K. & BOYD, P. W. 2018. Insights Into the Biogeochemical Cycling of Iron, Nitrate, and Phosphate Across a 5,300 km South Pacific Zonal Section (153°E–150°W). *Global Biogeochemical Cycles*, 32, 187-207.
- EVERETT, J.D., BAIRD, M.E., OKE, P.R. AND SUTHERS, I.M., 2012. An avenue of eddies: Quantifying the biophysical properties of mesoscale eddies in the Tasman Sea. *Geophysical Research Letters*, 39(16).

- FITZSIMMONS, J. N., ZHANG, R. & BOYLE, E. A. 2013. Dissolved iron in the tropical North Atlantic Ocean. *Marine Chemistry*, 154, 87-99.
- GABRIC, A. J., CROPP, R., MCTAINSH, G., BUTLER, H., JOHNSTON, B. M., O'LOINGSIGH, T. & VAN TRAN, D. 2016. Tasman Sea biological response to dust storm events during the austral spring of 2009. *Marine and Freshwater Research*, 67, 1090-1102.
- GONZÁLEZ-DAVILA, M., SANTANA-CASIANO, J. M. & MILLERO, F. J. 2005. Oxidation of iron (II) nanomolar with H₂O₂ in seawater. *Geochimica et Cosmochimica Acta*, 69, 83-93.
- GONZÁLEZ-DÁVILA, M., SANTANA-CASIANO, J. M. & MILLERO, F. J. 2006. Competition between O₂ and H₂O₂ in the oxidation of Fe (II) in natural waters. *Journal of solution chemistry*, 35, 95-111.
- GONZALEZ, A. G., SANTANA-CASIANO, J. M., GONZÁLEZ-DÁVILA, M., PÉREZ-ALMEIDA, N. & SUÁREZ DE TANGIL, M. 2014. Effect of *Dunaliella tertiolecta* organic exudates on the Fe (II) oxidation kinetics in seawater. *Environmental science & technology*, 48, 7933-7941.
- GONZALEZ, A. G., SANTANA-CASIANO, J. M., PEREZ, N. & GONZALEZ-DAVILA, M. 2010. Oxidation of Fe(II) in Natural Waters at High Nutrient Concentrations. *Environmental Science & Technology*, 44, 8095-8101.
- HABER, F. & WEISS, J. 1932. Über die katalyse des hydroperoxydes. *Naturwissenschaften*, 20, 948-950.
- HANSEL, C.M. AND DIAZ, J.M., 2021. Production of extracellular reactive oxygen species by marine biota. *Annual Review of Marine Science*, 13, pp.177-200.
- HELLER, M. I., WUTTIG, K. & CROOT, P. L. 2016. Identifying the Sources and Sinks of CDOM/FDOM across the Mauritanian Shelf and Their Potential Role in the Decomposition of Superoxide (O₂⁻). *Frontiers in Marine Science*, 3.
- HOLMES, T. M., WUTTIG, K., CHASE, Z., SCHALLENBERG, C., VAN DER MERWE, P., TOWNSEND, A. T. & BOWIE, A. R. 2020. Glacial and Hydrothermal Sources of Dissolved Iron (II) in Southern Ocean Waters Surrounding Heard and McDonald Islands. *Journal of Geophysical Research: Oceans*, 125, e2020JC016286.
- HOLMES, T. M., WUTTIG, K., CHASE, Z., VAN DER MERWE, P., TOWNSEND, A. T., SCHALLENBERG, C., TONNARD, M. & BOWIE, A. R. 2019. Iron availability influences nutrient drawdown in the Heard and McDonald Islands region, Southern Ocean. *Marine Chemistry*, 211, 1-14.
- HOPPE, C. J., HASSLER, C. S., PAYNE, C. D., TORTELL, P. D., ROST, B. & TRIMBORN, S. 2013. Iron limitation modulates ocean acidification effects on Southern Ocean phytoplankton communities. *PLoS One*, 8, e79890.
- HURD, C. L., LENTON, A., TILBROOK, B. & BOYD, P. W. 2018. Current understanding and challenges for oceans in a higher-CO₂ world. *Nature Climate Change*, 8, 686-694.

- HUTCHINS, D. & BOYD, P. 2016. Marine phytoplankton and the changing ocean iron cycle. *Nature Climate Change*, 6, 1072-1079.
- HWANG, H. & DASGUPTA, P. K. 1985. Thermodynamics of the hydrogen peroxide-water system. *Environmental science & technology*, 19, 255-258.
- ITO, A., PERRON, M. M., PROEMSE, B. C., STRZELEC, M., GAULT-RINGOLD, M., BOYD, P. W. & BOWIE, A. R. 2020. Evaluation of aerosol iron solubility over Australian coastal regions based on inverse modeling: implications of bushfires on bioaccessible iron concentrations in the Southern Hemisphere. *Progress in Earth and Planetary Science*, 7, 1-17.
- KEELING, R. F., KÖRTZINGER, A. & GRUBER, N. 2010. Ocean deoxygenation in a warming world. *Annual review of marine science*, 2, 199-229.
- KIEBER, R. J., PEAKE, B., WILLEY, J. D. & JACOBS, B. 2001a. Iron speciation and hydrogen peroxide concentrations in New Zealand rainwater. *Atmospheric Environment*, 35, 6041-6048.
- KIEBER, R. J., WILLIAMS, K., WILLEY, J. D., SKRABAL, S. & AVERY JR, G. B. 2001b. Iron speciation in coastal rainwater: concentration and deposition to seawater. *Marine chemistry*, 73, 83-95.
- KING, D. W., LOUNSBURY, H. A. & MILLERO, F. J. 1995. Rates and mechanism of Fe (II) oxidation at nanomolar total iron concentrations. *Environmental science & technology*, 29, 818-824.
- KÖNIG, I., HAECKEL, M., DRODT, M., SUESS, E. & TRAUTWEIN, A. X. 1999. Reactive Fe (II) layers in deep-sea sediments. *Geochimica et Cosmochimica Acta*, 63, 1517-1526.
- LAGLERA, L. M., TOVAR-SANCHEZ, A., SUKEKAVA, C. F., NAIK, H., NAQVI, S. W. A. & WOLF-GLADROW, D. A. 2020. Iron organic speciation during the LOHAFEX experiment: Iron ligands release under biomass control by copepod grazing. *Journal of Marine Systems*, 207, 103151.
- LANNUZEL, D., BOWIE, A. R., REMENYI, T., LAM, P., TOWNSEND, A., IBISANMI, E., BUTLER, E., WAGENER, T. & SCHOEMANN, V. 2011. Distributions of dissolved and particulate iron in the sub-Antarctic and Polar Frontal Southern Ocean (Australian sector). *Deep Sea Research Part II: Topical Studies in Oceanography*, 58, 2094-2112.
- LAUFER, K., RØY, H., JØRGENSEN, B. B. & KAPPLER, A. 2016. Evidence for the Existence of Autotrophic Nitrate-Reducing Fe(II)-Oxidizing Bacteria in Marine Coastal Sediment. *Applied and Environmental Microbiology*, 82, 6120-6131.
- LYLE, M. 1983. The brown-green color transition in marine sediments: A marker of the Fe (III)-Fe (II) redox boundary 1. *Limnology and Oceanography*, 28, 1026-1033.
- MARTIN, J. H. 1990. Glacial-interglacial CO₂ change: The iron hypothesis. *Paleoceanography*, 5, 1-13.
- MATA, M. M., WIJFFELS, S. E., CHURCH, J. A. & TOMCZAK, M. 2006. Eddy shedding and energy conversions in the East Australian Current. *Journal of Geophysical Research: Oceans*, 111.

- MCNEIL, B. I. & MATEAR, R. J. 2008. Southern Ocean acidification: A tipping point at 450-ppm atmospheric CO₂. *Proceedings of the National Academy of Sciences*, 105, 18860-18864.
- MILLERO, F. J. 1979. Effects of pressure and temperature on activity coefficients. *Activity coefficients in electrolyte solutions*, 2, 63-151.
- MILLERO, F. J. 1985. The effect of ionic interactions on the oxidation of metals in natural waters. *Geochimica et Cosmochimica Acta*, 49, 547-553.
- MILLERO, F. J. & IZAGUIRRE, M. 1989. Effect of ionic strength and ionic interactions on the oxidation of Fe (II). *Journal of Solution Chemistry*, 18, 585-599.
- MILLERO, F. J. & SOTOLONGO, S. 1989. The oxidation of Fe (II) with H₂O₂ in seawater. *Geochimica et Cosmochimica Acta*, 53, 1867-1873.
- MILLERO, F. J., SOTOLONGO, S. & IZAGUIRRE, M. 1987. The oxidation kinetics of Fe(II) in seawater. *Geochimica et Cosmochimica Acta*, 51, 793-801.
- MILLERO, F. J., WOOSLEY, R., DITROLIO, B. & WATERS, J. 2009. Effect of Ocean Acidification on the Speciation of Metals in Seawater. *Oceanography*, 22, 72-85.
- MOFFETT, J. W. & ZIKA, R. G. 1987. Reaction kinetics of hydrogen peroxide with copper and iron in seawater. *Environmental Science & Technology*, 21, 804-810.
- MOREL, F. M. M., KUSTKA, A. B. & SHAKED, Y. 2008. The role of unchelated Fe in the iron nutrition of phytoplankton. *Limnology and Oceanography*, 53, 400-404.
- MORROW, R., DONGUY, J.-R., CHAIGNEAU, A. & RINTOUL, S. R. 2004. Cold-core anomalies at the subantarctic front, south of Tasmania. *Deep Sea Research Part I: Oceanographic Research Papers*, 51, 1417-1440.
- NISHIOKA, J., OBATA, H. & TSUMUNE, D. 2013. Evidence of an extensive spread of hydrothermal dissolved iron in the Indian Ocean. *Earth and Planetary Science Letters*, 361, 26-33.
- OBERNOSTERER, I., RUARDIJ, P. AND HERNDL, G.J., 2001. Spatial and diurnal dynamics of dissolved organic matter (DOM) fluorescence and H₂O₂ and the photochemical oxygen demand of surface water DOM across the subtropical Atlantic Ocean. *Limnology and oceanography*, 46(3), pp.632-643.
- OKE, P.R. AND MIDDLETON, J.H., 2000. Topographically induced upwelling off eastern Australia. *Journal of Physical Oceanography*, 30(3), pp.512-531.
- OKE, P. R., ROUGHAN, M., CETINA-HEREDIA, P., PILO, G. S., RIDGWAY, K. R., RYKOVA, T., ARCHER, M. R., COLEMAN, R. C., KERRY, C. G. & ROCHA, C. 2019. Revisiting the circulation of the East Australian Current: Its path, separation, and eddy field. *Progress in Oceanography*, 176, 102139.
- ORSI, A. H., JOHNSON, G. C. & BULLISTER, J. L. 1999. Circulation, mixing, and production of Antarctic Bottom Water. *Progress in Oceanography*, 43, 55-109.
- PERRON, M. M., PROEMSE, B. C., STRZELEC, M., GAULT-RINGOLD, M., BOYD, P. W., RODRIGUEZ, E. S., PAULL, B. & BOWIE, A. R. 2020. Origin, transport and

- deposition of aerosol iron to Australian coastal waters. *Atmospheric Environment*, 117432.
- PHILLIPS, H. E. & RINTOUL, S. R. 2002. A Mean Synoptic View of the Subantarctic Front South of Australia. *Journal of Physical Oceanography*, 32, 1536-1553.
- PRICE, D., WORSFOLD, P. J. & C. MANTOURA, R. F. 1992. Hydrogen peroxide in the marine environment: cycling and methods of analysis. *TrAC Trends in Analytical Chemistry*, 11, 379-384.
- REES, C., PENDER, L., SHERRIN, K., SCHWANGER, C., HUGHES, P., TIBBEN, S., MAROUCHOS, A. & RAYNER, M. 2019. Methods for reproducible shipboard SFA nutrient measurement using RMNS and automated data processing. *Limnology and Oceanography: Methods*, 17, 25-41.
- RIDGWAY, K. & GODFREY, J. 1997. Seasonal cycle of the East Australian current. *Journal of Geophysical Research: Oceans*, 102, 22921-22936.
- RIDGWAY, K. & HILL, K. 2009. The east Australian current. *A marine climate change impacts and adaptation report card for Australia*, 5.
- RINTOUL, S., DONGUY, J. & ROEMMICH, D. 1997. Seasonal evolution of upper ocean thermal structure between Tasmania and Antarctica. *Deep Sea Research Part I: Oceanographic Research Papers*, 44, 1185-1202.
- RINTOUL, S., HUGHES, C. & OLBERS, D. 2001. The Antarctic circumpolar current system. *In: Ocean Circulation and Climate/G. Siedler, J. Church and J. Gould, eds. New York: Academic Press. p.*
- ROEMMICH, D., GILSON, J., DAVIS, R., SUTTON, P., WIJFFELS, S. & RISER, S. 2007. Decadal spinup of the South Pacific subtropical gyre. *Journal of Physical Oceanography*, 37, 162-173.
- ROZAN, T. F., TAILLEFERT, M., TROUWBORST, R. E., GLAZER, B. T., MA, S., HERSZAGE, J., VALDES, L. M., PRICE, K. S. & LUTHER III, G. W. 2002. Iron-sulfur-phosphorus cycling in the sediments of a shallow coastal bay: Implications for sediment nutrient release and benthic macroalgal blooms. *Limnology and Oceanography*, 47, 1346-1354.
- RYAN-KEOGH, T. J., THOMALLA, S. J., MTSHALI, T. N., HORSTEN, N. R. V. & LITTLE, H. J. 2018. Seasonal development of iron limitation in the sub-Antarctic zone. *Biogeosciences*, 15, 4647-4660.
- SAMPERIO-RAMOS, G., GONZÁLEZ-DÁVILA, M. & SANTANA-CASIANO, J. M. 2018. Impact on the Fe redox cycling of organic ligands released by *Synechococcus* PCC 7002, under different iron fertilization scenarios. Modeling approach. *Journal of Marine Systems*.
- SANTANA-CASIANO, J., GONZALEZ-DAVILA, M. & MILLERO, F. 2006. The role of Fe (II) species on the oxidation of Fe (II) in natural waters in the presence of O₂ and H₂O₂. *Marine Chemistry*, 99, 70-82.

- SANTANA-GONZÁLEZ, C., SANTANA-CASIANO, J. M., GONZÁLEZ-DÁVILA, M., SANTANA-DEL PINO, A., GLADYSHEV, S. & SOKOV, A. 2018. Fe(II) oxidation kinetics in the North Atlantic along the 59.5° N during 2016. *Marine Chemistry*.
- SARMIENTO, J. L. & ORR, J. C. 1991. Three-dimensional simulations of the impact of Southern Ocean nutrient depletion on atmospheric CO₂ and ocean chemistry. *Limnology and Oceanography*, 36, 1928-1950.
- SARTHOU, G., BUCCIARELLI, E., CHEVER, F., HANSARD, S., GONZÁLEZ-DÁVILA, M., SANTANA-CASIANO, J., PLANCHON, F. & SPEICH, S. 2011. Labile Fe (II) concentrations in the Atlantic sector of the Southern Ocean along a transect from the subtropical domain to the Weddell Sea Gyre. *Biogeosciences*, 8, 2461-2479.
- SCHALLENBERG, C., VAN DER MERWE, P., CHEVER, F., CULLEN, J. T., LANNUZEL, D. & BOWIE, A. R. 2016. Dissolved iron and iron (II) distributions beneath the pack ice in the East Antarctic (120 E) during the winter/spring transition. *Deep Sea Research Part II: Topical Studies in Oceanography*, 131, 96-110.
- SCHLITZER, R. 2015. Ocean data view. 2018. Available: *odv. awi. de*.
- SEDWICK, P., BOWIE, A., CHURCH, T., CULLEN, J., JOHNSON, R., LOHAN, M., MARSAY, C., MCGILLICUDDY JR, D., SOHST, B. & TAGLIABUE, A. 2020. Dissolved iron in the Bermuda region of the subtropical North Atlantic Ocean: Seasonal dynamics, mesoscale variability, and physicochemical speciation. *Marine Chemistry*, 219, 103748.
- SEDWICK, P., SOHST, B., USSHER, S. & BOWIE, A. 2015. A zonal picture of the water column distribution of dissolved iron (II) during the US GEOTRACES North Atlantic transect cruise (GEOTRACES GA03). *Deep Sea Research Part II: Topical Studies in Oceanography*, 116, 166-175.
- SHAKED, Y. & LIS, H. 2012. Disassembling iron availability to phytoplankton. *Frontiers in microbiology*, 3.
- SHARMA, V. K. & MILLERO, F. J. 1989. The oxidation of Cu(I) with H₂O₂ in natural waters. *Geochimica et Cosmochimica Acta*, 53, 2269-2276.
- SHI, D., XU, Y., HOPKINSON, B. M. & MOREL, F. M. M. 2010. Effect of Ocean Acidification on Iron Availability to Marine Phytoplankton. *Science*, 327, 676-679.
- SMETACEK, V., KLAAS, C., STRASS, V. H., ASSMY, P., MONTRESOR, M., CISEWSKI, B., SAVOYE, N., WEBB, A., D'OVIDIO, F. & ARRIETA, J. M. 2012. Deep carbon export from a Southern Ocean iron-fertilized diatom bloom. *Nature*, 487, 313-319.
- STRZEPEK, R. F., BOYD, P. W. & SUNDA, W. G. 2019. Photosynthetic adaptation to low iron, light, and temperature in Southern Ocean phytoplankton. *Proceedings of the National Academy of Sciences*, 201810886.
- TAGLIABUE, A., BOWIE, A. R., BOYD, P. W., BUCK, K. N., JOHNSON, K. S. & SAITO, M. A. 2017. The integral role of iron in ocean biogeochemistry. *Nature*, 543, 51-59.
- TALLEY, L. D. 2011. *Descriptive physical oceanography: an introduction*, Academic press.

-
- TILBURG, C.E., SUBRAHMANYAM, B. AND O'BRIEN, J.J., 2002. Ocean color variability in the Tasman Sea. *Geophysical Research Letters*, 29(10), pp.125-1.
- TRACEY, K. L., WATTS, D. R., MEINEN, C. S. & LUTHER, D. S. 2006. Synoptic maps of temperature and velocity within the Subantarctic Front south of Australia. *Journal of Geophysical Research: Oceans*, 111.
- TRIMBORN, S., THOMS, S., BRENNEIS, T., HEIDEN, J. P., BESZTERI, S. & BISCHOF, K. 2017. Two Southern Ocean diatoms are more sensitive to ocean acidification and changes in irradiance than the prymnesiophyte *Phaeocystis antarctica*. *Physiologia plantarum*, 160, 155-170.
- UCHIDA, T., BALWADA, D., ABERNATHEY, R., MCKINLEY, G., SMITH, S. & LEVY, M. 2019. Eddy iron fluxes control primary production in the open Southern Ocean.
- WANG, M., LIU, X., JIANG, L. & SON, S. 2017. Visible Infrared Imaging Radiometer Suite (VIIRS) Ocean Color Products Algorithm Theoretical Basis Document Version 1. *J. Quant. Spectrosc. Radiat. Transf.*, 188, 181-187.
- WILLEY, J. D., KIEBER, R. J., WILLIAMS, K. H., CROZIER, J. S., SKRABAL, S. A. & AVERY, G. B. 2000. Temporal variability of iron speciation in coastal rainwater. *Journal of Atmospheric Chemistry*, 37, 185-205.
- WRIGHT, S., JEFFREY, S. & MANTOURA, R. 2005. *Phytoplankton pigments in oceanography: guidelines to modern methods*, Unesco Pub.
- WUTTIG, K., HELLER, M. I. & CROOT, P. L. 2013. Pathways of superoxide (O₂⁻) decay in the Eastern Tropical North Atlantic. *Environmental science & technology*, 47, 10249-10256.
- YEALA, S., B., K. A. & M., M. F. M. 2005. A general kinetic model for iron acquisition by eukaryotic phytoplankton. *Limnology and Oceanography*, 50, 872-882.
- YUAN, J. & SHILLER, A. M. 1999. Determination of subnanomolar levels of hydrogen peroxide in seawater by reagent-injection chemiluminescence detection. *Analytical Chemistry*, 71, 1975-1980.
- ZHUANG, G., YI, Z. & WALLACE, G. T. 1995. Iron (II) in rainwater, snow, and surface seawater from a coastal environment. *Marine Chemistry*, 50, 41-50.

Chapter 5: General Discussion and Conclusion

5.1 Summary and aims of this work

Climate change parameters ocean acidification (OA) and ocean warming are becoming more of a concern day by day. Numerous published studies display results of these two parameters impacting flora and fauna in marine systems. However, only little is known about how OA and warming might impact nutrient composition in future oceans. Nutrients are key for phytoplankton growth in seawater and especially iron (Fe) is considered an important element for photosynthesising organisms. In the past, a focus has been on the stable Fe species Fe(III). Less studies have examined the rapidly oxidising species Fe(II).

In this thesis, I have therefore investigated the presence, availability, and oxidation of dissolved (d) Fe(II) in the Southern Ocean (SO). It is thought to be the more bioavailable form of Fe, meaning dFe(II) is more easily available to phytoplankton in this oxidative, unbound state. The interplay of oxidation and reduction between dFe(II) and dFe(III) are highly governed by changes in pH and temperature coming from ocean acidification and warming. The location of this study, the SO, is a large region rich in macronutrients but low in the micronutrient Fe. The SO plays an important role in carbon (C) export. Hence, studying the impact of OA and warming on the dFe(II) oxidation with respect to bioavailability in an Fe-limited area like the SO, was the aim for this study.

Dissolved Fe(II) is a transient species due to its reduced character and, therefore, very challenging to work with. For one, the oxidation is influenced by the oxygen (O₂) and hydrogen peroxide (H₂O₂) concentrations in the water column. Secondly, pH and temperature alter the oxidation time. Third, other parameters such as depth (pressure), salinity, excess nutrients, ultraviolet (UV) light, ligands and other biological parameters can impact this redox reaction from dFe(II) to dFe(III). However, Fe is generally scarce in the open SO, and the concentrations of dFe(II) lie in the pico-molar range. For that reason, and due to the many potential influencing factors to consider, the impact of ocean acidification and warming on dFe(II) may be underestimated.

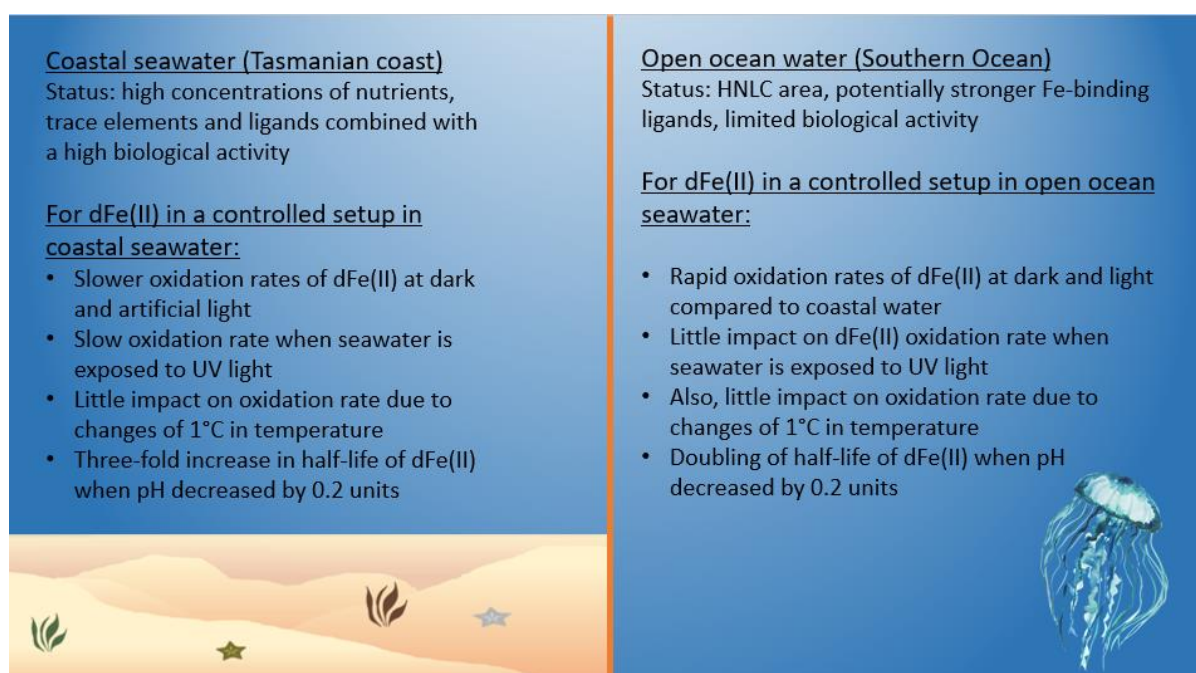


Figure 5.1 Summary of key findings for the dFe(II) oxidation from chapter 2 comparing coastal and open ocean seawater.

In my first data chapter (see Chapter 2 and **Figure 5.1** for summarising outcomes), I used a purely chemical approach, investigating the changes of the oxidation behaviour due to altered pH, temperature, and light conditions in coastal and open ocean water. These two distinctive water types were chosen to record differences in dFe(II) oxidation, which are potentially linked to the water composition of each.

I found that the dFe(II) oxidation is overall much slower in coastal water from the coast (here the Tasmanian coast) compared to open ocean water from the SO (**Figure 5.2 a**). Also, UV light had a greater impact on the oxidation in coastal water compared to open ocean water. I found that it is most likely that a higher concentration in ligands, organic material and biology led to a faster oxidation in coastal areas.

When observing the first climate change linked parameter temperature, I found that an increase by 1°C only impacted the oxidation rate minimally in coastal waters and also had little impact in open ocean water (see **Figure 5.2 b**). Based on my findings, the dFe(II) half-lives are halved in coastal and open ocean water starting at temperature increases of 5°C and more, which exceeds the worst-case scenario of the IPCC (Change, 2018) for future ocean temperatures. Additionally, it should be considered that 1°C warmer water could also lead to enhanced

leaching of Fe from the sediments (de Jong et al., 2013), which would likely impact coastal areas more than the open ocean.

When looking at the decrease in pH, my results had a greater impact on the oxidation rate than a change of 2°C (see **Figure 5.2 c**). The acidification experiments led to a doubling of the half-life in open ocean water and a three-fold increase in coastal water. This could mean that even though the water may be more acidic in both environments, it provides a Fe-enriched milieu due to extended times of ‘freely’ available dFe(II) (Yeala et al., 2005, Shaked and Lis, 2012). Besides the already proven resilience or growth-stimulating effects of OA for cold water phytoplankton species (Hoppe et al., 2013, Trimborn et al., 2017, Hoppe et al., 2017), easily available Fe might be an additional benefit for phytoplankton.

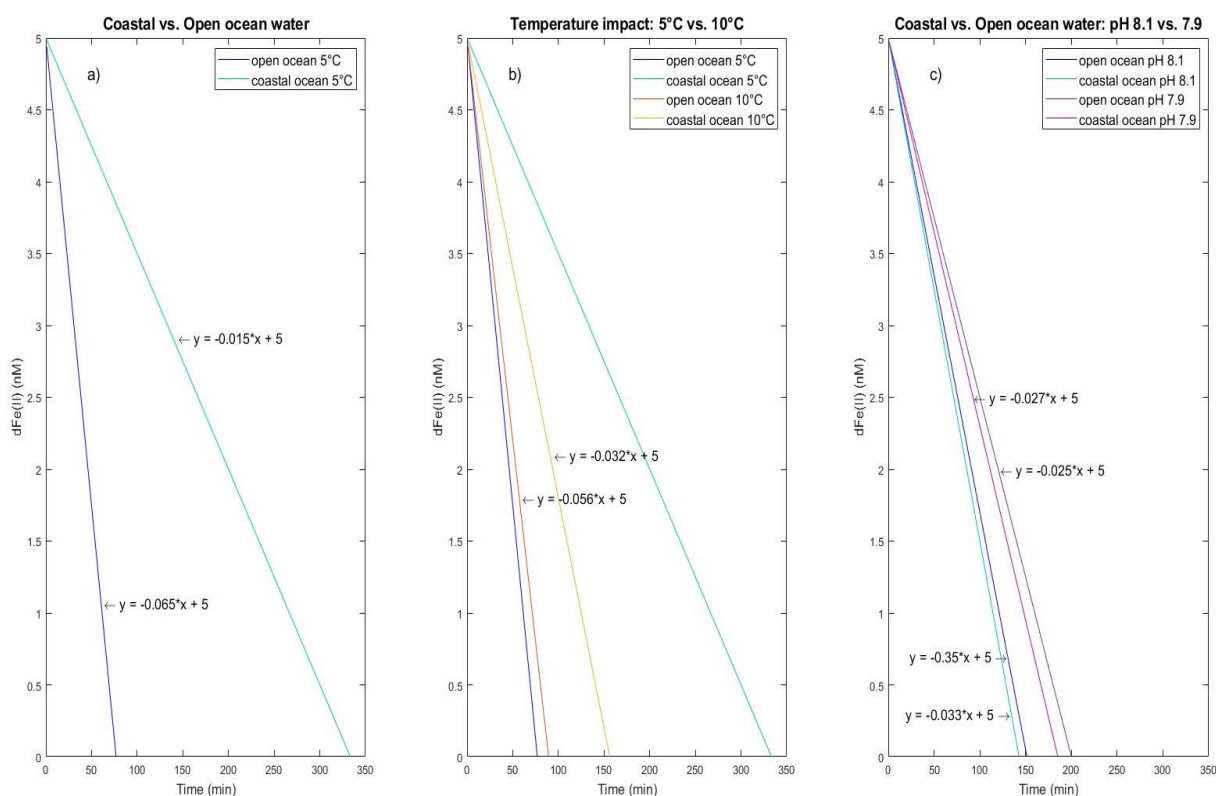


Figure 5.2 Dissolved Fe(II) oxidations comparing coastal and open ocean water (a), impacts of a temperature increase by 5°C (b) and comparing pH decreases by 0.2 units (c). (a) and (b) are based on the measured findings of **Table 2.2** from Chapter 2 and (c) is based on modelled values presented in **Table 2.4**.

My outcomes from Chapter 2 show how important the combination of several factors for predicting dFe(II) oxidation in the ocean are. Up until now, there are no studies displaying how much an increase in 1°C combined with a change in pH of 0.2 and, for example, UV light influences dFe(II) oxidation. Therefore, I included UV into my thesis to observe its impacts on dFe(II) oxidation, knowing that UV impacts/destroys ligands and organic matter. My findings indicated that excessive UV light had a large impact on coastal water (high concentrations in organic matter), leading to rapid oxidation. The oxidation time was more than halved when exposed to UV and extended waiting times (min 30 days) before the observations would have increased the strength of this dataset. On the other hand, in open ocean water it had almost no impact on the oxidation rate. This could be due to less reactive oxygen species in open ocean water compared to coastal water impacting the dFe(II) oxidation. While the UV exposure of our samples was likely highly above any expected future UV radiation, UV could become an increasingly important parameter affecting oxidation in future oceans due to the reasons below.

Ocean warming in open ocean water is thought to induce stratification and shoaling of the upper water layers (Toggweiler and Russell, 2008), hindering the redistribution of nutrients from deeper water masses to surface waters (Dong et al., 2019). Fewer nutrients in surface waters could further lead to less primary production and, therefore, less turbidity in the surface layer, enabling more UV light to penetrate deeper into the ocean. For Fe, a higher UV exposure would lead to an acceleration of the Fe-cycle, especially in the open ocean (Rijkenberg et al., 2005). In the coastal areas, impacts from UV radiation is already quite intense as it is combined with high diel fluctuations in temperature and other parameters such as organic matter. When this is further combined with H₂O₂ concentrations (reducing or oxidising dFe(II)) (Millero and Sotolongo, 1989), it adds a high degree of complexity, making it difficult to project for future coastal dFe(II) circumstances.

Another factor to consider when looking at the dFe(II) oxidation is the concentration of oxygen (O₂). Higher O₂ concentrations lead to faster oxidation, lower concentrations to retarded oxidation (Millero et al., 1987)). It is predicted that oceanic O₂ concentrations will decrease due to increased stratification (Keeling et al., 2010). While the changes in the O₂ concentrations are thought to be small (4%) (Pörtner et al., 2019), this could still have an impact on dFe(II) concentrations and their half-lives (extended) in open ocean water. Predictions for the impact

on dFe(II) and overall O₂ concentrations in coastal water are equally complex as predicting impacts by UV light exposure. Therefore, developing a model and including additional parameters such as organic matter and ligands might facilitate our interpretations.

In my third chapter, I addressed temperature combined with dFe(II) fertilising effects on phytoplankton using incubation experiments. I chose two common and frequently used SO species, *Fragilariopsis cylindrus* – a diatom, and *Phaeocystis antarctica* – a haptophyte. Both are bloom-forming and found in coastal and open ocean environments of the SO (Kropuenske et al., 2009), presenting differing characteristics towards growth and Fe demand. *Fragilariopsis cylindrus* is a member of the diatom family, which helps to regulate the silicate (SiO₄²⁻) cycle in the SO, while *P. antarctica* has a significantly higher capacity for carbon dioxide (CO₂) drawdown (Alderkamp et al., 2012). I chose to run an experiment using three different temperatures (3°C, 5°C, and 7°C) based on the thermal optimum for these two species. Also, an increase from 3°C or 5°C to 5°C or 7°C respectively, is well within the predicted increase for our future oceans (Change, 2018).

My results displayed an overall decrease in growth for the temperature-sensitive diatom *F. cylindrus* in both environments. The growth of *F. cylindrus* was inferior in coastal water compared to open ocean water. When 5 nM of dFe(II) was added though, the growth was significantly improved for coastal and open ocean water. While a better growth in open ocean water could be a result from increased SiO₄²⁻ (22 µM, no data for coastal water), it is also likely that higher toxicity from other trace elements such as copper (Cu) retarded growth (Pascal et al., 2010, Lombardi and Maldonado, 2011, Chu et al., 2019). In the case of *P. antarctica*, a decreased growth was also observed when no dFe(II) was added but overall, their growth interestingly improved with increasing temperatures.

This difference between the two species highlights how their success in growth depends on the water characteristics, nutrient availability, and tolerance to temperature. While temperature might be a physiologically limiting parameter for the diatom, it seems beneficial for the haptophyte in this study (Arrigo et al., 2010, Alderkamp et al., 2012). This difference in the thermal window (see section 3.2.4) and their likely differing adaptation capacity to temperature might be the downfall for many species such as *F. cylindrus* (Thomas et al., 2012, Boyd, 2019).

However, elevated growth for both species was observed when dFe(II) was added, even at relatively high temperatures of 7°C. Considering that there might be higher dFe(II) concentrations in the future, this might be beneficial for both species. On the other hand, many other species might not be able to cope with high temperatures, despite sufficient Fe available.

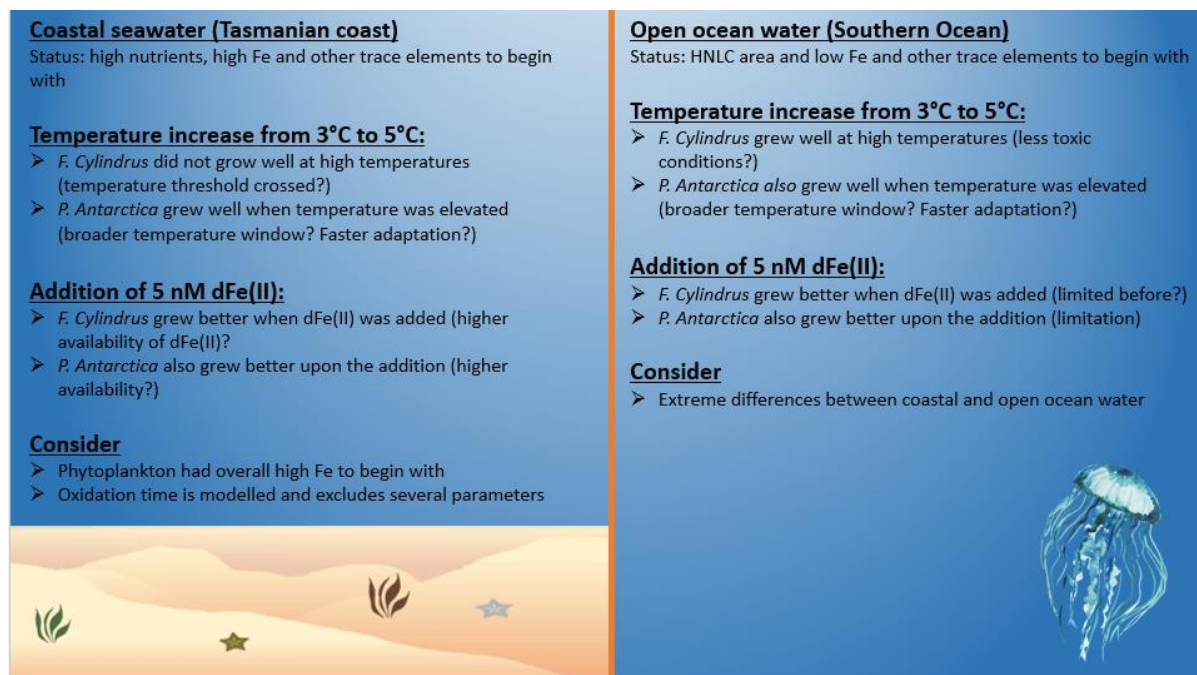


Figure 5.3 Summary of findings for chapter 3.

The half-life time ($t_{1/2}$) defines the time for half of the initial concentration to oxidise. To put the $t_{1/2}$ into perspective, I applied a model to project for oxidative trends under a warmer scenario. In coastal water, there were generally higher concentrations of nutrients and trace elements such as Fe to begin with (**Figure 5.3**). An increase in temperature from 3°C to 7°C would have reduced the $t_{1/2}$ at pH 8.1 (current) from 13 minutes to 6.5 minutes (modelled data, see **Supplementary Table 11**). This model, however, does not account for other parameters such as depth/pressure or organic material. Therefore, I suggest that the actual time that dFe(II) was present could have been much longer and was subject to ligand binding complexes, as seen in our experiments in Chapter 2 (**Figure 2.5**). In this case, not only the elevated initial Fe concentration but also the addition of 5 nM dFe(II) were beneficial for our two model species. In open ocean water, which we defined as high in nutrients and low in Fe to begin with, an increase by 5°C would theoretically decrease the $t_{1/2}$ by 30% at pH 8 (from 40 to 29 minutes;

modelled data, see **Supplementary Table 11**). That could mean that the overall time that dFe(II) was available to phytoplankton was sufficient to boost their growth despite probably lacking other nutrients.

In my final chapter, I looked at the concentrations of dFe(II) and H₂O₂ from a voyage along the east coast of the Australian continent into water from the SO. I aimed to assess sources and concentrations of dFe(II) and H₂O₂ in these areas and put it into context with future ocean scenarios. My findings revealed low concentrations of dFe(II) (< 0.2 nM) in most areas below 1000 m depth. Some exceptions were observed closer to seamounts or sediments. In the surface layer, however, multiple parameters influenced the dFe(II) concentrations and oxidation leading to concentrations above 0.2 nM. Sources explaining these higher concentrations up to 0.5 nM in the northern regions were likely due to biological parameters, input from continental margins and eddy based deep mixed layers. In the south, I only found higher concentrations close to process station (PS) 1, which was likely due to proximity to the South Tasman Rise.

Considering that most models for the dFe(II) oxidation do not account for other parameters such as changes in O₂ and organic matter, it is very likely that the oxidation and overall availability is stronger impacted by temperature changes in colder areas of the SO than by pH. Modelled results from this study display (**Table 4.3**) that temperature plays the dominant role for the dFe(II) oxidation with a $t_{1/2}$ of 5.2 min in the north (19°C, Transit Station (TS) 7) and an even faster $t_{1/2}$ when the temperature is increased to 21°C (4.3 min). In a southern station (PS 1), where the temperature was 9.5°C, I modelled a $t_{1/2}$ of 11.5 minutes. When combining a 2°C increase in temperature with a decrease in 0.2 units in pH, the oxidation at the northern station at TS 7 displayed changes of 14.7 % relative to the values today. In PS 1, I found combined changes of 15.8 %. Overall, it remains to improve models in order to interpret better for the dFe(II) oxidation and availability.

5.2 Future recommendations

The demand for green chemistry to answer climate change related questions is on the rise. Therefore, this is a promising field of work. This thesis is rooted in several major research fields

like ocean acidification, ocean warming, Fe and dFe(II) oxidation and impacts on phytoplankton. It is difficult to combine and interpret each aspect by itself, not to speak of them combined. I observed several issues linked to methodological differences of the dFe(II) assessments between research groups from different institutes and countries, but also found room for improvement when combining OA, warming and dFe(II) oxidations. Furthermore, there is hardly any real data when considering dFe(II) uptake by phytoplankton and a huge need for multi-stressor studies in the experimental but also the modelling field, which I would like to address here.

In the case of Fe, the task to experimentally observe oxidative processes, is often far greater than observing it in its stable form. For dFe(II) measurements, this is true for field observations but also for experiments carried out in laboratories. There are several methods developed to analyse for dFe(II) (Stookey, 1970, King et al., 1995, Bowie et al., 2002, Landing and Hansard 2009) and each method has its strength, differing (amongst others) in their execution, range of measurements and environmental application. This is likely cause and effect for why there is no generalised method for the dFe(II) analysis. As an example, methods are adjusted for different environments e.g., when measuring dFe(II) in sediments vs. open ocean, whereby one needs to be aware of the higher concentration in marine sediments compared to very low concentrations in the open ocean, which might either be undetectable or max out the measurement. While defining standard protocols for improved comparability between studies will remain difficult, it would however be useful to introduce a procedure for a standardised preparation of dFe(II) standards to generalise the starting point/concentration for each method. Currently, methods differ hugely in preparation and the time that the stock solution is considered valid, which could be standardised. Secondly, when only looking at oceanographic work, a standardised method to account for the time lost due to sampling in greater depth until the sample is analysed would also be helpful. Currently it is not clear how depth/pressure impacts the dFe(II) concentration and how to resolve that issue. Having a standardised method (either ignoring it or agreeing on applying a calculation) would resolve that issue.

Regarding primary producers, we know that phytoplankton can directly utilise dFe(II). An attempt to assess short-term extracellular dFe(II) production was made (Strzepek et al., 2011). As far as I know, this is one of only few studies that made and attempt to actually look into the concentration of dFe(II) during uptake. While I am aware that dFe(II) is not the only element,

but part of large elemental orchestra, having a method for an in-line long term observations of uptake or production of dFe(II) by phytoplankton would be recommended. Through this, one could combine the actual uptake, production, and oxidation of dFe(II). This could also be transferred onto other oxidising trace elements such as Cu and might also facilitate ligand studies in the Fe-Cu field.

A more general recommendation is concerning multi-stressor studies in our future oceans. Many studies focus on one or maybe two parameters linked to either chemical or biological processes. Ocean acidification and temperature-based studies often have a major interest for biologists in coastal areas with calcifying organisms such as corals or mammals (e.g., whales), due to a rather simple economic justification of the study (e.g., world heritage, recreational habitat etc.). In the case of nutrients like dFe(II), environmental scientists often face the challenge to link their concern to one of the hot topics mentioned above, in order to sell their story. Nutrients and their concentrations however are crucial for life and should therefore pose a high priority. The little output of publications combining trace-metals, future parameters, and organisms, highlights the difficulty of combining these fields, but it is clear that a combination of ideas and knowledge could be put to use through combining parameters, creating multi-stressors over extended times in maybe differing ecosystems (open vs. coastal water).

Another way to combine knowledge and collected data is to use models. Several parameters such as O_2 , H_2O_2 , temperature and salinity are already incorporated into most dFe(II) oxidation functions (Millero et al., 1987, Millero and Sotolongo, 1989). More thought, however, needs to be given into how to incorporate pressure/depth, UV light, organic material, ligands and uptake to create more realistic models. Therefore, collecting more background data would help to improve models and link them better to the role of OA and temperature for dFe(II) oxidation and project for future scenarios. I observed a major difference in my experimental observations compared to the modelling that I did not base on my experimental data but on published equations. This was especially true for the coastal water, where I could not integrate high CDOM, high UV or ligands in the models. I personally consider this as an important gap to close, as coasts are areas with a great importance due to high biodiversity in fauna and flora with major implications for human interactions. Considering a tool that contains more of the mentioned parameters might really help to project for future outcomes and therein hopefully protect coastal but also other ecosystems.

5.3 Conclusion

Both, the chemical and the biotic aspects of this work have left me with a series of challenging and unfortunately unsolved questions. For example, I intended to answer how much dFe(II) is taken up by phytoplankton and how it varies between species and what exact role ligands play hereby. While I was time limited, my work will help to better understand current and future oxidation processes of dFe(II) and are a part of the puzzle in working towards exploring the uptake of dFe(II) by the two SO species *P. antarctica* and *F. cylindrus*. This work further adds to a deeper understanding of the dFe(II) presence and cycling in the SO and closer to the Australian continent, which can also be incorporated into modelling work.

5.4 References

- ALDERKAMP, A. C., KULK, G., BUMA, A. G., VISSER, R. J., VAN DIJKEN, G. L., MILLS, M. M. & ARRIGO, K. R. 2012. The effect of iron limitation on the photophysiology of *Phaeocystis antarctica* (prymnesiophyceae) and *Fragilariopsis cylindrus* (bacillariophyceae) under dynamic irradiance. *Journal of Phycology*, 48, 45-59.
- ARRIGO, K. R., MILLS, M. M., KROPUENSKE, L. R., VAN DIJKEN, G. L., ALDERKAMP, A.-C. & ROBINSON, D. H. 2010. Photophysiology in two major Southern Ocean phytoplankton taxa: photosynthesis and growth of *Phaeocystis antarctica* and *Fragilariopsis cylindrus* under different irradiance levels. *Integrative and comparative biology*, 50, 950-966.
- BOWIE, A.R., ACHTERBERG, E.P., SEDWICK, P.N., USSHER, S. AND WORSFOLD, P.J., 2002. Real-time monitoring of picomolar concentrations of iron (II) in marine waters using automated flow injection chemiluminescence instrumentation. *Environmental science & technology*, 36 (21), pp.4600-4607.
- BOYD, P. W. 2019. Physiology and iron modulate diverse responses of diatoms to a warming Southern Ocean. *Nature Climate Change*, 9, 148-152.
- CHANGE, I. P. O. C. 2018. Special Report on the Ocean and Cryosphere in a Changing Climate. IPCC Geneva.

- CHU, W.-L., DANG, N.-L., KOK, Y.-Y., IVAN YAP, K.-S., PHANG, S.-M. & CONVEY, P. 2019. Heavy metal pollution in Antarctica and its potential impacts on algae. *Polar Science*, 20, 75-83.
- DE JONG, J., SCHOEMANN, V., MARICQ, N., MATTIELLI, N., LANGHORNE, P., HASKELL, T. & TISON, J.-L. 2013. Iron in land-fast sea ice of McMurdo Sound derived from sediment resuspension and wind-blown dust attributes to primary productivity in the Ross Sea, Antarctica. *Marine Chemistry*, 157, 24-40.
- DONG, S., BARINGER, M. O. & GONI, G. J. 2019. Slow down of the Gulf Stream during 1993–2016. *Scientific Reports*, 9, 1-10.
- GILLE, S. T. 2002. Warming of the Southern Ocean Since the 1950s. *Science*, 295, 1275-1277.
- HANSARD, S.P. AND LANDING, W.M., 2009. Determination of iron (II) in acidified seawater samples by luminol chemiluminescence. *Limnology and Oceanography: Methods*, 7(3), pp.222-234.
- HOPPE, C. J., HASSLER, C. S., PAYNE, C. D., TORTELL, P. D., ROST, B. & TRIMBORN, S. 2013. Iron limitation modulates ocean acidification effects on Southern Ocean phytoplankton communities. *PLoS One*, 8, e79890.
- HOPPE, C. J. M., SCHUBACK, N., SEMENIUK, D. M., MALDONADO, M. T. & ROST, B. 2017. Functional Redundancy Facilitates Resilience of Subarctic Phytoplankton Assemblages toward Ocean Acidification and High Irradiance. *Frontiers in Marine Science*, 4.
- KEELING, R. F., KÖRTZINGER, A. & GRUBER, N. 2010. Ocean deoxygenation in a warming world. *Annual review of marine science*, 2, 199-229.
- KENNEDY, F., MCMINN, A. & MARTIN, A. 2012. Effect of temperature on the photosynthetic efficiency and morphotype of *Phaeocystis antarctica*. *Journal of Experimental Marine Biology and Ecology*, 429, 7-14.
- KING, D.W., LOUNSBURY, H.A. AND MILLERO, F.J., 1995. Rates and mechanism of Fe (II) oxidation at nanomolar total iron concentrations. *Environmental science & technology*, 29(3), pp.818-824.
- KROPUENSKE, L. R., MILLS, M. M., VAN DIJKEN, G. L., BAILEY, S., ROBINSON, D. H., WELSCHMEYER, N. A. & ARRIGOA, K. R. 2009. Photophysiology in two major Southern Ocean phytoplankton taxa: photoprotection in *Phaeocystis antarctica* and *Fragilariopsis cylindrus*. *Limnology and Oceanography*, 54, 1176-1196.
- LOMBARDI, A. T. & MALDONADO, M. T. 2011. The effects of copper on the photosynthetic response of *Phaeocystis cordata*. *Photosynthesis research*, 108, 77-87.
- MILLERO, F. J. & SOTOLONGO, S. 1989. The oxidation of Fe (II) with H₂O₂ in seawater. *Geochimica et Cosmochimica Acta*, 53, 1867-1873.
- MILLERO, F. J., SOTOLONGO, S. & IZAGUIRRE, M. 1987. The oxidation kinetics of Fe(II) in seawater. *Geochimica et Cosmochimica Acta*, 51, 793-801.

- PASCAL, P. Y., FLEEGER, J. W., GALVEZ, F. & CARMAN, K. R. 2010. The toxicological interaction between ocean acidity and metals in coastal meiobenthic copepods. *Marine Pollution Bulletin*, 60, 2201-2208.
- PÖRTNER, H.-O., ROBERTS, D., MASSON-DELMOTTE, V., ZHAI, P., POLOCZANSKA, E., MINTENBECK, K., TIGNOR, M., ALEGRÍA, A., NICOLAI, M. & OKEM, A. 2019. IPCC, 2019: Technical Summary. *IPCC Special Report on the Ocean and Cryosphere in a Changing Climate*.
- RAVEN, J. A. & GEIDER, R. J. 1988. Temperature and algal growth. *New phytologist*, 110, 441-461.
- RIJKENBERG, M. J. A., FISCHER, A. C., KROON, J., GERRINGA, L., TIMMERMANS, K., WOLTERBEEK, H. T. & DE BAAR, H. 2005. The influence of UV irradiation on the photoreduction of iron in the Southern Ocean. *Marine Chemistry*, 93, 119-129.
- SHAKED, Y. & LIS, H. 2012. Disassembling iron availability to phytoplankton. *Frontiers in microbiology*, 3.
- STOOKEY, L.L., 1970. Ferrozine - a new spectrophotometric reagent for iron. *Analytical chemistry*, 42(7), pp.779-781.
- STRZEPEK, R. F., MALDONADO, M. T., HUNTER, K. A., FREW, R. D. & BOYD, P. W. 2011. Adaptive strategies by Southern Ocean phytoplankton to lessen iron limitation: Uptake of organically complexed iron and reduced cellular iron requirements. *Limnology and Oceanography*, 56, 1983-2002.
- THOMAS, M. K., KREMER, C. T., KLAUSMEIER, C. A. & LITCHMAN, E. 2012. A global pattern of thermal adaptation in marine phytoplankton. *Science*, 338, 1085-1088.
- TOGGWEILER, J. R. & RUSSELL, J. 2008. Ocean circulation in a warming climate. *Nature*, 451, 286-288.
- TRIMBORN, S., BRENNEIS, T., HOPPE, C. J., LAGLERA, L. M., NORMAN, L., SANTOS-ECHEANDÍA, J., VÖLKNER, C., WOLF-GLADROW, D. & HASSLER, C. S. 2017. Iron sources alter the response of Southern Ocean phytoplankton to ocean acidification. *Marine Ecology Progress Series*, 578, 35-50.
- YEALA, S., B., K. A. & M., M. F. M. 2005. A general kinetic model for iron acquisition by eukaryotic phytoplankton. *Limnology and Oceanography*, 50, 872-882.
- ZEEBE, R. E. & WOLF-GLADROW, D. A. 2001. *CO₂ in seawater: equilibrium, kinetics, isotopes*, Amsterdam ; New York : Elsevier, 2001.

Appendix A

Supplementary data for Chapter 2

Supplementary Table 1 Tukey's HSD post hoc test comparing the light treatments in coastal water for the 1st t½.

Multiple Comparisons^a

Dependent Variable: thalf_observed_considered

Tukey HSD

(I) dark1_light2_UV3	(J) dark1_light2_UV3	Mean Difference (I-J)	Std. Error	Sig.	95% Confidence Interval	
					Lower Bound	Upper Bound
1	2	-25,53827	13,28549	,145	-57,8153	6,7387
	3	25,80185	16,27133	,263	-13,7292	65,3329
2	1	25,53827	13,28549	,145	-6,7387	57,8153
	3	51,34012*	13,28549	,001	19,0631	83,6171
3	1	-25,80185	16,27133	,263	-65,3329	13,7292
	2	-51,34012*	13,28549	,001	-83,6171	-19,0631

*. The mean difference is significant at the 0.05 level.

a. open_coastal = 2

Supplementary Table 2 Tukey's HSD post hoc test comparing the light treatments in open ocean water for the 1st t½.

Multiple Comparisons^a

Dependent Variable: thalf_observed_considered

Tukey HSD

(I) dark1_light2_UV3	(J) dark1_light2_UV3	Mean Difference (I-J)	Std. Error	Sig.	95% Confidence Interval	
					Lower Bound	Upper Bound
1	2	-1,85894	4,11438	,894	-11,6969	7,9790
	3	12,59580*	5,15765	,044	,2633	24,9283
2	1	1,85894	4,11438	,894	-7,9790	11,6969
	3	14,45474*	4,39846	,004	3,9375	24,9719
3	1	-12,59580*	5,15765	,044	-24,9283	-,2633
	2	-14,45474*	4,39846	,004	-24,9719	-3,9375

*. The mean difference is significant at the 0.05 level.

a. open_coastal = 1

Supplementary Table 3 ANOVA for the 1st t½ in open ocean water comparing filtered vs. unfiltered conditions.

ANOVA^a

thalf_observed_considered

	Sum of Squares	df	Mean Square	F	Sig.
Between Groups	4727,272	1	4727,272	25,682	<,001
Within Groups	13989,470	76	184,072		
Total	18716,742	77			

a. open_coastal = 1

Supplementary Table 4 Tukey's HSD post hoc test comparing filtered light treatments in open ocean water for the 1st t½.

Multiple Comparisons^a

Dependent Variable: thalf_observed_considered

Tukey HSD

(I) dark1_light2_UV3	(J) dark1_light2_UV3	Mean Difference (I-J)	Std. Error	Sig.	95% Confidence Interval	
					Lower Bound	Upper Bound
1	2	-14,64430*	3,37687	<,001	-22,8009	-6,4877
	3	1,30103	4,40290	,953	-9,3338	11,9359
2	1	14,64430*	3,37687	<,001	6,4877	22,8009
	3	15,94532*	3,54169	<,001	7,3906	24,5000
3	1	-1,30103	4,40290	,953	-11,9359	9,3338
	2	-15,94532*	3,54169	<,001	-24,5000	-7,3906

*. The mean difference is significant at the 0.05 level.

a. open_coastal = 1, f_uf = 1

Supplementary Table 5 Tukey's HSD post hoc test comparing unfiltered light treatments in open ocean water for the 1st t $\frac{1}{2}$.

Multiple Comparisons^a

Dependent Variable: thalf_observed_considered

Tukey HSD

(I) dark1_light2_UV3	(J) dark1_light2_UV3	Mean Difference (I-J)	Std. Error	Sig.	95% Confidence Interval	
					Lower Bound	Upper Bound
1	2	-.05926	6,72726	1,000	-16,9586	16,8400
	3	23,15450*	7,19174	,011	5,0884	41,2206
2	1	,05926	6,72726	1,000	-16,8400	16,9586
	3	23,21376*	7,19174	,010	5,1476	41,2799
3	1	-23,15450*	7,19174	,011	-41,2206	-5,0884
	2	-23,21376*	7,19174	,010	-41,2799	-5,1476

*. The mean difference is significant at the 0.05 level.

a. open_coastal = 1, f_uf = 2

Supplementary Table 6 Tukey's HSD post hoc test comparing filtered light treatments in coastal ocean water for the 2nd t $\frac{1}{2}$.

Multiple Comparisons^a

Dependent Variable: sec_thalf_observed

Tukey HSD

(I) dark1_light2_UV3	(J) dark1_light2_UV3	Mean Difference (I-J)	Std. Error	Sig.	95% Confidence Interval	
					Lower Bound	Upper Bound
1	2	-2,07593	4,83107	,904	-14,1405	9,9886
	3	27,09074*	4,83107	<,001	15,0262	39,1553
2	1	2,07593	4,83107	,904	-9,9886	14,1405
	3	29,16667*	4,83107	<,001	17,1021	41,2312
3	1	-27,09074*	4,83107	<,001	-39,1553	-15,0262
	2	-29,16667*	4,83107	<,001	-41,2312	-17,1021

*. The mean difference is significant at the 0.05 level.

a. open_coastal = 2, f_uf = 1

Supplementary Table 7 Tukey's HSD post hoc test comparing filtered coastal water for all light treatments in the 1st and 2nd t½.

Multiple Comparisons^a

Tukey HSD

Dependent Variable	(I) dark1_light2_UV3	(J) dark1_light2_UV3	Mean Difference (I-J)	Std. Error	Sig.	95% Confidence Interval	
						Lower Bound	Upper Bound
sec_thalf_observed	1	2	,74111	1,65706	,896	-3,4512	4,9334
		3	,08133	1,96066	,999	-4,8791	5,0418
	2	1	-,74111	1,65706	,896	-4,9334	3,4512
		3	-,65978	1,96066	,940	-5,6202	4,3007
	3	1	-,08133	1,96066	,999	-5,0418	4,8791
		2	,65978	1,96066	,940	-4,3007	5,6202
thalf_observed_considered	1	2	1,22478	1,48174	,691	-2,4860	4,9356
		3	1,30103	1,52734	,675	-2,5239	5,1260
	2	1	-1,22478	1,48174	,691	-4,9356	2,4860
		3	,07625	1,52734	,999	-3,7487	3,9012
	3	1	-1,30103	1,52734	,675	-5,1260	2,5239
		2	-,07625	1,52734	,999	-3,9012	3,7487

a. open_coastal = 1, f_uf = 1, t_co2 = 1

Supplementary Table 8 Tukey's HSD post hoc test comparing open ocean pH in the 1st t½ during the CO₂ experiment.

Multiple Comparisons^a

Dependent Variable: thalf_observed_considered

Tukey HSD

(I) para_pH	(J) para_pH	Mean Difference (I-J)	Std. Error	Sig.	95% Confidence Interval	
					Lower Bound	Upper Bound
6,00	7,00	1,43519	2,11854	,779	-3,8554	6,7258
	8,10	8,48519*	2,11854	,001	3,1946	13,7758
7,00	6,00	-1,43519	2,11854	,779	-6,7258	3,8554
	8,10	7,05000*	2,11854	,008	1,7594	12,3406
8,10	6,00	-8,48519*	2,11854	,001	-13,7758	-3,1946
	7,00	-7,05000*	2,11854	,008	-12,3406	-1,7594

*. The mean difference is significant at the 0.05 level.

a. t_co2 = 2, open_coastal = 1

Supplementary Table 9 Tukey's HSD post hoc test comparing coastal ocean pH in the 1st t/2 during the CO₂ experiment.

Multiple Comparisons^a

Dependent Variable: thalf_observed_considered

Tukey HSD

(I) para_pH	(J) para_pH	Mean Difference (I-J)	Std. Error	Sig.	95% Confidence Interval	
					Lower Bound	Upper Bound
7,50	7,90	-24,81944	13,76401	,202	-60,5710	10,9322
	8,10	65,65834*	13,76401	<,001	29,9067	101,4099
7,90	7,50	24,81944	13,76401	,202	-10,9322	60,5710
	8,10	90,47778*	13,76401	<,001	54,7262	126,2294
8,10	7,50	-65,65834*	13,76401	<,001	-101,4099	-29,9067
	7,90	-90,47778*	13,76401	<,001	-126,2294	-54,7262

*. The mean difference is significant at the 0.05 level.

a. t_co2 = 2, open_coastal = 2

Supplementary Table 10 Calculated $t_{1/2}$ for coastal and open ocean water at pH 8.1 and 7.9 for temperature range from 0°C to 20°C.

Temp (C°)	Open ocean water			Coastal water		
	pH 8.1	pH 8	pH 7.9	pH 8.1	pH 8	pH 7.9
	$t_{1/2}$ (min ⁻¹)					
0	39.24	59.16	87.46	22.21	28.93	41.64
0.2	38.46	57.94	85.65	21.45	28.58	41.31
0.4	37.70	56.75	83.86	20.71	28.24	40.98
0.6	36.95	55.58	82.10	20.00	27.91	40.65
0.8	36.22	54.44	80.36	19.32	27.57	40.33
1	35.50	53.32	78.64	18.66	27.24	40.01
1.2	34.80	52.22	76.95	18.02	26.92	39.69
1.4	34.11	51.14	75.28	17.41	26.60	39.37
1.6	33.44	50.09	73.64	16.81	26.28	39.06
1.8	32.78	49.06	72.02	16.23	25.97	38.75
2	32.13	48.05	70.42	15.68	25.66	38.44
2.2	31.49	47.06	68.85	15.14	25.35	38.13
2.4	30.87	46.09	67.30	14.63	25.05	37.83
2.6	30.26	45.14	65.78	14.13	24.75	37.53
2.8	29.66	44.21	64.28	13.64	24.45	37.23
3	29.07	43.30	62.81	13.18	24.16	36.93
3.2	28.49	42.41	61.36	12.72	23.87	36.64
3.4	27.93	41.54	59.93	12.29	23.59	36.34
3.6	27.38	40.68	58.53	11.87	23.31	36.05
3.8	26.83	39.85	57.15	11.46	23.03	35.77
4	26.30	39.03	55.79	11.07	22.76	35.48
4.2	25.78	38.22	54.46	10.69	22.48	35.20
4.4	25.27	37.44	53.16	10.33	22.22	34.92
4.6	24.77	36.67	51.87	9.97	21.95	34.64
4.8	24.28	35.91	50.61	9.63	21.69	34.36
5	23.80	35.17	49.38	9.30	21.43	34.09
5.2	23.33	34.45	48.17	8.99	21.17	33.82
5.4	22.87	33.74	46.98	8.68	20.92	33.55
5.6	22.41	33.04	45.82	8.38	20.67	33.28
5.8	21.97	32.36	44.68	8.09	20.43	33.02
6	21.53	31.70	43.57	7.82	20.18	32.75
6.2	21.11	31.04	42.48	7.55	19.94	32.49
6.4	20.69	30.41	41.41	7.29	19.70	32.23
6.6	20.28	29.78	40.37	7.04	19.47	31.98
6.8	19.88	29.17	39.35	6.80	19.24	31.72
7	19.49	28.57	38.36	6.57	19.01	31.47
7.2	19.10	27.98	37.39	6.34	18.78	31.22
7.4	18.72	27.40	36.44	6.13	18.56	30.97
7.6	18.35	26.84	35.52	5.92	18.33	30.72
7.8	17.99	26.29	34.62	5.72	18.12	30.48
8	17.63	25.74	33.75	5.52	17.90	30.24
8.2	17.28	25.21	32.90	5.33	17.69	30.00
8.4	16.94	24.70	32.08	5.15	17.48	29.76
8.6	16.60	24.19	31.28	4.97	17.27	29.52
8.8	16.28	23.69	30.50	4.80	17.06	29.28
9	15.95	23.20	29.74	4.64	16.86	29.05
9.2	15.64	22.72	29.02	4.48	16.66	28.82
9.4	15.33	22.26	28.31	4.33	16.46	28.59
9.6	15.02	21.80	27.63	4.18	16.26	28.36
9.8	14.73	21.35	26.97	4.04	16.07	28.14
10	14.44	20.91	26.34	3.90	15.88	27.91
10.2	14.15	20.48	25.73	3.76	15.69	27.69

Temp (C°)	Open ocean water			Coastal water		
	pH 8.1	pH 8	pH 7.9	pH 8.1	pH 8	pH 7.9
	t/2 (min ⁻¹)					
10.4	13.87	20.06	25.15	3.64	15.50	27.47
10.6	13.59	19.65	24.59	3.51	15.31	27.25
10.8	13.33	19.24	24.05	3.39	15.13	27.03
11	13.06	18.84	23.54	3.28	14.95	26.82
11.2	12.80	18.46	23.05	3.16	14.77	26.60
11.4	12.55	18.08	22.58	3.05	14.60	26.39
11.6	12.30	17.70	22.14	2.95	14.42	26.18
11.8	12.06	17.34	21.73	2.85	14.25	25.97
12	11.82	16.98	21.34	2.75	14.08	25.77
12.2	11.58	16.63	20.97	2.66	13.91	25.56
12.4	11.36	16.29	20.62	2.57	13.75	25.36
12.6	11.13	15.96	20.30	2.48	13.58	25.15
12.8	10.91	15.63	20.01	2.39	13.42	24.95
13	10.69	15.31	19.74	2.31	13.26	24.76
13.2	10.48	14.99	19.49	2.23	13.10	24.56
13.4	10.27	14.68	19.26	2.16	12.95	24.36
13.6	10.07	14.38	19.06	2.08	12.79	24.17
13.8	9.87	14.08	18.89	2.01	12.64	23.98
14	9.68	13.79	18.74	1.94	12.49	23.78
14.2	9.48	13.51	18.61	1.88	12.34	23.60
14.4	9.30	13.23	18.51	1.81	12.19	23.41
14.6	9.11	12.96	18.43	1.75	12.05	23.22
14.8	8.93	12.69	18.37	1.69	11.90	23.04
15	8.76	12.43	18.34	1.63	11.76	22.85

Appendix B

Supplementary data for Chapter 3

Supplementary Table 11 Summary of the p-values from the statistical analysis. Significant values are shown in bold.

What is compared/assumption	Test type	P-value
Highest growth rates when no Fe was added for <i>P. antarctica</i> in coastal water	Post Hoc	3°C to 5°C: 0.679 3°C to 7°C: 0.006 5°C to 7°C: 0.003
Highest growth rates when no Fe was added for <i>P. antarctica</i> in open ocean water	Post Hoc	3°C to 5°C: 0.048 3°C to 7°C: 0.164 5°C to 7°C: 0.005
Highest growth rates when no Fe was added for <i>F. cylindrus</i> in coastal water	Post Hoc	3°C to 5°C: 0.99 3°C to 7°C: 0.010 5°C to 7°C: 0.010
Highest growth rates when no Fe was added for <i>F. cylindrus</i> in open ocean water	Post Hoc	3°C to 5°C: 0.379 3°C to 7°C: 0.269 5°C to 7°C: 0.955
Highest growth rates of <i>P. antarctica</i> when Fe was added to coastal water	Post Hoc	3°C to 5°C: 0.99 3°C to 7°C: 0.04 5°C to 7°C: 0.04
Highest growth rates of <i>P. antarctica</i> when Fe was added to open ocean water	Post Hoc	3°C to 5°C: 0.775 3°C to 7°C: 0.005 5°C to 7°C: 0.011
Highest growth rates of <i>F. cylindrus</i> when Fe was added to coastal water	Post Hoc	3°C to 5°C: 0.665 3°C to 7°C: 0.442 5°C to 7°C: 0.910
Highest growth rates of <i>F. cylindrus</i> when Fe was added to open ocean water	Post Hoc	3°C to 5°C: 0.654 3°C to 7°C: 0.057 5°C to 7°C: 0.019
Growth difference when Fe was added for <i>P. antarctica</i> in coastal water	ANOVA	3°C: 0.010 5°C: 0.021 7°C: 0.045
Growth difference when Fe was added for <i>P. antarctica</i> in open ocean water	ANOVA	3°C: 0.008 5°C: 0.001 7°C: 0.006
Growth difference when Fe was added for <i>F. cylindrus</i> in coastal water	ANOVA	3°C: 0.762 5°C: 0.079 7°C: 0.012
Growth difference when Fe was added for <i>F. cylindrus</i> in open ocean water	ANOVA	3°C: 0.729 5°C: 0.065 7°C: 0.027
Interactions between Fe addition and temperature in coastal water for <i>P. antarctica</i>	2-way ANOVA	0.269
Interactions between Fe addition and temperature in open ocean water for <i>P. antarctica</i>	2-way ANOVA	0.029
Interactions between Fe addition and temperature in coastal water for <i>F. cylindrus</i>	2-way ANOVA	0.013
Interactions between Fe addition and temperature in open ocean water for <i>F. cylindrus</i>	2-way ANOVA	0.025

Appendix C

Supplementary data for Chapter 4

Supplementary Table 12 Depth (cm), salinity, pH, temperature, and dilution factors for the analysis of sediment samples.

Depth (cm)	Salinity	pH	Temperature, °C	Dilution
25	35	7.53	3	x 60
1	35	7.28	3	x 60
- 1	32	7.6	3	x 60
- 2	No data	No data	No Data	x 10
- 3	32	7.58	3	x 20
- 4	32	7.63	3	x 20
- 5	32	7.76	3	x 20
- 6	34	7.6	3	x 10
- 7	33.5	7.6	3	x 6
- 8	33	7.72	3	x 6
- 9	32	7.72	3	x 6

Supplementary Table 13 Location, depth, CTD and nutrient data (NO_3^- , PO_4^{3-} , SiO_4^{2-} , NH_4^+) with Chl-*a* together with the data of dFe(II), dFe (tot) and H_2O_2 from V04_2018.

Station	Latitude	Longitude	Depth (m)	Temperature (C°)	Salinity	O_2 (μM)	NO_3^- (μM)	PO_4^{3-} (μM)	SiO_4^{2-} (μM)	NH_4^+ (μM)	Chl- <i>a</i> (μg)	H_2O_2 (nM)	dFe(II) (nM)	dFe (nM)	Ratio %
TS 9	-34.18	152.28	15	19.10			0.98	0.19	0.60	0.03	0.52	27.85	0.03	0.22	13.70
			40	19.11			0.97	0.19	0.70	0.03	0.49	20.07	0.03	0.29	10.24
Bottom depth: 4866 m			70	19.11			1.00	0.18	0.60	0.05	0.49	22.67	0.03	0.45	6.60
			100	19.11	35.74	230.81	1.65	0.22	0.70	0.04		16.01	0.03	0.45	6.68
			150	18.66			2.33	0.25	0.80	0.00	0.15	10.83	0.03	0.61	4.89
			200	18.39			2.52	0.27	0.90	0.00	0.15	12.44	0.03	0.22	13.62
			250				5.95	0.49	1.70	0.00		5.93	0.03	0.50	5.97
			300	16.25	35.49	202.63	7.60	0.60	2.40	0.00	0.01	6.94	0.03	0.91	3.31
			500	12.11	35.05	212.18	14.64	1.04	5.20	0.00		6.58	0.03	0.63	4.75
			750	9.00			22.92	1.57	11.90	0.00		6.09	0.03	1.00	3.00
			1000	6.14			28.31	1.94	26.70	0.00		6.52	0.03	0.66	4.54
			1250	4.22	35.05	174.00	32.53	2.26	55.00	0.00		5.54	0.03	0.84	3.58
			1500	3.35	34.55	159.71	34.99	2.46	81.00	-0.01		6.66	0.08	0.92	9.02
			1756	2.75	34.61	159.17	35.46	2.50	94.40	-0.01		6.11	0.05	1.15	4.00
			2000	2.39	34.66	168.06	34.64	2.44	95.50	-0.01		4.54	0.10	0.90	10.70
			2250	2.17	34.69	177.13	33.84	2.37	95.60	-0.01		5.49	0.05	0.75	6.11
			2500	2.01	34.71	183.24	33.31	2.33	98.60	-0.01		4.39	0.05	0.82	5.61
			2750	1.81	34.72	189.59	33.02	2.32	102.20	-0.01		5.13	0.05	0.92	4.98
			3000	1.61	34.72	193.34	33.04	2.32	107.20	-0.01		3.85	0.05	0.72	6.41
			3250				33.12	2.33	112.30	-0.01		4.26	0.05	1.07	4.27
			3500	1.30	34.72	199.14	33.29	2.34	116.10	-0.01		4.85	0.05	1.11	4.14
			3750				33.40	2.34	118.20	-0.01		3.56	0.05	0.68	6.72
			4000	1.20	34.72	201.20	33.43	2.36	119.40	0.01		3.71	0.05	0.77	5.95
TS 8	-34.40	154.33	15	19.33	35.75	229.33	4.57	0.44	2.00	0.09	1.21	22.32		0.43	
			40	19.33			1.73	0.26	0.80	0.15		14.25		0.47	

Station	Latitude	Longitude	Depth (m)	Temperature (C°)	Salinity	O ₂ (μ M)	NO ₃ ⁻ (μ M)	PO ₄ ³⁻ (μ M)	SiO ₄ ²⁻ (μ M)	NH ⁺ (μ M)	Chl- <i>a</i> (μ g)	H ₂ O ₂ (nM)	dFe(II) (nM)	dFe (nM)	Ratio %		
Bottom depth: 4871 m			70	19.33			3.20	0.36	1.10	0.17	0.94	8.42	0.02	0.49	3.56		
			100	19.33	35.75	228.62	5.82	0.50	1.80	0.01	0.07	6.84			0.76		
			250				11.99	0.89	3.80	0.00		6.71	0.10	0.92	11.03		
			300	17.26			14.43	1.04	4.70	0.00		6.61	0.39	0.83	47.30		
			500	12.03	35.10	213.17	21.39	1.48	9.20	0.00		6.45	0.12	0.82	14.15		
			750	9.58	34.77		28.88	1.99	29.00	0.10		6.52		0.73			
			1000	6.55	34.46	199.86	32.57	2.28	52.20	0.01		6.06	0.16	1.02	15.61		
			1500	3.61	34.53	163.46	35.35	2.49	91.00	0.00		7.02	0.08	1.14	6.60		
			1750	2.93	34.59	158.50	34.88	2.48	95.70	0.00		5.96	0.08	1.21	6.24		
			2000	2.52	34.64	166.54	33.86	2.39	94.30	0.00		6.53	0.08	1.05	7.18		
			2250	2.28	34.68	174.49	33.15	2.33	96.00	0.00		6.37	0.08	0.75	10.10		
			2500	2.09	34.71	183.38	32.77	2.31	100.00	0.00		6.13	0.08	0.71	10.61		
			2750	1.88	34.72	189.01	32.81	2.32	105.60	0.00		6.68	0.08	0.73	10.30		
			3000	1.70	34.73	192.94	32.88	2.32	111.00	0.00		5.80	0.08	1.34	5.63		
			3250						0.00				6.30	0.08	1.55	4.87	
			3500	1.35	34.72	199.14	33.00	2.33	115.10	0.00		6.28	0.08	0.85	8.84		
3750						0.00				5.81	0.11	0.67	16.08				
TS 7	-35.57	152.52	15	19.31			0.98	0.19	0.70	0.01	0.64	19.77		0.18			
			40	19.32			0.98	0.19	0.70	0.01	0.51	20.63		0.30			
Bottom depth: 4852 m			70	19.33			0.98	0.19	0.70	0.01	0.48	16.09		0.37			
			100	19.33	35.75	229.02	1.00	0.18	0.70	0.01			0.10				
			150	19.33			1.11	0.19	0.70	0.01	0.29	15.00		0.18			
			250				4.62	0.40	1.40	0.00	0.02	1.62		0.50			
			300	17.33	35.59	207.00	5.92	0.48	1.90	0.00		3.40		0.42			
			500	11.92	35.05	207.50	13.75	0.98	4.90	0.00		1.79	0.25	0.60	40.76		
			750	8.49	34.61	208.61	20.32	1.40	9.50	0.00		0.96	0.33	0.78	42.68		
			1000	6.46			27.70	1.90	24.10	0.00		0.00		0.67			
			1250	4.45	34.47	178.33	32.06	2.23	49.40	0.00		0.00	0.17	0.77	22.73		

Station	Latitude	Longitude	Depth (m)	Temperature (C°)	Salinity	O ₂ (μ M)	NO ₃ ⁻ (μ M)	PO ₄ ³⁻ (μ M)	SiO ₄ ²⁻ (μ M)	NH ₄ ⁺ (μ M)	Chl- <i>a</i> (μ g)	H ₂ O ₂ (nM)	dFe(II) (nM)	dFe (nM)	Ratio %
TS 6	-37.23	150.54	15	17.64			1.55	0.25	1.10	0.06	1.55	11.37	0.03	0.49	6.14
			40	14.06			2.21	0.29	1.30	0.14	1.37	6.30	0.03	0.23	13.30
Bottom depth: 4667 m			70	13.84			4.60	0.43	1.80	0.00	0.06	6.83	0.03	0.17	17.61
			100	13.63	35.44	250.15	8.30	0.65	2.80	0.00	0.03	6.84	0.03	0.22	13.94
			150	13.58			8.74	0.67	3.00	0.00	0.02	27.85	0.03	0.27	10.93
			200	13.56			10.76	0.80	3.70	0.00	0.02	23.11	0.03	0.44	6.83
			250				15.50	1.09	5.60	0.00		4.75	0.03	1.07	2.79
			300	13.52	35.44	251.80	17.32	1.20	6.50	0.00		3.80	0.03	0.81	3.72
			500	10.50	34.90	226.43	23.50	1.61	12.80	0.00		4.81	0.03	0.32	9.40
			750	6.90	34.48	200.39	28.47	1.95	27.30	0.00		5.25	0.03	0.47	6.39
			1000	5.13	34.44	187.89	31.98	2.21	49.50	0.00		4.89	0.03	0.43	6.91
			1500	2.79	34.60	160.74	35.42	2.49	90.20	0.01		2.61	0.19	1.23	15.09
			1756	2.56	34.63	163.73	35.01	2.46	94.20	0.00		4.75	0.08	0.87	8.83
			2000	2.31	34.67	172.17	34.24	2.40	94.60	0.09		3.26	0.17	0.92	18.56
			2250	2.12	34.70	181.15	33.39	2.34	94.80	0.00		2.88	0.06	1.28	5.05
			2500	1.95	34.72	186.95	32.95	2.31	97.80	0.00		5.14	0.02	1.17	1.48
			2750	1.79	34.72	190.61	32.84	2.30	102.80	0.01		1.73	0.02	1.17	1.48
			3000	1.63	34.73	194.50	32.81	2.29	107.00	0.00		1.94	0.02	1.32	1.31
			3500	1.31	34.72	200.35	33.07	2.33	115.60	0.00		3.02	0.02	1.25	1.38
			4000	1.17	34.72	202.14	33.40	2.34	120.20	0.15		2.75	0.02	1.40	1.23
			4500	1.15	34.71	203.74	33.33	2.34	122.10	0.00		2.71	0.02	0.87	2.00
			4600	1.13	34.71	205.75	33.33	2.34	121.80	0.00			0.02		
TS 5	-39.09	149.05	40	14.06			3.70	0.39	1.50	0.06	7.89	34.27	0.03	0.48	5.30
			70	13.84			6.08	0.54	2.10	0.01	1.49	15.97	0.02	0.45	3.81
Bottom depth: 1674 m			100	13.63	35.44	250.15	6.42	0.55	2.20	0.00	0.14	14.43	0.07	0.59	11.73
			150	13.58			6.55	0.56	2.30	0.00	0.09	12.97	0.08	0.56	14.75
			200	13.56			6.33	0.55	2.20	0.00	0.16	9.49	0.08	0.48	15.88
			250				6.41	0.55	2.20	0.00		1.24	0.08	0.68	12.10

Station	Latitude	Longitude	Depth (m)	Temperature (C°)	Salinity	O ₂ (μ M)	NO ₃ ⁻ (μ M)	PO ₄ ³⁻ (μ M)	SiO ₄ ²⁻ (μ M)	NH ⁺ (μ M)	Chl- <i>a</i> (μ g)	H ₂ O ₂ (nM)	dFe(II) (nM)	dFe (nM)	Ratio %
			300	13.52	35.44	251.80	6.45	0.56	2.20	0.00		1.32	0.12	0.60	20.10
			500	10.50	34.90	226.43	17.71	1.25	6.40	0.00		1.64	0.04	0.90	4.21
			750	6.90	34.48	200.39	25.93	1.79	18.50	0.00		2.04	0.06	0.87	7.27
			1000	5.13	34.44	187.89	30.81	2.16	41.20	0.00		2.45	0.07	1.00	6.98
			1250	3.93	34.50	171.77	34.29	2.43	72.90	0.00		2.85	0.06	0.80	7.13
TS 4	-39.47	150.59	15	14.33			3.93	0.41	1.60	0.28	3.00	28.01	0.13	0.35	36.54
			40	14.33			4.09	0.41	1.60	0.09	2.51	24.51	0.07	0.42	17.74
Bottom depth: 6475 m			70	14.18			4.58	0.45	1.80	0.13	2.39	4.61		0.32	
			100	14.09	35.49	256.89	5.19	0.49	1.90	0.10	1.91	18.46		0.38	
			150	13.77			6.63	0.56	2.20	0.00	0.18	10.15	0.13	0.51	25.25
			200	12.92			10.32	0.78	3.30	0.00	0.05	6.81	0.06	0.76	7.26
			250				11.71	0.87	3.90	0.00		5.06	0.06	1.14	5.67
			300	11.24			13.69	1.00	4.70	0.00		4.58	0.39	1.07	36.44
			500	8.66	34.63	216.07	21.00	1.46	9.60	0.00		4.94	0.53	1.16	45.65
			750	6.46	34.46	198.38	27.64	1.91	23.30	0.00		5.09	0.24	0.94	25.54
			1000	4.77	34.45	183.33	31.76	2.22	46.30	0.00		5.23	0.31	1.04	29.54
			1250	3.66	34.52	166.36	35.39	2.51	89.00	0.00		3.81	0.30	0.86	34.20
			1756	2.54	34.64	164.89	34.90	2.44	93.40	0.01			0.17		
			2000	2.29	34.68	173.87	34.04	2.38	93.20	0.00		2.54	0.14	0.95	14.31
			2250	2.11	34.71	182.08	33.11	2.32	94.30	0.01			0.12		
			2500	1.94	34.72	187.44	32.72	2.29	98.20	0.00			0.14		
			2750	1.79	34.73	191.33	32.61	2.28	102.70	-0.01		1.31	0.12	1.13	10.76
			3000	1.63	34.73	194.54	32.56	2.28	106.60	0.00		3.27	0.12	0.98	12.43
			3250				32.82	2.30	111.80	0.00		3.40	0.12	1.18	10.29
			3500	1.29	34.72	200.71	32.98	2.31	115.60	-0.01		0.24	0.12	0.74	16.43
			3750				33.14	2.33	118.00	-0.01		0.13	0.12	0.67	18.23
			4000	1.16	34.72	202.54	33.21	2.34	119.70	-0.01		1.54	0.16	1.08	14.47
PS 3	-40.25	153.22	15	14.01			6.01	0.44	1.80	0.04	1.61	51.92	0.11	0.35	29.99

Station	Latitude	Longitude	Depth (m)	Temperature (C°)	Salinity	O ₂ (μM)	NO ₃ ⁻ (μM)	PO ₄ ³⁻ (μM)	SiO ₄ ²⁻ (μM)	NH ₄ ⁺ (μM)	Chl- <i>a</i> (μg)	H ₂ O ₂ (nM)	dFe(II) (nM)	dFe (nM)	Ratio %
Bottom depth: 3426 m			40	13.99			4.70	0.45	1.90	0.04	1.39	46.63	0.07	0.33	21.54
			100	13.62	35.42	250.15	17.02	0.54	2.20	0.03	0.78	18.84	0.02	0.39	4.40
			200	12.90			14.12	0.59	2.30	0.13	0.47	25.88	0.02	0.29	5.90
			250				6.88	0.63	2.30	0.00		16.15	0.06	0.66	8.92
			300	12.40	35.23	256.00	7.68	0.66	2.40	0.00	0.10	14.50	0.02	0.49	3.51
			500	9.22	34.68	229.20	8.18	1.28	6.40	0.00		11.65	0.29	0.76	38.89
			750	6.79	34.48	199.50	18.44	1.76	16.90	0.00		11.05	0.29	0.74	39.55
			1000	4.74	34.44	185.17	25.62	2.11	35.10	0.00		6.87	0.34	0.81	42.12
			1250	3.73	34.49	171.90	30.47	2.38	62.90	0.00		8.28	0.02	0.76	3.08
TS 3	-42.03	152.60	15	12.70			6.46	0.58	2.10	0.01	1.20	55.72	0.32	0.67	48.23
			40	12.74			6.46	0.58	2.00	0.01	1.16	39.22		0.32	
			70	12.70	35.26	268.59	6.47	0.58	2.10	0.02	1.21	37.47	0.12	0.55	21.92
			100	12.70	35.27	264.88	6.50	0.59	2.10	0.02	1.21	41.68		0.20	
			150	12.64	35.26	260.87	7.15	0.62	2.20	0.00	0.19	24.70	0.12	0.33	36.33
			200	12.39	35.20	255.42	8.47	0.69	2.40	0.00		18.10	0.12	0.33	36.33
			250				8.67	0.70	2.40	0.00		17.73		0.22	
			300	11.52	35.04	247.96	11.64	0.87	3.40	0.00	0.02	13.84	0.12	0.59	20.38
			500	8.98	34.64	232.82	19.72	1.38	7.30	0.00		12.87	0.12	1.21	10.02
			750	7.24	34.49	205.75	26.59	1.83	18.90	0.00		11.69	0.12	1.26	9.63
			1000	5.39	34.43	193.29	30.84	2.14	38.20	0.00		10.44	0.12	0.96	12.64
1250	3.93	34.47	175.70	33.73	2.36	60.60	0.00		10.66	0.12	1.02	11.93			
TS 2	-43.51	153.34	15	12.14			7.40	0.63	2.10	0.04	0.39	44.18	0.08	0.20	37.15
			40	12.14			7.38	0.63	2.10	0.04	0.35	49.80	0.09	0.34	25.60
			70	12.14			7.37	0.63	2.10	0.03	0.36	45.96		0.30	
			750	8.24	34.55	223.53	22.56	1.57	10.50	0.00	0.14	20.60	0.08	0.48	15.80
			1000	5.95	34.41	202.85	28.43	1.97	23.90	0.00		22.42	0.08	0.56	13.45
PS 2	-45.47	153.32	15	12.13	35.18	266.85	11.11	0.86	2.80	0.00	0.39	30.57	0.12	0.31	37.84
			40				11.15	0.86	2.80	0.00	0.35	29.08	0.12	0.45	27.40

Station	Latitude	Longitude	Depth (m)	Temperature (C°)	Salinity	O ₂ (μ M)	NO ₃ ⁻ (μ M)	PO ₄ ³⁻ (μ M)	SiO ₄ ²⁻ (μ M)	NH ₄ ⁺ (μ M)	Chl- <i>a</i> (μ g)	H ₂ O ₂ (nM)	dFe(II) (nM)	dFe (nM)	Ratio %
Bottom depth: 4546 m			70				11.15	0.86	2.80	0.00	0.36	27.80	0.14	0.48	29.23
			100	12.15	35.19	264.39	11.17	0.86	2.80	0.00	0.14	27.43	0.04	0.26	16.13
			750	8.24	34.55	223.53	13.03	0.97	4.40	0.00		22.63	0.06	0.52	10.69
			1500	3.56	34.51	168.19	35.04	2.45	78.00	0.00		12.91	0.06	0.95	6.47
			2000	2.50	34.64	170.69	33.28	2.31	83.30	0.00		12.66	0.04	0.86	4.94
			2500	2.09	34.71	184.36	32.02	2.23	92.40	0.00		13.19	0.04	1.05	4.04
			3000	1.76	34.73	193.70	32.27	2.25	105.80	0.00		12.91	0.04	1.25	3.39
			3500	1.40	34.73	199.59	32.80	2.29	116.60	0.00		12.19	0.04	0.96	4.42
			4000	1.19	34.72	202.72	33.04	2.31	121.30	0.00		13.24	0.04	1.45	2.92
			4500	1.13	34.71	205.44	33.02	2.31	123.30	0.00	13.97	0.04	1.38	3.08	
TS 1	-46.20	148.06	15	9.13	34.56	286.81	13.52	1.01	2.80	0.00	0.05	47.74		0.24	
			40				13.52	1.02	2.70	0.00	0.05	31.63		0.15	
Bottom depth: 2614 m			70				13.51	1.02	2.70	0.00		30.65		0.30	
			100	9.14	34.57	285.70	13.49	1.02	2.80	0.00	0.03	22.62		0.16	
			150				13.40	1.02	2.80	0.00		43.67	0.17	0.35	47.36
			200				13.31	1.01	2.80	0.00	0.02	37.52		0.16	
			250				14.79	1.09	3.60	0.00		20.63	0.17	0.55	29.93
			300	9.11	34.60	266.85	15.74	1.14	4.00	0.00	0.02	19.14	0.17	0.41	39.96
			500	8.70	34.59	257.78	18.43	1.32	5.80	0.00		16.67		0.34	
			750	6.35	34.40	214.33	25.89	1.79	17.10	0.00		12.36	0.17	1.04	15.93
			1000				30.41	2.11	31.00	0.00		15.68	0.28	0.88	31.37
			1250	3.53	34.48	175.07	34.20	2.41	63.70	0.00	14.58	0.17	0.86	19.15	
PS 1	-47.03	141.52	15				12.60	0.98	2.60	0.01	0.04	27.99		0.54	56.32
			40	9.44	34.65	282.48	12.62	0.98	2.60	0.00	0.06	23.16		0.33	
Bottom depth: 4866 m			70				12.59	0.97	2.60	0.00		24.17		0.33	
			100	9.45	34.65	282.08	12.50	0.97	2.60	0.00		21.59	0.21	0.52	40.27
			150				12.46	0.97	2.60	0.01	0.04		0.19		
			200	9.44	34.64	282.03	12.60	0.98	2.60	0.01	0.03	19.03	0.16	0.52	30.80

Station	Latitude	Longitude	Depth (m)	Temperature (C°)	Salinity	O ₂ (μ M)	NO ₃ ⁻ (μ M)	PO ₄ ³⁻ (μ M)	SiO ₄ ²⁻ (μ M)	NH ₄ ⁺ (μ M)	Chl- <i>a</i> (μ g)	H ₂ O ₂ (nM)	dFe(II) (nM)	dFe (nM)	Ratio %
			250				12.63	0.97	2.60	0.00		18.46	0.09	0.39	22.51
			300	9.27	34.66	259.12	15.87	1.14	4.30	0.00	0.02	7.78	0.04	0.34	10.55
			500	8.75	34.59	264.71	17.20	1.23	4.90	0.00		6.68	0.03	0.71	4.25
			750				25.36	1.75	14.80	0.00		6.02	0.03	0.67	4.46
			1000				30.56	2.12	30.00	0.00		4.94	0.03	0.58	5.19
			1250	3.82	34.41	189.94	33.85	2.35	53.50	0.00		5.65	0.03	0.72	4.16
			1500	3.16	34.48	178.06	35.00	2.45	73.00	0.00		6.33	0.30	0.70	42.36
			1750	2.57	34.63	174.76	34.50	2.42	80.80	0.00		6.90	0.29	0.83	34.85
			2000	2.42	34.68	178.56	33.25	2.34	84.30	0.00		4.98	0.30	0.79	38.27
			2250				33.23	2.34	92.60	0.00		7.19	0.24	0.77	30.93
			2500	2.08	34.73	182.40	32.99	2.33	99.60	0.00		6.36	0.22	0.83	26.09
			2750				32.96	2.32	105.20	0.00		6.05	0.24		
			3000	1.77	34.73	190.17	32.88	2.31	108.50	0.00			0.22	0.79	27.60
			3500	1.49	34.73	199.14	32.72	2.30	113.90	0.00		7.36	0.23	0.71	32.69
			3750				32.80	2.30	116.50	0.00		6.11	0.30	0.91	32.46
			4000	1.28	34.72	204.10	32.87	2.30	119.60	0.00		8.96	0.28	1.18	23.41

Supplementary Table 14 Pearson correlations matrix for all data.

dFe2	Pearson Correlation	1	,021	-,113	-,190 ^{**}	,228 ^{**}	,138	,076	-,228 ^{**}	,000	,067	-,155 [*]	-,138	-,171 [*]	-,141	-,036	-,090	,771 ^{**}
	Sig. (2-tailed)		,784	,132	,009	,004	,138	,417	,014	,998	,362	,036	,062	,020	,055	,642	,222	<,001
	N	186	179	179	186	155	117	116	116	60	186	184	184	184	185	173	185	179
H2O2	Pearson Correlation	,021	1	-,574 ^{**}	-,485 ^{**}	,456 ^{**}	,244 ^{**}	,660 ^{**}	-,565 ^{**}	,194	,265 ^{**}	-,544 ^{**}	-,544 ^{**}	-,496 ^{**}	-,338 ^{**}	-,085	-,412 ^{**}	,221 ^{**}
	Sig. (2-tailed)	,784		<,001	<,001	<,001	,010	<,001	,142	<,001	<,001	<,001	<,001	<,001	<,001	,275	<,001	,003
	N	179	179	178	179	149	111	110	110	59	179	177	177	177	179	168	179	178
Fetot	Pearson Correlation	-,113	-,574 ^{**}	1	,668 ^{**}	-,712 ^{**}	-,383 ^{**}	-,638 ^{**}	,693 ^{**}	,013	-,155 [*]	,718 ^{**}	,723 ^{**}	,687 ^{**}	,535 ^{**}	,102	,581 ^{**}	-,377 ^{**}
	Sig. (2-tailed)	,132	<,001		<,001	<,001	<,001	<,001	,924	,039	<,001	<,001	<,001	<,001	<,001	,187	<,001	<,001
	N	179	178	179	179	150	112	111	111	59	179	177	177	177	179	168	179	179
Depth	Pearson Correlation	-,190 ^{**}	-,485 ^{**}	,668 ^{**}	1	-,829 ^{**}	-,332 ^{**}	-,526 ^{**}	,796 ^{**}	-,302 [*]	-,124	,790 ^{**}	,793 ^{**}	,954 ^{**}	,822 ^{**}	,087	,674 ^{**}	-,281 ^{**}
	Sig. (2-tailed)	,009	<,001	<,001		<,001	<,001	<,001	<,001	,019	,093	<,001	<,001	<,001	<,001	,257	<,001	<,001
	N	186	179	179	186	155	117	116	116	60	186	184	184	184	185	173	185	179
Temperature	Pearson Correlation	,228 ^{**}	,456 ^{**}	-,712 ^{**}	-,829 ^{**}	1	,753 ^{**}	,692 ^{**}	-,958 ^{**}	,097	,091	-,950 ^{**}	-,957 ^{**}	-,883 ^{**}	-,713 ^{**}	-,136	-,782 ^{**}	,362 ^{**}
	Sig. (2-tailed)	,004	<,001	<,001	<,001		<,001	<,001	<,001	,489	,259	<,001	<,001	<,001	<,001	,105	<,001	<,001
	N	155	149	150	155	155	117	116	116	53	155	155	155	155	155	144	155	150
Salinity	Pearson Correlation	,138	,244 ^{**}	-,383 ^{**}	-,332 ^{**}	,753 ^{**}	1	,474 ^{**}	-,673 ^{**}	,459 [*]	,044	-,729 ^{**}	-,751 ^{**}	-,423 ^{**}	-,357 ^{**}	-,121	-,558 ^{**}	,309 ^{**}
	Sig. (2-tailed)	,138	,010	<,001	<,001	<,001		<,001	<,001	,036	,635	<,001	<,001	<,001	<,001	,209	<,001	<,001
	N	117	111	112	117	117	117	116	116	21	117	117	117	117	117	110	117	112
Oxygen	Pearson Correlation	,076	,660 ^{**}	-,638 ^{**}	-,526 ^{**}	,692 ^{**}	,474 ^{**}	1	-,865 ^{**}	-,035	,224 [*]	-,830 ^{**}	-,840 ^{**}	-,714 ^{**}	-,435 ^{**}	-,168	-,645 ^{**}	,386 ^{**}
	Sig. (2-tailed)	,417	<,001	<,001	<,001	<,001	<,001		<,001	,881	,016	<,001	<,001	<,001	<,001	,080	<,001	<,001
	N	116	110	111	116	116	116	116	116	21	116	116	116	116	116	109	116	111
AOU	Pearson Correlation	-,228 ^{**}	-,565 ^{**}	,693 ^{**}	,796 ^{**}	-,958 ^{**}	-,673 ^{**}	-,865 ^{**}	1	-,470 [*]	-,172	,965 ^{**}	,976 ^{**}	,916 ^{**}	,642 ^{**}	,211 [*]	,741 ^{**}	-,478 ^{**}
	Sig. (2-tailed)	,014	<,001	<,001	<,001	<,001	<,001	<,001		,032	,066	<,001	<,001	<,001	<,001	,028	<,001	<,001
	N	116	110	111	116	116	116	116	116	21	116	116	116	116	116	109	116	111
Chl_a	Pearson Correlation	,000	,194	,013	-,302 [*]	,097	,459 [*]	-,035	-,470 [*]	1	-,104	-,322 [*]	-,320 [*]	-,220	-,131	-,120	-,075	-,009
	Sig. (2-tailed)	,998	,142	,924	,019	,489	,036	,881	,032		,431	,012	,013	,091	,323	,389	,574	,944
	N	60	59	59	60	53	21	21	21	60	60	60	60	60	59	54	59	59
PAR	Pearson Correlation	,067	,265 ^{**}	-,155 [*]	-,124	,091	,044	,224 [*]	-,172	-,104	1	-,077	-,076	-,125	-,086	-,022	-,076	,128
	Sig. (2-tailed)	,362	<,001	,039	,093	,259	,635	,016	,066	,431		,300	,308	,090	,243	,778	,301	,087
	N	186	179	179	186	155	117	116	116	60	186	184	184	184	185	173	185	179
NOx	Pearson Correlation	-,155 [*]	-,544 ^{**}	,718 ^{**}	,790 ^{**}	-,950 ^{**}	-,729 ^{**}	-,830 ^{**}	,965 ^{**}	-,322 [*]	-,077	1	,994 ^{**}	,870 ^{**}	,673 ^{**}	,131	,795 ^{**}	-,337 ^{**}
	Sig. (2-tailed)	,036	<,001	<,001	<,001	<,001	<,001	<,001	<,001	,012	,300		<,001	<,001	<,001	,088	<,001	<,001
	N	184	177	177	184	155	117	116	116	60	184	184	184	184	183	171	183	177
Phopshate	Pearson Correlation	-,138	-,544 ^{**}	,723 ^{**}	,793 ^{**}	-,957 ^{**}	-,751 ^{**}	-,840 ^{**}	,976 ^{**}	-,320 [*]	-,076	,994 ^{**}	1	,875 ^{**}	,678 ^{**}	,131	,804 ^{**}	-,328 ^{**}
	Sig. (2-tailed)	,062	<,001	<,001	<,001	<,001	<,001	<,001	<,001	,013	,308	<,001		<,001	<,001	,089	<,001	<,001
	N	184	177	177	184	155	117	116	116	60	184	184	184	184	183	171	183	177
Silicate	Pearson Correlation	-,171 [*]	-,496 ^{**}	,687 ^{**}	,954 ^{**}	-,883 ^{**}	-,423 ^{**}	-,714 ^{**}	,916 ^{**}	-,220	-,125	,870 ^{**}	,875 ^{**}	1	,795 ^{**}	,153 [*]	,758 ^{**}	-,281 ^{**}
	Sig. (2-tailed)	,020	<,001	<,001	<,001	<,001	<,001	<,001	<,001	,091	,090	<,001	<,001		<,001	,046	<,001	<,001
	N	184	177	177	184	155	117	116	116	60	184	184	184	184	183	171	183	177
Cu	Pearson Correlation	-,141	-,338 ^{**}	,535 ^{**}	,822 ^{**}	-,713 ^{**}	-,357 ^{**}	-,435 ^{**}	,642 ^{**}	-,131	-,086	,673 ^{**}	,678 ^{**}	,795 ^{**}	1	,076	,830 ^{**}	-,225 ^{**}
	Sig. (2-tailed)	,055	<,001	<,001	<,001	<,001	<,001	<,001	<,001	,323	,243	<,001	<,001	<,001		,319	<,001	,002
	N	185	179	179	185	155	117	116	116	59	185	183	183	183	185	173	185	179
Pb	Pearson Correlation	-,036	-,085	,102	,087	-,136	-,121	-,168	,211 [*]	-,120	-,022	,131	,131	,153 [*]	,076	1	,276 ^{**}	,110
	Sig. (2-tailed)	,642	,275	,187	,257	,105	,209	,080	,028	,389	,778	,088	,089	,046	,319		<,001	,157
	N	173	168	168	173	144	110	109	109	54	173	171	171	171	173	173	173	168
NI	Pearson Correlation	-,090	-,412 ^{**}	,581 ^{**}	,674 ^{**}	-,782 ^{**}	-,558 ^{**}	-,645 ^{**}	,741 ^{**}	-,075	-,076	,795 ^{**}	,804 ^{**}	,758 ^{**}	,830 ^{**}	,276 ^{**}	1	-,219 ^{**}
	Sig. (2-tailed)	,222	<,001	<,001	<,001	<,001	<,001	<,001	<,001	,574	,301	<,001	<,001	<,001	<,001	<,001		,003
	N	185	179	179	185	155	117	116	116	59	185	183	183	183	185	173	185	179
ratio_dFe2_Fetot	Pearson Correlation	,771 ^{**}	,221 ^{**}	-,377 ^{**}	-,281 ^{**}	,362 ^{**}	,309 ^{**}	,386 ^{**}	-,478 ^{**}	-,009	,128	-,337 ^{**}	-,328 ^{**}	-,281 ^{**}	-,225 ^{**}	,110	-,219 ^{**}	1
	Sig. (2-tailed)	<,001	,003	<,001	<,001	<,001	<,001	<,001	<,001	,944	,087	<,001	<,001	<,001	<,001	,002	,157	,003
	N	179	178	179	179	150	112	111	111	59	179	177	177	177	179	168	179	179

**. Correlation is significant at the 0.01 level (2-tailed).

*. Correlation is significant at the 0.05 level (2-tailed).

Supplementary Table 15 Correlations of proximity to landmass and/or seamounts for the first 250 m of dFe(II), H₂O₂ and dFe.

		Distance to nearest landmass	Distance to nearest landmass or seamount	H2O2	Fe2	Fetot
Distance to nearest landmass	Pearson-Korrelation	1	,675**	,463**	,106	-,073
	Sig. (2-seitig)		<,001	<,001	,397	,565
	N	66	66	64	66	64
Distance to nearest landmass or seamount	Pearson-Korrelation	,675**	1	,156	,223	,058
	Sig. (2-seitig)	<,001		,220	,072	,649
	N	66	66	64	66	64
H2O2	Pearson-Korrelation	,463**	,156	1	-,049	-,378**
	Sig. (2-seitig)	<,001	,220		,699	,002
	N	64	64	64	64	64
Fe2	Pearson-Korrelation	,106	,223	-,049	1	-,049
	Sig. (2-seitig)	,397	,072	,699		,702
	N	66	66	64	66	64
Fetot	Pearson-Korrelation	-,073	,058	-,378**	-,049	1
	Sig. (2-seitig)	,565	,649	,002	,702	
	N	64	64	64	64	64

*. Correlation is significant at the 0.05 level (2-tailed).

Appendix D

Acknowledgements & tasks performed for methods in this thesis

Supplementary Table 16 People & tasks thankfully performed, listed by chapters

Chapter	Description	Task	Name
1	Literature Review	No analytical work was done for this chapter	
		Writing & editing	Helene Aflenzer, Delphine Lannuzel, Pier van der Merwe, Kathrin Wuttig, Andrew Bowie
2	Fe(II) oxidation rates	Cleaning & vessel preparations	Helene Aflenzer
		Sampling of open ocean seawater during 'HEOBI'	Thomas Holmes, Pier van der Merwe, Manon Tonnard, Lavenia Ratnarajah
		Sampling of coastal seawater	Helene Aflenzer
		Designing and building the cooling unit for dFe(II)	Pier van der Merwe & Helene Aflenzer

Chapter	Description	Task	Name
		Modifying the overall dFe(II)-FIA system	Kathrin Wuttig, Pier van der Merwe & Helene Aflenzer
		dFe(II) & dFe(III) analysis	Helene Aflenzer
		CO ₂ installation & bubbling	Helene Aflenzer
		pH, O ₂ , temperature & salinity	Helene Aflenzer
		Macronutrient analysis	Catriona Hurd & Nils Jansen
		SF-ICP-MS analysis & preparations	Ashley Townsend, Kathrin Wuttig, Melanie Gault Ringold, Pauline Latour
		CDOM analysis	Kathrin Wuttig & Helene Aflenzer
		Experimental conductions	Helene Aflenzer
		Plotting & statistics	Helene Aflenzer with the initial help of Pier van der Merwe
		Writing & editing	Helene Aflenzer, Pier van der Merwe, Kathrin Wuttig, Andrew Bowie

Chapter	Description	Task	Name
3	Biological chapter	Cleaning & vessel preparations	Helene Aflenzer
		Sampling of open ocean seawater during 'SR3'	Pauline Latour, Pier van der Merwe, Melanie Gault-Ringold, Thomas Holmes, Christine Weldrick & Matt Corkill
		Sampling of coastal seawater	Helene Aflenzer
		Study organisms	Provided by Andrew McMinn & Fraser Kennedy
		Temperature, pH and salinity	Helene Aflenzer
		Macronutrients	Catriona Hurd & Damon Britton
		Trace elements	Ashley Townsend, Kathrin Wuttig, Melanie Gault Ringold, Pauline Latour, Pier van der Merwe
		Voltammetry	Cristina Genovese & Helene Aflenzer
		Growth rates	Helene Aflenzer
		Statistical analysis, plotting & experimental conduct	Helene Aflenzer

Chapter	Description	Task	Name
		Writing & editing	Helene Aflenzer, Robert Strzepek (comments), Linn Hoffmann, Kathrin Wuttig, Thomas Holmes, Andrew Bowie
4	EAC Chapter	Preparation of collection vessels	Helene Aflenzer & Pauline Latour
		Collection of TM free water column samples	Rob Gruen, Sarah Andrew, Pamela Barrett, Michael Ellwood, Pauline Latour
		Collection of seawater for hydrochemistry	CSIRO & MNF staff
		Analysis of hydrochemistry	CSIRO
		Macronutrients	CSIRO
		Chlorophyll- <i>a</i>	Rob Grun, Prayna Maharaj Riteshma Devi and Sarah Andrew
		dFe(II) & dFe(III) analysis	Helene Aflenzer
		H ₂ O ₂ analysis	Pauline Latour

Chapter	Description	Task	Name
		Rainwater collection	Helene Aflenzer & Pauline Latour
		Sediment pore water collection	Rob Grun, Prayna Maharaj Riteshma Devi and Sarah Andrew. Thank you to April Abott, Dave Janssen, Hannah Kumar, Hannah Wilson, and Annabel Payne
		dFe(II) Sample preparation from sediment core	Dave Janssen
		Plotting & illustrating	Helene Aflenzer & Thomas Holmes
		Writing & editing	Helene Aflenzer, Pier van der Merwe (comments), Thomas Holmes, Kathrin Wuttig, Pauline Latour, Andrew Bowie
5	Synopsis	Plotting & summarizing	Helene Aflenzer
		Writing & editing	Helene Aflenzer, Delphine Lannuzel, Pier van der Merwe,

Chapter	Description	Task	Name
			Kathrin Wuttig, Andrew Bowie